QUANTITATIVE TWO-DIMENSIONAL ECHOCARDIOGRAPHY

A thesis

presented for the degree of

Doctor of Philosophy in Electrical Engineering

in the

University of Canterbury,

Christchurch, New Zealand

by

W.H. ROUND B.Sc.(Tech.),M.Sc.

1982

To Glenys

".... I did not marvel that Andreas Laurentius wrote that the motion of the heart was perplexing as the flux and reflux of Euripus was to Aristotle.....I found it so truly difficult that I almost believed with Fracastorius that the motion of the heart was to be understood by God alone."

William Harvey, M.D.
Exercitatio Anatomica de Motu Cordis et Sanguinis in Animalibus (1628)

ACKNOWLEDGEMENTS

First, I would like to thank my wife Glenys for supporting me over the last three years, especially over the last three months.

I would also sincerely like to thank my supervisor, Professor Richard Bates, for his advice, encouragement and interest. I know that I am a far better scientist and engineer from the experience of working under his guidance.

My associate supervisor, Dr Hamid Ikram must also be thanked for his advice on the medical aspects of the research presented in this thesis. I also thank him for his perpetual enthusiasm and encouragement.

Dr Philip Bones, who often acted as an 'unofficial supervisor', was always willing to offer advice on the technical aspects of my work. I thank him for this.

I also thank the staff of the Princess Margaret Hospital for providing me with a pleasant environment in which to work. Special thanks must go to the echocardiographer at PMH, Christine Wilson, for always being willing to scan subjects for my studies. I thank her for her hard work and dedication.

Several of the staff and students at the University of Canterbury also contributed ideas and advice. In particular, I wish to thank Robin Williams, Dr Fred Cady, Bill Kennedy, Brent Robinson, Robert Minard and the technicians in the Electrical Engineering Departments' workshops.

The National Heart Foundation have generously supported my work financially over the past three years. I thank them for this.

Finally, thanks go to Merryl Woodhead for faithfully typing this thesis.

ERRATA

QUANTITATIVE TWO-DIMENSIONAL ECHOCARDIOGRAHY

BY W. H. ROUND

Page 4, para 2, line 2 'available'	should be	'able'
Page 4, Table 1.2 Page 5, para 1, line 5 Page 19, Fig 1.2 'mammilian'	should be	'mammalian'
Page 6, para 1, line 2 'acqueous'	should be	'aqueous'
Page 8, para 2, line 7 'longer'	should be	'larger'
Page 9, para 2, line 2 'or'	should be	'of'
Page 18, para 3, line 9 'is'	should be	'are'
Page 31, para 3, line 6 'hand-copy'	should be	'hard-copy'
Page 32, para 5, line 2 'M-mode'	should be	'C-mode'
Page 47, para 2, line 3 'defector'	should be	'detector'
Page 51, para 3, line 13 'pizels'	should be	'pixels'
Page 63, para 5, line 10 'systol'	should be	'systole'
Page 65, para 2, line 15 'end-diastolic'	should be	'end-systolic'
Page 73, para 2, line 7 'distance along'	should be	'distance ℓ along'
Page 90, para 3, line 6 ' 'low pass filtering' or smoothing' '	should be	' 'low pass filtering' or 'smoothing' '
Page 98, para 2, line 3 'Robison'	should be	'Robinson'

TABLE OF CONTENTS

ABSTRACT

This thesis reports studies of the motion and shape of the walls of the heart using data extracted from two-dimensional echocardiograms.

The relevant literature and clinical practice are first reviewed at length.

The development of hardware and software systems for digitally recording two-dimensional echocardiograms (scans) is described. Computer techniques for enhancing scans of the left ventricle of the heart are presented. Methods of interactively extracting the endocardial outlines seen in the scans are described.

The outlines of the left ventricular walls were extracted from the scans of two groups of subjects. One group consisted of nine normal volunteers, the other consisted of nine coronary artery disease (CAD) patients known to have abnormal left ventricles. The outlines obtained were used to study methods of analysing left ventricular wall motion and shape under exercise and drug interventions. Two cardiac drugs were used: nifedipine and metoprolol.

Wall motion was measured in terms of the change in distance of the walls from the ventricular centroid. CAD patients with apical infarctions were found to have hyperkinetic regions of the walls adjacent to their infarctions. The hyperkinesia decreased when the patients were subjected to isometric exercise. Under the influence of nifedipine the hyperkinesia increased. However under the influence of metoprolol it decreased. These observations are consistent with the known effects of exercise and the drugs on the motion of the heart.

Ventricular shape was described using a trigonometric Fourier series. Descriptors derived from the coefficients of the series were developed. The values of some of the descriptors of the CAD patients with apical infarctions were found to be larger than those of the normal volunteers. Under exercise the value of the descriptors of the normal volunteers did not change, while those of the apical infarction patients increased further. Nifedipine was found to increase the values of the descriptors of the patients. Metoprolol in contrast, reduced the values. These findings are consistent with the expected effects of exercise and the drugs on the shape of the left ventricle. Therefore, the methods developed may be used to quantitatively assess the

effects of other exercise and drug interventions on ventricular wall motion and shape. The quantitative analysis of ventricular shape may also be used as a means of identifying patients with ventricular wall abnormalities.

PREFACE

In 1978 I was employed as a physicist in the Departments of Radiotherapy and Nuclear Medicine at Waikato Hospital in Hamilton, New Zealand. I was fascinated with the relatively new (to New Zealand) field of medical ultrasonic imaging but my chances of venturing further into this at Waikato Hospital were somewhat limited. While passing through Christchurch in October of that year, I took the opportunity to visit Professor R.H.T. Bates at the Electrical Engineering Department at the University of Canterbury. Professor Bates and some of his colleagues had been experimenting with ultrasonic computed tomography and speckle imaging techniques. I was impressed with what I saw and told Professor Bates that I was interested in doing a Ph.D. in 'something to do with medical ultrasonics'. At later meetings with Dr. Philip Bones and Dr. Hamid Ikram at the Princess Margaret Hospital a proposal was put forward that we should apply for a grant from the National Heart Foundation of New Zealand to finance a suitable project.

Eventually funding to undertake a study of left ventricular wall motion was granted by the National Heart Foundation. It was proposed to interface an SKI echocardiographic sector scanner to the Cardiology and Respiratory Departments' PDP 11/10 computer. This would allow images from the scanner to be processed by the computer to help extract the desired wall motion data thus enabling ventricular wall motion to be quantified. It was recognised at this stage that the 'stop-frame' sector scan images produced by the SKI were of poor quality and, in general, the inner wall of the ventricle (the endocardium) could not be identified. Therefore image processing techniques would have to be employed to improve the image quality.

A sector scanner-to-computer interface was eventually constructed. Scans of several volunteers were recorded and were used to help develop appropriate image processing techniques.

The systems developed were then used to study left ventricular wall motion in two groups of volunteers. The first of these was a group of normal subjects with no history of cardiac disease. The second was a group of coronary artery disease patients who were known to have a wall motion defect. The volunteers were studied while resting, exercising, and during certain drug interventions. Quantitative methods of analysing ventricular wall motion and

shape were developed. It was shown that it may be possible to classify patients as having normal or abnormal ventricles by quantitatively assessing wall motion and shape using the data from their sector scans.

The first four chapters of this thesis review the research literature and describe the clinical techniques relevant to the original work presented in the final three chapters.

In Chapter 1, the interaction of ultrasound with human tissues is reviewed. This provides those readers who are unfamiliar with medical ultrasonic imaging with the necessary physical and biological background. The equations used to describe the propagation of sound through tissues are presented. The basic acoustic parameters, such as velocity and attenuation, related to sound travelling through tissue are discussed. Also the mechanisms by which ultrasound is absorbed and scattered by tissues are considered.

Chapter 2 discusses the instrumentation side of medical ultrasonic imaging. Emphasis is placed on pulse-echo techniques rather than on the transmission techniques which are less popular.

A brief description of cardiac anatomy is presented at the start of Chapter 3. The qualitative and quantitative methods used to analyse ventricular wall motion and shape in cineangiography and echocardiography are described. Angiographic methods are discussed in detail because angiography in the past has been the 'gold standard' technique for analysing wall motion. The literature contains many more accounts of the quantification of wall motion and shape by this technique than by echocardiography.

Image processing techniques are now widely employed in commercial ultrasonic scanning equipment to improve image quality. These techniques are reviewed in Chapter 4. Estimation of the position of the ventricular walls in angiograms and echocardiograms by semi- and fully-automatic computational procedures are also reviewed.

Chapter 5 describes the construction of the scanner-to-computer interface which was developed as part of the research reported in this thesis. The images it presents to the computer are generally of poor quality. Therefore image processing was employed to improve their visual appearance and to make the endocardial outline more obvious to an observer. The methods used to do this are described in detail. A technique called 'simultaneous scanning' was developed to allow an observer to accurately identify the position of the endocardial border in a sector scan. This was developed further and as

a result a new mode of scanning,' R-mode' scanning, was introduced. A computer program developed to extract the endocardial border in a series of scans is described in this chapter.

The above-mentioned techniques were employed to obtain the data for the experiments described in Chapter 6. In these experiments the regional heart wall motion of normal volunteers and coronary artery disease patients was studied. Wall motion was measured in terms of the percentage decrease in the distance of the walls from the ventricular centroid. The effects of various exercise and drug interventions on wall motion were also studied. The results of these experiments are detailed and shown to correlate with the known effects of these drugs on wall motion. A method of describing ventricular shape in terms of trigonometrical Fourier series is described. It was found that changes in the coefficients of the series due to the effects of the interventions can be related to expected changes in the ventricular shapes.

Conclusions are presented in Chapter 7 which also contains suggestions on how this research may be developed further.

While the research described in this thesis was being carried out, the following papers and presentations were prepared:-

1) W.H. Round and R.H.T. Bates
'Ultrasonic spectrum modification by subwavelength scatterers'
Presented at 20th Conference on Physical Sciences and Engineering in Medicine and Biology, Christchurch, New Zealand. 25-29 August 1980.

2) W.H. Round, P.J. Bones, H. Ikram and R.H.T. Bates
'Digitising and processing echocardiographic images'
Presented at 21st Conference on Physical Sciences and Engineering in Medicine and Biology, Melbourne, Australia. 17-21 August 1981.
Also published in 'Australasian Physical and Engineering Sciences in Medicine, 1982, 5, 113-121.

The following papers are also to be submitted.

1) W.H. Round, P.J. Bones, R.H.T. Bates, H. Ikram
'The simultaneous scanning technique : an aid for endocardial detection in sector scans' To be submitted to The Journal of Cardiovascular Ultrasound.

2) W.H. Round and R.B. Williams
'Inconsistent estimation of ventricular outlines'.
To be submitted to Journal of Clinical Ultrasound.

3) W.H. Round, P.J. Bones, H. Ikram, R.H.T. Bates
'Echocardiographic studies of left ventricular wall motion'.
To be submitted to The Journal of Cardiovascular Ultrasound.

4) W.H. Round, R.H.T. Bates, R.B. Williams, H. Ikram
'A Fourier description of ventricular outlines'.
To be submitted to Computers and Biomedical Research.

CHAPTER 1

THE INTERACTION OF ULTRASOUND WITH TISSUES

1.1 INTRODUCTION

In this chapter, the interaction of ultrasound with soft tissues is discussed. This will provide those unfamiliar with medical ultrasonic imaging with an appreciation of the relevant acoustical and biological background. It will also provide an insight into the difficulties encountered when obtaining data to image tissues using ultrasonic methods.

While the physics of ultrasound traversing homogeneous, low-loss media is well understood (cf. Wells, 1977, Chap. 1), it is difficult to obtain a satisfactory description of the propagation of an ultrasonic wave through biological tissues. Tissues exhibit spatial variations in density, refractive index and attenuation. The effects of these variations on ultrasonic waves have been analysed theoretically using simple tissue models (cf. Twersky, 1962a, 1962b, 1964; Atkinson and Berry, 1974).

In §1.2 the propagation of ultrasound in homogeneous media is discussed. The various acoustic parameters relevant to ultrasonic imaging are introduced. One of these, acoustic velocity, is treated in greater depth in §1.3. The range of values of this parameter for various biological tissues is presented. The scattering of sound by inhomogeneous media is considered in §1.4. Scattering is considered in detail for three tissues: blood, heart muscle and liver. Blood is a highly disordered tissue while liver is highly structured. Heart muscle represents the intermediate case and shows some degree of disorder in its structure. Finally, in §1.5, the absorption of ultrasound by tissues is described in terms of several of the mechanisms by which it may occur.

1.2 PROPAGATION OF SOUND WAVES IN FLUID MEDIA

The wave equation describing propagation of mechanical disturbances in dissipationless, isotropic, elastic media is (Dunn, 1976)

$$\frac{\delta^2\psi}{\delta t^2} = \frac{K + 4G/3}{\rho_o} \nabla\nabla.\psi - G\nabla x\nabla x\psi \qquad (1.1)$$

where ψ is the instantaneous displacement of a particle of the medium from its equilibrium position

K is the adiabatic modulus of compressibility of the medium

G is the modulus of shear rigidity of the medium

ρ_o is the mean density of the medium

The assumption is made that the medium is unable to support shear waves. Hence only longitudinal waves can propagate in the medium. This is in accord with experience with soft tissues (Wells, 1977). Setting the modulus of shear rigidity to zero (1.1) reduces to

$$\frac{\delta^2\psi}{\delta^2 t} = \frac{K}{\rho_o} \nabla\nabla.\psi \qquad (1.2)$$

This equation is an approximation of the more general hydrodynamic equations. It is valid under the conditions that the maximum particle velocity amplitude is small compared to the velocity of sound in the medium and that the adiabatic compressibility is not significantly dependent on pressure over the range of pressure variations occuring in the sound field. Under these conditions, the sound propagation velocity for longitudinal waves is

$$c = \left(\frac{K}{\rho_o}\right)^{\frac{1}{2}} \qquad (1.3)$$

The solution to the wave equation (1.2) for a one-dimensional wave travelling in the direction of the x axis is

$$\psi(x,t) = A\, e^{i(\omega t - kx)} \tag{1.4}$$

where A is the amplitude of the wave

ω is the angular frequency of the wave

k is the wave number ω/c

The characteristic impedance Z_o of the medium is defined as

$$Z_o = \rho_o c = \sqrt{K\rho_o} \tag{1.5}$$

This important parameter is discussed in §1.4. The acoustic pressure p at a point in the field can be defined as

$$p = p_i - p_o \tag{1.6}$$

where p_i is the instantaneous pressure at that point and p_o is the equilibrium pressure in the medium. The acoustic pressure and the particle displacement are related by

$$p = -\rho_o c^2 \frac{\delta\psi}{\delta x} \tag{1.7}$$

The intensity I of the acoustic wave is defined as the time average of the rate of transport of energy through unit area normal to the direction of propagation. It is given by

$$I = \frac{\rho_o c v_{max}}{2} \tag{1.8}$$

where v_{max} is the maximum velocity of a particle under the influence of the wave.

Medical ultrasonic imaging equipments use sound with a frequency in the range 1-10 MHz. The sound waves which they transmit have an intensity of approximately $10^{-2} W/cm^2$. The propagation of ultrasound in water in this frequency range is similar to that in soft tissues. It is therefore advantageous to know the magnitudes of the above parameters for water.

These are presented in Table 1.1 for 1 MHz sound waves.

Table 1.1 Field parameters for plane acoustic waves in water at 1 MHz

Parameter	Magnitude	Units
Peak particle displacement	1.8×10^{-9}	m
Peak particle velocity	12	m/sec
Peak particle acceleration	7×10^{4}	m/sec^{2}
Peak particle pressure	1.8×10^{4}	Nm^{-2}
Wavelength	1.5×10^{-3}	m
Wave velocity	1.5×10^{3}	m/sec
Density	1×10^{3}	kgm^{-3}
Characteristic impedance	1.5×10^{6}	$kgm^{-2}s^{-1}$

1.3 ACOUSTIC VELOCITY IN TISSUES

Most medical ultrasonic imaging systems require accurate estimates of the velocity of sound in various tissues to be available to produce undistorted images. Parry and Chivers (1979) collate the results of many researchers who have measured acoustic velocity in various tissue types. Estimates of acoustic velocity for selected tissues are presented in Table 1.2.

Table 1.2 The velocity of ultrasound in mammilian tissues (from Parry and Chivers, 1979)

Tissue		Velocity (m/sec)
Blood	(normal)	1550 - 1570
Fat	(normal)	1440 - 1582
Liver	(normal)	1553 - 1599
	(abnormal)	1570 - 1607
Kidney	(normal)	1558 - 1572
Spleen	(normal)	1515 - 1595
Lung	(normal)	650 - 1180
	(abnormal)	340
Connective tissue	(normal)	1545
Muscle	(normal)	1545 - 1631
Nervous tissue	(normal)	1506 - 1644
	(abnormal)	1500 - 1569
Bone	(normal)	2870 - 4060
	(abnormal)	2442 - 3371
Breast	(normal)	1450 - 1570
	(abnormal)	1478 - 1573

The velocity estimates reported in the literature for each tissue type tend to vary over an appreciable range of values (cf. Wells, 1977; Parry and Chivers, 1979). This variation has several sources, some being normal biological variation between tissue samples. In addition, not all of the values reported are for human tissues, although all are mammilian. It appears that there may be little difference from species to species (cf. Parry and Chivers, 1979). Several different techniques are used to measure ultrasonic velocity (cf. Andreae and Edmonds, 1961; Pellam and Galt, 1946; Greenspan and Tscheigg, 1957). While there should be no difference in the velocity estimates obtained using the various techniques, the reported values may well be functions of the instrumentation used. Some of the data reported in the literature are for tissues which have been 'fixed' in preserving chemicals, while others are for freshly excised or refrigerated samples. While the various preservation methods alter the acoustic velocity slightly (Bamber et al., 1979), greater variation is observed if the samples are not preserved. Presumably tissue decay over short periods of time has a greater effect than does preservation.

Velocity in tissues is known to be temperature dependent (cf. Bowen et al., 1979). Few of the estimates reported in the literature were measured with the samples at body temperature. Rather, the range of temperatures used by various researchers is from 19°C to 43°C. The velocity of ultrasound in most soft tissues increases by approximately 1 m/sec for each 1°C increase in tissue temperature (Bowen et al., 1979).

Soft tissues are dispersive media. The velocity dispersion is small however. It is less than 1% of the velocity in the 1-10 MHz frequency range (Wells, 1977). Since the magnitude of the dispersion is small, it is neglected in most imaging situations.

The range of velocities in soft tissue is small (1440 m/sec for post menopausal breast tissue to 1670 m/sec for collagen). It is common practice to assume an average velocity in soft tissues of 1540 m/sec. Bone has a much higher acoustic velocity than soft tissue. It has been reported to range from 2500 m/sec to 4400 m/sec (Parry and Chivers, 1979). The velocity in lung is much lower and has been reported as having values from 600 m/sec to 1200 m/sec.

1.4 THE SCATTERING OF SOUND BY TISSUES

1.4.1 Scattering by Inhomogeneous Media

In §1.1 the propagation of sound in lossless, homogeneous media (such as the acqueous and vitreous humours of the eye) is considered. However, few tissues can be considered homogeneous and almost all tissues exhibit spatial variations in density and compressibility. When an acoustic wave encounters a region where one of these parameters changes, some of the energy of the wave is scattered (Reid, 1976). In simple situations such as large planar or isolated subwavelength spherical scatterers, the scattering can be readily described theoretically. However the analysis is much more complicated for tissues, since to predict the acoustic parameters of a scattered wave, the spatial distributions of the density and compressibility of the tissues must be known. They are usually not available (Shung et al., 1976).

Scattering of ultrasound occurs at boundaries between organs and within the tissues themselves. Scattering at organ boundaries appears to be caused by the connective tissue membranes surrounding the organs (Reid, 1976). The echoes are strong and highly angle - dependent. This indicates that the scatter takes the form of specular reflections at the surface of the organs. The sources of the small echoes seen to arise from scatterers within tissues have not, in general, been identified.

In this section, scattering of sound from objects possessing simple shape and distributions is discussed. Scattering from three tissues (blood, heart muscle and liver) which exhibit differing degrees of order in their structure is related to the theoretical descriptions of scattering.

1.4.2 Scattering by Specular Reflectors

Acoustic waves with a wavelength which is appreciably less than the dimensions of a planar interface on which they are incident obey Snell's laws. This situation is illustrated in Figure 1.1.

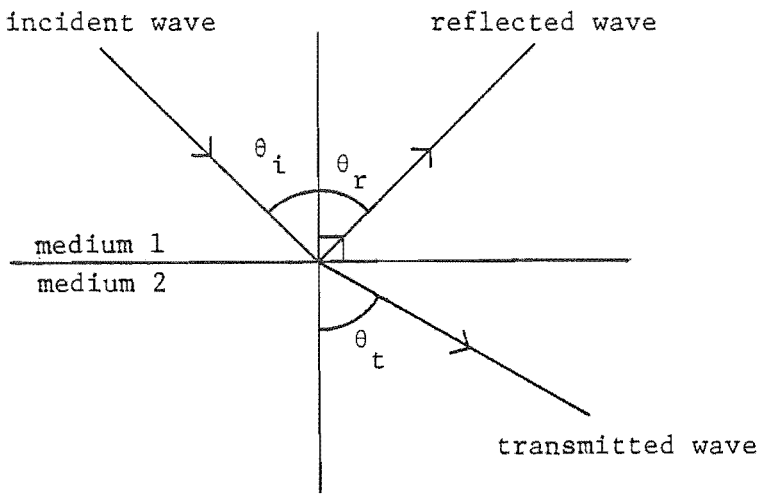

Figure 1.1: Reflection and transmission of sound at a plane boundary

At the interface some of the wave is transmitted while the rest is reflected. The angles θ_i and θ_r of the direction of the incident and reflected waves to the normal to the plane are such that

$$\theta_i = \theta_r \quad . \tag{1.9}$$

The angle θ_t describes the direction of the wave transmitted through the interface satisfies

$$\frac{\sin(\theta_t)}{\sin(\theta_i)} = \frac{c_2}{c_1} \tag{1.10}$$

where c_1 and c_2 are the velocities of the waves in media 1 and 2 respectively.

At the interface there can be no discontinuities in either particle velocity or particle pressure. In physical terms, this means that the two media remain in contact. By applying these two conditions the ratios of the intensities of the reflected and transmitted waves to the intensity of the incident wave are respectively

$$\frac{I_r}{I_i} = \left[\frac{Z_2\cos(\theta_i) - Z_1\cos(\theta_t)}{Z_2\cos(\theta_i) + Z_1\cos(\theta_t)}\right]^2 \qquad (1.11)$$

and

$$\frac{I_t}{I_i} = \frac{4Z_2Z_1\cos(\theta_i)\cos(\theta_t)}{\left[Z_2\cos(\theta_i) + Z_1\cos(\theta_t)\right]^2} \qquad (1.12)$$

where Z_1 and Z_2 are the characteristic impedances of media 1 and 2.

This analysis provides a satisfactory description of ultrasonic transmission and reflection at boundaries between organs (Reid, 1976; Round, 1977). The reflectivities, I_r/I_i, of boundaries between various tissues for waves perpendicular to the interface are presented in Table 1.3. It is seen that the reflectivities of soft tissue interfaces are in general small. Therefore little energy is lost from the incident wave by reflection. The reflectivities of interfaces between soft tissue and bone are much longer with the reflected wave having over half the intensity of the incident wave.

Table 1.3 Reflectivities of boundaries between selected tissues

	Water	Fat	Muscle	Skin	Brain	Liver	Blood	Skull Bone
Water	0.0	0.047	0.02	0.029	0.007	0.035	0.007	0.57
Fat			0.067	0.076	0.054	0.049	0.047	0.61
Muscle				0.009	0.013	0.015	0.02	0.56
Skin					0.022	0.0061	0.029	0.56
Brain						0.028	0.00	0.57
Liver							0.028	0.55
Blood								0.57

1.4.3 Scattering by Small Particles

Variations in density and compressibility in tissues are recognised as occuring over distances of much less than the wavelength of 1-10 MHz ultrasound (cf. Chivers, 1978; Gore and Leeman, 1977). It is informative to discuss the scattering of ultrasound by subwavelength particles. Some tissues appear to scatter ultrasound in a manner which can be described by modelling the scatterers as small spheres or cylinders (cf. Shung and Reid, 1977; Shung et al., 1976).

The scattering of sound by a sphere with a diameter much less than a wavelength is considered by Morse and Ingard (1968). If a sphere or radius a is suspended in a frictionless (i.e. non viscous) medium, the intensity I_s of the scattered sound at an angle θ to the direction of the incident wave with wavenumber k and intensity I_i is given by

$$I_s = \frac{I_i k^4 a^6}{9} \left(\frac{K_e - K}{K} + \frac{3\rho_e - 3\rho}{2\rho_e - \rho} \cos(\theta) \right)^2 \qquad (1.13)$$

where K and K_e are the compressibilities of the medium and the sphere respectively, and ρ and ρ_e are the densities of the medium and the sphere respectively. It is not realistic to consider the medium to be non-viscous in most biological situations. The above expression has been extended by Ahuja (1972) for a sphere suspended in a medium with viscosity ν_m:

$$I_s = \frac{I_i k^4 a^6}{9} \left[\frac{K_e - K}{K} + \frac{3E}{2} \left\{ \frac{\left(\frac{\rho_e - \rho}{\rho} \right)^2}{s^2 + \left(\frac{\rho_e}{\rho} + \tau \right)^2} \right\}^{\frac{1}{2}} \cos(\theta) \right]^2 \qquad (1.14)$$

where

$$E = 1 + 3\frac{d}{a} + \frac{9}{2}\left(\frac{d}{a}\right)^2 + \frac{9}{2}\left(\frac{d}{a}\right)^3 + \frac{9}{4}\left(\frac{d}{a}\right)^4$$

$$d = \left(\frac{2\nu_m}{\rho\omega}\right)^{\frac{1}{2}}$$

$$\tau = \frac{1}{2} + \frac{9}{4}\left(\frac{d}{a}\right)$$

$$s = \frac{9}{4}\left(\frac{d}{a}\right)\left(1 + \frac{d}{a}\right) .$$

The above equations also apply to a non spherical scatterer of volume $4\Pi a^3/3$ all of whose dimensions are much less than the wavelength (cf. Reid, 1976).

Many tissues, such as muscle, are made up of networks of fibres. It is relevant therefore to consider the scattering of sound from cylindrical objects. Morse and Ingard (1968) derive the equation for the intensity I_s of a wave scattered off a cylinder of radius a much less than the wavelength as

$$I_s = \frac{I_i \pi k^3 a^4 (1 - 2\cos(\theta))}{8r} \qquad (1.15)$$

where the scattered wave is observed at a distance r from the cylinder and at an angle θ to the direction of the incident wave.

Equations (1.13) to (1.15) show that the intensity of the wave scattered off a sphere varies as the fourth power of frequency and that off a cylinder as the third power.

1.4.4 Scattering by Distributions of Scatterers

'Grey scale' ultrasonic images of tissues reveal that within tissues there exist many closely spaced scattering centres. It is reasonable therefore to model tissues as being 'clouds' of subwavelength scatterers (cf. Twersky 1962a, 1962b, 1964 ; Aks and Vezzetti,1980; Vezzetti and Aks, 1980)

When sound traverses a cloud of scatterers, each object produces a scattered wave. These waves reinforce in some directions and interfere in others. This gives rise to coherent, incoherent and multiple scatterings. In soft tissues, the scattering from a single scatterer is small (cf. Gore and Leeman, 1977). Therefore it is usual to neglect multiple scattering.

The wave scattered from a cloud of subwavelength objects is the sum of the waves arising from each of the objects, each having a relative phase and amplitude determined by the particular object's size and position. If the spheres are regularly placed, the phases add up in certain directions to produce diffracted beams, as with the Bragg diffraction of X-rays from crystals. The maxima of these diffracted beams are found at angles θ to the direction of the wave incident on the cloud is satisfied by

$$\sin(\theta) = \frac{n\lambda}{2d} \qquad (1.16)$$

where n is an integer and d is the separation of the scatterers. However, the objects scattering the sound waves are often found to be randomly distributed. In this case little reinforcement occurs except in the direction of the incident wave.

Consider now a region R containing randomly distributed subwavelength scatterers having a concentration of N/unit volume and whose separations are also less than the wavelength of an incident plane wave of wavenumber k. Let the nth scatterer have a radius a_n, a compressibility K_n and a density ρ_n, the supporting medium has a compressibility K_o and a density ρ_o. In the forward direction, coherent scattering modifies the incident wave as though it were traversing a region of constant density ρ_R and compressibility K_R given by

$$\rho_R = \frac{1}{\rho_o} + \sum_{n=1}^{N} \frac{4}{3}\pi a_n^3 \left(\frac{1}{\rho_n} - \frac{1}{\rho_o}\right)^{-1} \qquad (1.17)$$

$$K_R = K_o + \sum_{n=1}^{N} \frac{4}{3}\pi a_n^3 (K_n - K_o) \qquad (1.18)$$

(Morse and Ingard, 1968).

Incoherent scattering is observed due to the variation in density and compressibility of the scatterers about the average values of ρ_R and K_R. The nth scatterer behaves like a scatterer of density ρ_n and compressibility K_n in a medium of density ρ_R and compressibility K_R. It can be shown (Morse and Ingard, 1968) that the ratio of the incoherent scattered intensity I_s to the incident wave intensity I_i is

$$\frac{I_s}{I_i} = NV \frac{\sqrt{2\pi}}{9} \frac{k_R^4 a^6}{r^2} \left| \gamma_K + \gamma_\rho \cos(\theta) \right|^2 \left\{ \frac{1}{8} k_R^2 a^2 \sin\left(\frac{\theta}{2}\right) \right\}$$

$$\cdot \exp\left\{-2k_R^2 a^2 \sin^2\left(\frac{\theta}{2}\right)\right\} \qquad (1.19)$$

where a is the mean radius of the spheres, γ_K is the mean value of $(K_n - K_o)/K_o$, γ_ρ is the mean value of $3(\rho_n - \rho_o)/(2\rho_n + \rho_o)$ and k_R is the wavenumber of the incident wave in the region R.

If it is assumed that the scatterers in R scatter sound independently and that each wavelet does not interfere with any other so that the scattered intensities merely add, the ratio of the intensity of the scattered wave to that of the incident wave is

$$\left(\frac{I_s}{I_i}\right)_o \simeq \frac{1}{9} NV \frac{k_o^4 a^6}{r^2} \left| \gamma_K + \gamma_\rho \cos(\theta) \right|^2 \qquad (1.20)$$

By comparing (1.19) and (1.20) it can be seen that interference between the wavelets modifies the angular distribution of the scattered wave. It is reduced in the forward and augmented in the side and backward directions.

Twersky (1962a, 1962b, 1962c, 1964), Beard et al., (1967) and Shung et al., (1976) have estimated the magnitude of backscattering from dense clouds. That is, from distributions where the separations of the scatterers is so small in comparison to their dimensions that they can no longer be considered to be totally random. Two heuristic approximations were suggested: the 'two phase' system and the 'hole' approach. in the two phase system each scatterer is considered to move totally randomly as does a molecule in a gas or to be held in a rigid structure as is a molecule in a crystal. Only those scatterers in the random phase contribute to incoherent scattering. In the 'hole' approach, scattering is considered to occur at the cavity sites (i.e. by the space not occupied by the medium). In effect, the scatterers become the medium, and the medium becomes the scattering source.

All soft tissues have very similar densities. Under the approximation that the scatterer density ρ_n is similar to the medium density ρ_o the ratio of the backscattered intensity to that of the incident intensity in sparse concentrations can be shown to be

$$I_s = I_i \pi k^4 a^3 W_o \left(\left| \frac{K_e - K_o}{K_o} \right| + \left| \frac{\rho_e - \rho_o}{\rho_e} \right| \right)^2 \qquad (1.21)$$

where W_o, K_e and ρ_e are the volume concentration, compressibility and density

respectively of the scatterers. Then, using the 'hole' approach, the backscattered intensity, in very dense concentrations such that $W_o \simeq 1$, is given by

$$I_s = I_i \frac{k^4 a^3}{12\pi} (1 - W_o) \left(\left| \frac{K_e - K_o}{K_o} \right| + \left| \frac{\rho_e - \rho_o}{\rho_e} \right| \right)^2 . \qquad (1.22)$$

However, if the scatterers are rigid, then their volume concentration cannot approach unity. For example, if the scatterers are spheres, then the maximum volume concentration is only 0.64. Beard et al., (1967) assumed that the volume V_h of a hole at the maximum realisable concentration of scatterers can be expressed as

$$V_h = V_o(1 - bW_o) \qquad (1.23)$$

where V_o is the volume of each scatterer and b is a 'fitting constant'. The intensity of the backscattered wave can then be expressed as

$$I_s = I_i \frac{k^4 a^3}{12\pi} W_o(1 - W_o)(1 - bW_o) \left(\left| \frac{K_e - K_o}{(1 - W_o)K_e - K_o W_o} \right| + \left| \frac{\rho_e - \rho_o}{\rho_e} \right| \right)^2 . \qquad (1.24)$$

1.4.5 The Scattering of Ultrasound by Blood

Blood is a suspension of cells in a liquid called plasma. There are three major types of cell in blood: red blood cells, white blood cells, and platelets. By far the most numerous are the red blood cells. They are elastic biconcave disks with an average diameter of 7 μm and an average thickness of 2 μm. The percentage fraction by volume which the cells occupy in a sample of blood is called the haematocrit. Normally this is about 45%.

It has been demonstrated that the red blood cells are responsible for the scattering of medical frequency ultrasound by blood (Reid et al., 1969). Exactly which part of the red blood cell is responsible for scattering has not been precisely identified. Reid (1976) has found that a suspension of red blood cell membranes has almost the same scattering cross-section as an equivalent suspension of intact red cells. This suggests that the membrane itself may be the primary scattering source. Some important acoustic properties

of intact red blood cells are presented in Table 1.4, (Urick, 1947; Carstensen et al., 1953; Platt, 1953).

Table 1.4 Acoustically significant properties of blood

Material	Density ρ gm/cm^3	Adiabatic Compressibility 10^{-12} $cm^2/dyne$ (at 20°C)
Water	0.998	46.1
Plasma	1.021	40.9
Red blood cell	1.092	34.1

Red blood cells move in a more or less random manner through the plasma at low haematocrits. At 45% haematocrit the cells are separated by about only one tenth of a cell diameter (Shung et al., 1977). At haematocrits above 58% the cells touch each other and begin to deform. At such high haematocrits the blood resembles a crystalline solid (Kol'tsova and Mikhailov, 1970).

The scattering of ultrasound by blood has been studied extensively (Sigelman and Reid, 1972; Shung et al., 1976, 1977; Reid, 1976). In their experiements these authors irradiated samples of blood with short (4 μsec) bursts of monochromatic ultrasound in the frequency range 5-15 MHz.

The intensity of ultrasound backscattered by blood varies as the fourth power of frequency (Shung et al., 1976). This dependence has been observed at all haematocrits. This is predicted by (1.19) to (1.24).

The intensity of the backscattered ultrasound at any one frequency is dependent on the haematocrit. Up to haematocrits of approximately 8% the backscattered intensity is found to increase linearly with increasing haematocrit (Shung et al., 1976). This is predicted by Morse and Ingard's (1968) equations for scattering from clouds of random scatterers (cf. 1.19, 1.20). Above 8% the scatterers can no longer be considered independent. The intensity of the backscattered wave is maximum at haematocrits of 26%. It then decreases with increasing haematocrit. Shung et al., (1976) explains this phenomenon in terms of Twersky (1962a, 1962b, 1964) and Beard's (1967) 'two phase' and 'hole' models. They report excellent agreement between the measured backscattering and that predicted using the models.

Shung et al., (1977) report an investigation of the angular dependence of the scattering of ultrasound by blood at low haematocrit levels. They confirm that, assuming the red blood cells to be scatterers, the scattering has an angular dependence similar to that predicted by Ahuja (1972) for a subwavelength particle in a viscous medium (1.14). Only the density

difference between the plasma and the blood gives rise to the angular variation. Hence it is possible to separate scattering into its compressibility and density contributions. Thus these parameters for a sample of blood cells may be determined by measuring the angular dependence of the scattered wave. It is expected that the values of these parameters may be correlated with different pathological conditions (Shung et al., 1977).

The amplitude of a wave backscattered by a sample of blood is observed to fluctuate with time. The fluctuations can be attributed to the random movement of the cells due to convection within the sample. Using a statistical diffraction theory, Atkinson and Berry (1974) have calculated the rate at which the fluctuations occur in terms of the spatial and temporal dimensions of incident ultrasonic pulses. Their calculations are in agreement with the observed fluctuation rates.

A statistical approach has also been taken by Angelsen (1980) to describe the observed fluctuations in backscattered wave intensity due to red blood cell concentrations changing by the diffusion of the cells in the blood. He explains changes in the scattered wave in terms of the diffusion velocity of the cells.

1.4.6 The Scattering of Ultrasound by Cardiac Muscle

Cardiac muscle is composed of fibres approximately 10-30 μm in diameter. They are composed of separate cellular units joined end to end by intercalated disks, (Kadaba et al., 1980). The fibres do not have simple cylindrical shapes. They bifurcate and connect with adjacent fibres to form a three-dimensional network. Hence there is no single predominant fibre orientation. The fibres are separated by connective tissues and small blood vessels.

Backscattering experiments show that the amplitude of the scattered ultrasound is independent of the orientation of the sample to the incident wave (Lele, 1976; Kadaba et al., 1980). This is consistent with the diverse fibre orientation found in the myocardium.

Shung and Reid (1977) and Kadaba et al., (1980) report that the intensity of ultrasound backscattered from a sample of myocardial tissue has an $f^{3.3}$ dependency where f is the frequency of the incident wave. Cylinders of infinite length and subwavelength diameter are known to scatter sound with an f^3 dependency (Morse and Ingard, 1968). Because their experiments employ ultrasonic wavelengths in the range 150-750 μm, these authors postulate that

the primary source of backscattering in normal tissue may be the myocardial fibres.

Mimbs et al., (1980, 1981) and Kadaba et al., (1980) have measured the effect of differences between the backscattered intensities of normal and infarcted tissue. When a region of the myocardium suffers an infarct, the affected tissue fibroses (scars) and the content of elastin and collagen increases dramatically. The backscattered intensity from infarcted myocardium is much greater than that of normal tissue. This has been attributed to the increase in collagen content in the infarcted regions. Mimbs et al., (1980) have treated infarcted hearts chemically to break down the collagen fibres into smaller units. These are still units of collagen however. The level of backscatter is then seen to reduce in the infarcted regions. Therefore it appears that intact collagen is the primary source of scatter from within infarcted myocardium.

1.4.7 The Scattering of Ultrasound by Liver

Liver tissue shows a high degree of regularity in its structure. It is composed of large groups of cells called lobules. Between these are found lobular canals through which flow bile and blood. The connective tissue forming the lobular canal network is composed of the proteins elastin and collagen. The acoustic impedances of elastin and collagen are three or four orders of magnitude greater than those of other tissue constituents (Fields and Dunn, 1973). Nicholas (1976) comments that the network of lobular canals or the actual lobular structure itself may be responsible for scattering. In support of this theory Mountford and Wells (1972a, 1972b) find an increased ultrasonic backscattering in people with cirrhotic liver disease. This is also consistent with the results of investigations by Freese and Lyons (1973, 1979), who find a high correlation between ultrasonic backscattering coefficient and the protein content of excised livers. However, a high correlation is also found between the backscatter coefficient and the lipid (or fat) content in patients with fatty liver disease. This suggests that there may be more than one source of scattering within liver tissue.

The backscattering coefficient in liver tissue has been found to be proportional to $f^{2.1}$ (Kadaba et al., 1980) or $f^{2.2}$ (Chivers and Hill, 1975; Nicholas, 1976) where f is the frequency of the incident wave. These results have been obtained for frequencies in the range 1-5 MHz. Chernov (1960) shows that for scatterers whose dimensions are similar to one wavelength, the

backscattered intensity varies as the square of the frequency of the incident wave. It appears that the mean scatterer dimension in liver tissue may therefore be approximately 1mm (Nicholas, 1976).

Nicholas and Hill (1975) and Nicholas (1976) report experiments to determine the angular dependence of scattering. They report a phenomenon similar to that observed in Bragg X-ray crystallography which suggests a characteristic structural pattern within the tissue. Similar work has been reported by Waag and Lerner (1973), Waag et al., (1973), de Billy and Quentin (1973) and Braun and Robinson (1980).

1.4.8 Spectral Studies of Ultrasonic Backscatter

It is obvious, even from the earliest ultrasonic images of tissues (cf. Wild and Reid, 1952), that small but appreciable echoes may be observed from sources within tissues. Such small scale echoes can be readily seen in images obtained using modern 'grey scale' ultrasonic imaging equipment (cf. Kossoff and Garrett, 1973; Taylor et al., 1973). If a sufficiently short pulse of sound was to be transmitted into a tissue sample, it would be reasonable to expect each peak in the received echo train to correspond to a single scatterer. Commercial diagnostic imaging devices cannot produce such a pulse. The echo trains received by commercial systems is dependent on the spatial and temporal characteristics of their transmitted pulses. Gore and Leeman (1977) predict that scattering is observed from sources within tissue when their spatial separation frequency is in the range 2-50 cycles/mm. Diagnosing disease from the texture of the scatter seen in two-dimensional images is common clinical practice (McDicken, 1981).

An alternative method of analysing backscatter has been investigated by Chivers and Hill (1975). They irradiate samples of tissues with broadband ultrasonic pulses. An 8 μsec pulse of the backscattered wavetrain is gated through to a spectrum analyser. It is observed that each type of tissue appears to have its own characteristic spectrum.

Similar studies have been reported by Lizzi et al., (1976) and Lizzi and Elbaum (1979). They have catalogued the spectra of backscattered echoes from various eye tissues according to the type of disease. They claim that it is possible to distinguish between several different types of diseased tissues on the basis of the spectra. It is reasonable to expect that such methods could be most successfully applied to ocular diseases, as the eye is a superficial organ. If the technique was to be used to analyse scatter from

deeper organs, such as the liver, corrections would have to be made to the spectra to account for the effects of intervening tissues.

1.5 ATTENUATION OF ULTRASONIC WAVES BY TISSUES

Attenuation of an ultrasonic wave traversing a medium is described by an exponential law (Wells, 1977; Parry and Chivers, 1979), that is

$$A = A_o \exp(-\alpha x) \qquad (1.25)$$

where A is the amplitude of an acoustic wave of initial amplitude A_o after it has travelled a distance x into a medium having an attenuation coefficient α. The attenuation coefficient is a function of frequency for all tissues. This dependence for several tissues is illustrated in Figure 1.2. A comprehensive review of attenuation data in the literature has been published by Parry and Chivers (1979).

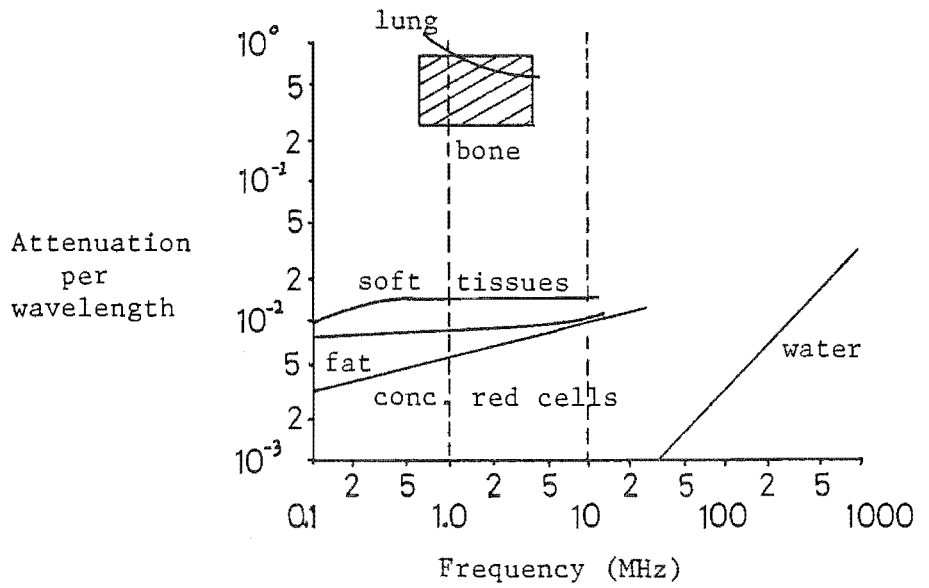

Figure 1.2 Graph of attenuation per wavelength vs. frequency for mammilian tissues. The region between the dashed vertical lines represents the diagnostic frequency region.

On the basis of the magnitude of the coefficients, the tissues can be grouped into several categories. These are water, red blood cells, fat, soft tissues, lung and bone. The range of the attenuation coefficients reported for each of these tissues is large (Carstensen, 1979). The variation is due to normal biological variability, inhomogeneous tissue samples, the method of measurement, the preservative process to which the samples have been subjected, the time after excision and the temperature at which the attenuation is measured. Also, much of the data reported is for species other than man (Parry and Chivers, 1979).

It is common practice to describe the attenuation coefficient of each tissue in terms of a power law of the form

$$\alpha = af^b \tag{1.26}$$

where a and b are characteristics of the tissue. For fat and soft tissues b is usually very close to unity, while for blood cells it is close to 1.2. Bone has a quadratic dependence up to 3.5 MHz, after which a lower power dependence is apparent. Water follows a quadratic law at all frequencies. Water is much less attenuating than fat, blood and soft tissues. Lung and bone are the most highly attenuating. Attenuation of ultrasound by tissues is due to two factors: absorption and scattering. Absorption is the conversion of acoustic energy into thermal energy. Scattering is the removal of some of the energy of an acoustic beam by reradiating it from regions where the acoustic parameters of the media change. In the literature, absorption is often confused with attenuation (Wells, 1977). Losses due to scattering within tissues are believed to be small (O'Donnell and Miller, 1979). This is because the acoustic properties of the scatterers do not differ significantly from the rest of the tissues. Therefore attenuation is due almost entirely to absorption. The mechanisms by which absorption occurs are not well understood (Carstensen, 1979). Several of the mechanisms which have been suggested are now described. It is unlikely that all of these mechanisms are equally applicable to the different tissue types.

1.5.1 Classical Absorption in Fluids

Ultrasonic absorption in fluids is due to frictional forces opposing the periodic motion of the particles of the fluid induced by an acoustic wave (Wells, 1977). The absorption coefficient α is

$$\alpha = \frac{2\omega^2 \eta_s}{3\rho_o c^3} \qquad (1.27)$$

where ω is the angular frequency of the acoustic wave travelling with velocity c in a medium of density ρ_o and a shear viscosity coefficient η_s (Dunn, 1976). Classical absorption indicates that the attenuation coefficient varies as the square of the frequency. This is not seen in biological tissues in the 1-10 MHz frequency range. Therefore, somewhat surprisingly perhaps, it cannot be considered to be an important mechanism. It may however be significant at frequencies above 1000 MHz.

1.5.2 Relaxation Mechanism

This is believed to be the most important mechanism (Wells, 1977). In an acoustic medium, energy may be considered to be stored in various 'compartments' which may be physical or chemical energy states such as translational molecular motion states (cf. Carstensen and Schwan, 1959; Pauly and Schwan, 1971). All of the compartments are coupled to each other so that energy may be shared among them. There are finite time constants associated with energy transfers between the compartments. When an acoustic wave passes through the medium, compressional energy is transfered from the wave into the compartments. Most energy is transfered to those with the smallest time constants. Energy is then shared with the other compartments. During the decompression half cycle of the acoustic wave, energy is transfered back from the compartments. The energy stored in the compartments with the short time constants returns to the wave almost immediately. That stored in compartments with time constants almost equal to the period of the wave returns out of phase and is absorbed. Little energy is stored in the compartments with longer time constants. Therefore there is little loss of energy via these compartments.

The absorption coefficients of soft tissues usually decrease with increasing temperature (cf. Gammell et al., 1979). This has been reported for blood (Carstensen and Schwan, 1959a), brain (Kremkau et al., 1979) and myocardium (O'Donnell et al., 1979). Carstensen (1979) has shown that this can be predicted for tissues whose absorption coefficient increases with

temperature by assuming absorption to be caused by relaxation mechanisms. Absorption by bone rises with increasing temperature (Kishimoto, 1959). This is also predicted by relaxation mechanisms because absorption by bone decreases with increasing frequency.

Absorption by central nervous tissue is more complicated as Dunn and Brady (1973, 1974) have reported for experiments on mice. It is found to both increase and decrease with temperature depending on the frequency of ultrasound used. It appears that this cannot be explained in terms of relaxation mechanisms.

If a single relaxation mechanism has a time constant τ, then the attenuation per wavelength α_λ, is (Markham et al., 1951)

$$\alpha_\lambda = \pi \frac{c^2}{c_o^2} \left(1 - \frac{c_o^2}{c_\infty^2}\right) \frac{\omega\tau}{1 + (\omega\tau)^2} \qquad (1.28)$$

where c is the velocity of a wave with angular frequency ω and c_o, c_∞ are the velocities at the wave at very low and very high frequencies respectively. This relation has been shown to be consistent with the observed absorption of ultrasound in haemoglobin (Carstensen and Schwan, 1959a).

Relaxation mechanisms also requires that dispersion occurs. The magnitude of the dispersion observed in soft tissues and solutions of biological macromolecules is consistent with that predicted by relaxation theory (Carstensen, 1979).

The approximately linear dependence of absorption coefficient with frequency cannot be explained by a single relaxation process model. The shape of the curve described by (1.28) is shown in Figure 1.3.

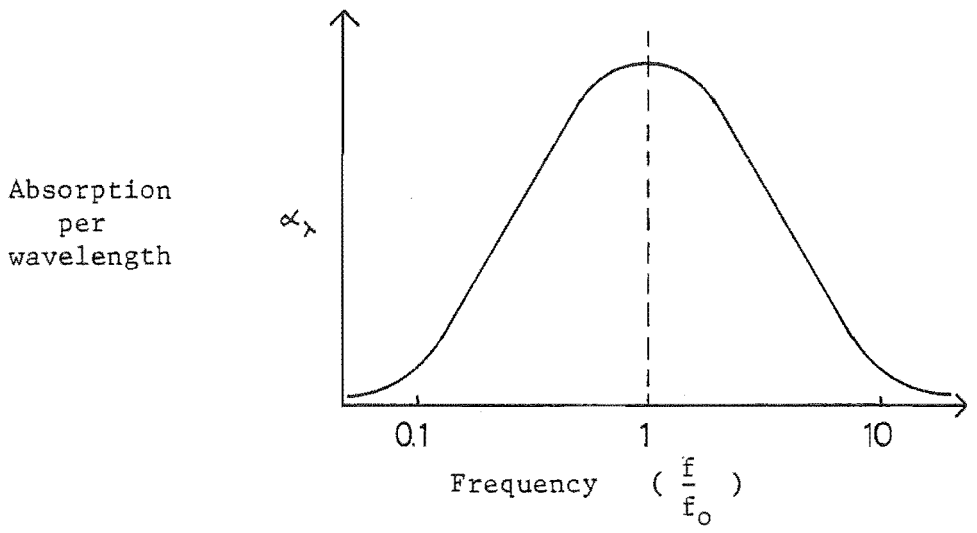

Figure 1.3 The dependence of absorption per wavelength on frequency for a single relaxation process.

Absorption is greatest when the time constant of the relaxation process is equal to the period of the ultrasonic wave. If absorption is due to several relaxation processes, then an almost linear dependence of absorption coefficient can be achieved over a wide range of frequencies. Suppose several relaxation processes occur at different frequencies as is illustrated in Figure 1.4. The overall absorption at any frequency is due to a combination of various relaxation processes. In the frequency range f_1 to f_4 the absorption coefficient is observed to have an almost linear dependence on frequency.

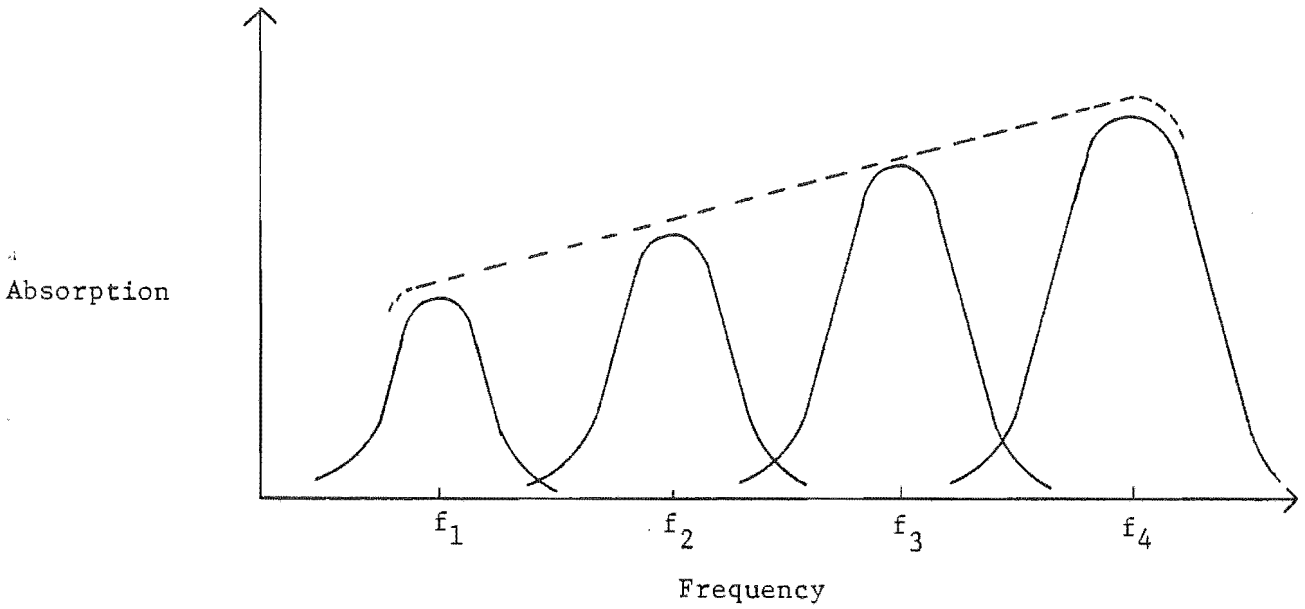

Figure 1.4 Illustration of how several relaxation processes at different frequencies can combine to produce an apparently linear dependence of absorption coefficient on frequency.

1.5.3 Relative Motion

Tissues can be considered to consist of small particles suspended in fluid media. For example, within a cell there exist many particles such as large protein molecules, which inhabit a liquid medium called the cytoplasm. When an acoustic wave passes through the fluid, the particles try to follow the motion of the medium. How well they manage to achieve this depends on the relative densities and viscosities of the particles and the fluid and on the frequency of the wave. Often the particles do not closely follow the motion of the fluid, and the particles move appreciably relative to the medium. This causes absorption by viscous drag. It has been demonstrated that relative motion between the very large molecules (macromolecules) found in cells and the cytoplasm may account for much of the absorption of ultrasound by heart muscle and skin and may also account for absorption by blood cells (O'Donnell and Miller, 1979). Absorption of ultrasound by blood may also be accounted for by considering the relative motion of red blood cells and plasma (Carstensen and Schwan, 1959b).

1.5.4 Thermal Losses

If tissues are considered to be composed of particles suspended in

fluid media, absorption of ultrasound also occurs from the thermal losses. The magnitude of such losses is dependent on the relative heat capacities, thermal conductivities and coefficients of thermal expansion of the particles and the media and on the frequency of the wave. O'Donnell and Miller (1979) have estimated the amount of acoustic energy absorption which can be attributed to thermal losses by subcellular particles in red blood cells, heart muscle and skin. They conclude that losses by such mechanisms are small. Approximately 100 times more energy is absorbed by relative motion losses.

1.5.5 Molecular Interaction

This is a poorly defined concept not based on any postulated mechanism. Kremkau and Carstensen (1972) have demonstrated that concentrated solutions of haemoglobin have a much greater absorption per molecule than do dilute solutions. Other experiments (cf. Ponder, 1945; Kremkau and Carstensen, 1973) show that if the molecular structure of haemoglobin is chemically altered, then a significant increase in absorption can result. It has been suggested that these observations may be explained in terms of interactions between macromolecules of haemoglobin (Carstensen, 1979).

1.5.6 Absorption by Macromolecules

Macromolecules are the structural components of living matter. They are polymers of smaller molecules, consisting of amino acids linked together in special ordered forms. The most important are nucleic acids, the proteins and some carbohydrates such as cellulose and starch. There is evidence that absorption in soft tissues and blood may be due to the interaction of ultrasound with the macromolecules.

Pauly and Schwan (1971) found that there is little difference between the magnitude of the absorption by whole liver and by that which has been homogenised to a subcellular level. This demonstrates that neither the ordered structure of liver tissue nor the structure of individual liver cells has any great influence on ultrasonic absorption.

It has also been found that the absorption coefficients of suspensions of red blood cells and haemoglobin solutions of equivalent concentrations are almost identical (Carstensen, 1979). Haemoglobin is the most plentiful protein in red blood cells. The slightly larger absorption by intact cells may be due to relative motion mechanisms between the cells and the medium which they inhabit (Carstensen and Schwan, 1959b).

Further evidence of macromolecular absorption is provided by the experiments of Kremkau and Carstensen (1972) and O'Brien and Dunn (1971). They demonstrate that a 10% solution of the amino acids which make up haemoglobin has a much smaller specific absorption (i.e. absorption per gram solute) than do solutions of intact haemoglobin. They also report that after chemically treating haemoglobin to break it down into smaller units solutions of smaller specific absorption result. This has been shown to be true for other proteins, nucleic acids and polysacchorides (cf. Kremkau and Carstensen, 1972; Johnson et al., 1979).

The results of these studies indicate that upon successive fractionation of the tissue macro and microstructure, no great decrease in absorption is observed until the macromolecules are broken down. This suggests that absorption in some soft tissues occurs mostly at the macromolecular level.

CHAPTER 2

MEDICAL ULTRASONIC IMAGING

2.1 INTRODUCTION

Medical ultrasonic imaging systems are usually designed to image internal organs by one of two techniques. These are the pulse-echo method and the transmission method. Details of these techniques are discussed in this chapter.

By far the most popular technique is the pulse-echo method pioneered by Wild (1950 ; Wild and Reid , 1952). With this technique, a series of pulses of very high frequency sound are transmitted into a patient. An image is then formed from the echoes returning from organs within the patient. The techniques of forming images using the pulse-echo method are reviewed in §2.2. Technical details of pulse-echo imaging systems are discussed in §2.3.

The second method, transmission imaging is similar to ordinary shadow X-ray imaging. A beam of ultrasound instead of X-rays is directed through a patient to create an 'ultrasonic attenuation shadowgram' of the patient's internal structure. This was the first medical ultrasonic imaging technique (Dussik et al., 1947). It has not proven to be popular and few such systems have been developed.

An obvious variation of transmission imaging is ultrasonic computed tomography. This technique is similar to X-ray computed tomography in that a map of the ultrasonic velocities or the ultrasonic attenuation coefficients within a patient are produced (Greenleaf et al., 1981; Bates and Dunlop, 1977; Whiting et al., 1981). Transmission imaging techniques are discussed in §2.4.

2.2 THE ECHO LOCATION PRINCIPLE

The echo location principle is the basis of medical pulse-echo imaging systems. The principle is illustrated in Figure 2.1. An ultrasonic probe is placed in contact with medium 1 and is directed towards the interface between medium 1 and medium 2. At a time $t = 0$ a pulse of ultrasound is emitted by the probe into medium 1 in which it travels with velocity v_1. At a time t_1 it impinges on the interface between medium 1 and medium 2. This interface is at a distance d_1 from the probe. At the interface, the acoustic impedance mismatch between medium 1 and medium 2 causes some of the

energy of the pulse to be reflected back to the probe while the rest is transmitted into medium 2. At a time $2t_1$ the reflected pulse is received back at the probe. If the value of v_1 is known then the distance d_1 to the interface from the probe is given simply by

$$d_1 = v_1 t_1 \qquad (2.1)$$

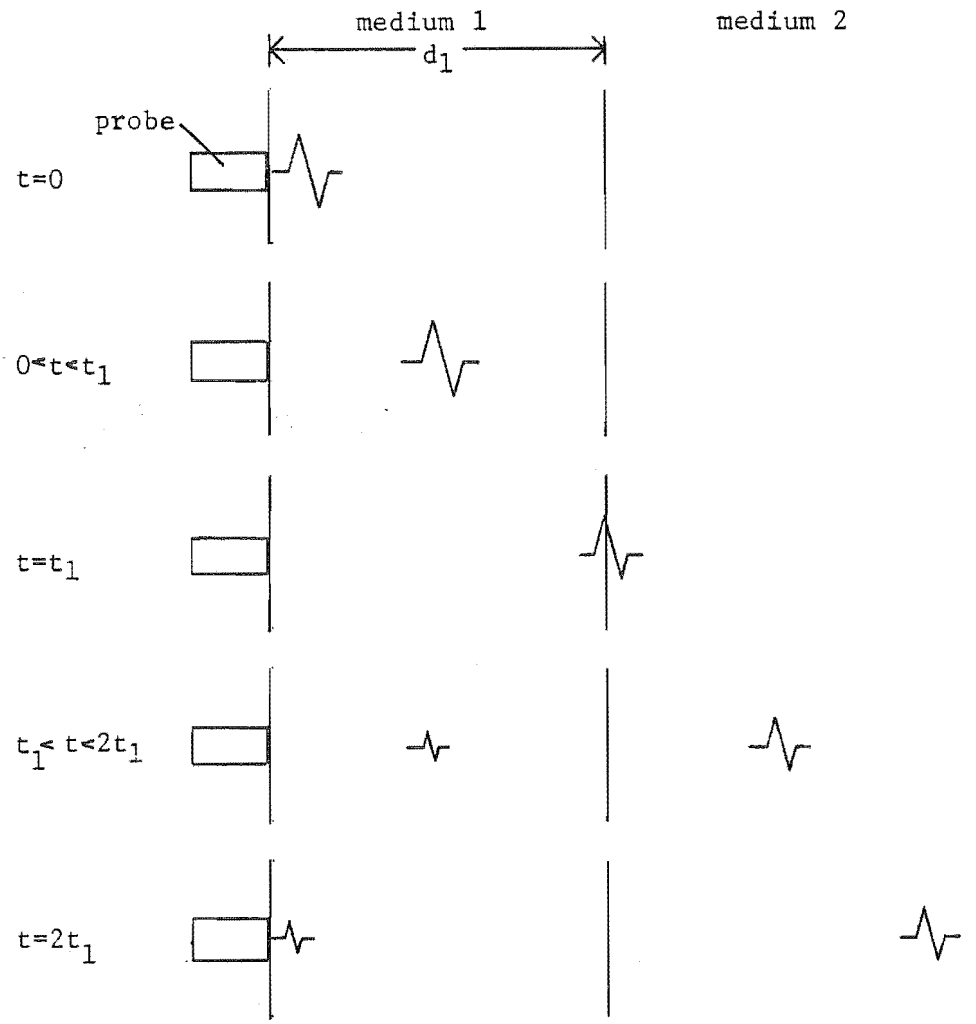

Figure 2.1 Principles of echo location

Hence the echo location (or the pulse-echo technique) provides a method of estimating distances to acoustic discontinuities within a region. In a clinical situation that region would be a part of a patient's anatomy which a clinician wishes to image. There are several methods of constructing images from such estimates of distances to acoustic discontinuities within a patient. These methods (or modes) are now discussed in turn.

2.2.1 The A-Mode Display

The amplitude modulated or 'A-mode' display is the simplest technique. It is illustrated in Figure 2.2.

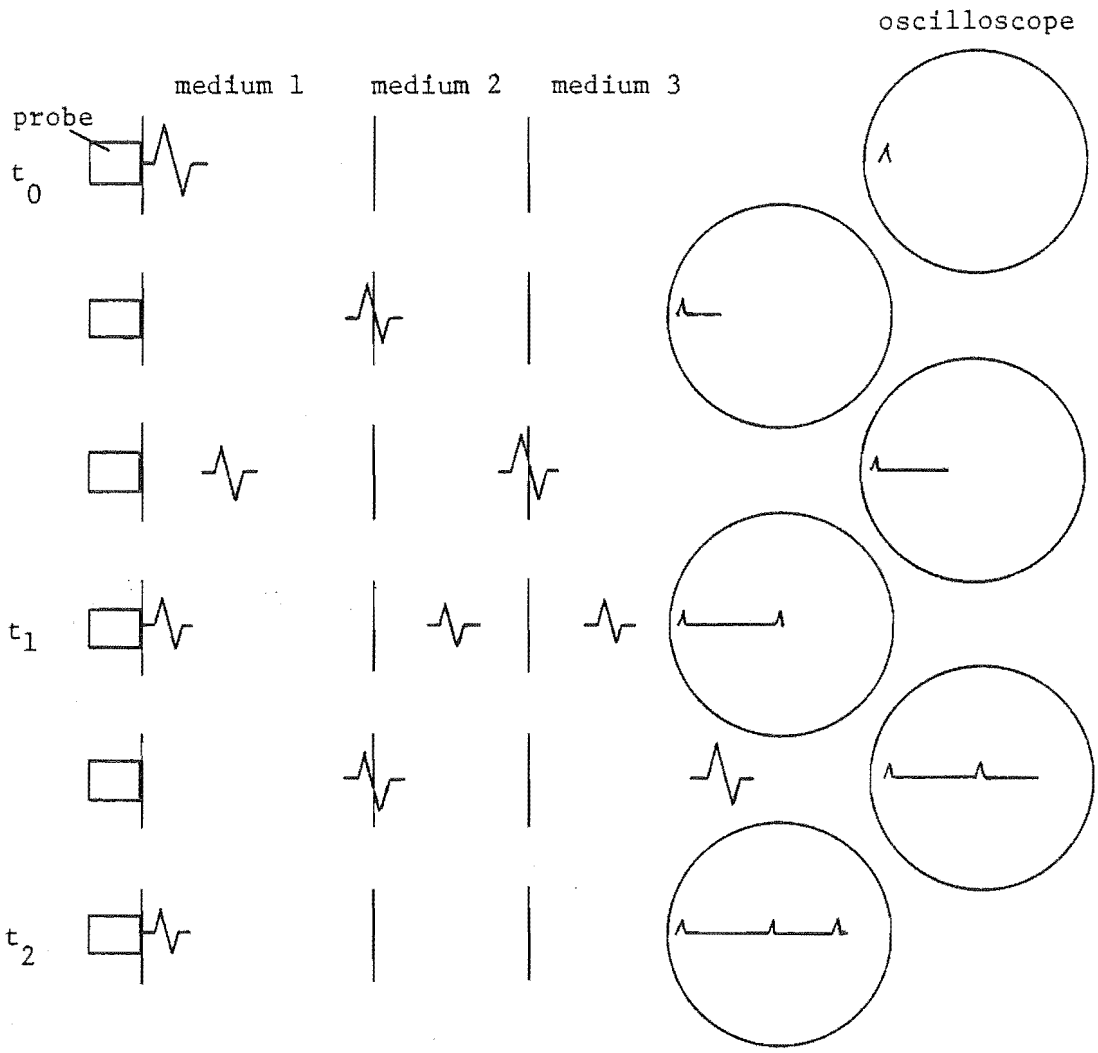

Figure 2.2. The generation of the A-mode display

The transducer probe is connected to an oscilloscope to display the envelope of the echoes which it receives. The oscilloscope's timebase is triggered at the same instant as the transducer is excited. On excitation, a deflection is displayed on the oscilloscope trace. Later, at times t_1 and t_2, echoes are received at the transducer. These are displayed as further deflections whose heights are proportional to the amplitudes of the echoes. The system is usually retriggered to refresh the display at a rate of about 1 KHz.

While this display reveals distances between organs within a body, it is unidimensional. Hence it reveals very little structural information concerning a patient's anatomy. Therefore its use has been restricted to

simple studies such as brain midline localisation or measurements of the length of the optic axis of the eye. Such information is easily abstracted from the A-scan (Robinson et al.,1970).

2.2.2 The B-Mode Display and the B Scan

Consider now a cross sectional slice of a patient as depicted in Figure 2.3(a)

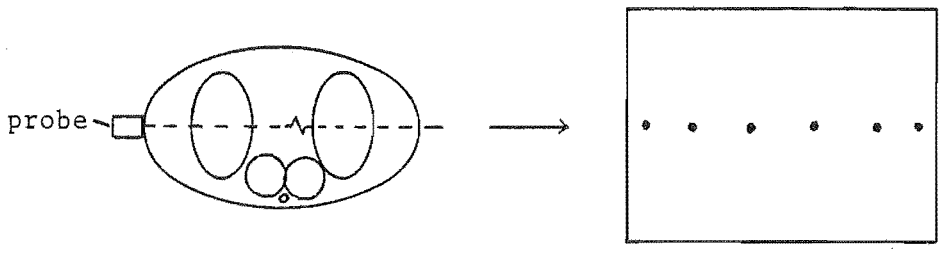

Figure 2.3 Formation of the B-mode display

It is usual to employ a transducer excitation and reception system similar to that used for the A-mode display. However, further circuitry is employed to display the detected echoes as a series of dots on a screen. The brightness of the dots is ideally proportional to the amplitude of the received echoes. Hence this is called a 'brightness modulated' or B-mode display.

The position and direction of the transducer is usually electronically encoded. Therefore it is possible to determine the relative origins of echoes from within the patient. Hence the dots representing received echoes can be displayed on the screen according to their origins. As the transducer is moved around the patient, the beam sweeps through the patient's anatomy. The dots displayed with the beam in different positions combine to form an image of the patient's anatomy. This is illustrated in Figure 2.4.

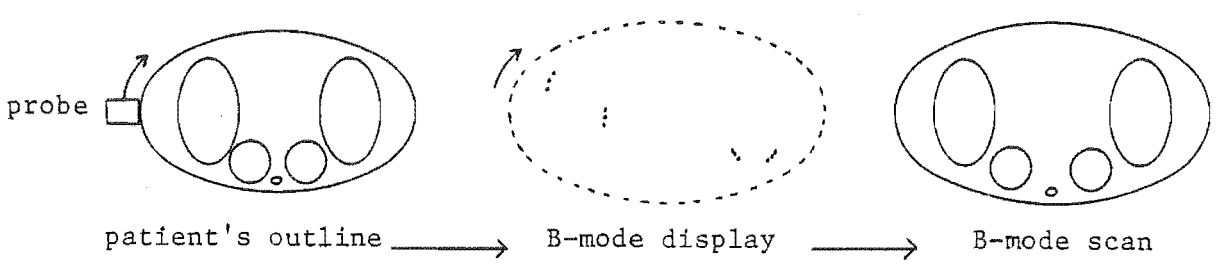

Figure 2.4 Formation of the B-mode scan

The resulting image is called a 'B-mode scan'. Such two-dimensional images are of great use and have found many applications in abdominal imaging.

2.3.3 The M-Mode Display and the M Scan

Not all organs within the human body are stationary. It is often desirable to study the motion of some organs such as the heart. Abnormal motion of such organs is often an indicator of disease. A useful method of displaying motion is illustrated in Figure 2.5.

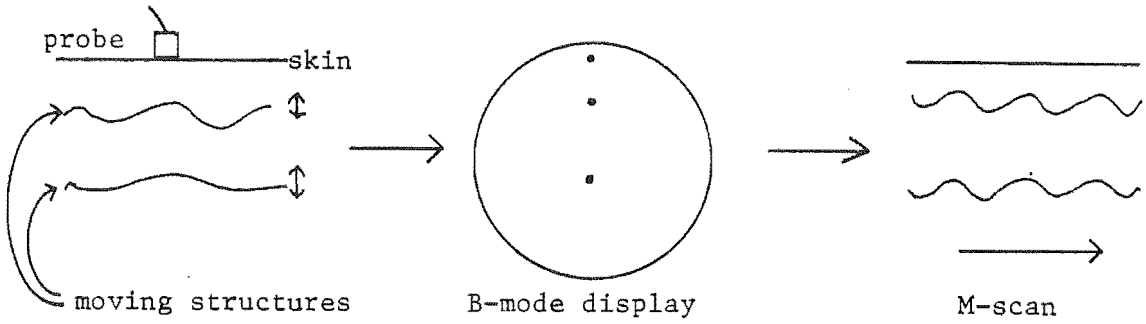

Figure 2.5 Formation of the M-mode display

A transducer probe is held against a patient. A B-mode display of structures in the path of the transducers beam is presented on a screen. The B-mode display is then swept across the screen. Any motion of the structures causes the B-mode display to change as it sweeps. The resulting image is called an M(motion) or TM (time-motion) scan. Often it is convenient to hold the B-mode display stationary, and to obtain a hand-copy by moving a strip of photographic paper past it.

Although M scans present motion information from only a single line into a patient, a clinician familiar with such scans can often readily recognise motion abnormalities in them.

2.2.4 The Real Time B Scan Display

While the M scan is a valuable tool for investigating structural motion, it is desirable to observe moving structures in real time on a two-dimensional display. This can be effected by arranging a transducer probe to scan its beam across the part of the patient's anatomy under investigation. The resulting B-mode scan is then displayed on a screen and the image is updated each time the beam rescans the patient.

The speed of sound in soft tissue is approximately 1500 m/sec. Since structures up to 15 cm from the transducer must be scanned, the highest frequency at which the transducer may be excited must often be no higher than 5 KHz. If a B-mode scan is to be updated even as slowly as 25 times per

second, each scan displays only 200 lines of data. Hence the information content of real-time B-scans is very limited.

Beam scanning can be effected by two methods. First, it can be done mechanically by physically moving the transducer probe, such as by wobbling it on its own axis. This makes the beam sweep through a sector. Various mechanical scanning systems have been developed, (cf. Kambe et al., 1977; Matzuk and Skolnick, 1978). Second, it can be done electronically by simultaneously pulsing adjacent members of a linear array of miniature transducers. The individual beams are combined to form a single narrow beam by introducing an appropriate delay between the pulsing of adjacent transducers. The direction of the beam is changed by altering the delay. This is covered in detail in §2.3.

2.2.5 With B-mode scanning it is not always possible to move the tranducer's beam in the plane which a clinician wishes to image. C-mode scanning is a technique which is occasionally employed to investigate structures at a constant depth within a patient. It is illustrated in Figure 2.6.

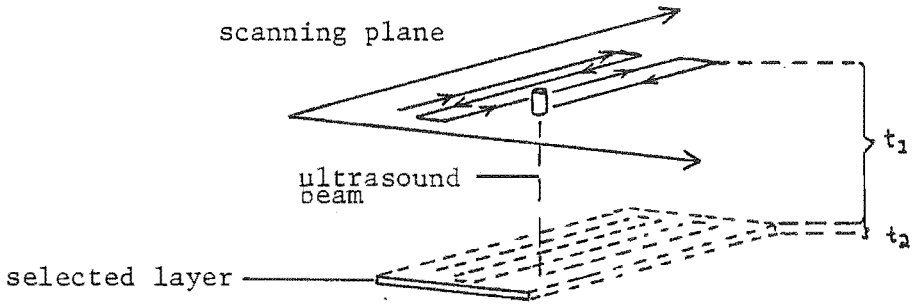

Figure 2.6 A basic C-scanning system

With this technique, a transducer is raster-scanned across a patient. The echoes from within a short interval of duration t_2, after a constant delay t_1, are stored and presented on a two-dimensional display. As the C-mode scan presents images in planes perpendicular to the transducer beam, it is possible to image in planes which are inaccessible with B-mode scanning.

Note that the C-mode is a two-dimensional version of the M-mode. With M-mode scanning only one point in the plane is imaged each time the transducer

is excited compared to many points with B-mode scanning. Therefore it takes considerably longer to perform a C-mode scan than it does a B-mode scan.

2.3 THE GENERALISED PULSE-ECHO IMAGING SYSTEM

A block diagram of a typical medical pulse-echo system is shown in Figure 2.7.

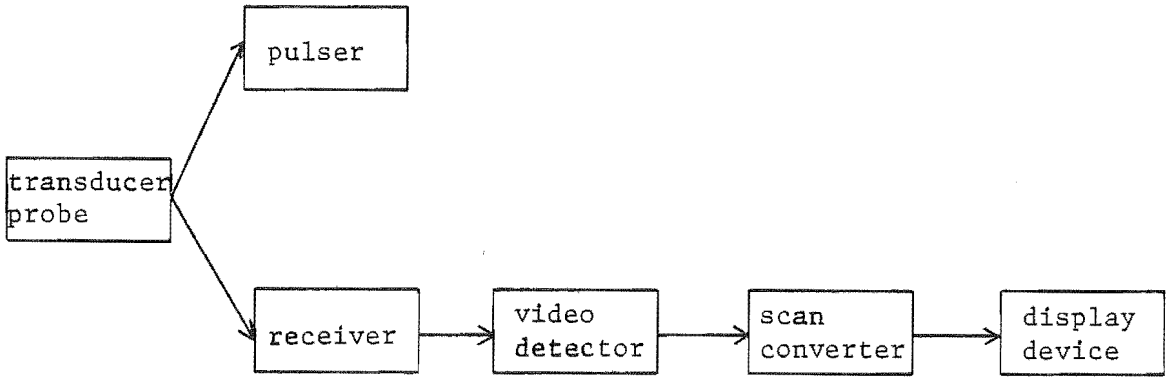

Figure 2.7 The major components of pulse echo imaging systems

The system components have the following functions:

i) transducer probe - to transmit an ultrasonic pulse and convert the received echoes into electrical signals

ii) pulser - to excite the transducer probe

iii) receiver - to receive and amplify electrical signals sent to it by the transducer probe

iv) video detector - to convert the bipolar echo signals passed to it by the receiver into a unipolar signal relative to echo amplitude

v) scan converter - to map echo signals into their correct positions in the resulting two-dimensional image

vi) display device - to present the resulting image to an observer.

Each of these components is discussed in more detail below.

2.3.1 Transducer Probes

Two types of probe are used in medical imaging: single element devices and multielement devices. At diagnostic frequencies, piezo-electric transducers are almost exclusively used due to their efficiency and ease of fabrication, especially when non-planar (eg. focussing) transducers are used.

i) Single Element Transducer Probes

The construction of a typical single element transducer probe

is shown in cross section in Figure 2.8

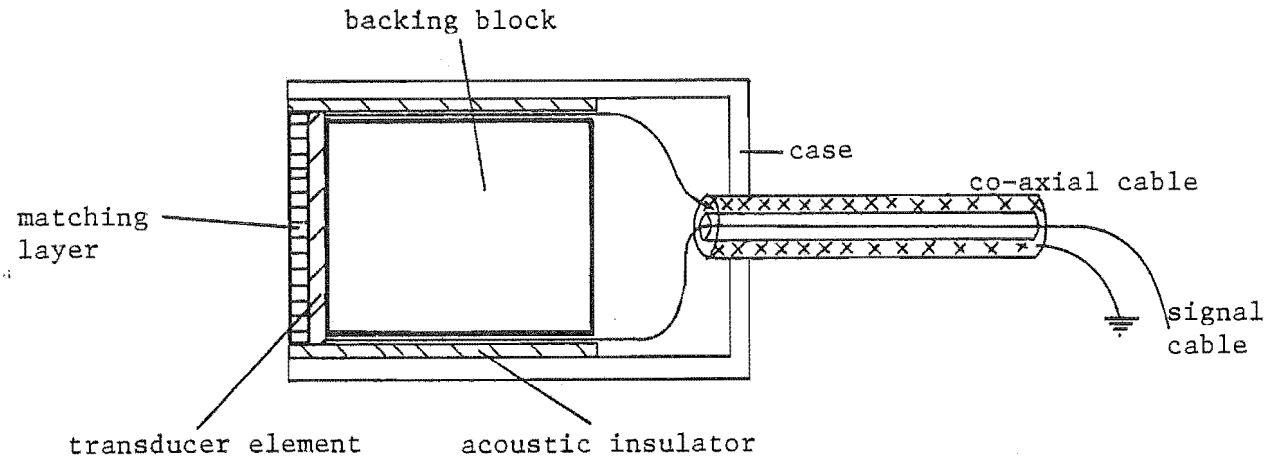

Figure 2.8 Construction of a piezo-electric single element transducer probe (Approx. 2-3 times real size)

The transducer element is a disc of piezoelectric material about one half-wavelength thick. Lead-zirconate-titanate (PZT) is the most popular material, although quartz and barium titanate are also used. PZT has a low electrical impedance, a moderate mechanical Q and is cheap. The matching layer is a plastic or epoxy based material about one quarter wavelength thick and of acoustic impedance $Z = (Z_{transducer}\ Z_{tissue})^{\frac{1}{2}}$. This matches the tissue loading to the transducer to allow almost complete coupling of all acoustic energy from the transducer into the patient. Behind the transducer is a backing block designed to have a similar acoustic impedance to that of the transducer. The backing block absorbs much of the energy transmitted into it by the back face of the transducer. This is often constructed of a mixture of araldite and tungsten powder. The entire assembly is mounted in a case from which it is acoustically and electrically isolated by a layer of rubber, nylon or PTFE. Acoustic insulation is necessary to prevent the case from ringing in response to acoustic transients. Excitation of the transducer is achieved electrically via the coaxial cable entering the back of the assembly. The same transducer is also used as a receiving element and the received signals are passed electrically back along the same cable (Wells, 1977, pp66-69).

Medical ultrasonic transducers are usually about 20 to 30 wavelengths in diameter. The transition between the Fresnel (near) zone and the Fraunhofer (far) zone of a transducer's beam therefore occurs between 400 and 900 wavelengths from it. Attenuation of the beam by tissue limits the maximum depth at which structures may be visualised to about 200 wavelengths.

Hence the echoes used for imaging come from structures within the near field of the transducer. In the near zone, the width of the beam is approximately the same as the transducer diameter, i.e. about 1 to 2 cm. Hence the lateral resolution of B scanning systems is also approximately 1 to 2 cm. It is desirable to reduce the bandwidth to increase the resolution. This can be achieved over part of the beam by focussing. The beam may be focussed either by mounting an acoustic lens in front of a planar transducer or by using a curved transducer element (Kossoff, 1979; O'Neill, 1949; Fry and Dunn, 1962). Focussing is achieved at the expense of broadening the beam at large distances from the transducer.

ii) Transducer Arrays

Transducer arrays are formed by mounting many small independent transducer elements in a line to form a probe of the type illustrated in Figure 2.9.

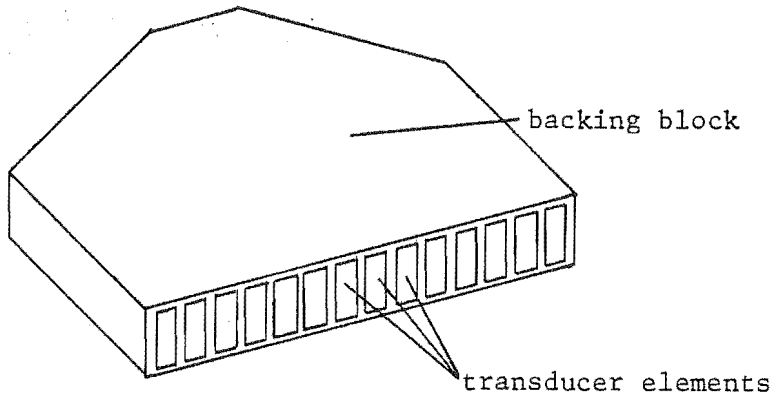

Figure 2.9 Representation of a transducer array

The array consists of a number of rectangular transducers about 1mm wide and 1 to 2 cm long mounted side by side on a backing block.

The transducer can be operated in 2 modes - as a linear scanner or as a phased array scanner. When operated as a linear scanner, the array simulates a single transducer moving across the patient. A single transducer element is excited at any one time. The one next to it is then excited, and so forth along the array so that it appears that a single beam is sweeping across the patient. Interfacing such an array to a television display is easily effected by associating each array element with a corresponding T.V. line (Ligtvoet et al., 1977). The raster scanning feature of the T.V. is used to present the image on the screen. This is illusted in Figure 2.10.

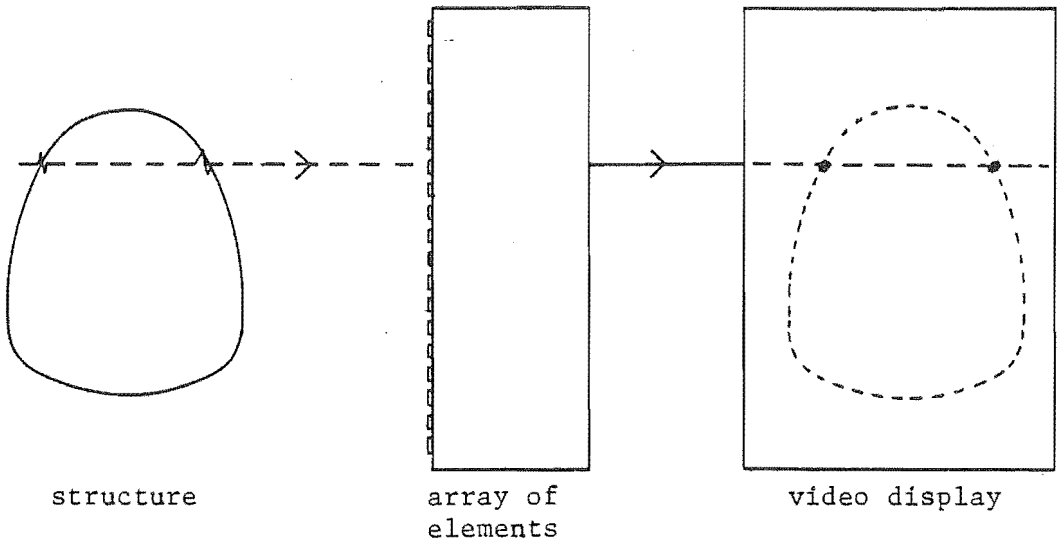

Figure 2.10 Simple display of a real-time B-mode image using a linear array

The width of each transducer element is often less than one wavelength. The beamwidth of each element is therefore very large and gives poor resolution. If adjacent elements are excited, the individual beams can combine to create an effectively narrower beam as is illustrated in Figure 2.11.

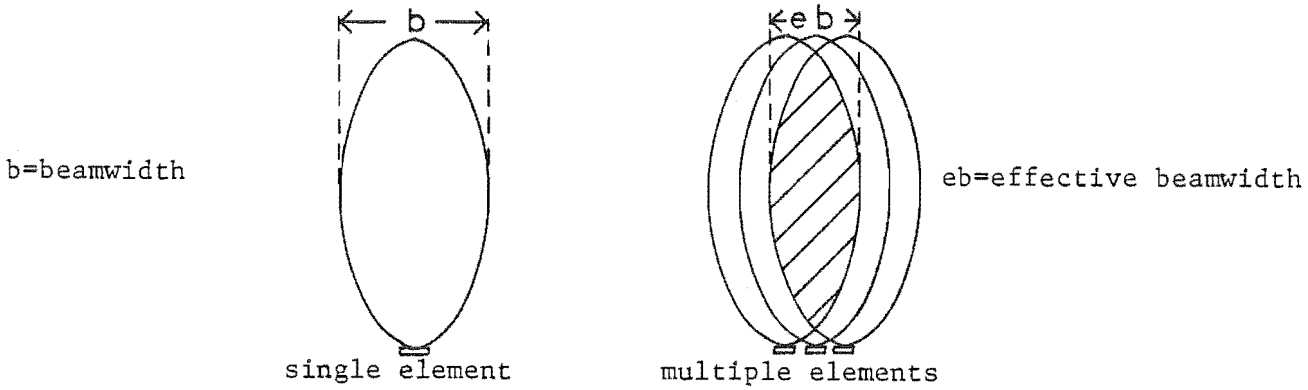

Figure 2.11 Formation of a narrow beam by combining those of several elements

It is therefore preferable to excite several adjacent elements in the linear array. Hence it is common practice in linear array scanning to excite a group of adjacent elements and to displace the group by one element along the array between each excitation. More sophisticated phased array techniques can produce a steerable beam from the array. Consider the array of 5 elements illustrated in Figure 2.12.

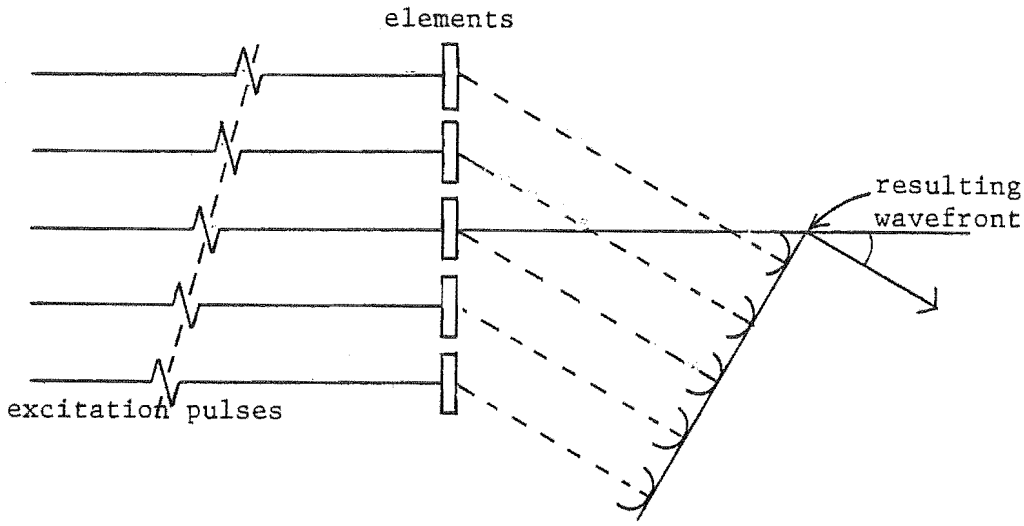

Figure 2.12 Beam steering with phased arrays

The top element is excited first producing an acoustic wave. After a short delay, the second is excited producing another acoustic wave. This process continues until the last element is excited. These five individual waves add, by the Huygen's summation principle, to form a plane acoustic wave at an angle determined by the time sequencing of the excitation pulses. Hence, by increasing or decreasing the relative delays at each excitation, the beam forms at greater or smaller angles. Hence the beam can be made to appear to scan through a sector centred on the array by systematically varying the relative delays on successive excitations (Morgan et al., 1978). Consider the array in Figure 2.13 which has n elements each separated by a distance d and which produce an acoustic wave which travels at a velocity V. If the time delays of the corresponding excitations are $\frac{m\ d\ \sin\theta}{V}$ with respect to the first element, the main beam has an angle θ to the normal.

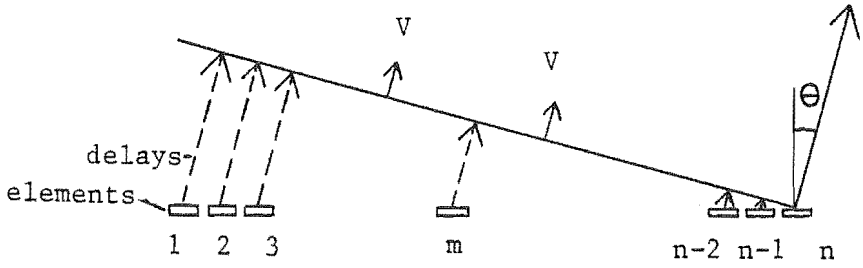

Figure 2.13 Beam angle formation of a phased array

The receiving beam may likewise be steered to coincide with the transmitted beam. This is effected by introducing delay lines into the signal paths

from each element in the array so that the appropriate delay relationships are maintained when the signals are combined. This reception steering can considerably improve the overall beam shape and sensitivity (Somer, 1968). It is also possible to electronically focus the acoustic beam of a phased array. This is effected by delaying the excitation of the inner elements compared to the outer elements as is illustrated in Figure 2.15 (Inuma et al., 1979).

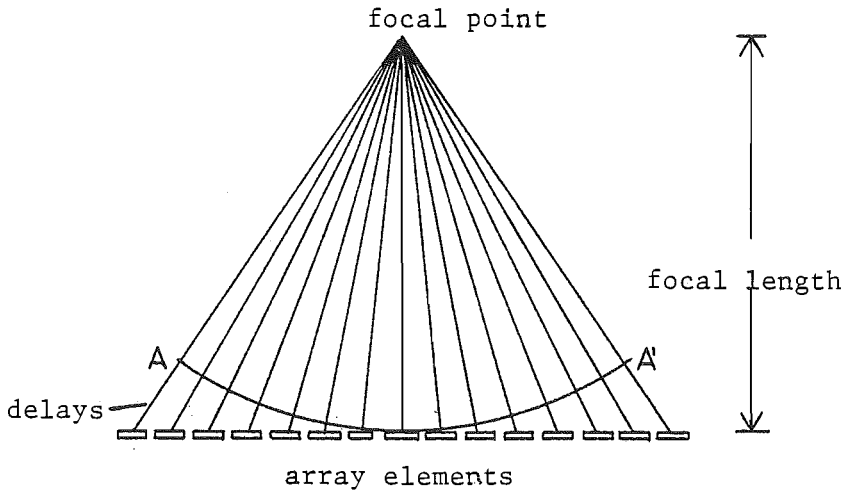

Figure 2.14 Electronic focussing of phased arrays

Appropriate delays are introduced so that the resulting wavefront is aligned along A-A'. This then concentrates in the vicinity of the focal point. A similar effect can be achieved by introducing delays on reception to focus the signals from a certain region. By continuously varying the delays on reception it is possible to focus at all ranges in front of the array. On transmission it is, of course, only possible to focus at a single range.

By adding together the delays necessary for beam-steering and for focussing, both effects can be combined.

2.3.2 Pulsers

Pulsers or transmitters are used to excite transducer elements to produce the short acoustic burst needed for pulse echo imaging. Two types of waveform commonly used for exciting transducer elements are described below.

i) Unipolar Pulse Excitation

This is the most popular form of excitation used in contemporary systems. A unipolar pulse of a few hundred volts and a rise time of approximately 10 nsec is applied to the transducer element. The pulse is usually generated by charging a capacitor to a high voltage then suddenly discharging it through an electronic switch (Wells, 1977). Satisfactory switches can be implemented

using either a thyratron, a thyristor or a transistor. Thyratrons and thyristors can be operated at higher voltages than transistors but they cannot operate as fast.

ii) Gated Sinewave Excitation

A gated sinewave oscillator is sometimes used, usually for pulsed doppler systems rather than B scan machines. A schematic diagram of how a gated sinewave excitation may be produced is illustrated in Figure 2.15.

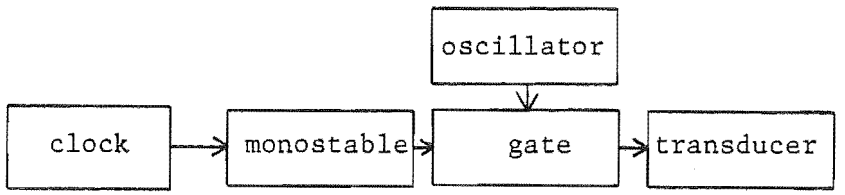

Figure 2.15 Components of a gated sinewave transmitter

A master clock is used to trigger a monostable which opens a gate for a short period to let a radio-frequency oscillator pass a small number of cycles through to the transducer. The resulting ultrasonic pulse waveform is usually of longer duration than that produced by the unipolar pulse method. Hence range resolution is degraded. This is not a popular form of excitation for B-mode scanners, but it has occasionally been used (Bom et al., 1973).

iii) Excitation of Phased Array Systems

It is technically difficult to delay a short high voltage pulse. Therefore phased array systems require a separate low voltage triggered transmitter for each transducer element. Each transmitter is triggered separately under the control of a master signal. A schematic layout of a typical system is shown in Figure 2.16.

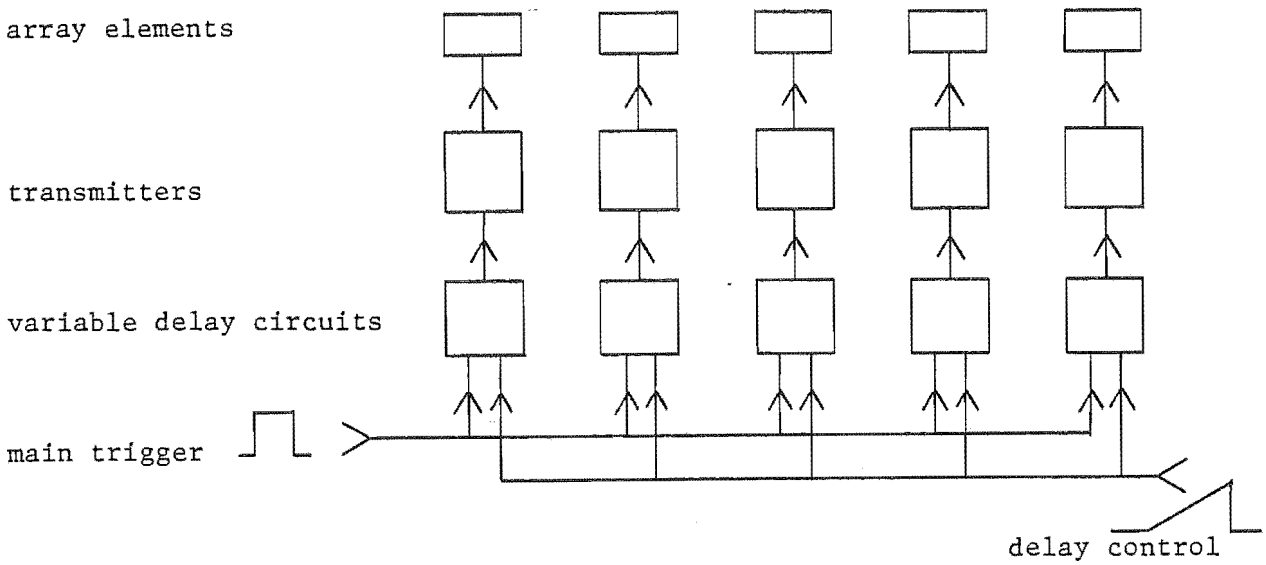

Figure 2.16 Schematic diagram of excitation system for a phased array scanner

In the system illustrated, excitation of the array is initiated by applying a low voltage pulse simultaneously to all of the delay circuits. The latter generate delays set by the voltage level sweep of the delay control. Thus the delay across the array can be changed by altering the main control voltage sweep. After the appropriate delay intervals, the transmitters are triggered to excite the array elements.

2.3.3 Receivers

The purpose of the receiver in a pulse-echo imaging system is to accept and amplify the electrical signals passed to it by the transducer probe. These signals have a dynamic range of some 100 dB (Wells, 1977). The receiver is usually made up of three parts as illustrated in Figure 2.17.

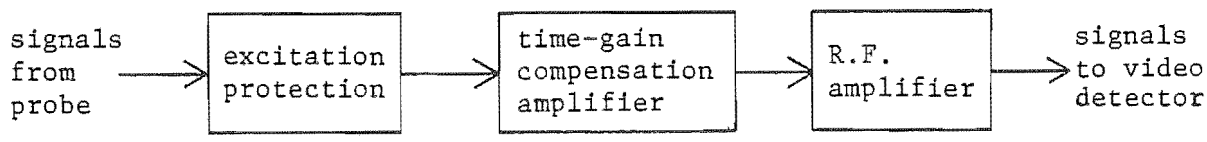

Figure 2.17 Components of a pulse-echo receiver

Signals from the transducer probe are passed to a time-gain compensation amplifier after passing through circuitry to protect the receiver from the high voltage triggering pulse. Because of the high attenuation experienced by ultrasound on passing through tissue, the time-gain compensation amplifier is used to amplify more distant echoes more strongly than closer echoes. The radiofrequency amplifier then buffers and amplifies the compensated signal to a suitable level for the video detector. Each of these components is now considered in more detail.

As the excitation pulse commonly has an amplitude of a few hundred volts, it is necessary to isolate the circuitry connected to the probe from it. Should the pulse be allowed to proceed into the receiver, there is a danger that it may destroy some of the receiver's components. Also the pulse would temporarily paralyse the receiver making it insensitive to small signals. The simplest form of protection is to provide earthed diodes at the receiver input. These effectively limit the amplitude of the received signals to the junction voltage of the diodes. Alternatively, by using a device such as a unitrode diode, it is possible to arrange a 'short circuit' to be switched in at the receiver input for the period of the transmitter pulse. An arrangement of this type has been described by Myers et al., (1972).

The 100 dB useful dynamic range of echoes received by conventional pulse-echo systems is divided between the variations in echo amplitude from structures at fixed distances from the transducer, and the attenuation due to tissue. In practice, at a fixed range, the echo amplitude variation is usually of the order of 30 dB. Hence compensation of up to 70 dB may be provided to allow for loss of echo amplitude by tissue attenuation. The average attenuation in tissue is somewhat less than 1 dB/cm/MHz in soft tissues. To compensate for such attenuation, an increasing amplification needs to be applied to echoes from more distant structures. This technique of increasing amplifier gain with time (which is very closely related to echo range) after transducer excitation is called 'swept-gain' or 'time-gain' compensation. Swept-gain needs to be applied at a rate of approximately 1.3f dB/cm where f is the centre frequency of the transmitted pulse. The exact rate of compensation is chosen to match each individual circumstance. It is usually under interactive operator control. The earlier stages of the receiver's amplification circuitry are usually designed to operate most satisfactorily on small signals. Since distortion must then occur when large signals are received, it is necessary to apply swept-gain to the earlier stages so that near echoes are not excessively amplified.

It is generally best for the swept-gain to be applied in such a way that it increases exponentially with time. This effectively assumes that all tissues traversed by the ultrasonic pulse have the same attenuation coefficient. This is never true of course in practice, but experience nevertheless suggests that exponential swept-gain, based on a 'mean' attenuation coefficient, is often the best practical compromise.

Swept-gain can be achieved by two methods. In one of these, the echo signal is passed through a multistage amplifier. The gains of each stage are made to vary with time, to obtain swept-gain by electronically altering with time, their feedback biasing conditions. In the other method, a multistage amplifier is again used but the gain of each stage is held constant. Each stage incorporates an attenuator whose characteristics are electronically controlled to decrease the amplitude of echo signals from the closest structures. This second method is found to be the easier to implement. The methods by which suitable attenuators may be constructed are reviewed by Wells (1977, pp 173-178).

Both of these methods require the provision of time varying voltage or current supplies to control the various amplifiers or attenuators. Usually this time variation is nonlinear, and in many cases, it should be specially programmed. A suggested method of generating a programmable sweep using a diode-based function generator has been described by Wells (1977, p178). Sophisticated swept-gain systems (Bom et al., 1973; Barnes et al., 1975) have been developed to allow an operator to alter the time-gain sweep to any desired amplification at a number of points along the beam. Such systems afford an operator ample control of a receiver's characteristics in situations where there is a wide variation in attenuation due to the tissues traversed by the beam. This often makes it possible to visualise structures which would be virtually invisible with purely exponential gain sweeping. Such systems are now available on some commercial scanners.

2.3.4 Video Detectors

Video detectors are used to convert the bipolar echoes from the receiver into unipolar signals suitable for driving display systems such as cathode ray storage tubes. The bipolar signals are rectified (or demodulated) to obtain unipolar signals. Demodulation is usually carried out by diode systems to provide either full-wave or half-wave rectification. Such systems have been discussed by Wells (1977,pp180-185). Full-wave rectification is more efficient than half-wave. Half-wave rectification allows greater

possibility of error in estimating the time of occurence or position of an echo, since the first half-cycle of a pulse may be rejected.

The insertion of diode demodulators into the signal path has the unfortunate effect of expanding the original signal dynamic range of some 30 dB by a further 5 dB. As a result, low level signals which contain important diagnostic information are further reduced in amplitude (Wells, 1977). The dynamic range of typical cathode ray tubes and other display devices is usually at most only 20 dB. If the 35 dB video signal is used to directly drive the display screen, the low level echoes are effectively invisible. At the other extreme, if the low level signals are maintained, the high level signals overdrive the screen. To avoid this difficulty, video amplifiers with a logarithmic response are usually employed to provide dynamic range compression. Several methods of constructing such amplifiers are discussed by Wells (1977, pp 186-188).

It is also necessary to incorporate within the video detector, ordinary linear-response video amplifiers. These are designed to have a pass-band equal to the frequency of the transducer used. If high frequency (5-15 MHz) transducers are used, it is possible to employ somewhat narrower bandwidth amplifiers. In all cases, it is necessary for the lower frequency cut-off to extend down to 1 KHz. If higher cut-offs are used, serious degradation of long pulses may occur and an excesive recovery time follows large signals (Wells, 1977).

Further processing of the video signal after dynamic range compression can lead to an improved image. Most common is some form of differentiation of the signal to highlight the positions of the echoes. Differentiation emphasises the edges as opposed to the durations of echoes.

Kossoff (1972) has introduced a method of combining the original video signal after logarithmic compression with its differential as in Figure 2.18. The resulting 'grey-scale' images have revolutionised two-dimensional ultrasonic imaging (Kossoff and Garrett, 1972; Taylor et al., 1973).

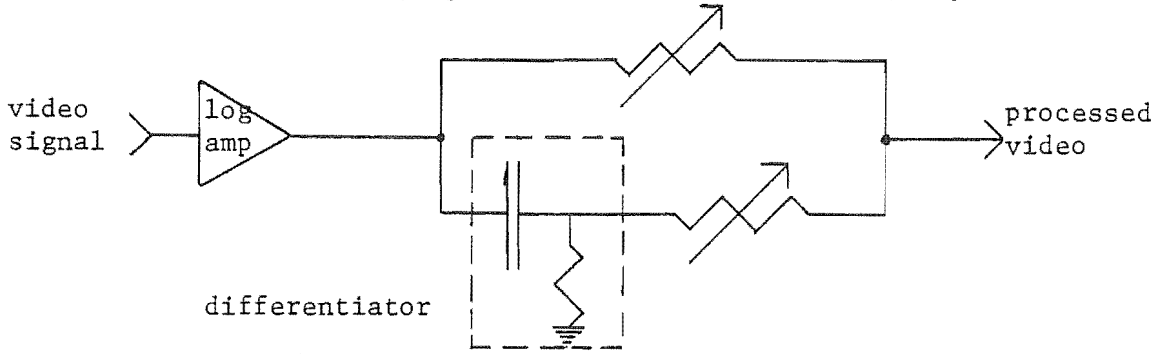

Figure 2.18 Kossoff's differentiate-and-add processor

The original video signal is combined with the differentiated signal in the ratio of 1:0.2 to 0.3. This emphasises changes in amplitude rather than absolute values of echo amplitude. Such processing allows an observer to notice sudden changes without losing sight of the overall amplitude as would happen if the signal was merely differentiated. Ide (1974) refers to images processed in this manner as being 'contour emphatic'.

A similar method of processing has been described by McDicken (1981). This is illustrated in Figure 2.19. The video signal is compressed and differentiated in parallel channels whose outputs are combined in a summing amplifier. This produces a video signal with enhanced edges.

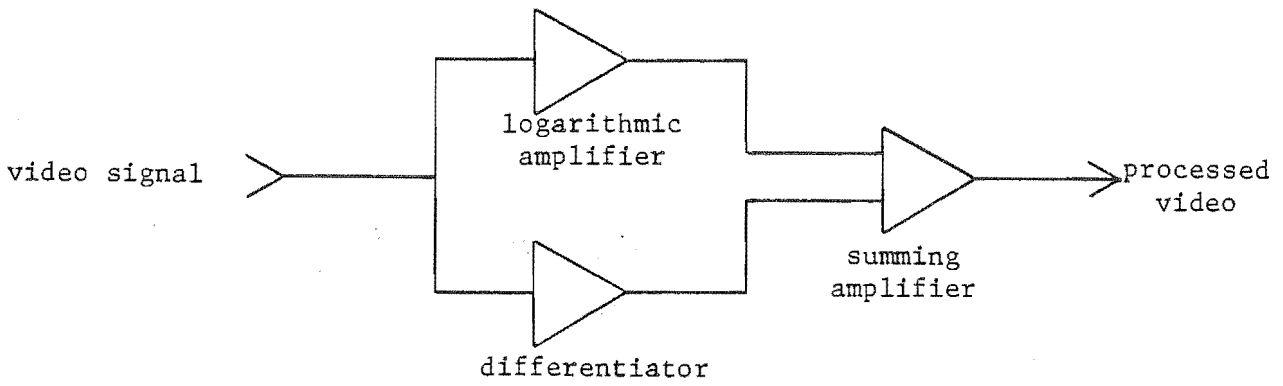

Figure 2.19 Edge enhancement circuit of McDicken (1981)

2.3.5 Signal Processing with Phased Array Systems

It is stated in §2.3.2 that when a phased array system is excited, a separate pulser circuit is required for each transducer element. Similarly, in the receiver system of a phased array, a separate receiver circuit is required for each element. This is because the dynamic range of the echo signals exceeds that of the delay devices. Time-gain compression provided by the receivers is necessary to reduce the echo signal dynamic range. A typical phased array system is illusted diagrammatically in Figure 2.20.

Each element is provided with a preamplifier to buffer the incoming signals, and a time-gain compensation amplifier. The signals are passed through electronic delays to bring them in to phase to effect beam steering and focussing. The delay time must be variable up to 10 μsec. Several devices have been used to implement the delays. These are discussed later in this section.

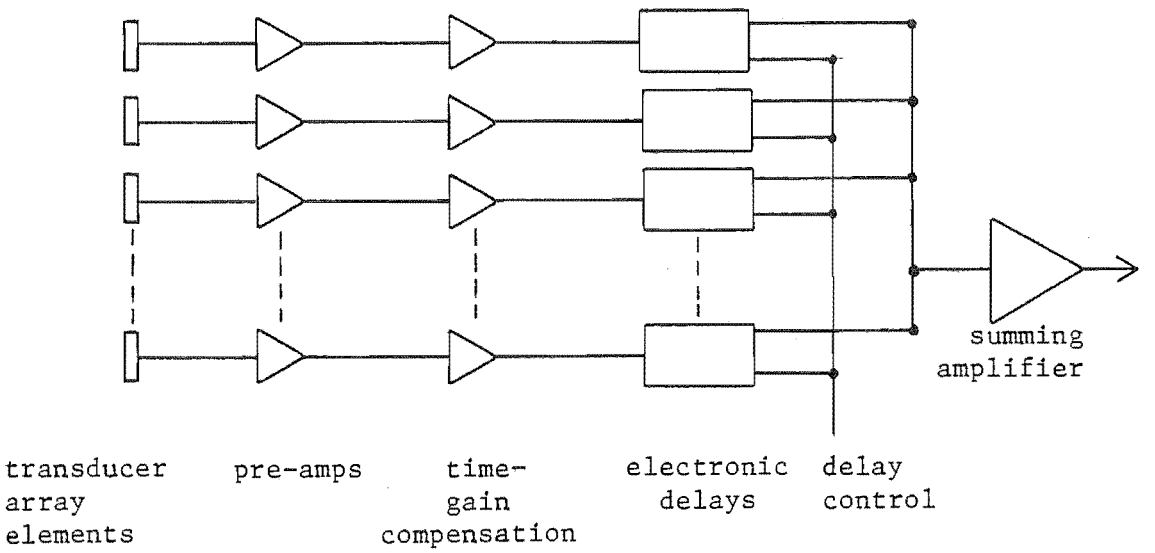

Figure 2.20 A typical phased array receiver system

The delayed signals are added in a summing amplifier to produce the signal for the video detector. It has been reported by Somer and Van Dael (1972) that azimuthal resolution is improved when the delayed signals are multiplied together rather than being added. This may be effected by introducing a logarithmic amplifier between each time-gain compensation amplifier and its associated delay circuit (Melton and Thurstone, 1978; Von Ramm and Thurstone, 1976). When the signals are combined by the summing amplifier, they are effectively multiplied together and logarithmically amplified. This form of processing is an effective means of matching the echo signal dynamic range to that of the display device.

Early phased array systems used various forms of tapped electromagnetic delay line (cf. Somer, 1968; Thurstone and Von Ramm, 1973). The appropriate delays are obtained by electronically switching the echo signal through the appropriate tap in the delay line. Such delay lines generally have a high dynamic range but are very bulky.

Doornbos and Somer (1972) report the development of a consecutively-commuted capacitor delay line with a dynamic range of 50 dB. Compact integrated circuit versions of such delay lines with dynamic ranges as high as 70 dB are now available. These are suitable for ultrasonic systems (Wells, 1977).

More recently charge-coupled-delay (CCD) lines have been developed with dynamic ranges of only 30 dB but which seem to be suitable for ultrasonic systems (McKeighen and Buchin, 1977). CCD lines are integrated circuits composed of a linear array of closely spaced metal oxide semiconductor capacitors (Melen et al., 1979). The echo signal is sampled and stored as charges on the capacitors. The stored charges are passed from each capacitor to its neighbour in the array in response to a clock pulse. At the same time the signal is again sampled and stored on the first capacitor. The signal may be tapped at any capacitor in the array. The delay for a sample to reach any tap is dependent on the clocking rate. Shott et al., (1976) have developed a single monolithic charge coupled device (CCD) integrated circuit which performs beam steering, focussing and summing operations.

McKeighen and Buchin (1979) have proposed systems based entirely on digital electronics. In such systems each receiver channel would contain an analogue-to-digital converter to sample the echo signals at a rate of about 15 MHz. The digitised signals would then be stored in high speed memories or shift registers. The signals would then be combined digitally after the appropriate delay. The advantage of such systems is that the signals would not be degraded as the delay time increases as happens with analogue delay systems. The dynamic range of such delay systems is dependent only on the accuracy with which the analogue signal is digitised.

It is not entirely satisfactory to simply add the delayed echo signals to achieve correct phasing. Random phase errors are introduced by each element, making it difficult to line up the echoes for correct focussing. This problem has been considered by Beaver (1977). A means of compensating for this has been proposed by Manes et al., (1979). They describe a method of separating the echo carrier from the echo envelope of the signal in each receiver channel. The phase of the carrier is corrected and reconciled with the envelope before the signals are added. Computer simulations show that a considerable gain in resolution can be achieved.

As the paths through tissue from any particular target to each array element are different, further phase distortions are introduced into the echoes received by each element. It is very difficult to remove such distortions.

2.3.6 Scan Converters

The origins of echoes from within a body can be determined using any of the many electronic 'position computers' that have been developed for this

purpose. To construct a two-dimensional image it is necessary to store the information gathered by the transducer in a manner which maintains the correct juxtaposition of the echoes.

The simplest way to reconstruct and store a scan is to write it on to a cathode ray storage screen. This is done using position calculators to drive the screen's deflection coils while the signal from the video defector modulates the screen's electron beam. Storage screens tend to have poor resolution and to be limited in the number of grey levels which they can display. Images stored on such screens tend to degrade with time. To overcome these limitations, electronic devices have been developed to store two-dimensional scans for long periods. Such devices are called scan converters (Wells, 1977; McDicken, 1981). Scans are then read from them and reproduced on a T.V. monitor capable of displaying a larger number of grey levels than can storage tubes. Scan converters have the added advantage that they allow the scans to be image processed before they are displayed. Two types of scan converter have been developed: analogue and digital. These are discussed below.

Analogue Scan Converters

Analogue scan converters are based on devices called scan conversion memory tubes. The construction of such devices, depicted in Figure 2.21 is similar to that of small cathode-ray tubes (CRT's) (Wells, 1977; McDicken, 1981). The main difference is that the screen phosphor is replaced by a storage target.

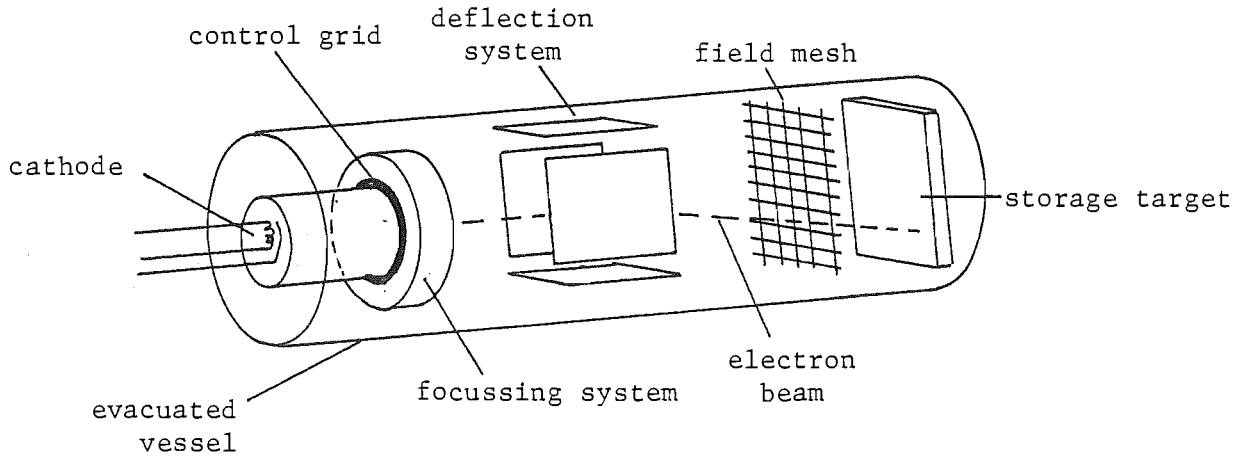

Figure 2.21 Construction of a scan convertion memory tube.

The latter consists of a conducting silicon wafer about 25mm in diameter onto which is mounted a matrix of minute squares of an insulating material such as silicon oxide (Figure 2.22). Scans are held on the target by storing a variable amount of charge on each square. As in a CRT, free electrons are produced by a heated cathode and are accelerated toward the target at the opposite end of the tube. The free electrons are focussed into a beam by an electrostatic or electromagnetic focussing system. The field mesh produces an electric field which causes the electrons in the beam to approach the target perpendicular to its plane.

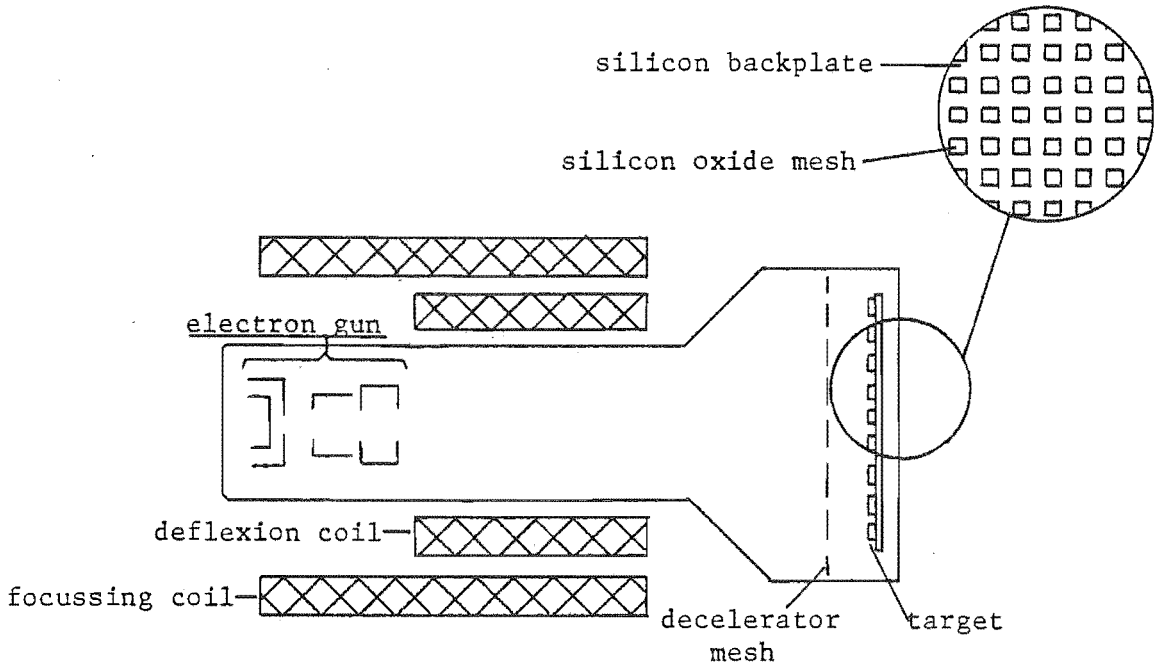

Figure 2.22 Construction of a storage target in a scan converter memory tube. From Wells (1977)

An image is written on the target in much the same manner as on a storage screen. Reading the image off the screen is effected by raster scanning the target matrix with a constant intensity electron beam. The potential of the target is adjusted so that the charge on the elements causes the electron beam to be deflected away from them. Elements with a high potential deflect the electrons back to the field mesh. Lower potential elements allow some of the electrons to land on the target backplate. The electrons flow through the backplate and the resulting current is used to drive a video monitor.

No electrons land on the elements themselves during the reading process. Hence the image is not destroyed by the reading process. It may be stored for over ten minutes before it starts to degrade.

Analogue scan converters are excellent scan storage devices as they accommodate about thirty shades of grey, which is greater than the eye can appreciate. As the target matrix has over 250,000 elements, high resolution images may be stored.

Digital Scan Converters

Digital scan converters are basically small computers with large memories to store the ultrasonic images. As they are based on computer technology, a great deal more image processing may be performed on scans thus stored than can be achieved with analogue scan converters. Images stored digitally are not affected by noise and low voltage drifting to the same extent as those stored by analogue devices. This is because digital images are stored using only two distinct voltages while analogue images are composed of many contiguous voltage levels. Digital images can be stored virtually indefinitely and can be recalled any number of times without being degraded.

The basic components of a typical digital scan converter are identified in Figure 2.23.

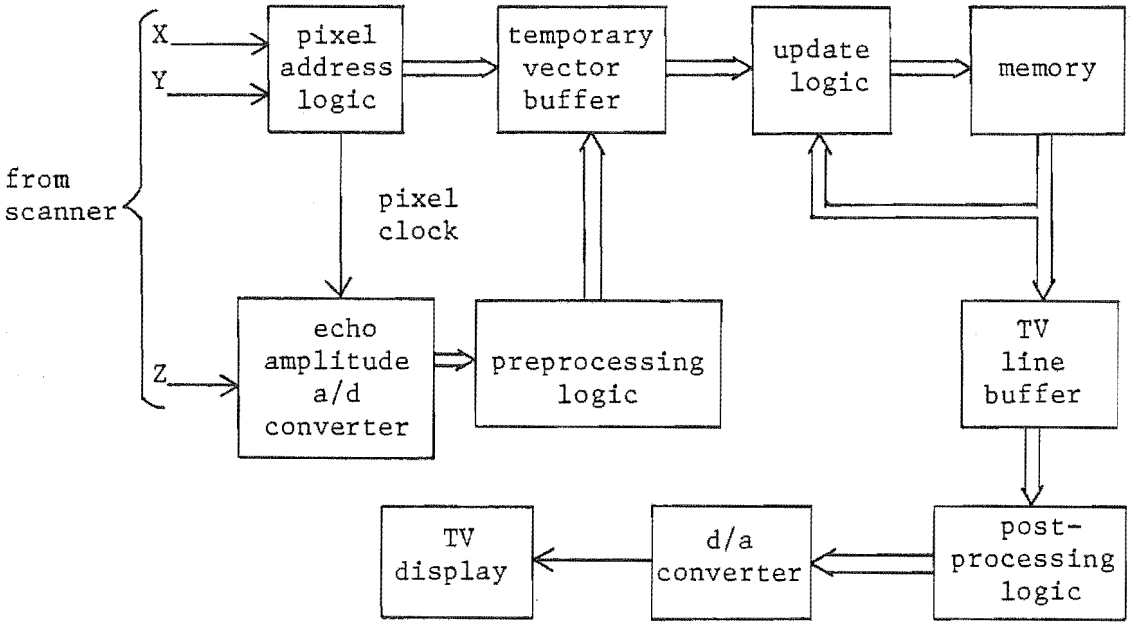

Figure 2.23 The basic components of a digital scan converter

Some imaging systems based on digital scan converters include a microcomputer for control and/or data processing purposes. It has been omitted from Figure 2.23, for clarity. Each of the blocks shown in this figure is now discussed.

i) Pixel Address Logic

The pixel address logic generates a sequence of digital addresses corresponding to image co-ordinates to correctly position received echoes in the image. The inputs to this block are the outputs from position calculators.

ii) Echo Amplitude Analogue-to-Digital Converter

This device converts the analogue ultrasonic video signal into a digital form at a rate of 10-20 MHz. The converter usually samples to a 4 or 5 bit accuracy according to a simple linear or a pre-programmed non-linear function stored in read-only memories.

iii) Pre-processing Logic Buffer

In this block the digitised video signal is processed by other non-linear functions, which are usually stored as look-up tables in read-only memories.

iv) Temporary Vector Buffer

This is a high-speed buffer memory which holds 512 or 1024 samples of echo data for transfer to the main image memory. The data stored at any one time is that obtained from the transmit/receive cycle of a single pulse.

v) Update Logic

The purpose of the update logic is to over-write the image in the main memory with new data. The values of the new data are determined from the contents of the temporary vector buffer and the spatially equivalent values in the main memory. Several common updating algorithms are described in Chapter 4.

vi) Main Image Memory

The memory contains the actual scan image. It is composed of an array of 512 x 512 four or five bit locations. Each location contains the intensity of a single pixel.

vii) T.V. Line Buffer

The T.V. line buffer contains the values of 16 horizontally adjacent memory locations which are passed to be the post-processing logic.

viii) Post-Processing Logic

This is used to further process an image as it is displayed. It allows a stored scan to be further modified to produce a diagnostically more useful image. The structure of this block varies considerably according to the type of processing to be performed.

ix) T.V. Display

The processed pixel intensities are converted to an analogue video signal by a high speed digital-to-analogue converter. This signal is then passed to a high quality wide-bandwidth black and white video monitor on which the image is presented.

While analogue scan converters are usually used only for non-real time scanning, digital versions can be designed for use with real time imaging systems. A frame rate of about thirty frames per second is used.

The rapid data transfer processes necessary are time consuming, leaving little time for processing and calculating the positions of echoes in the image memory. It is relatively simple to form an ultrasonic image on the display screen without the added complexity of a digital scan converter. This makes it seem superfluous to include digital scan converters in real time systems. However, there are several useful features which can be included in digital scan converter based real time systems (McDicken, 1981). Scan converters allow instantaneous frame-freeze facilities to be implemented. This is of use in cardiac imaging where the operator may wish to view the heart at a particular phase of the heart cycle. Digital scan converters make it possible to convert sector scans to standard T.V. format making video tape-recording possible. In addition, one can implement a small amount of image processing, such as smoothing between pizels, or insertion of extra lines of data between sector scan lines to make the images more presentable. Some systems have been developed which allow time averaging of a few frames to be performed to reduce random noise.

2.3.7 Display Systems

Several devices are used to display ultrasonic images. Some commonly used devices are storage and non-storage cathode ray tubes, video monitors and fibre-optic chart recorders. Almost any device with a suitable wide bandwidth can be adapted to display ultrasonic images.

The operational details of such devices are not discussed here; they can be found in many standard text-books on video and television electronics, (cf. Eastman, 1971; Sims, 1969).

Ultrasonic scans are usually displayed as black and white images. Some attempts have been made to provide colour-coded images (cf. Ito et al., 1974; Milan and Taylor, 1975), provide a much higher dynamic range that is more useful diagnostically. It is difficult, however, to match colour scales and grey scales. Also the eye cannot average the large numbers of colours

which are presented in areas where there are rapid changes in image intensity. Hence, black and white displays continue to be the most popular for presenting ultrasonic scan images, even though colour coding is available on some commercial systems.

2.4 ULTRASONIC TRANSMISSION IMAGING

2.4.1 The Direct Technique

The direct technique is analogous to the common X-ray imaging technique. The density of the image is proportional to the intensity of an ultrasonic beam after it has traversed an object.

The first transmission images were those reported by Dussik (1942, 1947). They were formed by scanning transmitting and receiving transducers past opposite sides of the head to produce images of the brain. Dussik claimed that an outline of the ventricles of the brain could be seen in these images, and that brain tumours could possibly be detected. Ballantine et al. (1950) experimented with a similar system. It was reported at the time (Hueter and Bolt, 1951) that transmission imaging of the ventricles was considerably more promising than the pulse-echo technique. However, experiments by Guttner et al. (1952) strongly suggested that ventriculography was not possible because the attenuation masking effect of the skull is much greater than the attenuation due to the brain. Ballantine et al. (1954) reached a similar conclusion from the results of their experiments, although they had been interpreted by Dussik (1954) and by Herrick and Kruesen (1954) as evidence that the method was potentially useful.

Further development of the technique had to wait until Green et al. (1974) constructed a sophisticated real time transmission scanner. Acceptable images of excised organs were obtained. A prototype scanner to image the abdomen was then developed (Zatz, 1975). However, when an object as complex as the abdomen is scanned, the resulting images are degraded by diffraction and refraction effects.

Attenuation of an ultrasonic beam is due to two effects: reflections at interfaces and acoustic absorption by the tissues. Ideally imaging should be performed purely on the basis of only one effect; absorption. Attenuation by reflection is not a property of each individual tissue, but of acoustic mismatch between tissues and the orientation of their interface to the beam. Attenuation is dependent mainly on reflections, especially at the lower (1-5 MHz) frequencies (Dunlop, 1978). Hence artifacts from reflections are

prominent in absorption images.

It would appear to be better to form transmission images of objects on the basis of the variation of the ultrasonic propagation velocity within them. Velocity can be estimated from the time-of-flight of a pulse of sound from a transmitter to a receiver. Partial reflection of the beam by interfaces has little effect on time-of-flight measurements, although refraction effects may distort the path to give a lower velocity estimate.

Heyser and Le Croisette (1974) produce two dimensional images from time-of-flight measurements of sound travelling between raster scanning transducers. They estimate the time-of-flight of the ultrasound from changes in a linear frequency sweep transmitted through the imaged object. Images have also been produced by other researchers measuring the time-of-flight of a pulse of ultrasound. Estimation of time-of-flight was effected either by computer analysis of the received signal to detect the pulse (Johnson et al., 1975; Greenleaf et al., 1975) or by detecting it electronically (Glover and Sharp, 1977).

2.4.1 Ultrasonic Computed Tomography (CT)

Ultrasonic computed tomography is analogous to X-ray computed tomography (cf. Hounsfield, 1973; Brooks and DiChiro, 1976; Dunlop, 1978). The ultrasonic attenuation coefficient or the velocity is used as the imaging parameter instead of the X-ray attenuation coefficient (cf. Greenleaf and Bahn, 1981; Klepper, 1981).

The details of the imaging techniques used in computed tomography can be found elsewhere (cf. Lewitt and Bates, 1978a, 1978b, 1978c; Lewitt, Bates and Peters, 1978, Dunlop, 1978; Heffernan, 1981). Figure 2.24 illustrates the principles involved. Transmitting and receiving transducers are positioned opposite each other and moved past the object. It is assumed that refraction effects are negligible so that the sound travels in a straight line from the transmitter to the receiver. Consider the case where an image of the ultrasonic attenuation coefficient is reconstructed. The output of the receiver is a measure of the total attenuation of the beam by the object. The attenuation of the beam is measured at many positions as the transducers are scanned past the object. Each measurement is called a projection. Projections are measured at many different angles (see Figure 2.24). The image is then reconstructed from the projections using the techniques developed for X-ray computed tomography (cf. Brooks and DiChiro, 1976). Other scanning geometrics such as the fan beam geometry have been used.

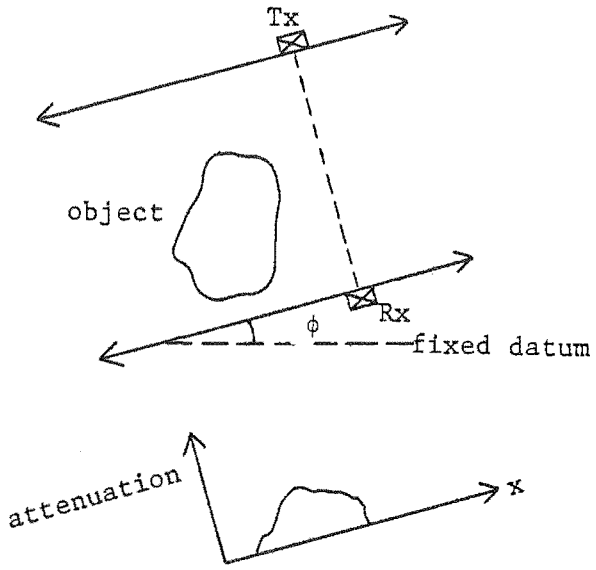

Figure 2.24 Principles of computed tomography

The fan beam geometry is illustrated in Figure 2.25.

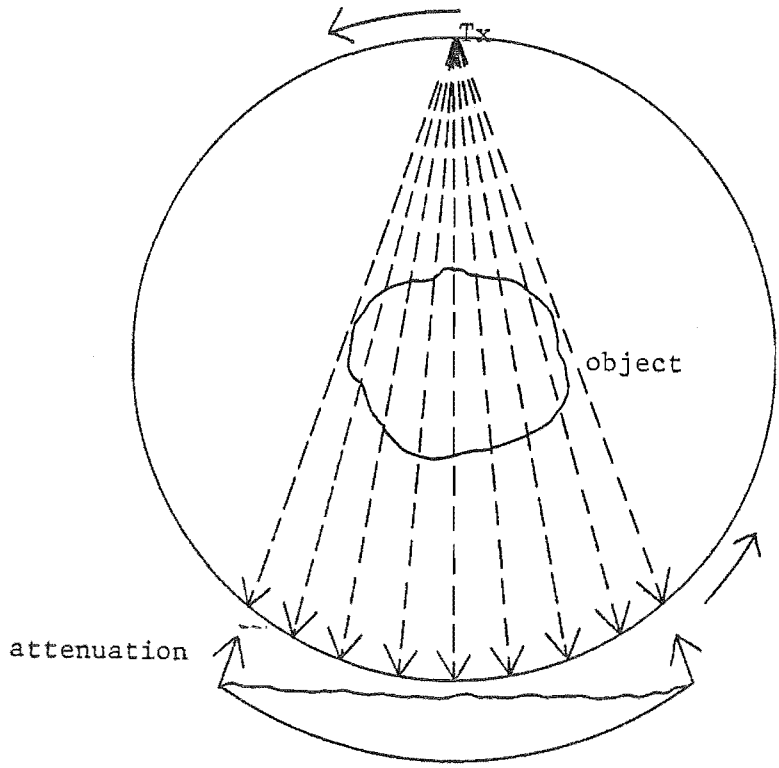

Figure 2.25 Fan beam geometry

X-ray CT uses a fan shaped X-ray beam wide enough to irradiate the whole of the object. Many projections are measured simultaneously by an array of detectors and therefore scan time is reduced. Also the source/detector system now has only to rotate and not translate as well. In ultrasound CT a fan beam is not used but a single receiver is swept around in an arc opposite the transmitter. The transmitter also rotates to follow the receiver (cf. Whiting et al., 1981).

Rather than measuring the attenuation of an ultrasonic beam, the time delays for pulses to travel to the receiver from the transmitter may be observed. The projections are then called 'delay projections'. The image is formed as a map of ultrasonic velocity within the object (Bates and Dunlop, 1977; Klepper et al., 1981; Greenleaf et al., 1974).

Application of the technique in view is limited to imaging only a few parts of the body (e.g. the female breast). The pressure of lung and bone which strongly attenuate and refract the beam prevent it from being used to image most organs. Pilot studies of imaging the female breast by the velocity method (Glover, 1977; Whiting et al., 1981) and the attenuation method (Greenleaf and Bahn, 1981) have been performed and suggest that it is possible to detect tumours with this technique.

CHAPTER 3

PROPERTIES OF THE HEART

3.1 INTRODUCTION

Most of the original work in this thesis is related to imaging the heart and to evaluating some of its properties. In this chapter, the relevant background information is presented.

In §3.2 the anatomy and the functioning of the heart are described. The heart is a very mobile organ. The motion of its walls are often assessed qualitatively to diagnose certain cardiac disorders. Quantitative assessment, while desirable, is extremely difficult to achieve. Ways of measuring heart wall motion are discussed in §3.3.

It is important for diagnosis to be able to assess the shape of the main pumping chamber of the heart (i.e. the left ventricle). §3.4 is concerned with the few reports of quantitative shape assessment that presently exist in the literature.

3.2 THE HEART

3.2.1 Cardiac Anatomy

A brief description of the heart and how it works is now presented. Only sufficient details are provided to enable the reader to understand the information presented in later chapters of this thesis. Further information can be found in, for instances, Gray (1973) and Silverman and Schlant (1974).

The function of the heart is to propel blood around the body. Its structure and relationship to the circulatory system and the rest of the body is illustrated in Figures 3.1 to 3.4.

The heart is composed of two pumps which act simultaneously. The right atrium and ventricle form one pump which accepts blood from the body and passes it to the lungs. The left atrium and ventricle then receive the blood from the lungs and propel it around the rest of the body.

The function of the atria is to pump the blood into the ventricles to 'prime' them before they contract. The atria contract just before the ventricles to forcibly increase the volume of blood in the ventricles by approximately 20%. This stretches the ventricles and aids in their contraction.

Figure 3.1 The heart and the circulatory system. The arrows show the direction of blood flow.

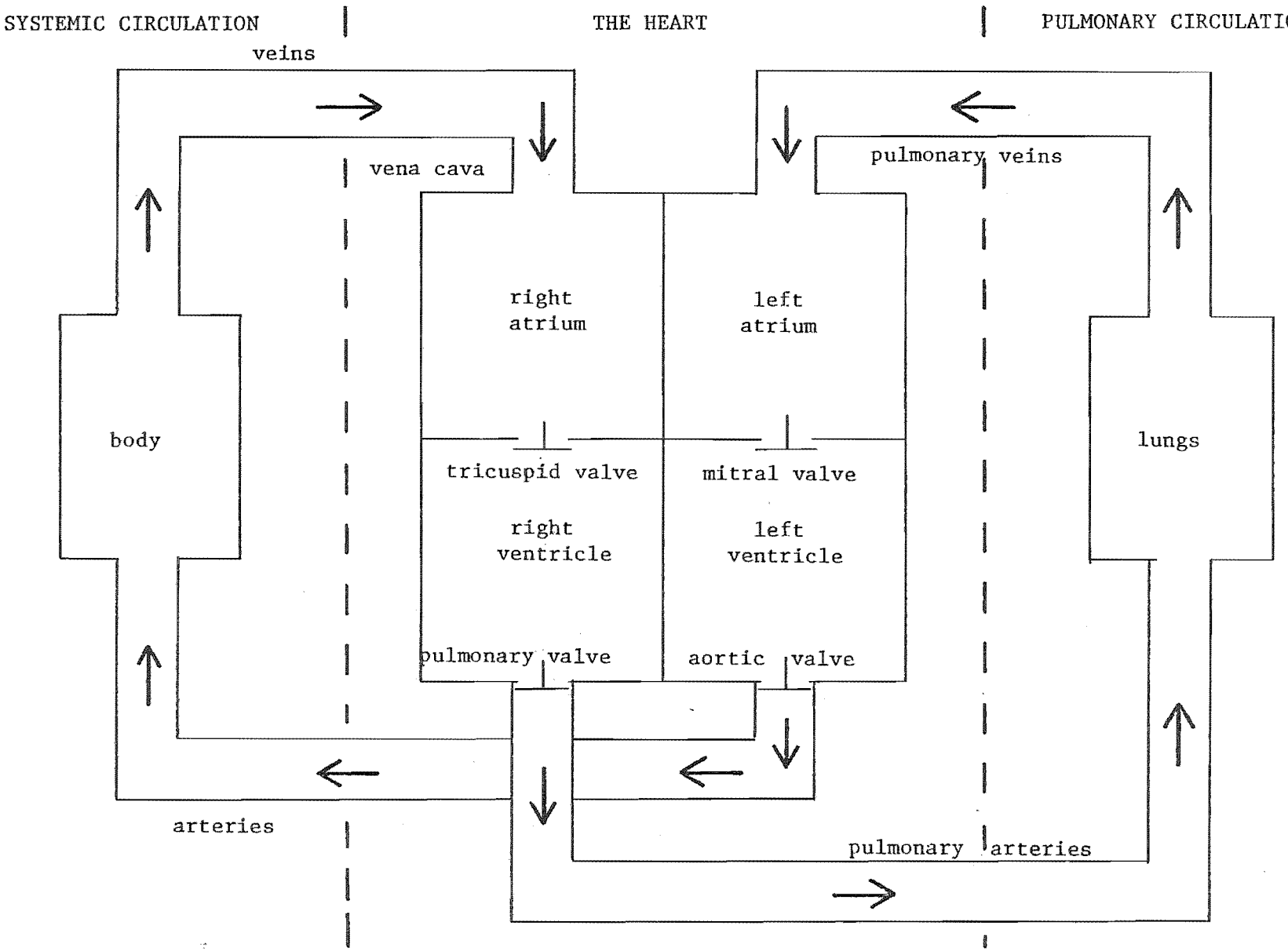

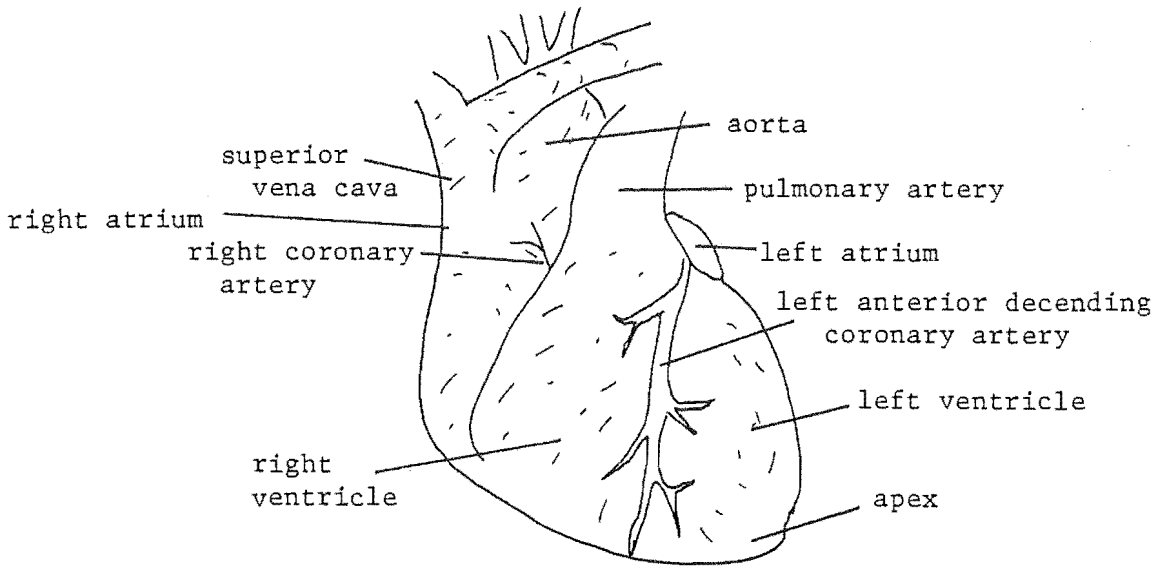

Figure 3.2 The external view of the heart.

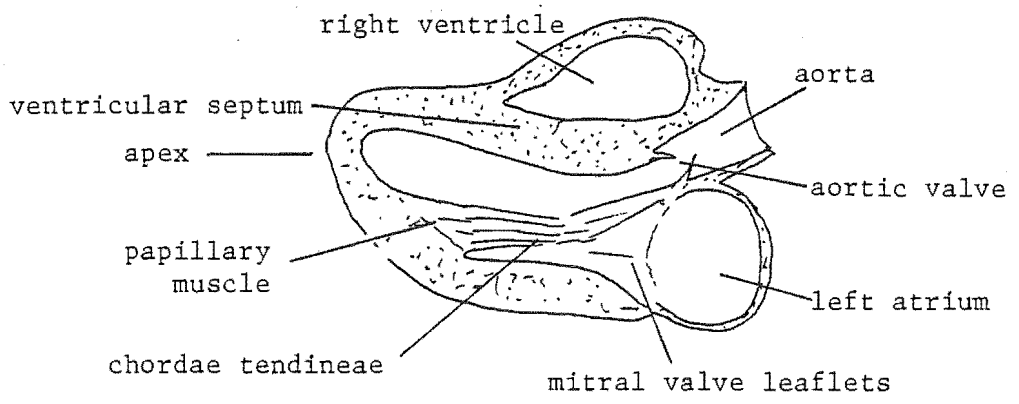

Figure 3.3 Longitudinal section through the heart.

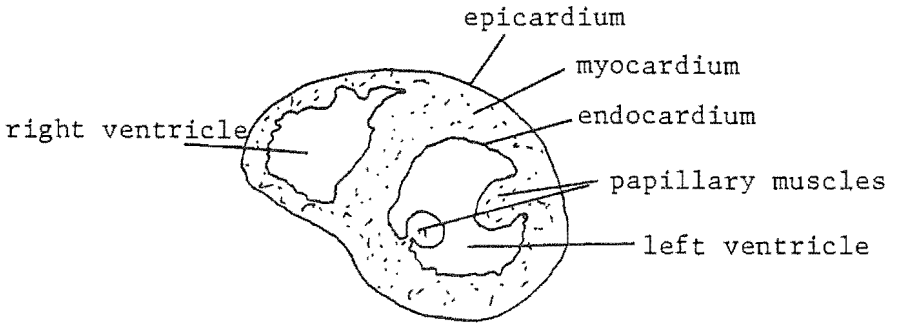

Figure 3.4 Transverse section through the ventricles.

(cf. Silverman and Schlant, 1974; Tajik et al., 1978; Edwards et al.,1981)

The pumping action of the atria alone is not sufficient to maintain life. It does, however, aid the overall efficiency of the heart.

The two atria together take the shape of a hemisphere placed on top of the ventricles. They are partitioned into the left and right chambers by the interatrial septum. The walls of the chambers are from 0.5mm to 4mm thick with the left atria having thicker walls than the right. They are composed of many bundles of muscle fibres joined by connective tissue. Several large blood vessels open into the atria. Blood from the venous side of the systemic circulation enters the right atrium through the superior vena cava. The blood supply to the heart itself returns through the coronary sinus into the same chamber. Oxygenated blood from the lungs enters the left atria through four or five pulmonary veins. The atria and the ventricles are connected by the fibrous atrio-ventricular (AV) ring which supports the four cardiac valves.

The ventricles provide the main propulsion of blood through the circulation. The left ventricle is the more muscular of the two as it supplies the high pressure systemic circulation. Its walls are approximately 15mm thick. The walls of the right ventricle are only about 4mm thick - they supply the pulmonary circulation at a much lower pressure. The ventricles are separated by the interventricular septum. It is slightly thicker than either wall.

The ventricles are often describes as being in the shape of a cone having the atrio-ventricular ring for its base. Indeed, it is usual to refer to the atrio-ventricular ring as the 'base' of the heart and to the point of the ventricles furthest from the base as being the 'apex'. The left ventricle is roughly elliptical in section while the right ventricle tends to be more flattened and wraps around the left (Figure 3.4). Its position is not exactly to the right of the heart, but is somewhat forward and rightward. The left ventricle itself does not point directly downwards. It lies on the diaphragm and is oriented forward, downward and leftward.

The blood enters the left and right ventricles through the mitral and tricuspid valves respectively. It is ejected through the aortic valve to the systemic circulation and the pulmonary valve to the pulmonary circulation (i.e. to the lungs).

Papillary muscles are located in the walls of the ventricles. Their function is to help close the mitral and tricuspid valves at the onset of ventricular contraction. They are attached to the valve leaflets by the chordae tendoneae.

The walls of the heart are composed of muscular tissue called myocardium. The inner surface of the chambers is lined with a tissue, endocardium. The inner walls of the ventricles are ridged with muscles called the trebeculae carnae. The outer surface of the myocardium is covered with a tissue called epicardium.

The heart muscle itself is supplied with blood via three coronary arteries. If an adequate blood supply to a region of the myocardium is interrupted, that region may die resulting in a condition called myocardial infarction (cf. Braunwald, 1980). The most common cause of this is coronary artery disease (CAD), in which the internal diameter of the coronary arteries is reduced by the buildup of fatty and calcified deposits. The affected myocardium permanently loses its contractile properties and is eventually replaced by fibrous tissue. Myocardial infarction is therefore a very serious condition.

A temporary inadequacy of blood supply to a region of the myocardium is called myocardial ischaemia. With its symptoms of chest pains, it is an indication of CAD and may forewarn a myocardial infarction. Ischaemia also occurs directly before infarction and in regions of myocardium which eventually recover around an infarction.

3.2.2 The Electrocardiogram

The electrocardiogram (ECG or EKG) is the time varying potential field produced on the body surface by the electrophysiological activity of the heart. It is commonly used as a time-reference system to which the mechanical activity of the heart is related.

The ECG is measured as the differential voltage between two electrodes (or sets of electrodes) on the body surface. The ECG of a normal subject is presented in Figure 3.5.

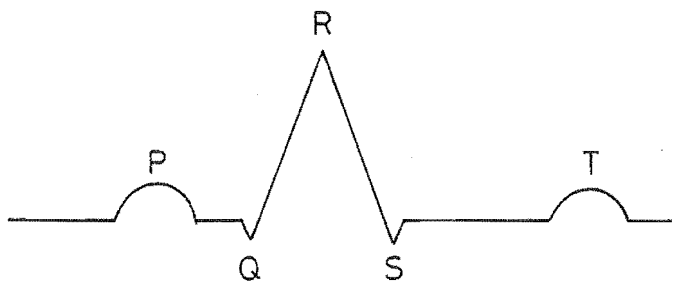

Figure 3.5 The normal ECG

The major features are

i) The P wave: caused by the depolarisation of the atrial myocardium which causes the atria to contract.

ii) The QRS complex: caused by the depolarisation of the ventricular myocardium which causes the ventricles to contract

iii) The T wave: which is caused by the repolarisation of the ventricular myocardium as the ventricles relax.

The contraction phase of the heart is called systole, the relaxation phase is called diastole.

3.3 MEASUREMENT OF VENTRICULAR WALL MOTION

Detecting the lack of contractility of a region of the heart walls due to myocardial ischaemia and infarction is of great importance to the clinician. To allow this, an imaging system capable of identifying individual pieces of myocardium and displaying their relative motion is required. The usual cardiac imaging techniques, namely echocardiography, cineangiography and radionuclide aniography, provide only a record of the time variation of position and shape of the ventricles. However, changes in these do allow the recognition of abnormal wall motion of a region of myocardium, and hence the indirect detection of abnormal contractility. Abnormal wall motion usually manifests itself as the lack of inward movement during systole. However, if an aneurysmal segment is present, the wall may bulge outwards.

The motion of a ventricle as seen in an image formed by one of the above techniques is not due entirely to the contraction of that ventricle alone. All of the parts of the heart are coupled. Therefore contraction in one region of the walls will cause all parts of the heart to be displaced slightly. During systole the heart translates left to right and downwards, rotates clockwise and rotates forwards slightly (Brower and Meester, 1976; Ingels et al., 1979). It also moves up and down under the influence of respiration.

It is very difficult to separate the inward motion of the heart walls due to their down contraction from its gross movement. Lack of contractility in one region of a ventricle's walls influences the overall as well as the region's motion. Apparently abnormal wall motion is sometimes observed in normal subjects and normal wall motion is sometimes seen in people known to have had an infarction (Morganroth et al., 1981). Therefore the presence of abnormal wall motion is not necessarily a precise indicator of the existence

of an infarction.

Analysis of ventricular wall motion is usually done in a qualitative or semi-quantitative manner. Although some fully quantitative systems are reported (cf. Fujita et al., 1981), no generally accepted procedure has yet been developed.

3.3.1 Wall Motion Analysis Using Cineangiography

Cineangiography is an X-ray technique for imaging the ventricles. It is the traditional standard technique to which the results of all new techniques are compared to assess their sensitivity and specificity.

In this technique, radiopaque dye is injected into a ventricle via a catheter to help define the ventricle. A cine X-ray film at a rate of 30 to 60 frames/second is taken of the ventricles over a few heart cycles. The heart is imaged from two directions to give the right anterior oblique (RAO) or left anterior oblique (LAO) views or projections. The angles at which these projections are taken are illustrated in Figure 3.6. Typical outlines of the left ventricle obtained using these projections are presented in Figure 3.7.

When studying a left ventricular angiogram clinicians usually assess wall motion in a semi-quantitative manner. A popular method of doing this is illustrated in Figure 3.7. The walls are partitioned into 'segments' (A-G) and the wall motion of each classified on a 'scale of abnormality' of 0-4. The values assigned to each segment are called 'scores'. They are assigned as:

0 normal - amplitude and timing of motion is correct
1 hypokinetic - low amplitude but timing of motion is correct
2 akinetic - not moving
3 hyperkinetic - amplitude too great
4 aneurysmal - wall moves outwards during systol

This assessment is subjective and classification of the motion of each segment for a single patient varies from observer to observer. Before quantitative analysis to provide consistent classification can be achieved several basic difficulties must be overcome (cf. Ingels et al., 1979). The first of these relates to the problem of separating left ventricular wall motion due to its own contraction from that due to the overall movement of the heart. Many workers have attempted to do this by defining a suitable axis (a 'reference axis') through the heart relative to which motion is measured. For instance, an axis from the junction of the aortic and mitral valves to the apex is often used (Figure 3.8). This is termed selecting a 'frame of

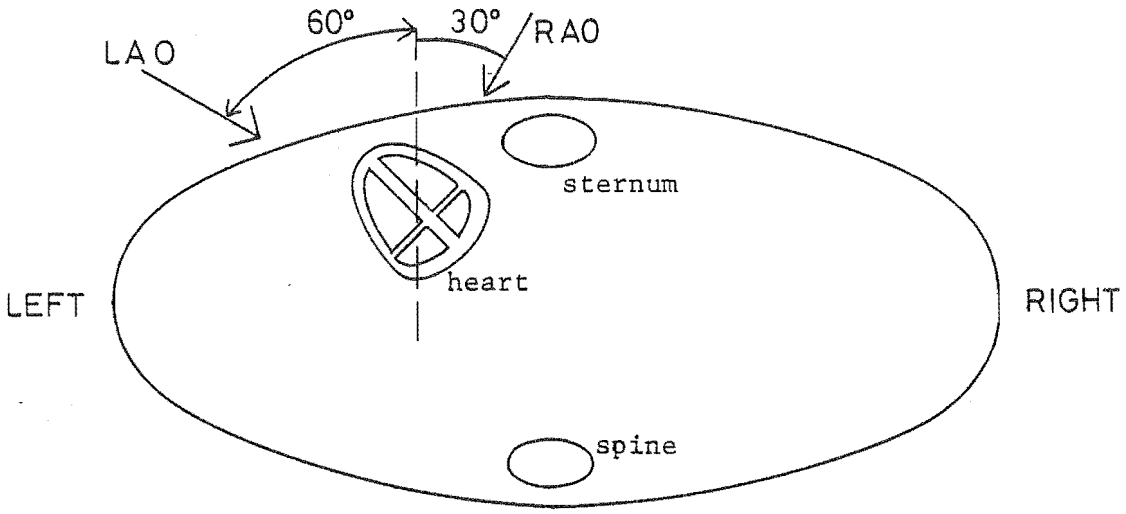

Figure 3.6 Orientation of the LAO and RAO views used in cineangiography. The cross section of the body is at the level of the eighth thoracic vertebra

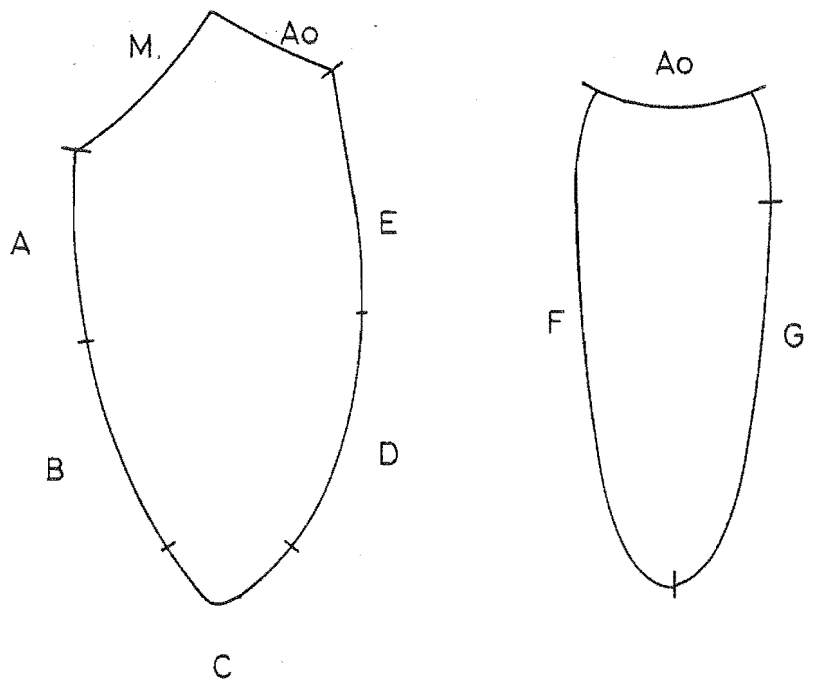

Figure 3.7 The RAO and LAO views of the left ventricle

Ao - aortic value
Mi - Mitral value

Segments				
	A	Posterobasal	E	Anterobasal
	B	Diaphragmatic	F	Septal wall
	C	Apical	G	Posterobasal
	D	Anterolateral		

reference'. Two types of frame of reference have been defined: external and internal (Ingels et al., 1979). Internal reference frames basically correct for the gross cardiac movement while external reference frames do not. When an external reference frame is used, wall displacement is measured from a reference axis which is fixed in space. A clinician employs such a frame of reference when qualitatively analysing wall motion using angiography. Motion is implicitly judged relative to the edges of the screen displaying the images (Ingels et al., 1979). Internal frames of reference require the reference axis to move during the heart cycle so that it passes through the same structures in the ventricle at all times (Figure 3.7). By translating and rotating the ventricle in all images so that the reference axes coincide, lateral and rotational movements are effectively removed (cf. Azancot, 1978). The vertical movement of the ventricle must also be removed. This can be done by moving the ventricular outlines up and down the reference axis until certain features (such as the aortic/mitral valve junction) coincide.

The second difficulty is that of determining a 'system of co-ordinates'. This relates to defining the direction of motion in which wall movement is measured. The two most popular, the hemiaxis and the radial axis systems, and two others (Gibson et al., 1976, 1978a; Bolson et al., 1980) are illustrated in Figure 3.9. The hemiaxis system measures motion along lines parallel to the reference axis. But it is intuitively more reasonable to assume that the motion is directed towards a single point such as the ventricular centre of mass (or centroid) (cf. Azancot et al., 1978) or a point along the reference axis (cf. Harris et al., 1974; Ingels et al., 1978). This is why the radial axis methods have been developed. Even though the methods of Gibson et al. (1976, 1978a) and Bolson (1980) are more complicated, they are based on more realistic assumptions of how the walls move. Gibson et al. divide the end-systolic and end-diastolic outlines into 40 segments of equal length. They then assume that each segment on the end-diastolic curve moves towards the nearest segment on the end-diastolic curve (Figure 3.9c). Bolson's approach is to plot a line midway between the end-diastolic and end-systolic curves. The motion is then assumed to be directed perpendicular to that line (Figure 3.9d).

All four of the above systems of co-ordinates are based on intuitive assumptions of how the ventricular walls move. Angiograms only allow changes in the shape of a ventricle to be observed. It is very difficult to identify a point on the ventricular wall and observe its motion with this technique. Only a few studies of the motion of individual points on the heart

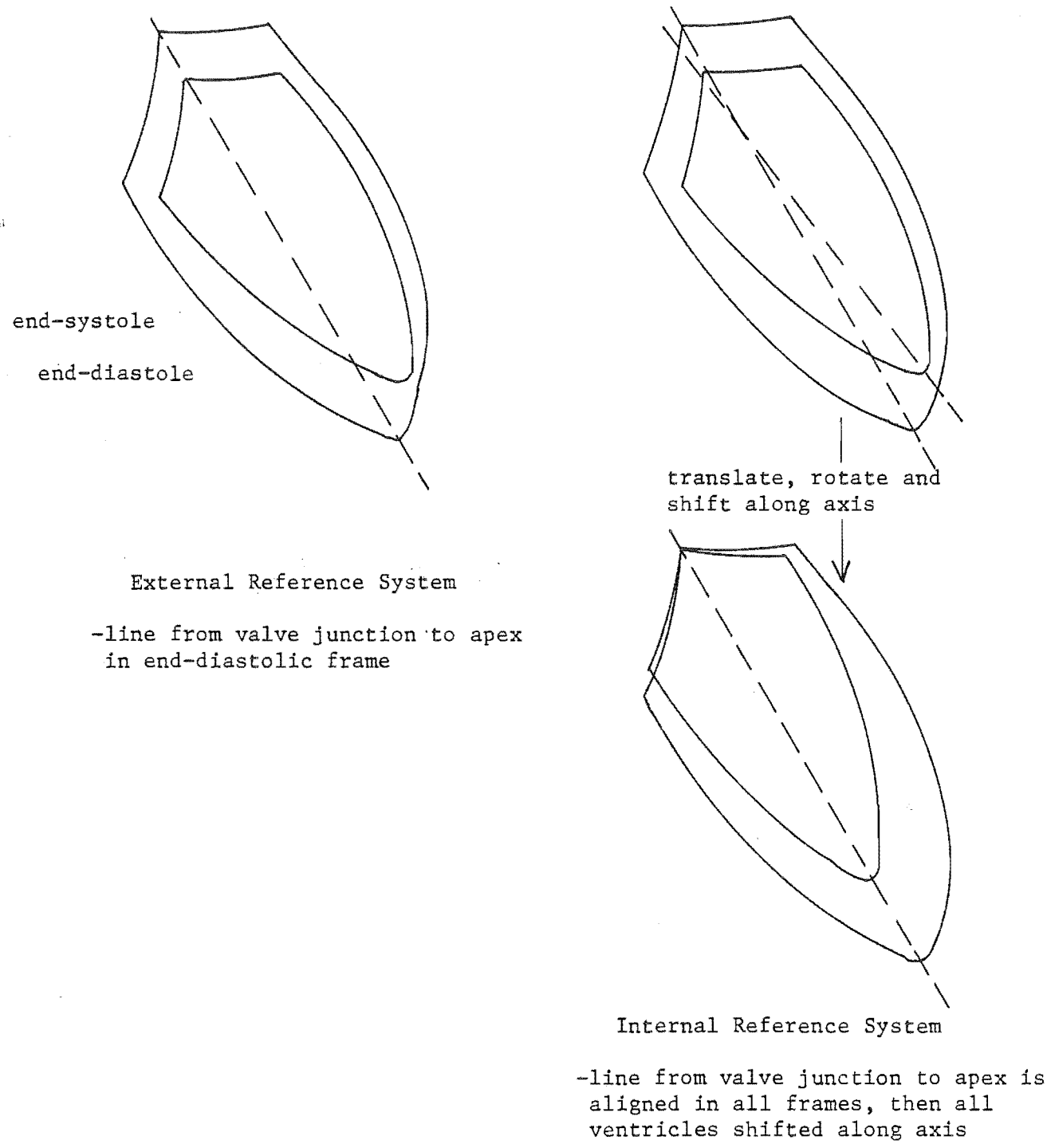

Figure 3.8 External and Internal Reference Systems.

wall are reported, notably those of Ingels et al. (1978); Alderman et al. (1979); Brower et al. (1978) and Slager et al. (1979).

Ingels et al. (1978) and Alderman et al. (1979) describe a technique where they implant several small radiopaque markers on patients ventricular walls. This is done while the patients are undergoing coronary artery

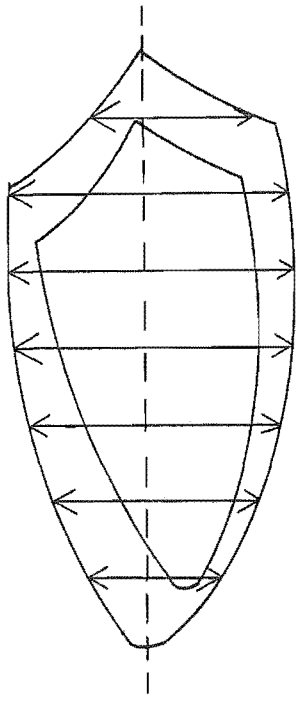

a) Hemiaxis

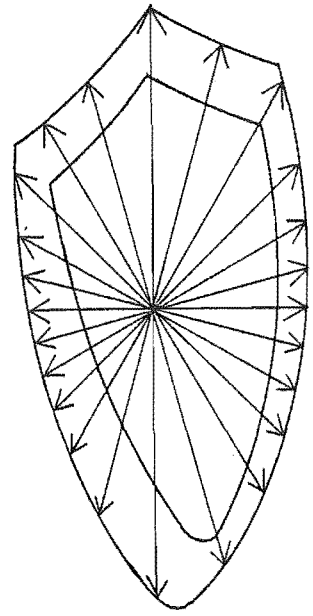

b) Radial

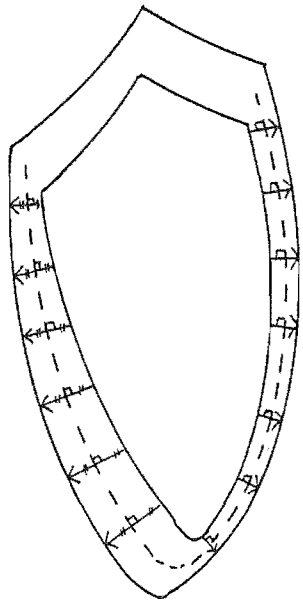

c) Perpendicular to mid-line between end-systolic and end-diastolic frames. (Bolson,1980)

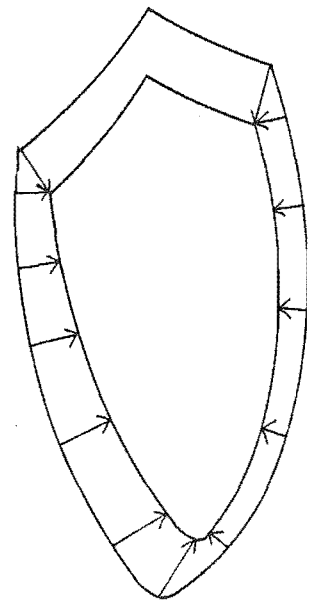

d) Nearest point on end-systolic outline from point on end-diastolic outline. (Gibson,1976,1978a)

Figure 3.9 Systems of co-ordinates.

surgery or cardiac transplant. The markers' motion is then observed using a cine X-ray technique. They claim that after surgery the ventricular walls return to a normal physiological state and therefore their motion also is normal. This claim is not easy to prove or refute. Their studies have been used to help define a centre of motion in left ventricular angiograms for use with radial axis systems of co-ordinates. They conclude that the motion is directed to a point on a line between the apex and the edge of the aortic valve. The point is situated on this line at 0.69 of the distance from the aortic valve to the apex.

The technique of Brower et al. (1978) is similar. They implant markers on poorly contracting areas of myocardium during coronary artery surgery. Their relative motion is then observed angiographically after surgery to observe the contractility of the affected myocardium.

An interesting study by Slager et al. (1979) provides a most detailed insight into myocardial movement. They identify the left ventricular boundary in cineangiograms using an automatic detection system (Slager et al., 1978). Successive images are studied and small details on the outlines are identified. The paths of the small details are then determined from frame to frame. This technique was tested using the angiograms of 23 subjects found to have normal ventricular motion. After averaging over the group to determine the motion of a 'normal' individual, it did not seem to correspond to any of the systems of co-ordinates in Figure 3.9. The motion appeared to be directed as shown in Figure 3.10.

Whichever combination of system of co-ordinates and frame of reference is used, it is also necessary to decide which parameter to measure. Some researchers measure motion in terms of fractional shortening from end-diastole to end-systole of the radial axis or hemiaxis (cf. Klausner et al., 1982). Others calculate the change in area of the sectors bounded by the radial axis during the heart cycle (cf. Baruthio, 1979; Hooghoudt et al., 1981). Some have also studied the rate of change of the lengths of the axis during the heart cycle (cf. Blair et al., 1981; Leighton et al., 1979).

Many papers have been written describing comparisons of the ability of the various combinations of reference frame, co-ordinate system and parameter to differentiate between normal and abnormal motion (cf. Papietro et al.,1978; Azancot et al., 1979; Shepertycki et al., 1979; Daughters et al., 1980). There appears to be no clear advantage in using any one combination. All exhibit some degree of success but all combinations produce a significant

number of false positive and false negative results.

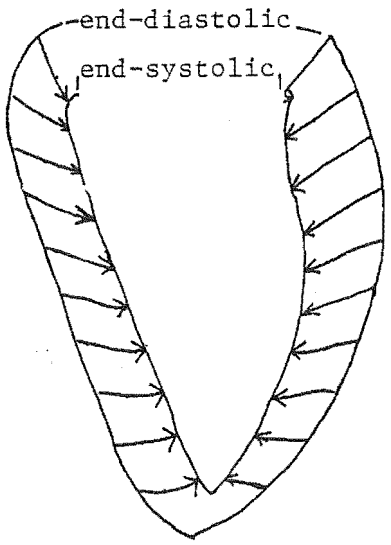

Figure 3.10 Mean systolic wall motion of 23 normal volunteers as determined by Slager et al. (1979)

3.3.2 Wall motion Using Echocardiography

Attempts at analysing regional left ventricular wall motion using two-dimensional echocardiography (2DE) have been reported only recently. Most of these are qualitative studies (cf. Horowitz et al., 1982; Visser et al., 1982a). They use scoring techniques, as in cineangiography, to classify the motion of the regions of the ventricular walls. More regions of the walls may be analysed using 2DE since transverse as well as longitudinal views can be obtained. Therefore more comprehensive studies may be performed.

Only a few quantitative analyses similar to those performed with cineangiography have been reported (cf. Bastiaans et al., 1980). Most of these analyse transverse rather than longitudinal views of the ventricles. The most comprehensive studies are those of Parisi et al. (1981) and Moynihan et al. (1981). They use a radial co-ordinate system with the chamber divided into 4 or 8 segments. While both internal and external reference systems are tried, it is of little consequence which is used. They find that fractional area changes in the sectors defined by each segment are more sensitive and specific indicators of wall motion abnormality than is fractional radial axis shortening.

Hestenes et al. (1978) report a technique similar to that used by Slager et al. (1979) to analyse motion in angiograms. Transverse views of the the left ventricles of dogs are used. They identify echoes from certain endocardial structures (such as the papillary muscles) and measure their separations throughout the heart cycle. Thus they are able to estimate the contraction in the regions between the structures. Changes in the separations are detected when the coronary arteries are blocked off.

Some researchers have attempted to construct three-dimensional ventricular outline images by combining the data obtained from several different views (cf. Matsumoto et al., 1977; Nixon and Saffer 1978; Ueda et al., 1980; Geiser et al., 1980, 1982). This allows a great deal of information about the ventricular volume, shape and movement to be extracted (cf. Geiser et al., 1980, 1982). Care must be taken to ensure correct registration of the views from which the three-dimensional reconstruction is composed.

Angiography is the 'gold standard' of cardiac imaging. Hence comparisons of echocardiographically and angiographically obtained estimates of various ventricular parameters are reported (cf. Visser et al., 1982b). Global wall motion parameters such as chamber volume and ejection fraction correlate well (cf. Gueret et al., 1980; Wyatt et al., 1979; Kronik et al., 1979).

Others have scanned dog and cadaver hearts in vitro and estimated their ventricular volumes and muscle masses from the echo images obtained (cf. Wyatt et al., 1980a, 1980b; Meerbaum et al., 1980). It is found that such parameters can be estimated accurately. Hence echocardiography is found to be suitable for studying ventricular parameters closely related to the ventricular wall position. Therefore it may be used to study wall motion.

3.4 QUANTITATIVE VENTRICULAR SHAPE DESCRIPTION

The recognition of abnormalities in the shape of the left ventricle in cardiac images is an established diagnostic procedure. For example, abnormalities are especially evident in the presence of aneurysms, local dilation, subaortic stenosis and severe hypertrophy (Brower and Meester, 1980). Few shape grading systems appear in the literature (cf. Cohen et al., 1981). These have been applied to angiographic images.

Gibson and Brown (1975) develop a shape index of

$$G = \frac{4\pi \text{ (ventricular area)}}{\text{(ventricular perimeter)}^2} \tag{3.1}$$

It is possible to classify normally shaped left ventricles (G = ·85 at end-diostole, .65 at end systole) from aneurysmal ventricles (G = .84 at end diastole, .78 at end systole). The index is aspecific in that non-ventricular shapes may have a normal shape index. For example, a square has a shape index of 0.79, which is within the range of indices for normal ventricles.

A better index is suggested by Brower (1980) and Brower and Meester (1981). They assume the shape of the ventricle to be elliptical. The length a of the major axis of an equivalent ellipse is taken to be the distance from the apex to the mitral valve/aortic valve junction. The length b of the minor axis is then calculated as

$$b = \frac{4(\text{area of ventricle})}{\pi a} \tag{3.2}$$

The eccentricity e of the ellipse defined as

$$e = \sqrt{1 - (b/a)^2} \tag{3.3}$$

is used as a shape descriptor. It allows normal and abnormal ventricles to be classified with somewhat greater specificity and sensitivity than the Gibson index.

Brower also develops a 'statistical' index to describe ventricular shape (Brower and Meester, 1981). They measure the distance from the centroid to the ventricular wall along 72 equally spaced radial axes. Their index B is then calculated as

$$B = \frac{1}{72} \sum_{i=1}^{72} \left| \frac{L_i - T_i}{S_i} \right| \qquad (3.4)$$

where T_i = average radial length along axis i in normal subjects

S_i = standard deviation of radial length along axis i in normal subjects

L_i = radial length of axis i of patient.

The sensitivity and specificity of this index for discriminating between normals and abnormals is less than Brower and Meesters' eccentricity index but is greater than that of the Gibson index.

To describe something as complex as ventricular shape using a single index is hardly feasible. The approaches of Van Wijk van Brievingh (1975) and Cohen et al. (1980) who describe it in terms of a mathematic series is more reasonable.

Van Wijk van Brievingh describes the shape using the series of coefficients in a Tschebycheff polynomial expansion of the function $r(\theta)$ where r is the centroid to wall distance at angle θ. (See Figure 3.11)

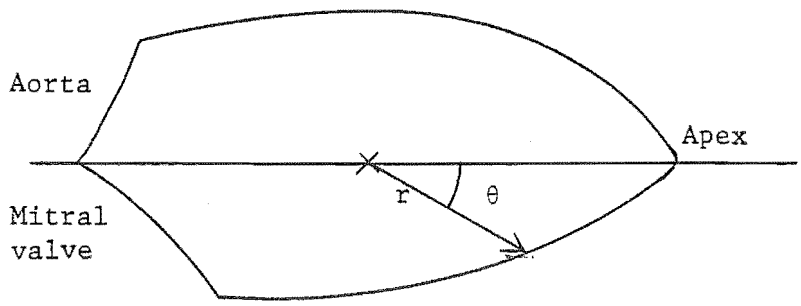

Figure 3.11 Co-ordinate system used by Van Wijk van Brievingh

The expansion is

$$r(\theta) \simeq \sum_{n=0}^{m} c_n T_n(\theta) \tag{3.5}$$

where the polynomial coefficients are defined

$$c_0 = \frac{1}{\pi} \int_{-1}^{+1} \frac{r(\theta)}{\sqrt{1 - \theta^2}} \, d\theta \tag{3.6a}$$

$$c_n = \frac{2}{\pi} \int_{-1}^{+1} \frac{r(\theta) T_n(\theta)}{\sqrt{1 - \theta^2}} \, d\theta \tag{3.6b}$$

and where the Tschebycheff polynomials are (cf. Morse and Feshbach, 1953)

$$T_o(\theta) = 1 \tag{3.7a}$$

$$T_i(\theta) = \theta \tag{3.7b}$$

$$T_{n+1}(\theta) = 2\theta T_n(\theta) - T_{n-1}(\theta) \tag{3.7c}$$

A Fourier series method of describing simple closed curves developed by Zahn and Roskies (1972) is used by Van Wijk van Brievingh (1975) and Cohen et al. (1981) to describe ventricular shape. The coefficients of the Fourier expansion

$$\phi(\ell) = \mu_o + \sum_{n=1}^{\infty} \{a_k \cos(n\ell) + b_k \sin(n\ell)\} \tag{3.8}$$

where ϕ is the angle of the tangent to the curve at a point of fractional distance along the curve from an origin (Figure 3.12) are used to describe the ventricular outline.

It is found that the coefficients are very sensitive to the shape of the curve. The ventricular outlines are input to computers by an operator

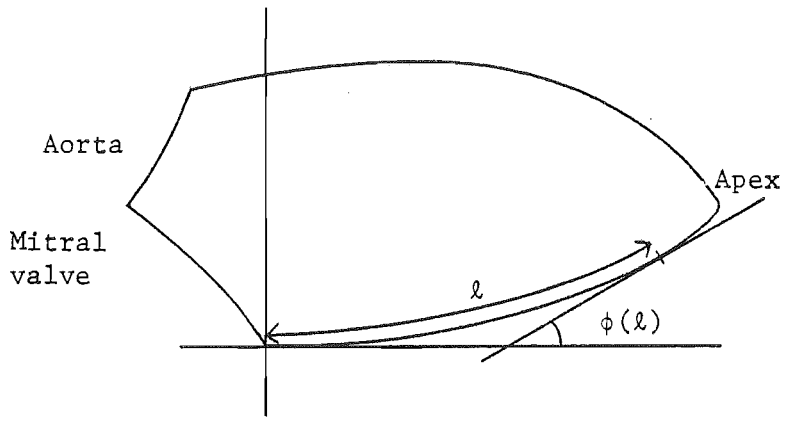

Figure 3.12 Fourier series co-ordinate system of Cohen et al., (1981) on Van Wijk van Brievingh (1975)

tracing around the outlines with such devices as light pens. The coefficients are significantly different each time the same curve is traced. Therefore these methods of describing ventricular shape have not been widely used in clinical situations.

CHAPTER 4

ECHOCARDIOGRAPHY AND IMAGE PROCESSING

4.1 INTRODUCTION

In this chapter the M-mode and two-dimensional echocardiographic techniques are discussed (§4.2). While useful diagnostic information can be obtained with these techniques, the images they produce are often of only marginal quality. This is especially true for two-dimensional scans. They tend to have a low signal-to-noise ratio (Feigenbaum, 1981) and they sometimes fail to display important cardiac structures (cf. Garcia et al., 1981a, 1981b). Better images may be obtained using digital image processing to reduce the level of noise and to enhance important details (Skorton et al., 1981). Modern commercial scanners use such techniques to produce images of high quality (cf. Ophir and Maklad, 1979). These techniques are reviewed in §4.3.

Image processing may also be used to overcome one of the major difficulties encountered when analysing heart wall motion and shape with two-dimensional echocardiography. This is the detection of the position of the endocardium. The techniques for detecting the heart walls in angiograms with the aid of computers are well developed (cf. Slager et al., 1978; Reiber et al., 1978). This is reviewed in §4.4, where it is pointed out that little research has been directed towards computer-aided heart wall detection in echocardiography.

4.2 ECHOCARDIOGRAPHY

4.2.1 M-Mode Echocardiography

Examining the heart with M-mode echocardiography can be compared to examining a darkened room with a pencil-beam torch (or flashlight). Only objects within the beam can be identified and only a limited amount of information can be recognised. While it does not provide a full two-dimensional image of the heart, M-mode echocardiography is very useful technique for evaluating cardiac function. A trained echocardiographer can readily identify abnormalities in valve and wall movement and in the size of certain structures (e.g. septal thickness). In fact, some cardiac boundaries (e.g. the endocardium) are easier to recognise in M-mode scans than they are in two dimensional scans (cf. Gibson, 1978b). A large amount of literature exists on methods of diagnosing cardiac disorders using this technique

(cf. Feigenbaum, 1976).

Echocardiographic scanning, both M-mode and two-dimensional echocardiography, is usually performed with the patient lying supine and slightly on the left side. This causes the heart to move towards the rib cage and out from behind the lungs which absorb the ultrasonic beam (Feigenbaum, 1976). M-mode scanning is usually performed with the transducer placed between the ribs at the third or fourth intercostal space. From here the heart can be examined from the atria right down to the apex. The areas of the heart traversed by the beam with the transducer pointed in different directions are illustrated in Figure 4.1. The M-mode scans which are obtained in each of these directions are presented in Figure 4.2

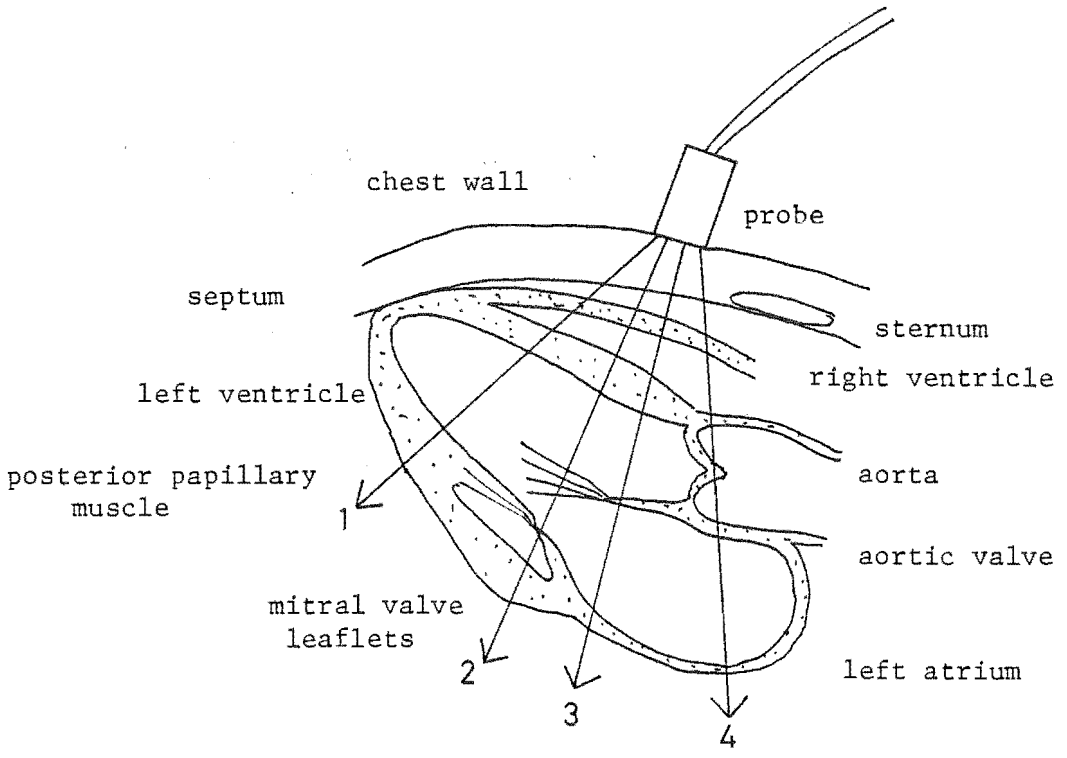

Figure 4.1 Longitudinal cross-section of the heart showing which structures are traversed by an ultrasonic beam with angled in four different directions.

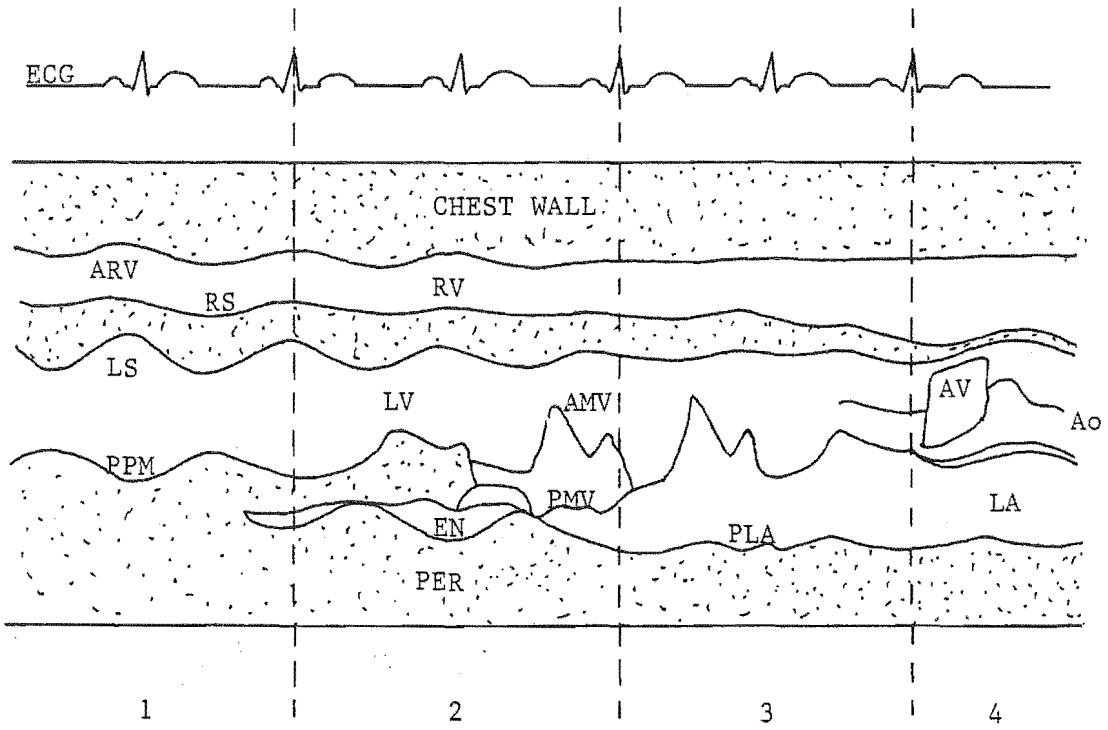

Figure 4.2 Schematic diagram of M-mode echocardiogram scanning from the apex (1) to the base of the heart (4). The regions (1) to (4) correspond to the beam positions (1) to (4) in Figure 4.1. Based on Feigenbaum (1976)

ARV - anterior right ventricular wall
RS - right septum
RV - right ventricle
LS - left septum
LV - left ventricle
AMV - anterior mitral valve leaflet
PMV - posterior mitral valve leaflet
PPM - posterior papillary muscle
EN - endocardium
LA - left atrium
PLA - posterior wall of left atrium
Ao - aorta
AV - aortic valve leaflets
PER - pericardium

4.2.2 Two-Dimensional Echocardiography

Real-time two-dimensional echocardiography (2DE) provides images of the heart which are easier to interpret than M-mode scans. The heart is seen in cross-section in which the different structures can be identified by their shape, position and motion. A reasonable knowledge of cardiac anatomy and function is necessary for an observer to understand what is being displayed as the images are often of poor quality. This is especially true of stop-frame images where there is no motion information available.

Better quantification of the size of cardiac structures is possible with 2DE. For instance, accurate estimates of ventricular volume may be obtained by combining the data from a few cross-sectional scans and a longitudinal scan (cf. Geiser et al., 1982).

Scanning is usually done at several different sites around the ribcage to obtain different cross sections. Some of the more commonly used views are illustrated in Figure 4.3 (Tajik et al., 1978)

4.2.3 Artefacts and Restrictions

While echocardiography is a useful technique it has significant limitations. First, useful images cannot be obtained on all patients. Only about 80% of the population are 'echoable' (cf. Morganroth, 1981; Maurer, 1981). There are several reasons why certain people cannot be usefully scanned. First, it is sometimes impossible to position a patient to allow the heart to move forward away from the lungs. This is especially true of people whose lungs have been enlarged by exercise or cigarette smoking (Feigenbaum, 1976). The lungs then tend to be imaged as a 'cloudiness' through which the walls and valves cannot be seen. Getting the patient to expire often reduces the apparent size of the lungs sufficiently to allow clear images to be obtained (Feigenbaum, 1981). Many obese or barrel-chested patients are 'unechoable'. There is a tendency for too much tissue to exist between the transducer and the heart in obese patients to allow sufficient signal to return to the transducer to form an image. With barrel-chested patients it is often difficult to find a position between the ribs through which the heart can be examined (Feigenbaum, 1981).

2DE images tend to contain many artifacts. An echocardiographer must be familiar with the capabilities and idiosyncracies of each scanner to be able to diagnose correctly using the images it produces.

One of the main sources of artifact is the width of the ultrasonic beam, which is more than 5 mm in some of the older scanners. More modern

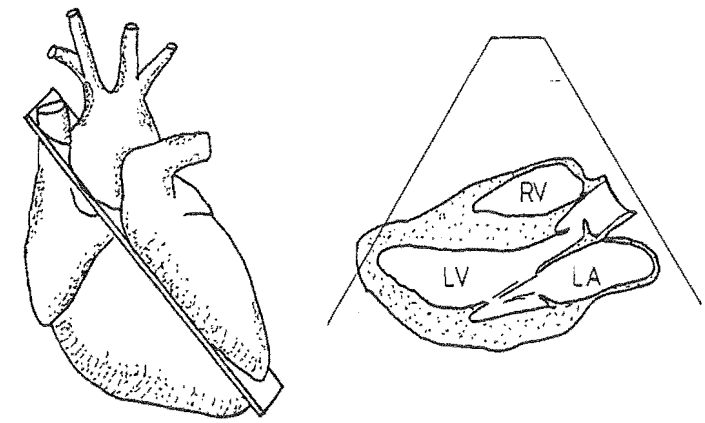

a) Parasternal long axis view.

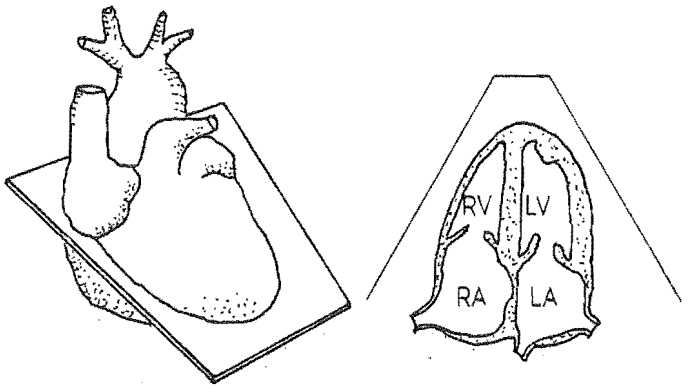

b) Apical four-chamber view.

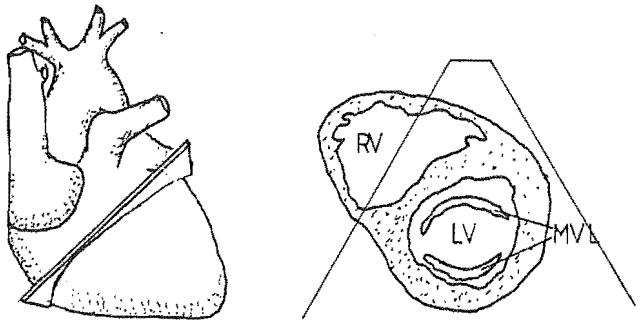

c) Parasternal short axis view at the level of the mitral valve.

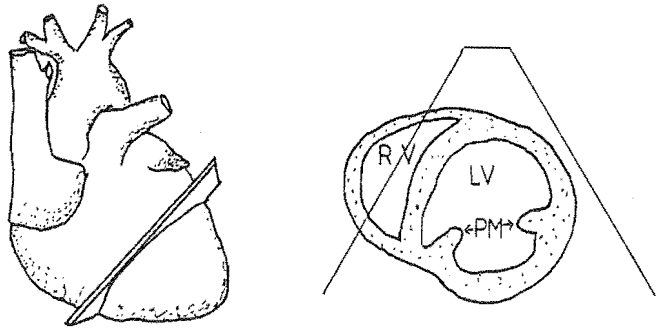

d) Parasternal short axis view at the level of the papillary muscles.

Figure 4.3 Commonly used two-dimensional echocardiographic views. The diagrams on the left indicate the plane through the heart in which the corresponding cross-section on the right is taken. LV = left ventricle, RV = right ventricle, LA = left atrium, RA = right atrium, MVL = mitral valve leaflet, PM = papillary muscles. Based on Henry et al. (1980), DeMaria et al. (1980).

machines have beamwidths of as low as 2 mm.(Latson et al., 1981). The beamwidth limits the lateral resolution of the echocardiogram (Wells, 1977). The longitudinal resolution is much less than this, typically 1 to 2 mm (Latson et al., 1981). The large beamwidth of some scanners can cause 'off-axis artifacts' which arise from structures outside the scanning plane being intercepted by the beam (Feigenbaum, 1981). The result is that echoes sometimes appear in what would be expected to be echo-free regions. This may be seen when scanning near the apex of the left ventricle. The chamber is very narrow in this region and echoes from the walls appear in the scan and make the chamber seem smaller than it really is. Also, the beam may intercept trebeculae carnae in the walls which causes a streak to appear in the middle of a ventricle (DeMaria et al.,1980)

The lateral and longitudinal resolution of a scanner is influenced by the gain of the ultrasonic receiver (Dekker and Piziali, 1972). Off-axis artefacts may be reduced by using as low a gain as possible while still obtaining a clear image. Using too high a gain may also cause echoes from the blood cells in the ventricles to be detected. This results in the chambers becoming 'cloudy', giving the appearance of structures existing within the chambers (Feigenbaum, 1981).

Some of the greatest difficulties in interpreting an image are caused by a phenomenon called 'echo dropout'. If two adjacent tissues are well matched acoustically then only a small echo is generated at their interface. This may not be large enough to be detected by the scanner (Garcia et al., 1981a). This difficulty is even more important if the interface is far from being perpendicular to the beam, since little of the echo is then scattered back to the transducer. Often the endocardium/blood boundary is not seen in two-dimensional echocardiograms because of echo dropout (cf. Skorton et al., 1981). The echoes from the epicardial or pericardial boundaries can be so much stronger than those from the endocardial boundary that the echoes from the latter are not recognised. In such cases the epicardium or the pericardium can be mistaken for the endocardium.

An ultrasonic beam does not consist of a single shaft of sound perpendicular to the transducer's face. Instead the beam consists of a central lobe of high intensity and several lower intensity sidelobes (Figure 4.4). If one of the sidelobes illuminates a strongly reflecting structure, the resulting echo detected by the scanner is positioned as though the echo came from within the central lobe. This artifact is seen

most often in phased-array scanners where the sidelobes become very intense when the beam is steered (Feigenbaum, 1981).

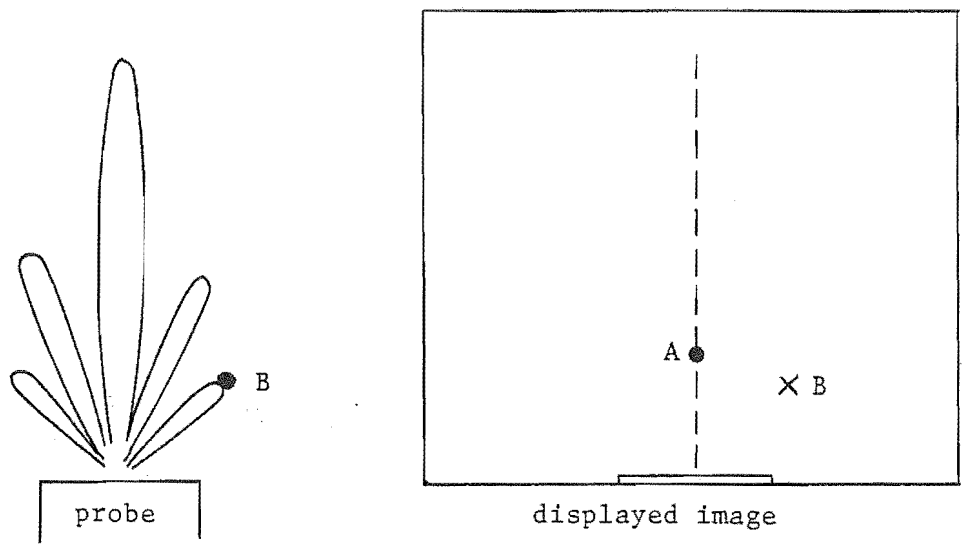

Figure 4.4 Formation of sidelobe artifacts. The true position of the object is at B where it is illuminated by a sidelobe, then is displayed at A.

Reverberation artifacts from echoes being reflected back and forth between the transducer and strongly reflecting structures are sometimes present. They appear as 'ghost images' occuring distal to the structure by which they are produced. A similar artifact occurs with mechanical scanners where reverberation occurs between the transducer elements and the plastic housing in which they rotate (Feigenbaum, 1981). This can cause multiple ghost images to form directly behind the structure from which the echo originated.

Many of these artifacts are more often recognised in two-dimensional scans. They are present in M-mode scans but, as only one spatial dimension is displayed, they are not as obvious.

4.3 IMAGE PROCESSING IN CARDIOLOGY

4.3.1 Digital Image Processing

When an image is displayed to an observer it should be presented in a form in which its details can be easily identified. The techniques used to do this constitute the science of image processing (Rosenfeld and Kak, 1976).

Since the mid-sixties when the third generation computers offered sufficient power and storage, digital image processing has developed rapidly. Modern electronic hardware has made it possible to perform image processing in real time. Such hardware is now used in many ultrasonic scanners to provide high quality images.

The more relevent aspects of image processing (cf. Pratt, 1978; Gonzalez and Wintz 1977; Bates et al., 1978) are now defined and discussed. Their application in pulse echo imaging is described in §§4.3.2 to 4.3.6.

Image reconstruction is the process of combining the data obtained by an imaging device according to a certain regime to create a useful picture. For example, a two-dimensional B-mode scan is reconstructed by combining many one-dimensional scans taken in the same plane.

Image enhancement is concerned with improving the visual appearance of pictures whose essential information is clouded but nonetheless apparent. This may be achieved by compensating for non-linearities in image recording systems by adjusting image contrast or by filtering in image or spatial frequency space.

Image restoration is the uncovering and displaying of information which has been made unrecognisable by an unwanted blurring process. The effects of the blurring on an image must first be estimated before restoration may be carried out. An example of this is the removal of the beamwidth artifact seen in many ultrasonic scans.

Image segmentation is the partitioning of an image into regions, each of which is associated with a certain feature. For instance, it may be desired to separate the region in a cineangiogram which represents the ventricle filled with radiopaque dye from the rest of the image.

4.3.2 Image Reconstruction

Digital scanners reconstruct B-mode scans by mapping many A-mode scans onto a two-dimensional array of picture elements (§2.3.6). This is easy to implement with linear array scanners. The A-mode scans are obtained along

parallel paths. They are then simply mapped into adjacent rows of pixels (Ligtvoet et al., 1977).

The mapping process with sector and compound scanners requires a series of pixel addresses describing the path of the beam in the scanning plane to be generated. The echo wave-form is sampled simultaneously. The sample values are recorded in the corresponding addresses. There are two techniques for computing the addresses, namely the 'X and Y' and the 'X or Y' boundary detection methods (Figures 4.5 and 4.6)(Ophir and Maklad, 1979)

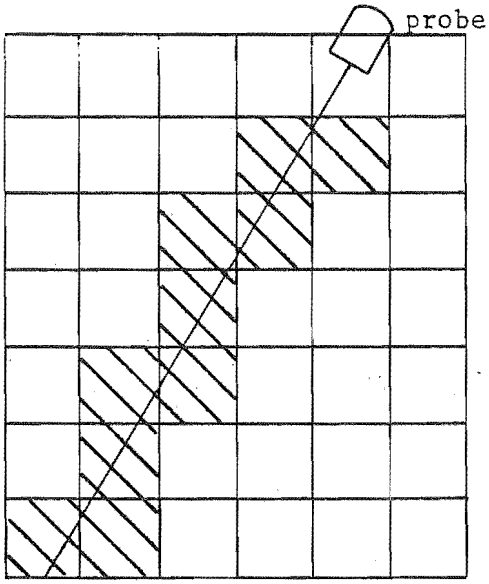

Figure 4.5 The 'X and Y' boundary detection method. With this technique more pixels are written to than with the 'X or Y' method in Figure 4.7 . The addresses of the shaded pixels are generated by the 'X and Y' method.

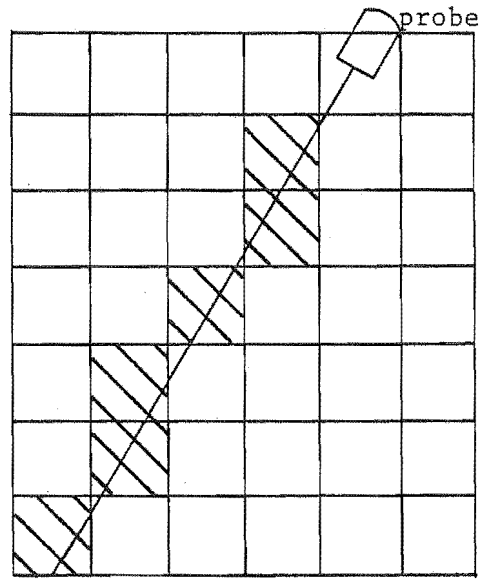

Figure 4.6 The 'X or Y' boundary detection method. The shaded pixels are those whose addresses are generated by this method.

When the 'X and Y' method is used, a pixel address is generated everytime a pixel boundary is crossed by the beam path. The 'X or Y' method, however, generates addresses only when boundaries parallel to one axis are crossed. The axis chosen is that which subtends the smallest angle to the direction of the beam. This method generates less addresses than the'X and Y' method allowing a lower sampling rate to be used.

When compound scanning is performed, any one pixel may be crossed by the beam many times as the image is generated. A similar situation arises with sector scanners close to the apex of the sector. Several algorithms

have been developed to determine the value to be stored in the pixel address. The algorithms are called 'modes'. Some of these are now described.

Survey mode: The previously stored pixel value is simply replaced with the latest value. A completely new image is generated each time an area is scanned (McDicken, 1981).

Peak mode: the old value is compared to the new value and is replaced by it if the new value is larger (Robinson, 1972). Hence as a region is successively rescanned, its brightness increases (even to saturation if it is done too often). A similar effect can be achieved by employing:

Integration mode: in this mode, the stored value is the sum of all the values assigned to that pixel (Ophir and Maklad, 1979). This saturation effect is overcome by using:

Average mode or Normalised mode: the scan of the values is divided by the number of values (McSherry and Keller, 1974). When operating in this mode, strong specular reflections in a scan tend to be diminished. This is because they are averaged with weaker reflections when the same point is viewed from different directions.

Peak-average mode: this technique, which has been developed by Ophir et al., (1974), involves recording both the average mode and the peak mode values. If the difference between the maximum value and the average value is greater than an operator defined threshold, then the maximum value is displayed. If not, the average value is displayed. In this way the specular echoes in the display are maintained along with the averaged values of the diffuse scatterers.

Exponential modes: each pixel is updated by a weighted average of the previously stored and the latest values (Ophir and Maklad, 1979; McDicken, 1981).

The relative usefulness of all the various modes has yet to be assessed (McDicken, 1981).

As well as some pixels being overwritten several times when compound scanning is used the possibility exists that any one pixel will not be crossed by the beam path at all. Various gap filling algorithms have been developed to fill the 'holes' in the scans (Ophir and Maklad, 1979).

4.3.3 Image Enhancement

The image enhancement techniques which are useful in processing B-mode scans may be classified as 'contrast manipulation' and 'filtering' techniques. Contrast manipulation is used extensively in commercial scanning systems.

It involves altering the echo-amplitude transfer function between the various stages of the ultrasonic receiver/amplifier/display system. It emphasises features such as small echoes scattered from within tissues or it matches the dynamic range of an image to that of the display. The latter is often called 'dynamic range compression'.

Filtering techniques are used with two-dimensional images reconstructed by B-mode scanners (cf. McSherry and Keller, 1974). Such processing is unfortunately not available with most commercial scanners. It is implemented using the transformation process illustrated in Figure 4.7 which is only feasible with the aid of a mini- or micro-computer.

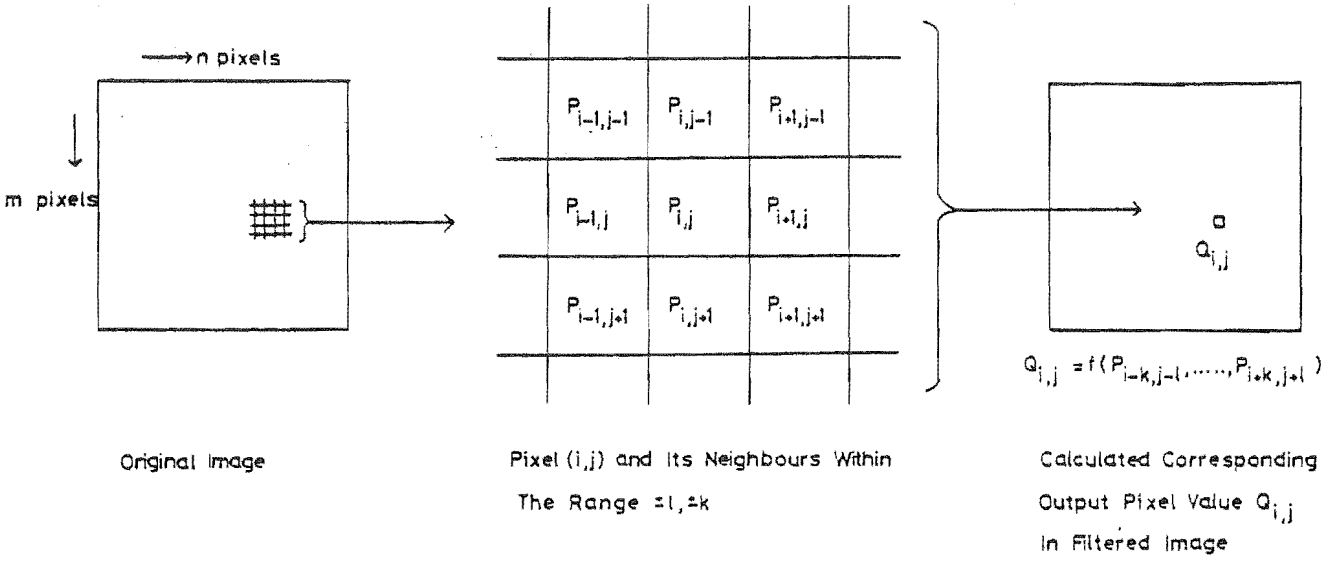

Figure 4.7 The image filtering transformation process.

The transformation process is as follows. A typical pixel (i,j) of an image, composed of an array of m x n pixels, is assigned the value $P_{i,j}$. Filtering is performed by assigning to each pixel in the filtered image a value $Q_{i,j}$ calculated from the values of the same pixel and its relatively close neighbours according to a specified rule called the filter function (Round et al., 1982).

In image enhancement, the selection of a filter function is done on a rather ad hoc basis (Rosenfeld and Kak, 1976) rather than by designing it to remove a recognised distortion according to a knowledge of how that distortion alters the image. There is, in fact, evidence that introducing distortions can produce images which are more appealing to the eye (Pratt, 1978).

4.3.4 Contrast Manipulation

Contrast manipulation is used to provide a suitable transfer function between an image and the device on which it is displayed. It is also used to correct non-linearities in the transfer functions between the components of imaging systems. Methods for determining a transfer function are found in many standard image processing textbooks (cf. Pratt, 1978; Kak and Rosenfeld, 1976; Gonzalez and Wintz, 1977). The principles involved and their application in ultrasonography are now discussed.

Suppose an image has been quantised to 256 grey levels (represented by 8 bits) and it is to be displayed on a device in only 16 grey levels (4 bits). The simplest transfer function is 'linear', this being illustrated in Figure 4.8. Each consecutive group of 16 input grey levels is mapped into a single display grey level.

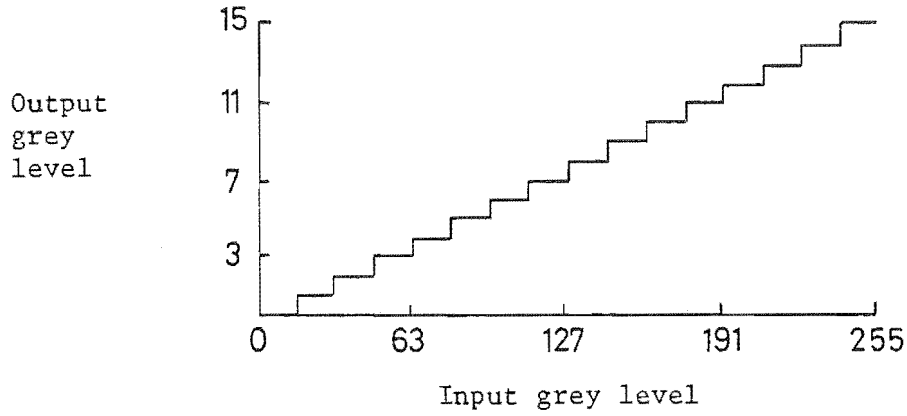

Figure 4.8 Linear transfer function from 8 bit input to 4 bit output

Not all of the possible input grey levels will necessarily be represented by the pixel values of an image. Suppose the lowest input grey level is A and the highest is B. Using the transfer function just described, a low contrast image which does not use all of the output grey levels is produced. In this case, it is better to use the 'clipped' linear transfer function which maps the input grey level range onto the display range as in

Figure 4.9.

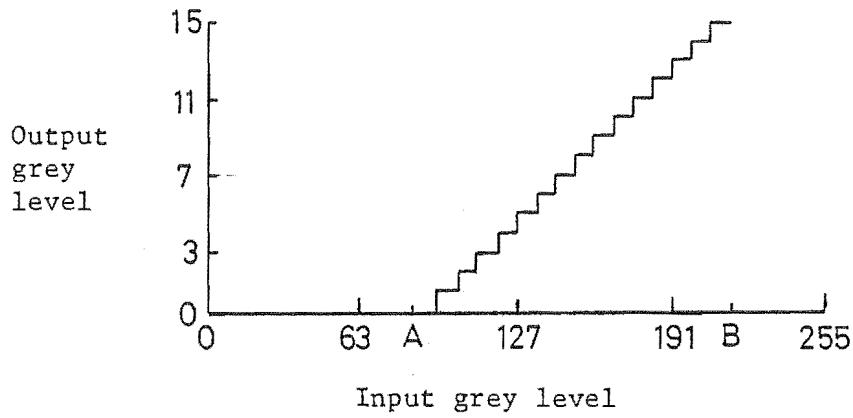

Figure 4.9 Clipped linear transfer function for an image with lowest input value A and highest B

Suppose that the distribution of grey levels is skewed so that more pixels have levels nearer A than B. Using a clipped linear transfer function will result in a dark toned image being displayed. By using non-linear transfer functions between the recorded image and the displayed image it is possible to fully utilize all of the grey levels in the display (cf. Gonzalez and Wintz 1977; Pratt, 1978). This is illustrated in Figure 4.10. Suppose an image has been recorded as 16 grey levels and is to be displayed on a device as 8 grey levels. The numbers of pixels in each of the 16 grey levels are represented in the histogram in Figure 4.10. There are more pixels with lower pixel values than higher ones. A transfer function is chosen so that the output intensities are made to appear in an approximately equal number of pixels. The resulting image is said to be 'histogram equalised'. Details in parts of the image containing more of the most popular intensities are usually more apparent in the equalised image.

More presentable images can sometimes be obtained by using transfer functions designed to produce an unequalised histogram. Frei (1978) suggests that the histogram of the output image should be designed so that the logarthmic response of the human eye is accounted for. This is done by choosing the output images histogram to have a hyperbolic shape. The process is therefore called 'histogram hyperbolisation'. Some image processing systems have been designed so that the operator can define any arbitrary transfer function. The operator decides on the best function for an image by trial and

error (Gonzalez and Wintz, 1977).

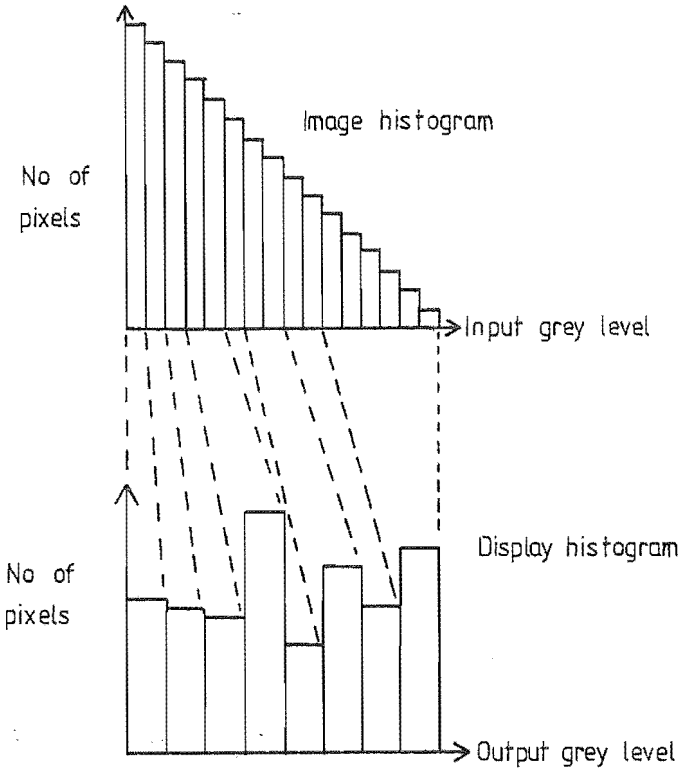

Figure 4.10 Histogram equalisation of an image sampled to an accuracy of 16 grey levels for display as only 8 grey levels. The histogram of the displayed image is approximately 'flat'.

In modern scanners with digital scan converters, contrast modification is performed by their pre-processing and post-processing units. In the pre-processing unit the video signal which is sampled to an 8 bit precision is mapped into the main memory of only 4 or 5 bit precision. Usually several different transfer functions are stored as 'look-up tables' in read-only memories (Ophir and Maklad, 1979). Four commonly used transfer functions are presented in Figure 4.11 (McDicken, 1981).

The post-processing unit permits further contrast manipulation to be performed between the main memory and the display screen. Four of these transfer function options are illustrated in Figure 4.12 Often the post-processing options are not used as a satisfactory image is usually obtained using only pre-processing.

Some researchers have found that histogram equalisation provides a satisfactory memory to display transfer functions (Round et al., 1982). Others have found that other transfer functions provide a better image (Robinson et al., 1982). A function which is satisfactory when imaging one organ may not necessarily be suitable for displaying others.

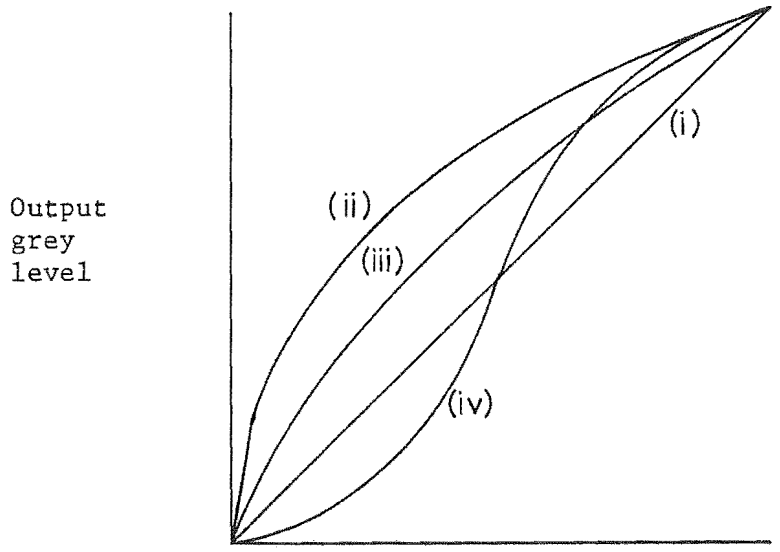

Figure 4.11 Suggested pre-processing transfer functions.

Function (i) linear transfer involving no contrast modification
" (ii) logarithmic compression to enhance weak echoes
" (iii) similar to (ii) but with less emphasis on weak echoes
" (iv) mid-range echoes favoured to delineate anatomic surfaces of internal structure.

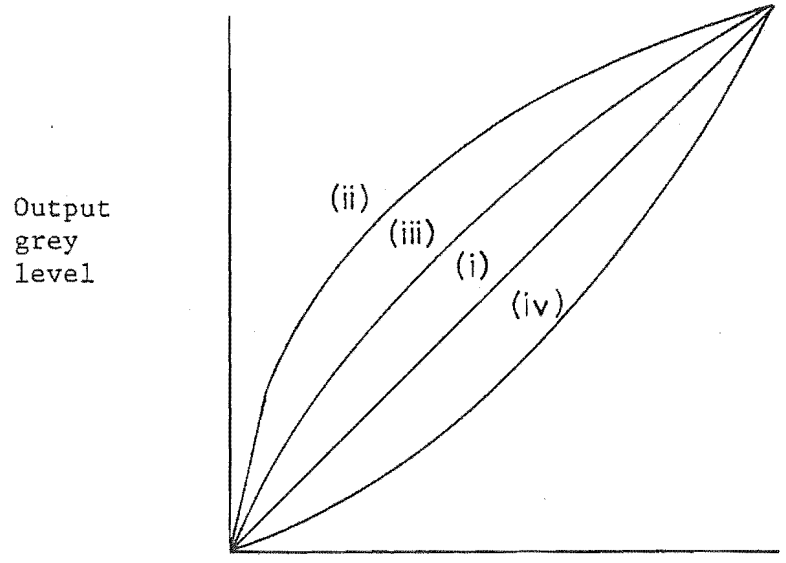

Figure 4.12 Suggested post-processing transfer functions.

Function (i) linear function involving no contrast modification
" (ii) high contrast output to compress high level signals
" (iii) medium contrast output
" (iv) low contrast output.

4.3.5 Filtering Techniques

Filtering techniques are used in image enhancement to reduce noise and to crispen the edges of details in images.

a) Noise Reduction

Noise often appears in an image as a 'graininess' or by some pixels having very different values from their near neighbours. Noise can be suppressed using one or more of the following filter functions:

Processing an image with the filter function (using the same notation as in Figure 4.8)

$$Q_{i,j} = \sum_{a=i-k}^{i+k} \sum_{b=j-\ell}^{j+\ell} W_{a,b} P_{a,b} \qquad (4.1)$$

where $W_{a,b} \geq 0$

and $\sum_{a,b} W_{a,b} = 1$

is known as 'local average filtering', low pass filtering' or smoothing' (Pratt, 1978). The value $Q_{i,j}$ of each pixel in the filtered image is found using the values of the corresponding pixel and its neighbours in the original image as estimates of that pixel's true value. $Q_{i,j}$ is calculated by taking a weighted average of these estimates. The elements of the weight array (or filter mask) $W_{a,b}$ are non-negative and their sum is unity. Noise smoothing of ultrasonic scans is described by McSherry and Keller (1974) who find it to be a useful technique for reducing noise in cardiac imaging. A similar technique is described by Parker et al. (1979), for enhancing echoes from the endocardium.

A further technique is to add together several images of the same scene with different noise content. The noise in the resulting image then tends to be only $1/\sqrt{N}$ times the noise in any one image (Garcia et al., 1981a). This has been applied in some real time scanners because successive images are often sufficiently similar to be considered identical. The scanners have several main memories each of which contains a different image which are added to the others, (Varian, 1980).

The appearance of noise as pixels with values which differ greatly from their neighbours is used as the basis of 'out-range filtering' (Pratt, 1978). Each pixel is sequentially examined and if its value is different from the mean of its neighbours, by a specified level, it is considered to contain noise. The mean of its neighbours is used as an estimate of its value in the filtered image. The filter function is

$$Q_{i,j} = P_{i,j} \qquad \text{if} \qquad |P_{i,j} - \text{est}(P_{i,j})| \leqslant R$$

$$= \text{est}(P_{i,j}) \qquad \text{otherwise}$$

where R is the threshold level and

$$\text{est}(P_{i,j}) = \frac{\left(\sum_{a=i-\ell}^{i+\ell} \sum_{b=j-k}^{j+k} P_{a,b} \right) - P_{i,j}}{(2\ell + 1)(2k + 1) - 1} \quad . \tag{4.2}$$

Median filtering (Tukey, 1971) is a noise reduction technique which also attempts to estimate the value assigned to a pixel according to that of itself and its neighbours. The estimate used is the median value of the pixels. The filter function is

$$Q_{i,j} = \text{med}(P_{a,b}) \qquad a \in i-\ell, i-\ell+1, \ldots\ldots, i+\ell \qquad b \in j-k, j-k+1, \ldots\ldots, j+k \tag{4.3}$$

where $\text{med}(P_{a,b})$ is the median value $P_{a,b}$ in the ranges of a and b defined in (4.3).

While these filters can reduce noise, they also blur images and reduce the sharpness of edges. Techniques to reduce noise in angiograms and radiocardiograms while maintaining edge crispness have been reported (cf. Keshavan et al., 1978). The assumption is made that if an edge passes through the region of a pixel and its neighbours, it may be possible to decide on which side of the line the pixel lies. The decision is made by considering the grey levels of each pixel in the neighbourhood. Smoothing is then done by one of the above techniques using the values of the pixels only on the same side

of the line (cf. Lev et al., 1977; Eklundh et al., 1980). Some of these techniques require excessive computation for them to be used very often. Other techniques are based on the assumption that the image can tolerate more noise in regions of large pixel values (cf. Trussel, 1977). Therefore, smoothing is applied only to regions containing low pixel values.

b) Edge Crispening

Psychophysical experiments indicate that a photograph or picture in which which the details have accentuated edges is often more pleasing to the eye than is an exact reproduction (Pratt, 1978). Such edge enhancement or crispening is accomplished by using one of the techniques now described.

One of the most common techniques is Laplacian filtering (cf. Gonzalez and Wintz, 1977; Rosenfeld and Kak, 1976). It involves calculating the differences in magnitude between the values of a pixel and its neighbours. This is done by convolving a weight array with an image as was described for local average filtering. The weights are now permitted to be negative as well as positive and are chosen so that their sum is zero. The filter functions are therefore of the form:

$$Q_{i,j} = \sum_{a=i-k}^{i+k} \sum_{b=j-\ell}^{j+\ell} W_{a,b} P_{a,b} \qquad (4.4)$$

where $\sum_{a,b} W_{a,b} = 0$.

Typical 3 x 3 element Laplacian filter arrays are

$$\begin{bmatrix} 0 & -1 & 0 \\ -1 & 4 & -1 \\ 0 & -1 & 0 \end{bmatrix} \qquad \begin{bmatrix} -1 & -1 & -1 \\ -1 & 8 & -1 \\ -1 & -1 & -1 \end{bmatrix} \qquad \begin{bmatrix} 1 & -2 & 1 \\ -2 & 4 & -2 \\ 1 & -2 & 1 \end{bmatrix}$$

(a) (b) (c)

Laplacian filters have an unfortunate tendency to act as edge detectors and produce images which are not very pleasing to the eye (Round et al., 1982). A visually more pleasing effect is obtained by combining the Laplacian image with the original in a certain ratio to maintain the character of the original while obtaining the advantage of having the edges well defined. This process

is similar to the 'grey scale' imaging described by Kossoff (cf. §2.3).

Another form of edge enhancement is called 'statistical differencing' (Wallis, 1976). It involves generating an image by dividing each pixel value by its statistical deviation $\sigma_{i,j}$ from its neighbours according to the relation

$$Q_{i,j} = \frac{P_{i,j}}{\sigma_{i,j}} \tag{4.5}$$

where $$\sigma^2_{i,j} = \sum_{a=i-k}^{i+k} \sum_{b=j-\ell}^{j+\ell} (P_{i,j} - \overline{P_{i,j}})^2$$

when $$\overline{P_{i,j}} = \frac{\sum_{a=i-k}^{i+k} \sum_{b=j-\ell}^{j+\ell} P_{i,j}}{(2k+1)(2\ell+1)}$$

= mean value of $P_{i,j}$ and its neighbours.

The enhanced image pixel values is increased in magnitude at edge points which deviate from their neighbours and decreased in amplitude elsewhere.

Many other edge enhancement functions are described in the literature (cf. Argyle, 1971; Roberts, 1965; Sobel, 1973; Kirsch, 1971; Rosenfeld, 1970; Rosenfeld and Thurston, 1971).

Implementing these filters in real tissue with echo scanners is usually very difficult due to the large amount of data to be processed and the complexity of the filter functions. Thurstone and Abbott (1977) report the development of a system capable of filtering echo images in real time. It was interfaced to a phased array scanner. Their system is capable of performing local average and Laplacian filtering in two dimensions with and 11 x 11 array and in time for up to 4 frames. Such processing cannot normally be done with commercially available scanners.

4.3.6 Image Restoration

When an image is recorded, it is usually subjected to degradation by noise and by the transfer function of the recording device. The objective of image restoration is to ameliorate the degradations so as to recover the best possible estimate of the original image (Pratt, 1978). This process has been termed 'inverse filtering'.

In pulse-echo imaging the main degradation to images is the beamwidth artifact (cf.§4.2.3). This causes single point reflectors to appear as a long streak perpendicular to the direction of the beam. It limits the axial resolution of the image. Similarly, the pulse length of the beam degrades the axial resolution. The image can be modelled as a series of point reflectors convolved with the point spread functions of the beam cross section and the pulse shape.

Several workers report attempts to design inverse filters to deconvolve the point spread functions and restore the image (cf. McSherry, 1973; McSherry and Keller, 1974). McSherry (1974) improves axial resolution by inverse filtering the radiofrequency wave train obtained by an echo scanning system. She utilizes filtering techniques described by Treitel and Robinson (1966). She also proposes removing the beamwidth artifact in a similar manner but notes that this is more difficult to achieve particularly when imaging moving organs. To do this effectively, the beamwidth must be sampled many times as it scans past each reflector. The reflector must not move as the beam passes it, or the received beam pattern will be distorted. Therefore it can be expected to be successful only when imaging static organs.

More recent attempts are reported by Hundt and Trautenberg (1980). They show that it is possible to almost double the resolution of images of needles scanned in a water bath. An increase in resolution of this order is predicted by Vollman (1982) provided that the signal-to-noise ratio is sufficiently large. McSherry (1974) and Hundt and Trautenberg (1980) do not present the results of any in vivo work. They both note that a single filter cannot be applied to remove the beamwidth artifact at all distances from the transducer, as the beam pattern changes with range. Also, if sector, or other non-parallel scanning patterns, are used the inverse filter changes as the beamwidth is sampled at different points and at different numbers of points in the image. Certain tissues and organs also tend to distort the beam (Round, 1977). Hence it is very difficult to design and implement an inverse filtering system to achieve this.

4.4 SEGMENTATION OF CARDIAC IMAGES

The objective of segmentation is to partition an image into 'meaningful regions' (Gonzalez and Wintz, 1977). The definition of a 'meaningful region' depends on the problem being considered. In chapter 6 of this thesis, studies of heart wall motion are described. For these, it is necessary to delineate the ventricular wall in echocardiograms. In this case the 'meaningful regions' are the left ventricular cavity and the areas outside that cavity.

Wall motion studies using cineangiograms are more common than those using echocardiograms (cf. Azancot et al., 1978; Hestenes et al., 1978). Computer-aided detection of ventricular walls in angiograms is better developed than in echocardiograms. In this section the techniques used with both imaging techniques are discussed.

4.4.1 Detection of Ventricular Walls in Angiograms

In many centres where heart wall motion using cineangiograms is analysed by computers, the ventricular outline is manually traced into the computer using lightpens, etc (cf. Besse et al., 1977; Balocchi et al., 1977). Some fully automatic boundary detection schemes are reported (cf. Smalling et al., 1975; Chow and Kaneko, 1973). These schemes usually only work on images in which the ventricular outline can be easily identified visually. Semi-automatic techniques are more commonly used (cf. Slager et al., 1978; Brunt et al., 1979). These require the operator to define certain points on the ventricular outline (or even the entire outline) in one image of a series. The computer then uses this information to define the contour in successive images.

Several characteristics of the different regions have been utilized to segment the images into ventricular and non-ventricular areas. Some systems utilize only one of these to estimate the position of the boundary between the regions (cf. Chow and Kaneko, 1972). Others take a weighted average of the estimates obtained by analysing several different characteristics (cf. Barrett et al., 1976, 1980). The methods employed by a number of researchers are presented in Table 4.1. The use of the various characteristics is now discussed.

Almost all schemes use pixel value thresholding. Pixels representing the ventricles tend to have higher values than those outside. A pixel value threshold is chosen and all pixels with values greater than the threshold are classified as being within the ventricle and those with lower values as being outside. The radiopaque dye used in angiography does not mix evenly within the ventricles. Therefore, even within the ventricles some pixel values tend to

Researchers \ Parameter	Grey level Threshold	Gradient Thresholding	Profile Matching	Contour Following	Time - Position Estimating	Model Outline
Fujita et al. (1981)				√		
Brunt et al. (1979)	√	√			√	
Barrett et al., (1976, 1980); Clayton et al., (1974)	√		√	√	√	√
Chow and Kaneko (1972, 1973)	√					
Smalling et al. (1976)	√	√				
Modestino et al. (1976)				√		
DeJong and Slager (1975); Slager et al., (1978)	√			√		
Balocchi et al. (1977)					√	
Tasto (1974)	√					

Table 4.1 Parameters used to detect ventricular boundaries in cineangiograms

be below the threshold. Within other organs, such as the ribs, some pixel values may be greater than the threshold. Hence, a single threshold value cannot be used over the entire image (Chow and Kaneko, 1972, 1973). A different threshold is often defined in different parts of the image (cf. DeJong and Slager, 1975).

If the image is scanned in a raster fashion, the pixel values rise quickly as the ventricle is entered and fall as it is exited. By detecting this change, the boundary is assumed to be crossed when the rate of change in pixel value is greater than a defined threshold (cf. Smalling et al, 1975). More sophisticated algorithms assume that the shape of the pixel value profile of the ventricular boundary is known. The boundary is then detected in the image by comparing the assumed profile with the actual image profile at all points across the image. The point of best match is taken to be the boundary position (cf. Barrett et al., 1976, 1980).

Some of the automatic detection systems raster-scan the angiograms. The boundary is detected twice on each raster line. The boundary positions

on the next raster line must necessarily be close to those on the preceeding lines. The expected position of the ventricle wall on that line is then calculated from the previous positions (cf. DeJong and Slager, 1975). This scheme is often employed in the weighted average systems (cf. Barrett et al., 1976, 1980).

Similarly, if a number of consecutive images taken throughout the same heart cycle are analysed, the wall position in any one frame can be estimated from its position in the preceeding images (cf. Brunt et al., 1979).

To confirm that realistic ventricular outlines are obtained, some systems compare them with a 'model' outline based on that of a normal subject. This scheme has been used in some automatic systems (cf. Barrett et al., 1976, 1980). Model outlines are also used to provide an initial estimate of boundary position in such systems (Brunt et al., 1979).

4.4.2 Detection of Ventricular Walls in Echocardiograms

It is difficult to detect the ventricular walls in echocardiographic images without the aid of a computer. Echo dropout over part or all of the wall makes it possible to mistake the epi- or pericardial echoes for the endocardial echo. Even in high quality scans the endocardium often seems to be discontinuous, like a series of closely spaced dots. The techniques which some workers have used to estimate its outline are similar to those used to detect the ventricular outline in angiograms.

Skorton et al., (1981) detect the endocardial echoes in images obtained by averaging several frames to reduce noise. The images are processed with a Sobel edge detector (cf. §4.3) to create a map of the boundaries in the image. The edge map is considered to correctly define the endocardial curve, although sections of it may be missing in the map due to echo dropout. The original image is then grey level thresholded to detect the walls (cf. §4.4.1) with the threshold set at several different values. Provided that the threshold is not set at too high a value, an unbroken endocardial outline is seen. The thresholded image in which the endocardial curve best matches the Sobel edge map curve is used to define the endocardium.

Garcia et al., (1981a) detect the ventricular walls by studying the variation in pixel values along radial lines from the centre of the ventricle. The endocardium is assumed to be detected when the pixel values rise above a certain threshold or when a point of inflexion in the second derivative of the pixel values is detected. They also note that the shape of the echoes is

not symmetrical, and that this may cause an operator who is manually tracing the boundary to follow different parts of the echo in different parts of a ventricular image. The echoes have a fast rising edge and a long trailing edge (Figure 4.13). Hence, when tracing around the posterior wall of the chamber, the operator follows the rising edge, but at the anterior wall the trailing edge is traced. Outlines are corrected for this factor.

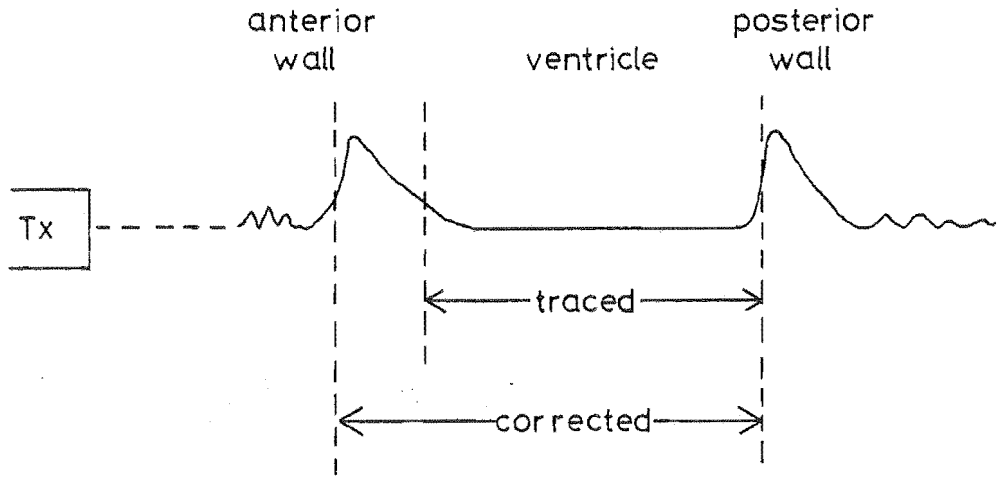

Figure 4.13 Incorrectly traced endocardial echoes at the anterior wall and their correct position

Automatic recognition of the ventricular borders (both peri- and endocardial) using a knowledge of the pixel value profile at these boundaries has has been performed by Robison et al., (1976). This is similar to the scheme used by Clayton et al., (1974) for detecting the walls in angiograms (cf.§4.4.1).

Detection of the endocardial border for studies of wall motion using M-mode images is also reported. This is usually performed manually (cf. De Coodt et al., 1975) although some automatic systems have been described (cf. Veerbeek et al., 1977). These usually require the operation to indicate to a computer which echo is to be detected. This echo is then followed in real time by the computer. The position of the echo is found using pixel value thresholding (cf. Ledley and Wilson, 1974) or by finding the longest echo within a window placed in the region where the wall is expected to be found (cf. Hirsch et al., 1973; Hosteler et al., 1980).

CHAPTER 5

ACQUIRING AND PROCESSING ECHOCARDIOGRAMS

5.1 INTRODUCTION

Much of the research described in this thesis is directed towards quantifying the shape and the motion of the left ventricle. The experimental work has been performed echocardiographically rather than angiographically. If the experiments had been carried out angiographically, very few studies of the same patient would have been possible, since the accumulated X-radiation dose would have been more than is ethically (or legally) permissible. Angiography is also a very traumatic and expensive procedure. The patient is usually sedated and is therefore unable to participate in studies of the effect of exercise on the heart.

Echocardiography suffers from none of the above difficulties. It is noninvasive in both the physical and radiation senses. Therefore serial studies may be performed and data can be collected readily with the patient co-operating fully. Few personnel are needed and little expense is involved.

The main disadvantage of echocardiography is that satisfactory images cannot be obtained with all patients. Usually it is old, obese or heavy smoking individuals (who are most at risk from heart disease) who are the hardest to image successfully. The endocardial echo is usually hard to identify in two-dimensional scans, because the signal from this boundary is weak. Often the epicardial or pericardial border is more obvious and can be mistaken for the endocardial border. This difficulty is not as great with M-mode scans because they have a much higher signal-to-noise ratio. They also display the motion of the various borders which can often be used to identify the endocardium.

It should be noted that there is a fundamental difference in the images obtained by the two techniques discussed above. Angiography provides shadow images of the ventricles and not true cross-sectional views. Hence some concavities within the ventricles may not be detected. Two-dimensional echocardiography does provide true cross-sections, although there may be some distortion due to beam refraction. It also enables many different cross-sectional views of the ventricles to be obtained whereas only a few views are usually obtained with angiography.

However, two-dimensional echocardiograms are inherently less reproducible than angiograms. Angiograms are 'shadow' images. Therefore translating the heart slightly in a direction perpendicular to the X-ray beam will not significantly change the image. Translating the heart slightly perpendicular to the scanning plane of a two-dimensional echocardiogram, however, significantly changes the image. A completely different slice through the heart is then imaged (see Figure 5.1). Its few disadvantages and several significant advantages indicated that my research should be done with echocardiography rather than angiography.

In §5.2 the development of an electronic system for obtaining echocardiograms from a commercial sector scanner is described. The echocardiograms obtained with this system are passed to a computer where they are processed to make them visually more pleasing and to enhance the endocardial curve. This is described in §5.3. Techniques for interactively extracting the curve in a series of sector scans are discussed in §5.4. The equipment and techniques developed have been used in the experiments described in Chapters 6 and 7.

5.2 A SYSTEM FOR ACQUIRING TWO-DIMENSIONAL ECHOCARDIOGRAMS

Several methods of recording two-dimensional echocardiograms in formats suitable for computer processing have been reported in the literature. The earliest, those of McSherry (1973) and Pryor et al., (1978) are not based on real time sector scanners but on A-mode or M-mode scanners. A transducer pulse repetition frequency of only 50 Hz is used so that single A-mode lines of data can be sampled at 2 MHz and stored in computer memory between each excitation. The transducer position and direction and the subject's E.C.G. are also recorded. Two dimensional images of the heart at a given point in its cycle are reconstructed by combining A-mode images obtained from many heart cycles observed from different positions and in different directions.

Hestenes et al., (1978) and Skorton et al., (1981) using commercial sector scanners record two-dimensional scans on videotape. The scans are replayed and photographed. A flying-spot scanner is then used to input the images to a computer.

Sophisticated interfaces between commercial scanners and computers are described by Garcia et al., (1981a,b) and Jensch et al., (1981). The Garcia system digitises and stores sector scans at rates of up to 30 frames per

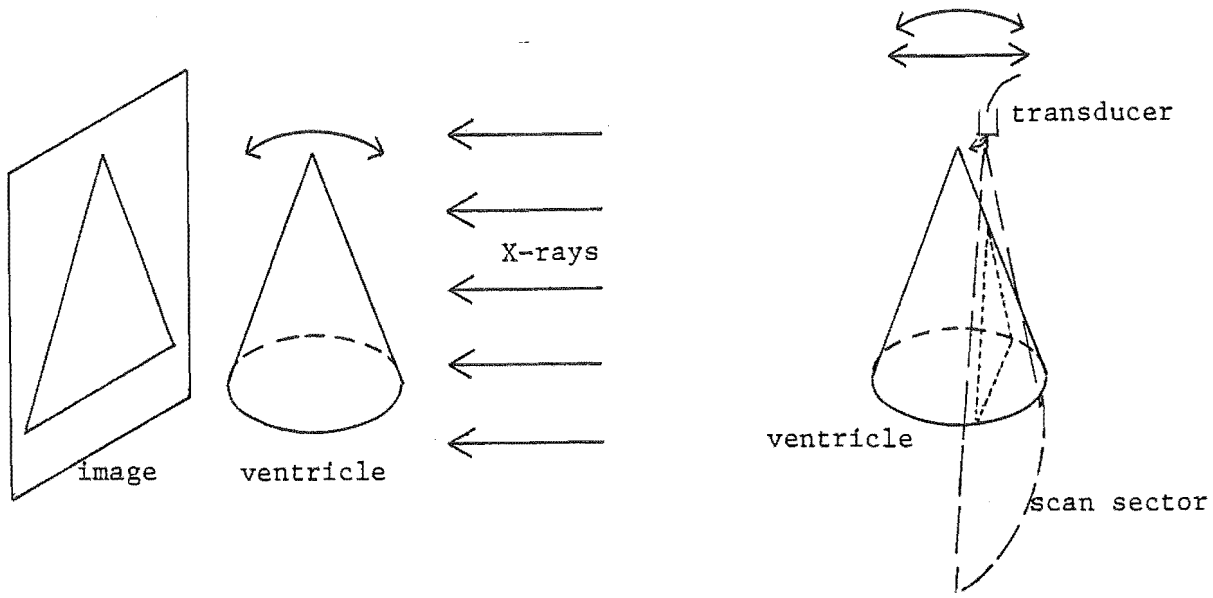

a) Angiography b) 2D Echocardiography

Figure 5.1 Sensitivity of angiograms and echocardiograms to translations and rotations of the ventricle. The ventricle is modelled as a cone. Translation and rotation of the ventricle in the direction of the arrows causes a different image to be obtained. The angiogram is only sensitive to rotation, but the 2DE is also sensitive to translation. If the ventricle is not a perfect cone, the different images will also be obtained by rotating the ventricle about an axis from the apex to the centre of the base of the cone.

Table 5.1 Specifications of SKI scanner.

Type:	Smith-Kline Industries 'Ekosector 1'
Modes:	A-mode M-mode 2D sector scan
Scanning transducers:	30° wobbler (2.25 MHz) 82° 4 element rotating (2.25 MHz)
Lines/scan:	30° transducer - 121 82° transducer - 54/55 lines (interlaced)
Pulse repetition frequency:	M-mode - 1000 Hz Sector - 3630 Hz
Frame rate:	30° transducer - 30 Hz 82° transducer - 60 Hz

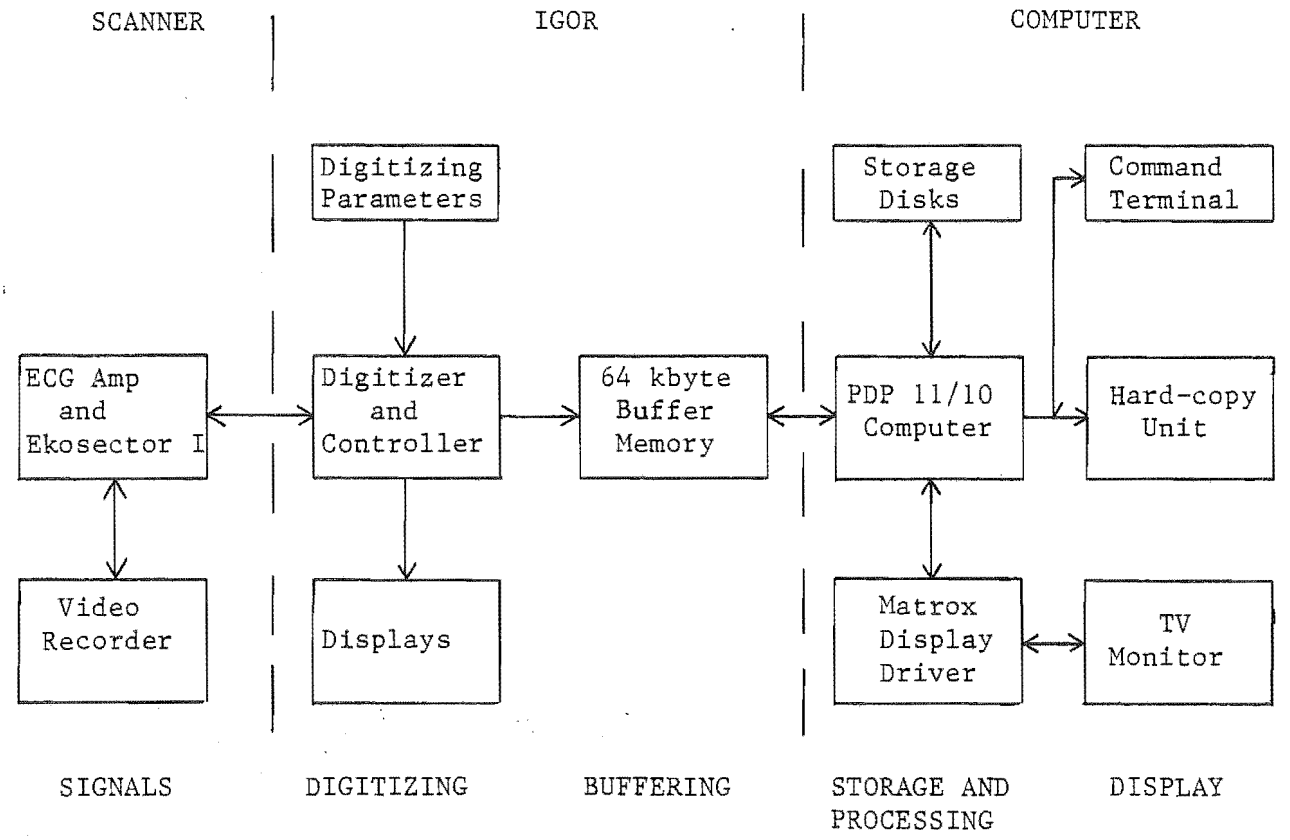

Figure 5.2 Block diagram of scanner/Igor/computer system.

Table 5.2 Specifications of computer system.

Type:	DEC PDP 11/10
Hardware:	Extended Arithmetic Element
Memory:	48 kbytes of user memory
Storage:	3 x 2.5 Mbyte RK05 removable disks
I/O ports:	2 x DL11 serial lines 1 x DR11K 16 bit parallel I/O port LPS11 Laboratory peripheral system (not DMA)
Terminals:	Teleray 10M Tektronix 4012 storage and line graphics
Hardcopy:	DECwriter LA36 Tektronix 4631 storage screen copier
Video:	Matrox URGB-256 video driver (256 x 256 pixel x 4 bit) 8 inch AWA black-and-white video monitor

second. The actual reconstructed image is sampled rather than the echo wavetrain. To achieve the highest frame rate, images are displayed as only 64 x 64 pixels. Much finer digitisation (400 x 512 pixel images) at lower frame rates is possible. Jensch's system is capable of sampling and storing 512 x 512 pixel scans for periods of up to 20 seconds in real time. Either the echo wavetrain or the reconstructed scans may be sampled. Real time filtering is also possible. Brinkley et al., (1978) and Garrison et al., (1977) describe systems where recorded sector scans are replayed on video screens onto which a computer superimposes suggested ventricular outlines. An operator interactively modifies the outlines until they correspond to the endocardial contour. No image enhancement is possible however.

The Department of Cardiology, at the Princess Margaret Hospital in Christchurch, possess an SKI Ekosector I real time sector scanner. It was one of the first commercially available cardiac two-dimensional scanners. It is a mechanical scanner with an 82^{o} field of view and a frame rate of 60 Hz. Full specifications are presented in Table 5.1.

It does not employ a scan converter but displays the video signal directly on a monitor by scanning its modulated electron beam in a sector rather than a raster format. A typical sector scan obtained and displayed by the scanner is shown in Figure 5.7a. The number of B-mode lines in alternate frames is either 54 or 55. This is because an interlace technique is used.

The Department of Cardiology also possess a PDP11/10 computer with line graphics, grey level graphics and printer outputs. Its specifications are listed in Table 5.2.

I have designed and constructed an interface to enable sector scans from the SKI scanner to be converted into digital form and to be passed to the computer for storage on disk. The scans can then be recalled from disk for processing, display and endocardial outline extraction. The interface has been affectionately named 'Igor' by those who have used it. For convenience, I will refer to it by that name.

The layout of the scanner/Igor/computer system is illustrated as a block diagram in Figure 5.2. A more detailed block diagram of Igor's layout is presented in Figure 5.3. A full set of circuit diagrams is provided in Appendix A.

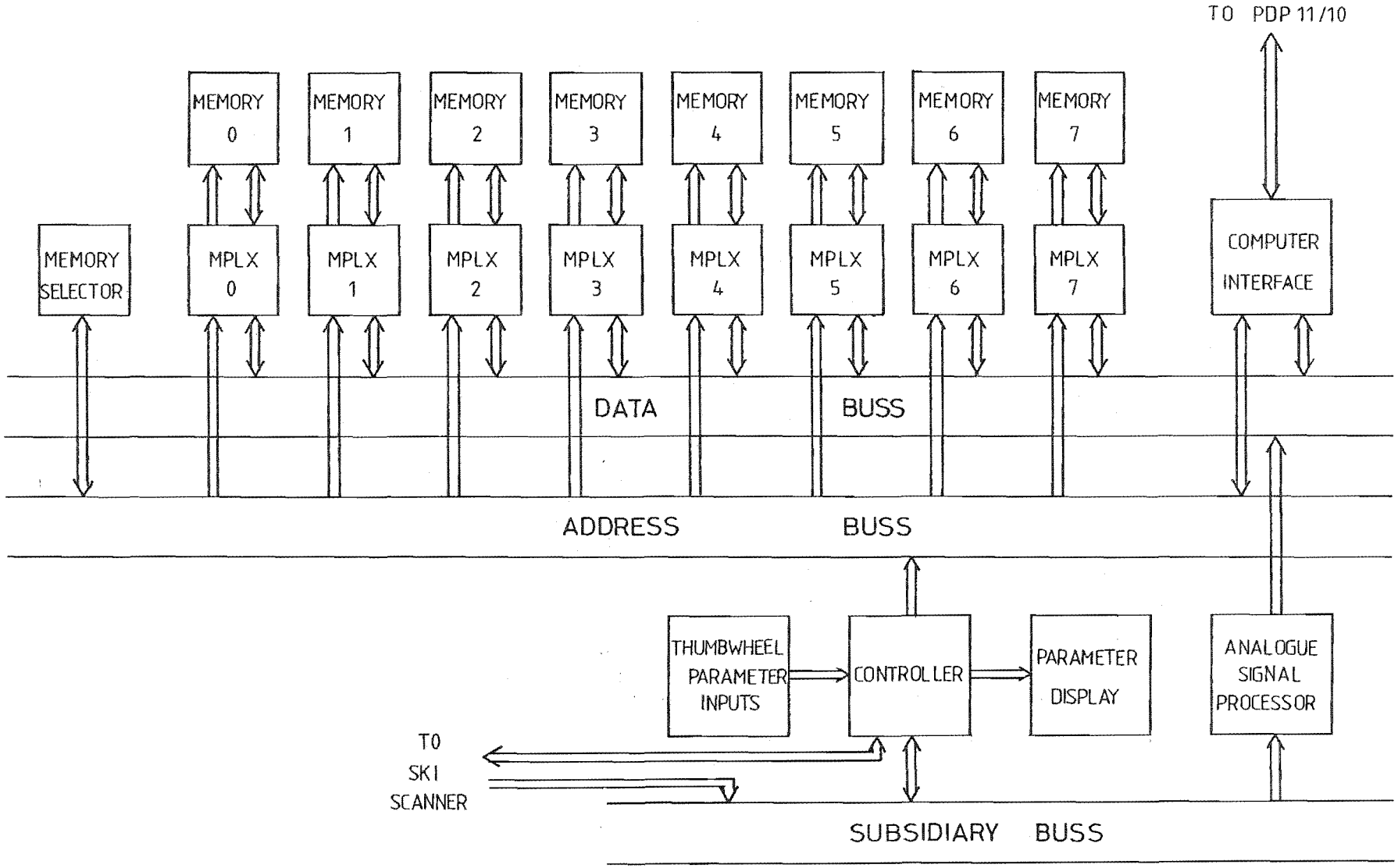

Figure 5.3 Block diagram of SKI sector scanner to PDP 11/10 computer interface.

Igor consists basically of a 64 kilobyte (8 bit bytes) memory and a high speed (20MHz) analogue-to-digital converter. Analogue ultrasound signals and the patient's ECG signal are obtained from the sector scanner and passed to the analogue signal processor board. Here the analogue signals are converted to digital form (8 bit precision) and are passed to the data buss. The R wave of the ECG signal is also detected by the analogue signal processor board to provide a trigger signal to the controller board, initiating data collection. Data is collected until Igor's memory is full at which point its contents are sent to the computer where they are stored on disk. It takes approximately two seconds to store all 64 kilobytes of data on disk. Hence data can only be collected in real time until all of Igor's memory is full as the rate at which data is collected by Igor (up to 7.26 MHz) is much greater than the rate at which it can be stored on disk (30 kHz).

The only data along each B-mode line which is usually of interest is that within a certain range gate. For the studies reported in Chapter 6, only the left ventricle is studied therefore data relating to regions outside the ventricle need not be stored. In this way more samples of relevant information may be collected and irrelevant information rejected. A range gate within which data is to be collected is selected by the operator using thumbwheel switches. The sampling rate which is within the range of 145 KHz to 7.26 MHz, is also selected by thumbwheel switches. Ninety-nine different rates are available. The rate selected is presented on LED displays on the front panel, as is the maximum number of times a B-mode line may be sampled at that rate. The images are usually sampled at 1.08 MHz with a gate approximately 110 samples long defined at the range of the left ventricle. Therefore, each frame is sampled about 6400 times. Thus ten sectors may be stored in Igor. Another switch allows the frame rate to vary from 6 to 60 frames per second. At the slower frame rates the sectors are sampled over a length of time greater than that of one heart cycle. Thus wall motion may be studied throughout the whole heart cycle.

All thumbwheel parameter inputs are connected to the controller board. This board processes all of the logical and timing signals needed to digitise and store ultrasonic and ECG data in the memories. It also provides a clock signal to the sector scanner to synchronise its operation with Igor. The scanner in turn provides logical signals to Igor to indicate when a new frame is being started and when the transducer is being excited. The controller board provides the analogue signal processor board with a logical signal each time the analogue signals are to be sampled. It also

generates the memory addresses where the sampled data is to be stored.

Igor's memory consists of 8 memory boards each having 8 kbytes of static random access-memory (RAM). As the data rate can be as high as 7.26 MHz and the access time of the boards is only 500 nsec, data can be generated faster than it can be stored directly in memory. So it is necessary to multiplex the data between the memory boards. Each memory board is interfaced to the buss by a board containing high speed batches to hold the data and addresses constant. The data and addresses on the buss may then change to allow data to be sent to another board while the batched data is written into the batched address. The memory selector board determines on which memory board the successive samples are to be stored.

When the memories are full, their contents are passed to a PDP 11/10 computer through the computer interface board. This is done as an 8-bit parallel transfer, that is, all 8 bits of a sample are transfered at once. It is possible to load Igor with data from the computer and then to transfer it back to the computer. This has proved to be invaluable for testing the memory boards and the multiplexing system.

The entire system was designed and constructed by myself with the exception of the memory boards and the case in which it is housed. The artwork for the memory boards was obtained from a local manufacturer. I only had to construct and test the boards. The case was designed by myself and constructed by technicians of the Department of Electrical Engineering, University of Canterbury.

The ultrasonic analogue output of the sector scanner is a half-wave rectified version of the echo signals. The carrier wave is not removed. If the analogue output signal were to be digitised, a sampling rate of approximately 7 MHz would be required to ensure that aliasing would not occur. At that sampling rate, only 1½ frames of data could be sampled and stored at a time. However, if the only echo envelope is sampled, digitising rates as low as 1 MHz may be used. The length of an echo pulse received by the scanner was seen on an oscilloscope to be approximately 2.5 μsec long. This suggested that filtering the echo envelope with a low pass filter having an upper cut-off frequency of 500 KHz will extract the envelope. This form of envelope extraction is used by many commercial sector scanners (Gammell,1981). An analogue interface unit consisting of a low-pass filter (having a 500 KHz upper cut-off) and a buffer amplifier, was constructed to extract the echo envelope signal and transmit it to Igor for sampling and storage. The circuit

diagrams for the unit are presented in Appendix A. A graph of its frequency response is presented in Figure 5.4. It is clear from this graph that the low-pass filtered echo wavetrain can be sampled at 1MHz without significant aliasing taking place.

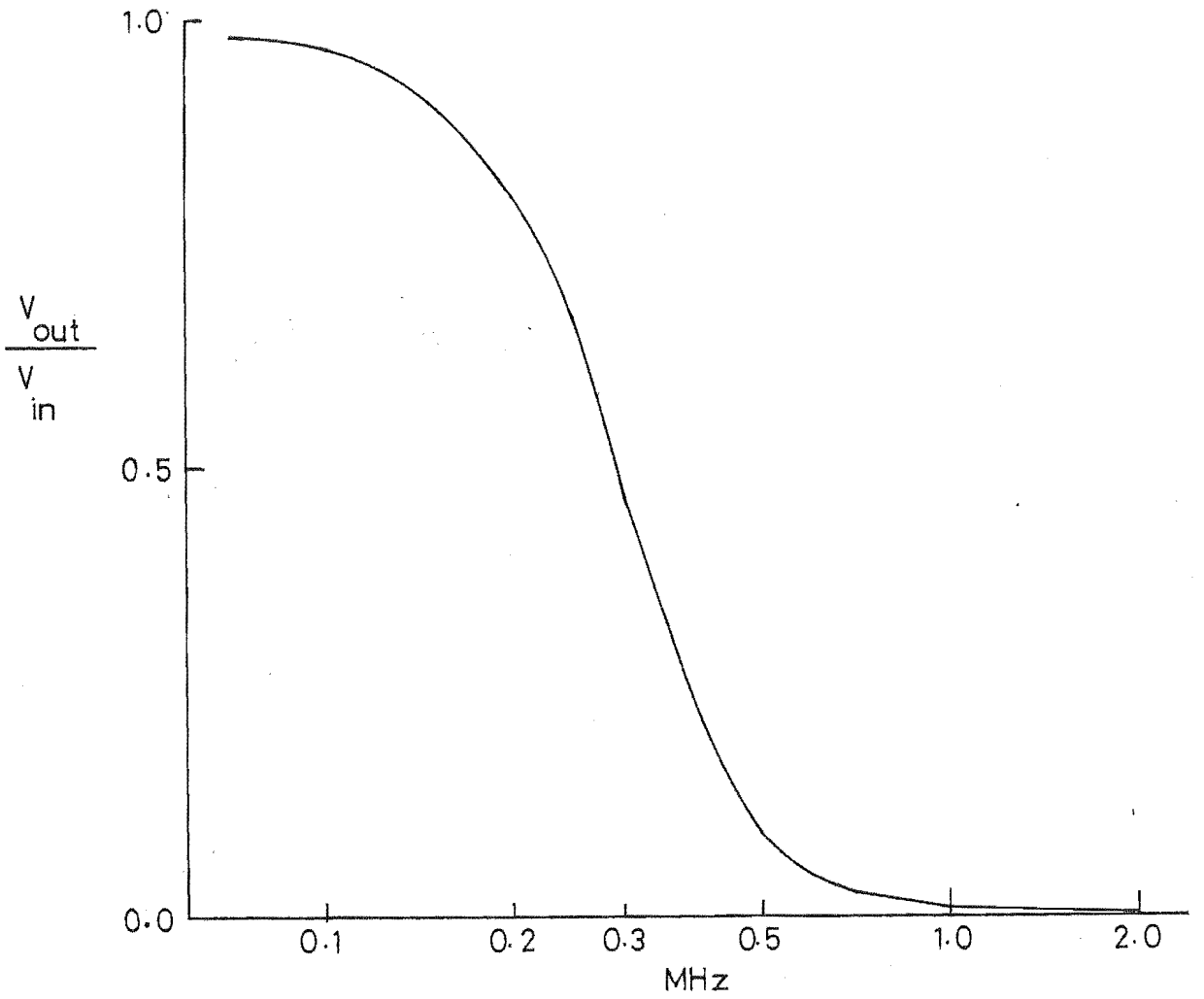

Figure 5.4 Frequency responce of analogue filter/buffer.

The scanner/Igor/PDP computer proved in practice to be somewhat limited. The computer was immobile, so it seemed that it would be necessary to perform all data collection in the computer/respiratory laboratory at the Princess Margaret Hospital. The laboratory contained a great deal of equipment. There was very little space left available for all of the equipment and personnel necessary to record the scans. As a result the sector scanner, echocardiographer and patient were situated in a room adjoining the laboratory while only Igor and myself were positioned by the computer. Myself at the computer and the echocardiographer in the next room communicated with the aid of an intercom. Hence there was little feedback between myself and the echocardiographer while data was being collected. Eventually, a mobile Systems Group North Star microcomputer was made available. This was interfaced to Igor without any modifications to the microcomputer or to Igor being necessary. It enabled data to be collected with the scanner, Igor and the microcomputer in close proximity anywhere within the hospital. Hence the frustration of being isolated from the patient and echocardiographer was eliminated.

The microcomputer stored the data on five-inch floppy disks. The data transfer rate from Igor to the floppy disks is much slower than to the PDP computer's disks; it takes 50 seconds to transfer the complete contents of Igor.

Data Format

Data sampled by Igor is stored in the order illustrated in Figure 5.5. B-mode lines of N samples are stored as sequences of N+2 eight bit binary numbers. The first number in each sequence is a 'marker' number. This number is $255_{10}(11111111_2)$ if the new line is the first line in a new frame. If it is not the first it is set to 254_{10} $(1111\ 1110_2)$. The next number is a sample of the ECG waveform taken just before excitation of the transducer. Following this are the N B-mode samples. The ECG and B-mode samples are binary numbers in the range 0_{10}-253_{10} $(0000\ 0000_2$ - $1111\ 1101_2)$. The output of the analogue-to-digital converter is monitored by hardware to detect if the output is either 254 or 255. If either of these numbers is detected the hardware produces the number 253 and passes this to the data buss instead. Thus the numbers 254 and 255 are unique to the start of lines and frames.

The marker numbers have proved to be very useful checks that the data collected by Igor and passed to the computer are correct. If Igor is not correctly connected to the sector scanner, it is possible for the system to

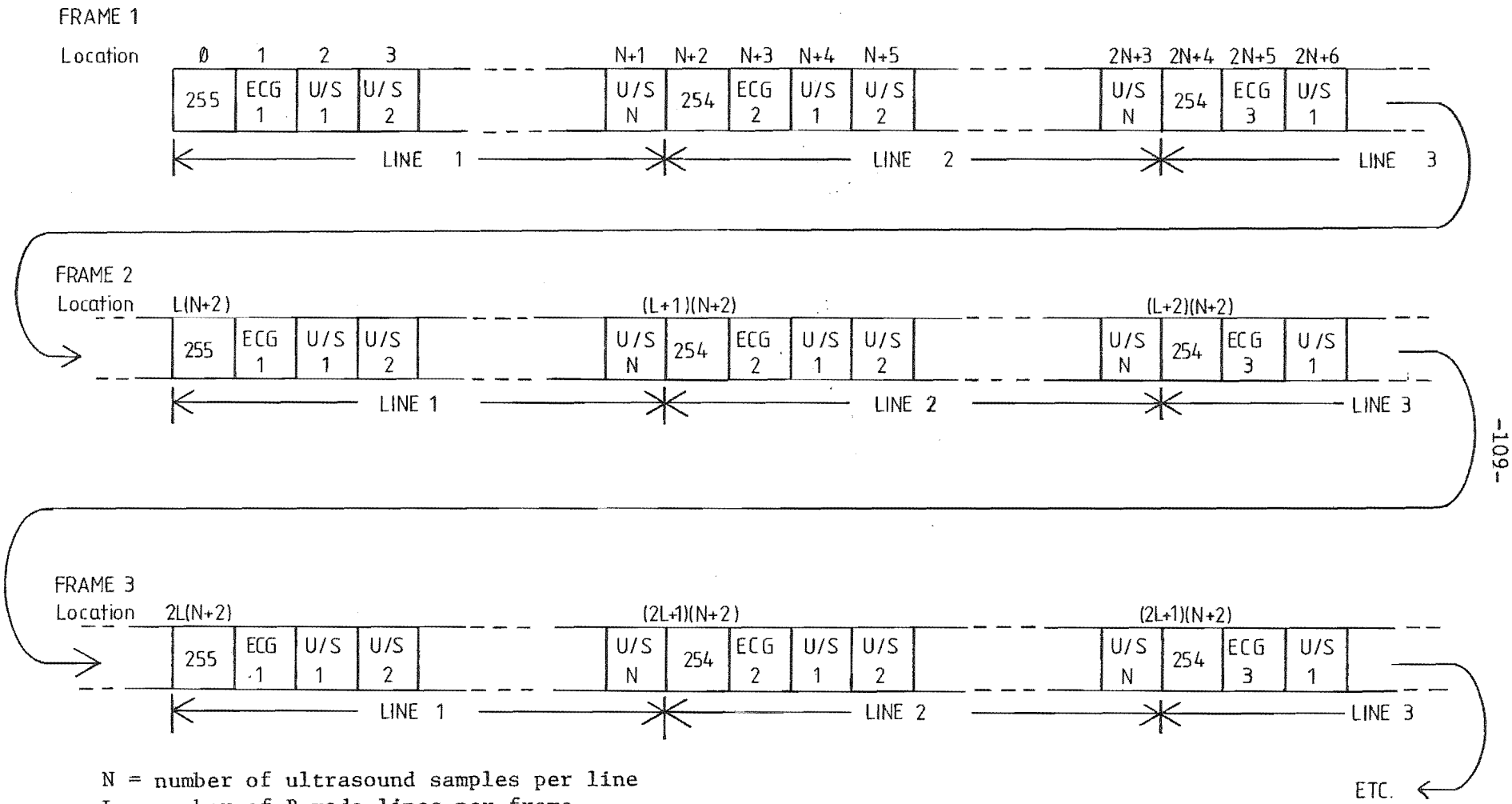

Figure 5.5 Format of data stored in Igor.

appear to be working correctly. However, when the data is analysed it may be found that some of the data is missing or that the data sequence does not start at the lowest address in memory as it should. Programs have been written to analyse the data and print out a table of the number of ECG and B-mode samples between each marker, the number of 'line start' markers in each frame, and the commencing address of each frame. Other programs have been written which allow the stored data string to be corrected if it does not conform to the format specified in Figure 5.5. The data must be in this format to allow the image processing programs to function correctly.

5.3 PROCESSING ECHOCARDIOGRAPHIC IMAGES

In this section the method of reconstructing sector scans from the sampled data is described. The effects of some of the filtering techniques discussed in Chapter 4 on the reconstructed scans are reported. Some of the conclusions as to the effectiveness of the various techniques do not agree with those in an earlier paper describing similar studies (Round et al., 1982). This is because the analogue ultrasonic signal has been altered by modifications which were made to the sector scanner and the analogue interface since the earlier studies were performed. The modifications were made to the scanner after the echocardiographers complained that the quality of the images produced had deteriorated over the past few years. Several faults were identified and corrected. The quality of the images improved greatly and the analogue interface was modified accordingly to its present specifications. The reconstructed images were somewhat altered in character, hence the ability of the various techniques to improve the images was changed. The studies reported here were carried out with the new interface, using images obtained after the scanner was overhauled.

5.3.1 Image Reconstruction

The scans sampled by Igor and stored on disk are recalled and displayed to an observer on a computer driven black-and-white monitor. It is driven by a Matrox URGB-256 video board within the PDP computer. The image is stored in memories on the board as an array of 256 x 256 pixels each of four bits (i.e. as 16 grey levels). The pixel values are read out sequentially line by line and converted to an analogue signal to drive the video in the same way as digital scan converters (cf. §2.3). The video screen is rectangular so that an image of only 256 pixels horizontally by 200 pixels vertically is visible.

Images are reconstructed by mapping the M-mode data into the sector format illustrated in Figure 5.6. The scan sector sweeps at 81.8 degrees of area and is 150 pixels in radius. Each line of sampled data is mapped into a line sector of 1.49 degrees. There are 55 line sectors in the scan sector. A data file permanently stored on disk contains the cartesian co-ordinates of the pixels and their distances (ranges) from the apex of the sector. The data is stored in order of increasing range.

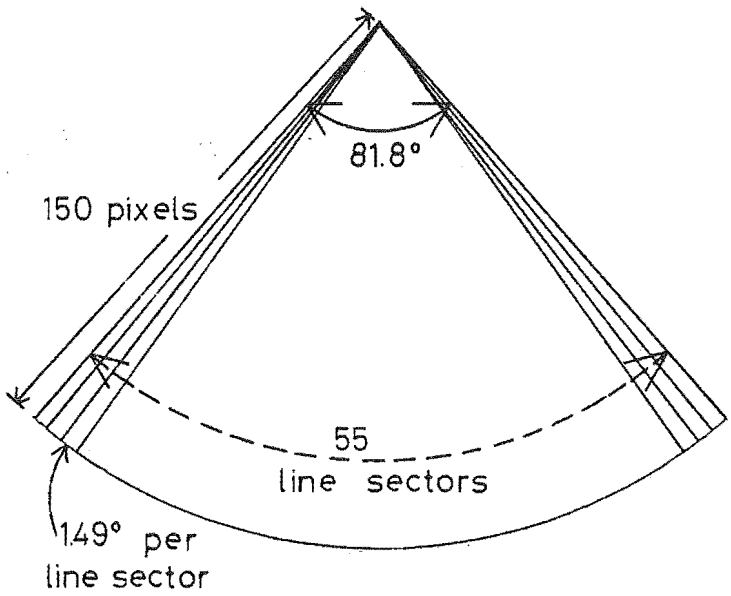

Figure 5.6 The format of the sector scans.

The mapping process is performed as follows. Each sample occupies a 'time gate' of length T_{GATE} equal to the delay between each sample. The time delays for sound to travel from the apex to the beginning and end of the time gate of sample N are

$$T_{G1} = T_{TRANS} + T_N - \tfrac{1}{2}T_{GATE} \qquad (5.1)$$

$$T_{G2} = T_{TRANS} + T_N + \tfrac{1}{2}T_{GATE} \qquad (5.2)$$

where T_N is the time delay between when the transducer is excited and when sample N is recorded, and T_{TRANS} is the time taken for sound to travel from the centre of the transducer drum to its circumference and back to the centre of the drum. Therefore pixels whose range is between

$$R_1 = 150 \frac{T_{G1}}{T_{SECTOR}} \qquad (5.3)$$

and

$$R_2 = 150 \frac{T_{G2}}{T_{SECTOR}} \qquad (5.4)$$

are contained within the time gate occupied by sample N. When mapping a sample into its equivalent pixels in the sector, R_1 and R_2 are first calculated for that sample. The pixel-range data file is searched to find the pixels which are within the gate. The value of the sample is then assigned to those pixels. Because the pixel co-ordinates are stored in increasing range, as are the sample values, the searching algorithm is very rapid. Each sector scan takes approximately 12 seconds to be reconstructed. The scans are either displayed directly on the monitor as they are reconstructed, or else they are stored on disk in the reconstructed form. Redisplaying the reconstructed scans which have been stored on disk takes just over 1 second.

Near the circumference of the sector, each sample is mapped into several pixels. Near the apex of the sector, there are more samples available

than there are pixels to map them into. Therefore, near the apex some of the samples are rejected and are not used in the reconstructed scan.

5.3.2 Endocardial Detection

One of the major difficulties encountered when analysing left ventricular wall motion with two-dimensional echocardiography is that the endocardium is not always visible (§4.2.3). Some cardiologists believe that the endocardium is almost never visible. Others are confident that it is easily seen and that no real difficulty exists. It is likely that cardiologists opinions are formed by their experience with their own scanner's imaging capabilities. Those with high quality scanners, which are also correctly adjusted find little difficulty. Cardiologists possessing scanners, which are either or poor quality or are badly adjusted, rarely see the endocardium and find that only the epicardial and pericardial borders are visible.

To test that the SKI scanner is capable of imaging the endocardial border an experiment using 'contrast echocardiography' was carried out. Contrast echocardiography is a technique where a solution of such substances as indocyanine green or saline are injected into the blood stream (cf. Weyman et al., 1979). When imaged ultrasonically the blood in the atria and the ventricles appears to be 'cloudy' rather than transparent. Thus, if the left ventricle is imaged with two-dimensional contrast echocardiography, and if the clouds do not appear to completely fill the chamber, then what appears to be the endocardium is really the pericardium or epicardium.

A patient was studied with the SKI scanner while undergoing angiography. While scanning the left ventricle in a transverse view, indocyanine green was injected into the left ventricle, through an intracardiac catheter, to identify the part of the image showing the blood in the chamber. Scans obtained before and after injection of the saline solution are presented in Figures 5.7a and 5.7b, respectively. The boundary which appears to be the endocardium is indicated in the scan taken before injection. After injection the chamber is clouded up to, but not beyond the boundary. Therefore, this boundary is in fact the endocardium. It was encouraging that it can be identified even in poor quality stop-frame images taken directly from the scanner. The application of image processing techniques which allow the endocardium to be more easily visualised are described in §§5.3.3 to 5.3.6.

5.3.3 Contrast Manipulation

A typical probability histogram of the frequency with each sample value appears in a reconstructed scan is presented in Figure 5.8.

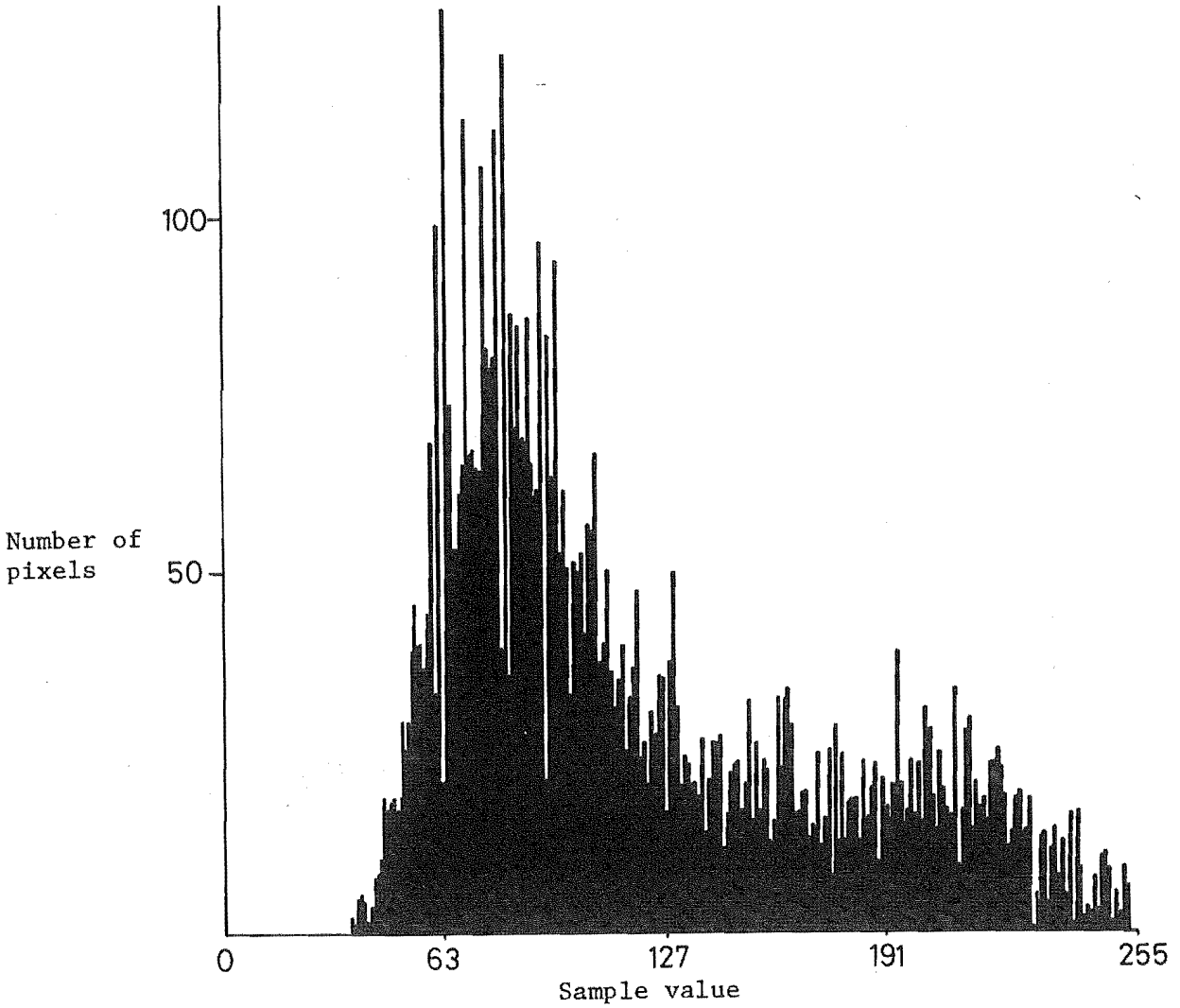

Figure 5.8 Sample frequency histogram for the scan shown in Figure 5.9

Figure 5.7 Images of the left ventricle obtained directly from the sector scanner a) before injection of the contrast agent
b) after injection of contrast agent
The contour which appears to be the endocardium is marked 'E'. The contrast agent fills right up to the boundary indicating that this is, in fact, the endocardial border.

Figure 5.9 Image of the left ventricle of a normal volunteer obtained by Igor. This image is displayed with a linear transfer function from sample value 65 to sample value 220. Scan is a short axis view at the level of the mitral valve.

Figure 5.10 Scan in Figure 5.9 displayed with a linear transfer function from sample value 35 to sample value 253. Note the noise signal from within the blood in the ventricle.

Figure 5.11 Scan in Figure 5.9 displayed with histogram equalisation with a lower sample value cut-off of 65. The endocardial border is easier to identify than in Figures 5.9 and 5.10.

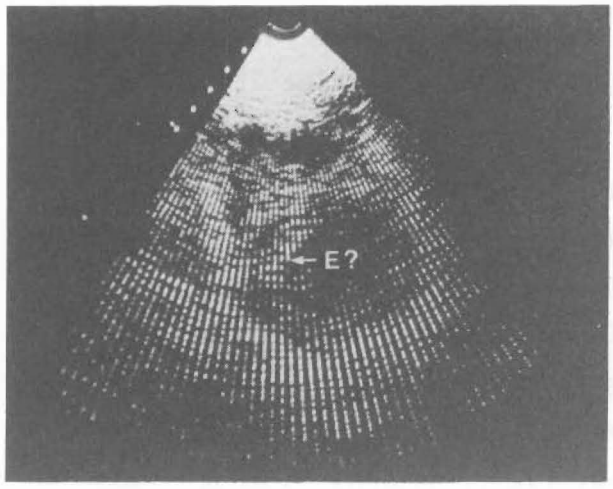

Figure 5.7a

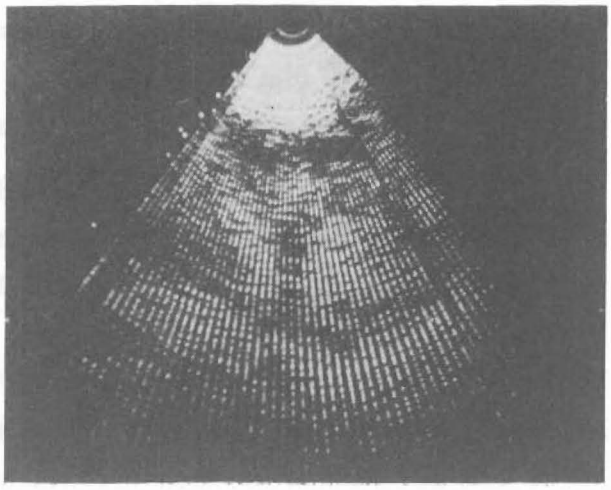

Figure 5.7b

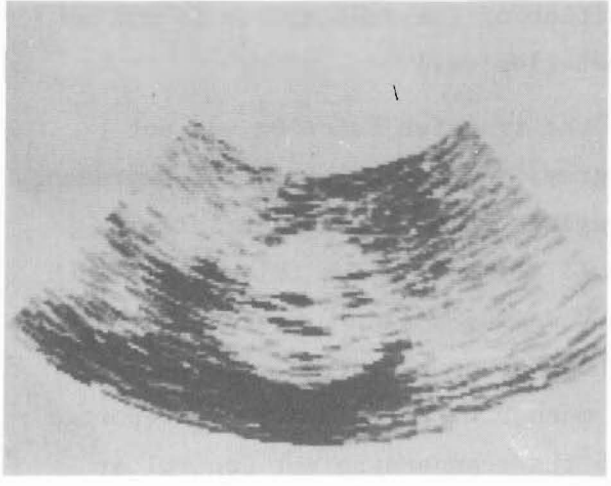

Figure 5.9

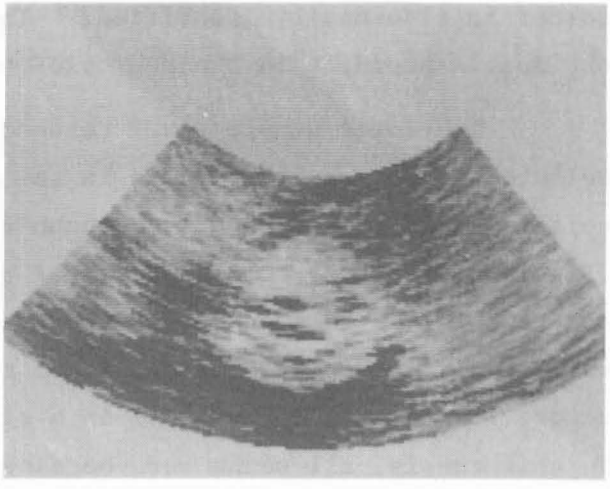

Figure 5.10

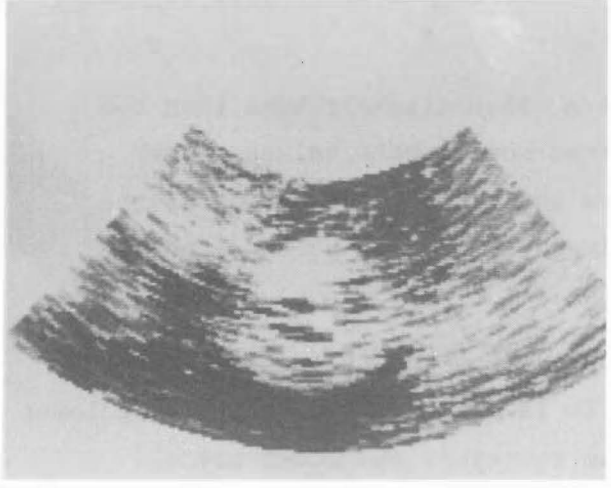

Figure 5.11

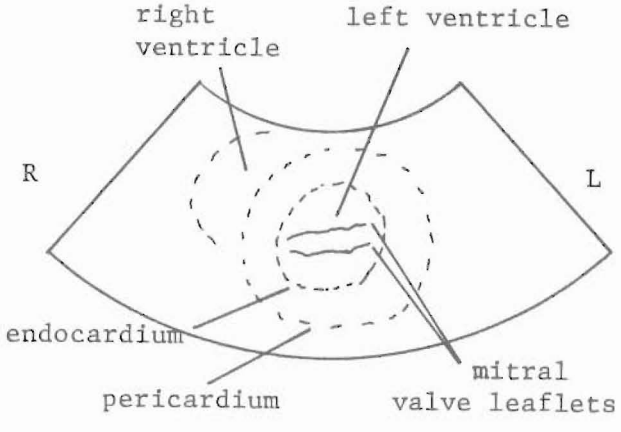

Key to Figs 5.9 to 5.11

Most of the sample values are in the range 50 to 120. Above this range the values occur with approximately equal frequency up to the value 220, after which the frequency decreases. The shape of this histogram is typical.

When a scan is to be displayed on the monitor, a transfer function must be defined between the 254 possible sample values and the 16 pixel values with which it is displayed. Figure 5.9 shows the scan from which the histogram in Figure 5.8 was obtained. A linear transfer function which maps the sample values from 65 to 220 into the pixel values of from 0 to 15 was used. All the sample values below 65 are displayed with a pixel value of 0, and those above 220 are displayed with a pixel value of 15. The scan is of a transverse view of the left ventricle taken in mid-systole at the level of the mitral valve. The anterior and posterior valve leaflets are clearly visible. The pericardial border is also easily identified. The position of the endocardium is not as obvious, especially in the region of the posterior wall.

The lower sample level threshold of the transfer function was not selected as the smallest value in the histogram. The smaller values represent noise signals in what should be echo-free regions such as the ventricles (Figure 5.10). By choosing a lower threshold slightly above this level, much of the noise is removed resulting in a more pleasing image. Most sector scans have a 'Reject' control which allows the echocardiographer to electronically remove low-level noise signals in a similar manner. For the studies reported in this thesis, all scans were obtained with the scanners reject control at its minimum setting so that all the echo and noise signal was sampled. A lower threshold level was defined when the scans were displayed by the computer. In this way there was no danger of the echocardiographer rejecting low amplitude endocardial echoes.

Setting the upper threshold level to a value slightly less than the maximum also improves the images. This forces more sample values to be mapped into the larger pixel values which are not displayed as often as the smaller values. If this is not done, the image appears to be too lightly shaded.

Histogram equalisation was found to provide a very effective way of calculating a suitable transfer function. It is again better to define a lower threshold level when equalising the histogram to reject low level noise. The sample values below the threshold are assigned pixel values of zero. The sample values above that level are equalised over the pixel value range of 0 to 15.

The effect of histogram equalisation is seen in Figure 5.11. The scan is aesthetically more pleasing and the low level echoes from the posterior endocardium are now plainly visible.

Histogram equalisation with a lower threshold was found to improve all scans significantly. Therefore it was always used to determine an appropriate transfer function to display the scans.

5.3.4 Noise Reduction

Stop frame two-dimensional echocardiograms are usually not very pleasing to the eye, because their noise level is so high that some of the detail is obscured. It is easier to interpret real time scans, since the noise is less obvious. Structures can also be identified by their motion. The noise comes from three major sources. First, there is electronic noise in the receiver amplifiers. It can be large compared to echo signals from within tissues. Second, the scans often suffer from a 'grainy' appearance called 'acoustic speckle'. This is caused by distortion of the scattered acoustic waves by tissues between the scatterers and the transducer. Third, the beam-width artifacts described in §4.2 are often seen in scans as small echoes in what should be echo-free regions such as blood-filled ventricles.

Visually improved images which are easier to interpret can be obtained by applying some of the noise clearing techniques described in §4.3.5.

The filtering process reviewed in Chapter 4 are normally performed on images reconstructed in two-dimensional arrays of pixels. However, in the studies reported here, filtering was performed on the raw sample values before they were reconstructed as an image in a sector format. Filtering the data is similar to filtering an image. The filters operate on a two-dimensional array of sample values rather than on individual pixel values. A filtered image is then created by transforming the filtered data into the sector format.

Data filtering rather than image filtering was necessary because, in the transformation process, one raw data sample is often mapped into several adjacent pixels. This is most evident at the bottom of the scans where the image appears to consist of blocks of pixels with the same value. Image filtering would then be effective only at the edges of the blocks.

Out-range Filtering (cf. §4.3.5)

The out-range filter was of limited value in removing noise from the scans. Figure 5.12 demonstrates the effect of out-range filtering on the

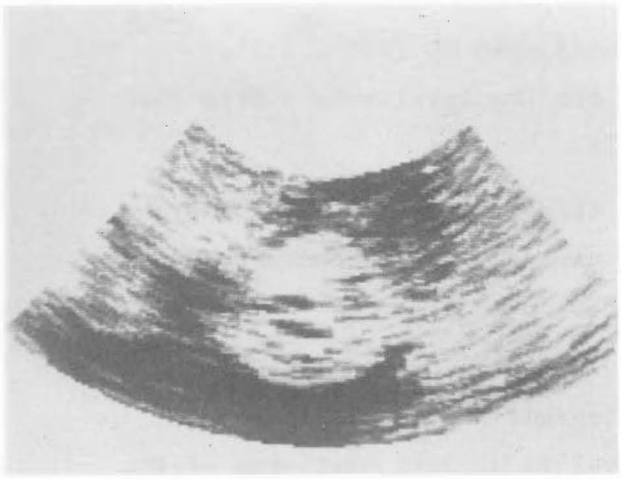

Figure 5.12
Scan in Figure 5.9 after it has been out-range filtered with a 3x3 window and threshold of 40. This image has been histogram equalised.

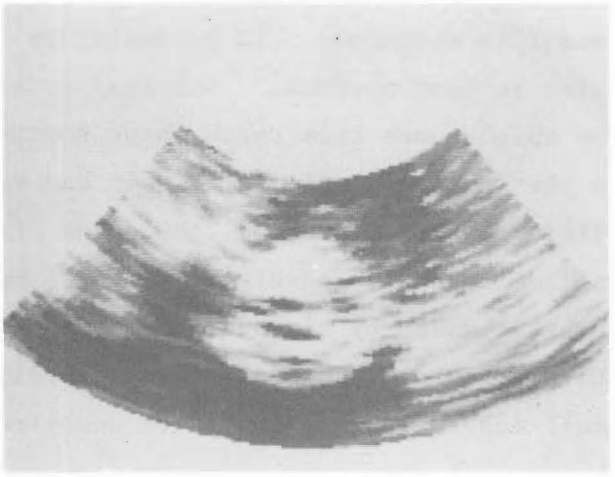

Figure 5.13
Scan in Figure 5.9 after it has been median filtered with a 3x3 sample window. This image has been histogram equalised.

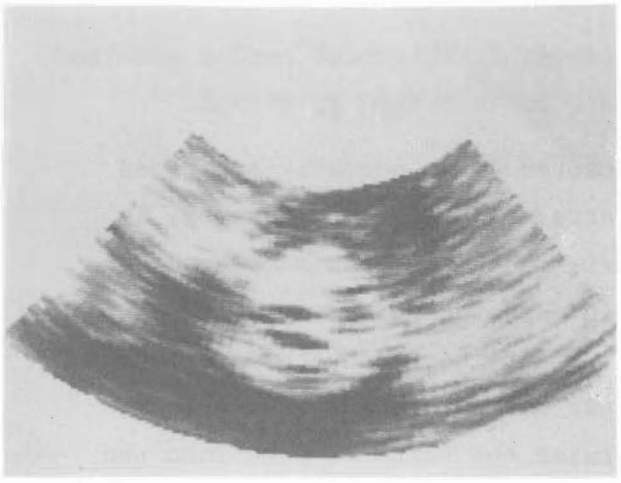

Figure 5.14
Scan in Figure 5.9 after it has been local average filtered. This image has been histogram equalised.

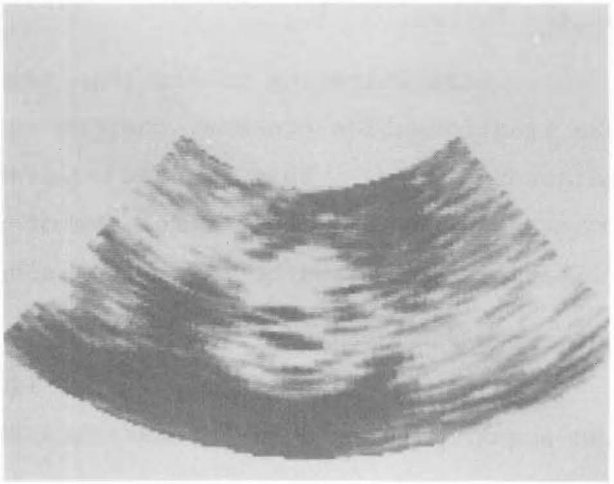

Figure 5.15
Scan in Figure 5.9 after it has been echo-shape filtered. This image has been histogram equalised.

scan shown in Figure 5.9. The out-range threshold was set at 40 and the image has been histogram-equalised with a lower threshold level of 65. Some noise suppression has taken place but little effect is evident within the ventricle which contains the detail of most interest. This technique is most useful where the noise is in the form of isolated pixels having values very different from their neighbours ('salt and pepper' noise).

Median Filtering (cf. §4.3.5)

The effect of median filtering on the scans is seen in Figure 5.13 where it has been applied to the data of Figure 5.9 using a 3 x 3 sample window. The image has been histogram-equalised with a lower cutoff of 65. Again the noise level is less than that in the original image but 'contouring' is now seen. This effect is most obvious near the posterior wall of the ventricle. It tends to degrade the image somewhat, even though the noise level is indeed less.

Local Average Filtering (cf. §4.3.5)

This has proved to be a very useful technique. Figure 5.14 shows the scan displayed in Figure 5.9 after it has been filtered using the weight array:

$$\begin{bmatrix} 1 & 2 & 1 \\ 2 & 4 & 2 \\ 1 & 2 & 1 \end{bmatrix}$$

The image has been histogram-equalised above a sample value threshold of 65. It no longer has a speckled character and the noise is well suppressed. Some edge definition is lost but the endocardium is quite apparent and is distinct from the pericardium.

There are many possible weight-arrays which could be used to obtain a similar effect. McSherry and Keller (1974) smooth the noise in their cardiac scans with 'beam-width filtering'. This is done by designing a filter weight array where the relative values of the weights are the same as the relative ultrasonic pressure amplitudes at the corresponding points across the beam. The image is in effect correlated with the beam profile.

A two-dimensional filter array for smoothing noise was designed on the same basis. This was done by mounting a wire in a water bath and imaging it with the scanner. The wire was positioned so that it was in the centre of the sample range-gate most often used when sampling scans of the left ventricle. A two-dimensional sector scan was taken of the wire and the sample values obtained were used as estimates of the beam profile and echo envelope shape.

The relative intensities in the beam were

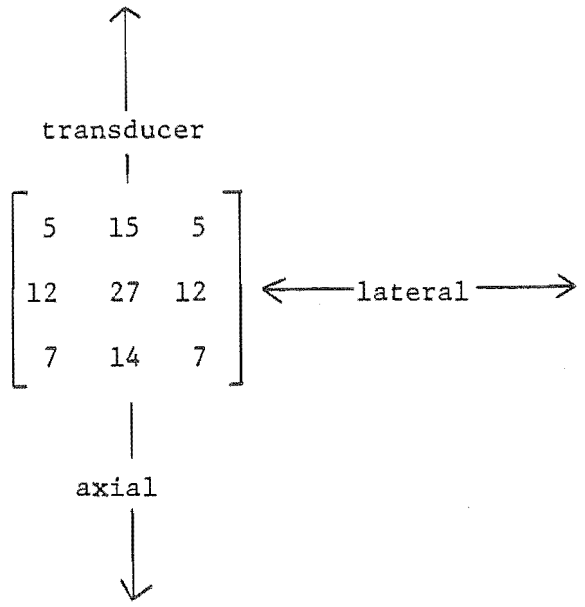

These relative intensities were used as the values of a weight array to local-average the scan in Figure 5.9. The resulting image, presented in Figure 5.15, is slightly more pleasing than is that in Figure 5.14. The endocardial echo is well defined although the crispness of the image is reduced.

Weight arrays designed according to the echo shape should ideally vary as the distance from the transducer is changed. This is because the echo shape and the number of B-mode lines within the beam alter with increasing range. The beam profile however, is also known to change with increasing receiver gain and to be altered by the tissues it traverses. It is very difficult to determine the true echo shape for any point in any scan. The weight array determined by the wire in the water bath experiment has proved to be a useful array for noise smoothing.

5.3.5 Edge Enhancement (cf. §4.3.5)

Edge crispening techniques often make images more presentable by making poorly defined outlines more obvious to an observer. Some of these techniques were applied to see if the endocardial border could be made easier to identify. Figure 5.16 demonstrates the effect of convolving the scan in Figure 5.9 with the Laplacian filter mask:

$$\begin{bmatrix} -1 & -1 & -1 \\ -1 & 8 & -1 \\ -1 & -1 & -1 \end{bmatrix}$$

(a)

The resulting image is of little value because, while the edges in the image have been enhanced, the noise level has also been amplified.

Better images can be obtained by combining the original image with the Laplacian filtered image in a certain ratio (cf. §4.3.3). Convolving the original image with the weight array

$$\begin{bmatrix} -1 & -1 & -1 \\ -1 & 12 & -1 \\ -1 & -1 & -1 \end{bmatrix}$$

(b)

combines that image with the Laplacian image in the ratio 4:1. The image thus produced is presented in Figure 5.17. The noise level is still very high and the image is not as pleasing to the eye as is the original. The high noise level can be reduced by convolving the echo-shape filtered image with array (b). The resulting image (Figure 5.18) is very similar to the unprocessed scan (Figure 5.9). Therefore, there is little advantage in applying Laplacian filtering techniques.

5.3.6 Regional Filtering

The character of two-dimensional echocardiograms often varies over an image. This variation can take many forms. For instance, it is often easy to define the anterior and posterior walls of a ventricle, because they are perpendicular to the beam. The lateral walls are usually much harder to identify as they lie parallel to the beam so that little energy is reflected back to the transducer. They therefore appear faint or invisible due to echo dropout. The ability to localise the lateral walls is limited by the lateral resolution of the beam. This may be three times worse than the axial resolution. This limits localisation of the anterior and posterior walls. It is reasonable to expect that the processing necessary to make the lateral walls more visible in the sector scans would be different from that needed to

Captions for Figures on p123.

Figure 5.16 Scan in Figure 5.9 after it has been filtered with Laplacian weight array (a). Edges and noise are detected. This image is of little value.

Figure 5.17 Scan in Figure 5.9 after it has been filtered with Laplacian weight array (b). This image is more pleasing to the eye than is that in Figure 5.16, but the noise level is still too high.

Figure 5.18 Scan in Figure 5.9 after it has been echo-shape filtered (Figure 5.15) and then Laplacian filtered with the weight array (b). This image is more pleasing than are those of Figures 5.16 and 5.17.

Figure 5.19a Four chamber view of the heart. Three regions have been defined within which the endocardium is not easily recognised due to echo dropout. These regions have been defined by the operator as being enclosed by the boxes superimposed on the scan.

Figure 5.19b The scan shown in Figure 5.19a after it has been regionally filtered by multiplying all of the sample values corresponding toregions within the boxes by 2.0 . The endocardium is now much easier to see.

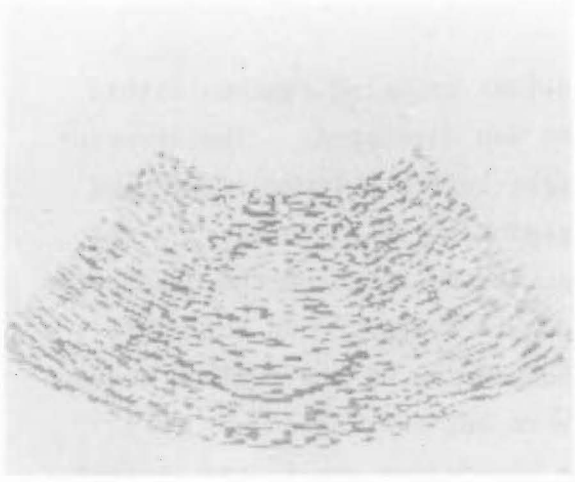

Figure 5.16

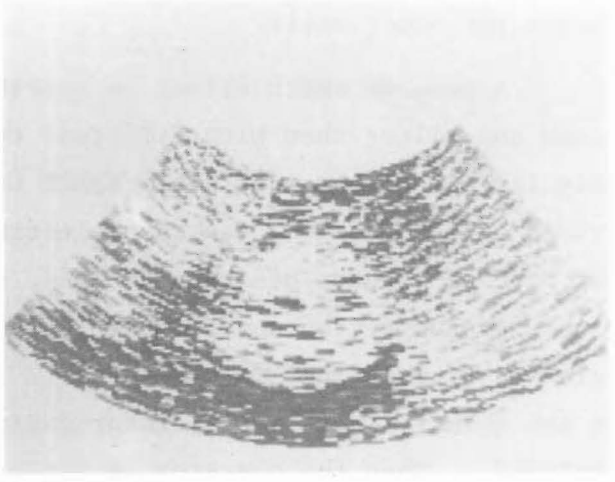

Figure 5.17

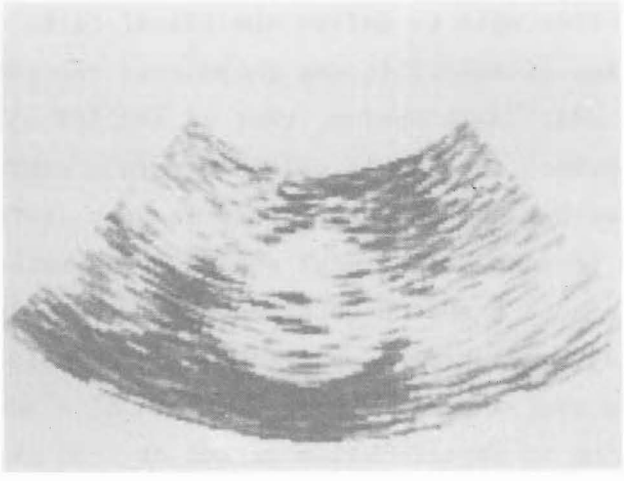

Figure 5.18

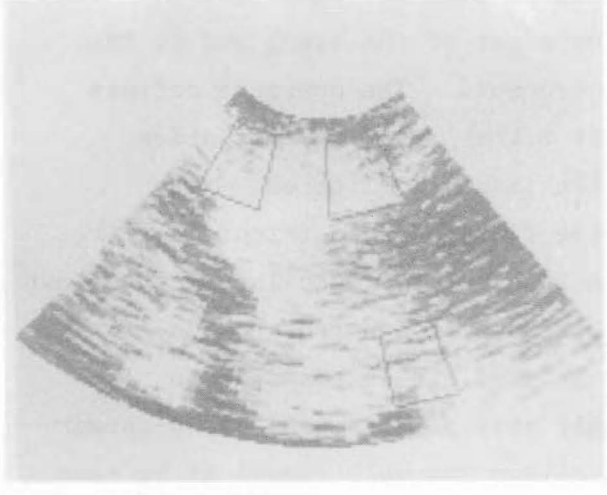

Figure 5.19a

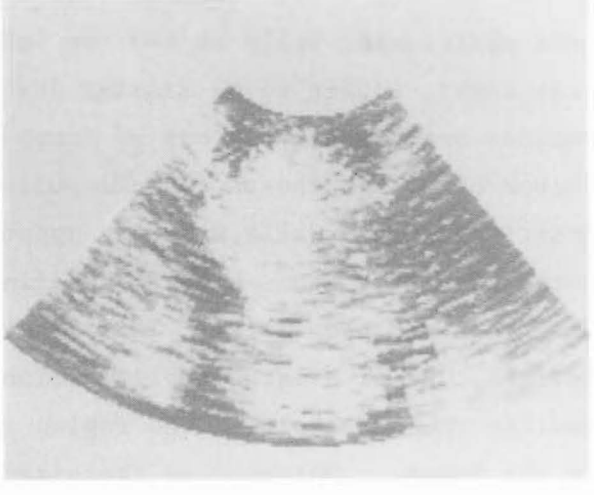

Figure 5.19b

enhance the other walls.

A program which allows an operator to define selected regions within a scan and filter them with different techniques was developed. The operator manipulates a cursor with a trackball to the upper left and lower right hand corners of each region, thereby selecting the region to be filtered. After each pair of corners has been defined, the computer superimposes the boundaries of the defined region on the sector scan (see Figure 5.19a). Up to four regions can be defined in each scan. If the boundaries of the regions chosen are not exactly where the operator desires them to be, the region may be redefined. When the operator is satisfied the boundaries are in the correct positions, the co-ordinates of the corners of the regions are stored on disk in terms of their position in the raw data file.

The operator is then able to define the filter to be used in each region of each scan. Any of the filtering techniques described in §§5.3.3 to 5.3.5 may be used. An additional option, that of amplification, is also provided. With this option, the sample values within a region may be multiplied by an operator-defined factor. This is very useful in regions where echo dropout occurs, as it enables the weak echoes to be selectively enhanced. It is also useful when a scan has been obtained where the correct time-gain compensation (cf. §2.3.3) has not been applied. For example, if the echoes from near the sector are over-amplified near the apex of a sector may appear to be too dark. By defining an amplification factor of less than 1.0 to this region, a more pleasing image is obtained.

The regional filtering process is illustrated by Figures 5.19a to 5.19b. A scan showing a four chamber view of the heart is seen in Figure 5.19a. The left ventricular walls at the top left and top right of the scan, and at the lower right, appear to be missing due to echo dropout. The operator defines regions enclosing the areas of dropout (Figure 5.19a). An amplification factor of 2.0 is chosen for all regions and the image is filtered. The positions of the walls are more apparent in the filtered scan (Figure 5.19b). Note that the regions have been defined to enclose an area much larger than that which contain the walls. This is necessary because if a narrow region is defined, and if a large amplification factor is used, it is possible to amplify the noise within the region so strongly that a false wall would appear in the image. Defining an oversized region allows the wall signal to be seen, as distinct from the signal due to noise within the ventricle.

Regional filtering is a very time consuming technique. A lot of

operator interaction is required to define the regions and several attempts to select the most appropriate filtering technique for each region may be necessary. If a series of scans taken throughout a single heart cycle are to be processed with this technique, it may be difficult to justify the time spent in terms of the value of the improvement to the scans. Therefore, while this technique can significantly improve a scan, I did not use it very frequently.

5.4 ENDOCARDIAL DETECTION IN A SERIES OF SECTOR SCANS

When a series of sector scans are taken during a single cardiac cycle, the endocardium is not obvious in all scans. Usually, the endocardium can be identified in a few of the scans. In others though, echo dropout and the endocardium's close proximity to other structures prevent it from being identified. The difficulties are demonstrated in Figures 5.20a to 5.20d. These are consecutive scans taken throughout the systolic phase. The endocardium is easily identified in Figures 5.20a and 5.20b. However, in the next two scans, the posterior leaflet of the mitral valve lies very close to the endocardium and therefore the scans are difficult to interpret. The mitral valve and the endocardium are often easier to identify in M-mode scans, as their motions allow them to be recognised. Techniques which allow the endocardium to be identified by using the motion information contained in a series of sector scans were developed and are described below.

5.4.1 M-mode Reformating

When Igor is used to obtain a series of sector scans throughout a heart cycle, ten scans each of 55 lines are usually obtained. It is easy to conceive these ten 55 line sector scans as 55 M-mode scans of only ten lines each (see Figure 5.21). If these are displayed simultaneously with the sector scans, the operator then has access to both the two-dimensional information and the time-varying information for the single line common to both displays. This is demonstrated in Figure 5.22. The dots above and below each scan indicate the line common to both scans. In the M-mode scan, the two dots mark out the third line, therefore the third sector scan of the series (cf. Figure 5.20c) is being displayed, the two M-mode dots would move to the right to mark out successive M-mode lines.

The position of the posterior endocardium can be seen in all lines of the M-mode scan, even in those corresponding to the sector scan lines in which it can not be identified (Figures 5.20c, 5.20d). From the position of the endocardium in the M-mode scan, its position in the sector scan can be deduced.

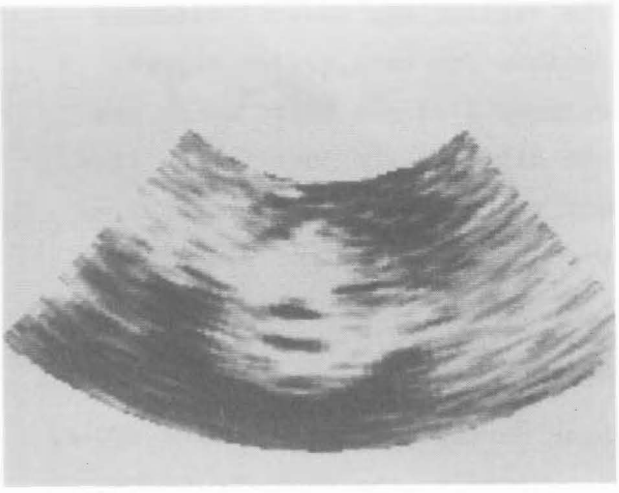

Figure 5.20a

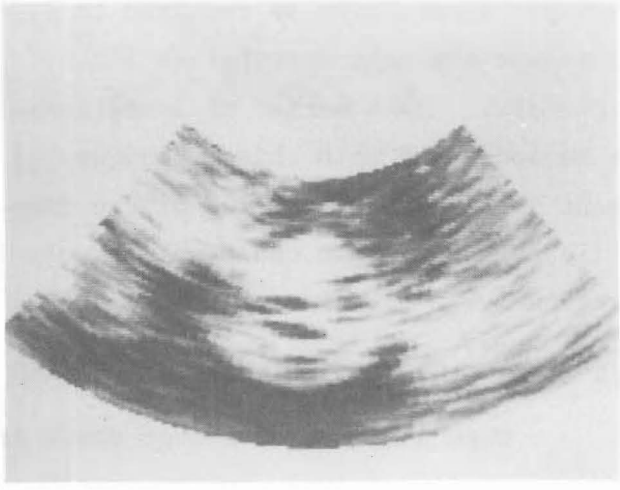

Figure 5.20b

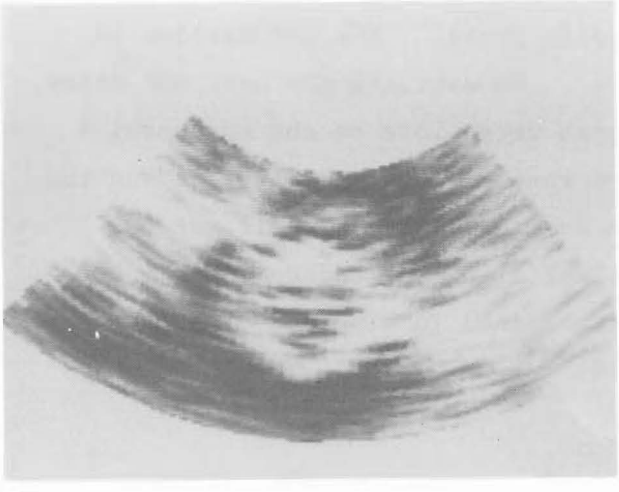

Figure 5.20c

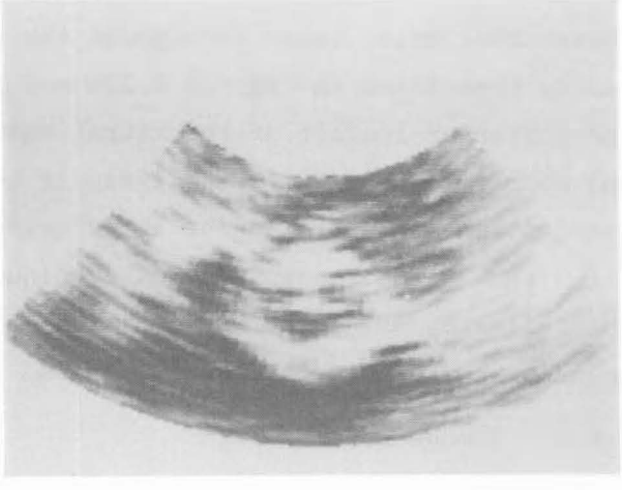

Figure 5.20d

Figures 5.20a to 5.20d A series of four sector scans taken at the level of the mitral valve. The scans go from end-diastole (5.20a) to end-systole (5.20d). The posterior endocardium is difficult to identify in Figures 5.20c and 5.20d.

Software was developed to allow a flashing cursor to be manipulated around the sector scans under manual control by an operator using a trackball. The cursor is moved around the endocardial contour as interpreted by the operator and the contour is stored by the computer. Simultaneously the computer displays a supplementary cursor on the corresponding M-mode line in registration with its position in the sector scan. As the cursor travels across the sector scan, the M-mode display refreshes in real time. This allows the operator to track the endocardium both in time on the M-mode scan and in two dimensions in the sector scan. Improved identification of the endocardial contour is achieved, which leads to a more accurate estimate of the endocardial position in the sector scan.

5.4.2 C-mode Reformatting

Simultaneous display of the M-mode and the sector scan is not always useful. When tracking along the lateral walls, the endocardial echo vanishes from the M-mode scan as the heart proceeds through systole. This can be seen in the M-mode scan in Figure 5.23 in which the endocardial curve disappears in the third to sixth lines. To overcome this difficulty a 'simultaneous C-mode' scan technique was developed. The principle is illustrated in Figure 5.24. The sector scans are reformatted as 150 C-mode scans of ten lines each formed from the echo data at a constant range from the transducer. These scans can be used to aid in tracking the endocardial echo at the lateral walls. However, resolution of the C-mode scans is poor, as is the lateral resolution of the sector scans (Figure 5.25a).

The software which allowed simultaneous sector and M-mode tracking was modified to include simultaneous C-mode tracking (Figure 5.25b). As the operator manipulates a cursor around the sector scans, both the M-mode and the C-mode scans refresh. Supplementary cursors in registration with those in the sector scan which mark the equivalent points in all three scans. It is possible to define all the endocardial contour by observing the M-mode scan when tracking along the anterior and posterior walls and the C-mode scan when tracking along the lateral walls. This technique has certain disadvantages. Firstly, the C-mode scans reconstructed from the sector scans are, in essence, M-mode scans taken along lines which cannot be imaged using conventional scanners. An observer must therefore exercise great care when interpreting the C-mode scans, at least, until sufficient experience is gained. Secondly, it is very difficult to follow all three cursors at once, especially when two of the displays are continually changing. Thirdly, a lot of the computer's time is spent in updating the scans tending to make the cursor respond slowly

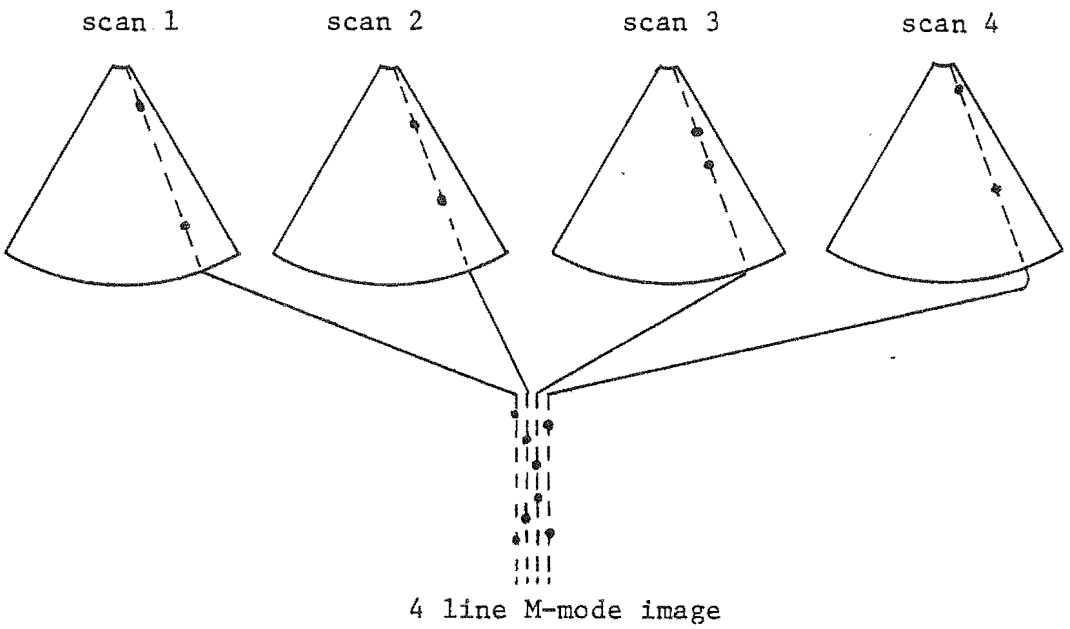

Figure 5.21 M-mode reformatting from a series of sector scans.

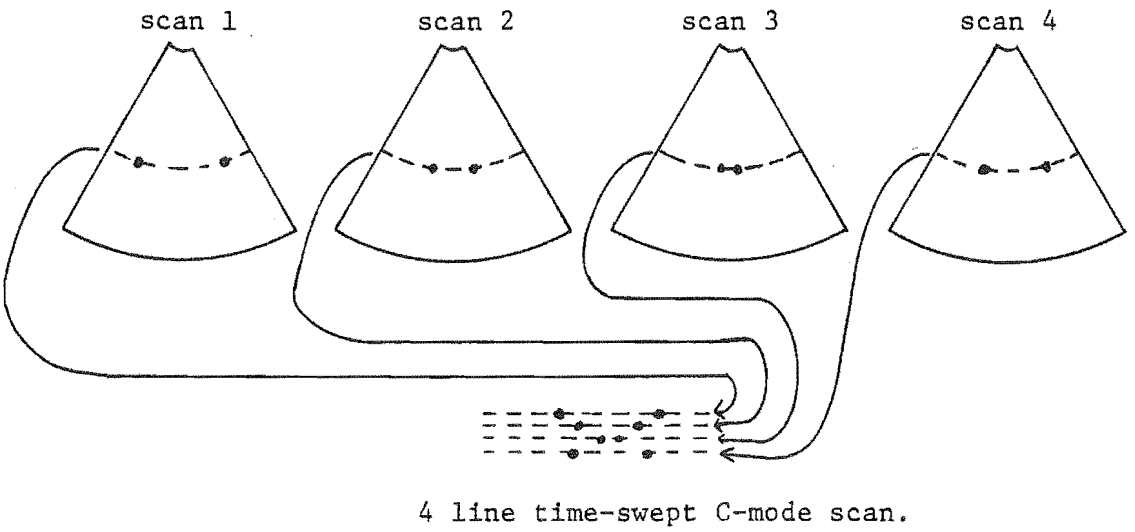

Figure 5.24 C-mode reformating from a series of sector scans.

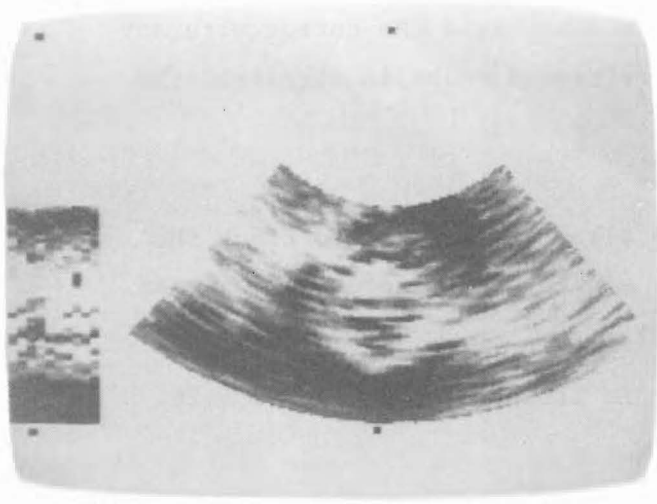

Figure 5.22
The simultaneous M-mode scan. The lines which are common to both scans are marked by the dots.

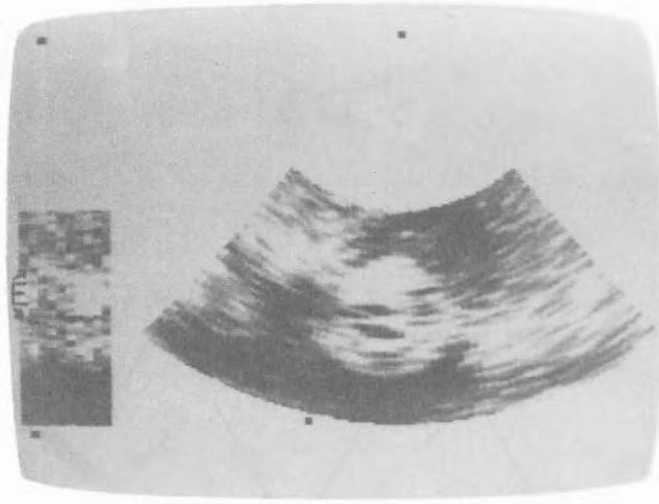

Figure 5.23
This figure demonstrates the difficulty in identifying the endocardium in the M-mode scan. The endocardium is marked by 'E' and arrows. It is difficult to identify in line 3 to 6 of the M-mode display.

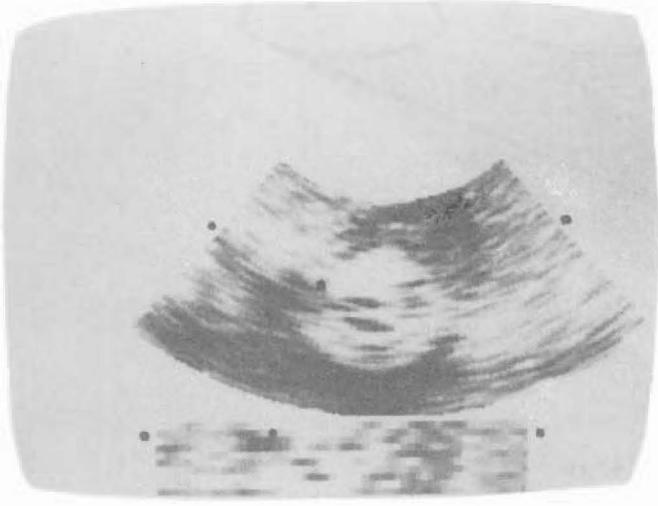

Figure 5.25a
The simultaneous C-mode scan. The lines which are common to both scans are marked by the dots.

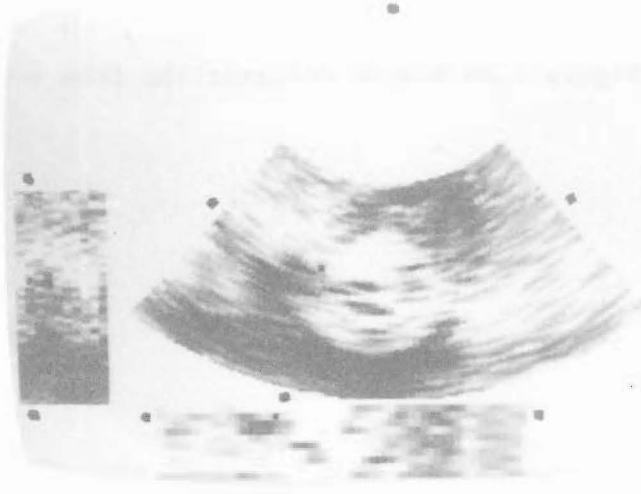

Figure 5.25b
The combined simultaneous M-mode and C-mode displays. The lines common to those in the sector scan are marked with dots.

to the trackball. This makes it difficult to manipulate the cursor with any degree of dexterity. When only one of the refreshed scans is displayed the cursor is much more responsive.

5.4.3 R-mode Reformatting

R-mode reformatting was developed to allow an operator to track the entire endocardial contour with the aid of a single simultaneous motion scan. Thus, there is no loss of cursor response.

The principle of R-mode reformatting is illustrated by Figure 5.26.

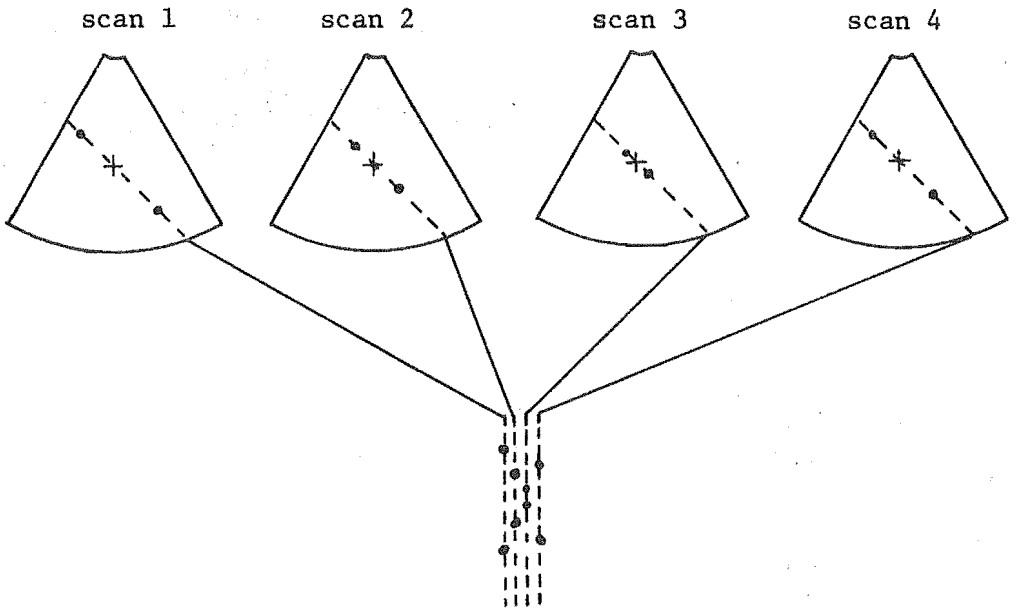

Figure 5.26 R-mode reformatting from a series of sector scans.

A point within the ventricle in all the sector scans in a series is selected. M-mode type scans are then constructed from the sector scans along a line through that point. Such scans (R-mode or radial-mode scans) tend to be formed along lines parallel to the direction of motion of the ventricular walls. Thus the endocardial curve does not disappear, as it does in the M-mode and C-mode scans.

A 'simultaneous R-mode' scan was implemented by constructing R-mode scans along lines through the point at two degree intervals. Again a supplementary cursor marked the point in the refresh R-mode scan corresponding to the position of a cursor in the sector scan (see Figure 5.27). The R-mode scan updates as it rotates around the central point. This simultaneous display was found to be superior to the others as it is possible to follow the entire endocardial curve using only one type of simultaneous display, thus not sacrificing cursor responsiveness.

5.4.4 Endocardial Detection using the Simultaneous Display Method

This section describes a program which was written to allow an operator to define the endocardial contour in a series of sector scans. The program makes full use of the simultaneous display method described in §§5.4.1 to 5.4.3. A flow diagram of the procedure involved is presented in Figure 5.28.

Before entering the program it is necessary to reformat the raw scan data into the sector, C- and M-mode scans. The reformatted scans are stored on disk and are recalled when needed by the program. The raw data is formatted into R-mode scans within the program itself.

The first step when running the program is to review the sector scans to find in which scan the endocardial curve is easiest to identify. The scans can be recalled in any order, it is not necessary to review them in the sequence in which they were obtained.

The operator then traces around the endocardial curve of the sector scan in which the endocardium is most easily identified (see Figure 5.29). This is done with aid of simultaneous display of the M-, C- or R-mode scan. If the R-mode scan is used, the operator must first define a point inside the ventricle through which the scans are to be reconstructed. This is done with the aid of a trackball-driven cursor. The computer then constructs 180 R-mode scans through that point.

Once traced, the operator is given the choice of retracing the curve, continuing on through the program to define its in all of the other scans, or

Figure 5.28 Flow chart of program to extract endocardial curves (§5.4.4)

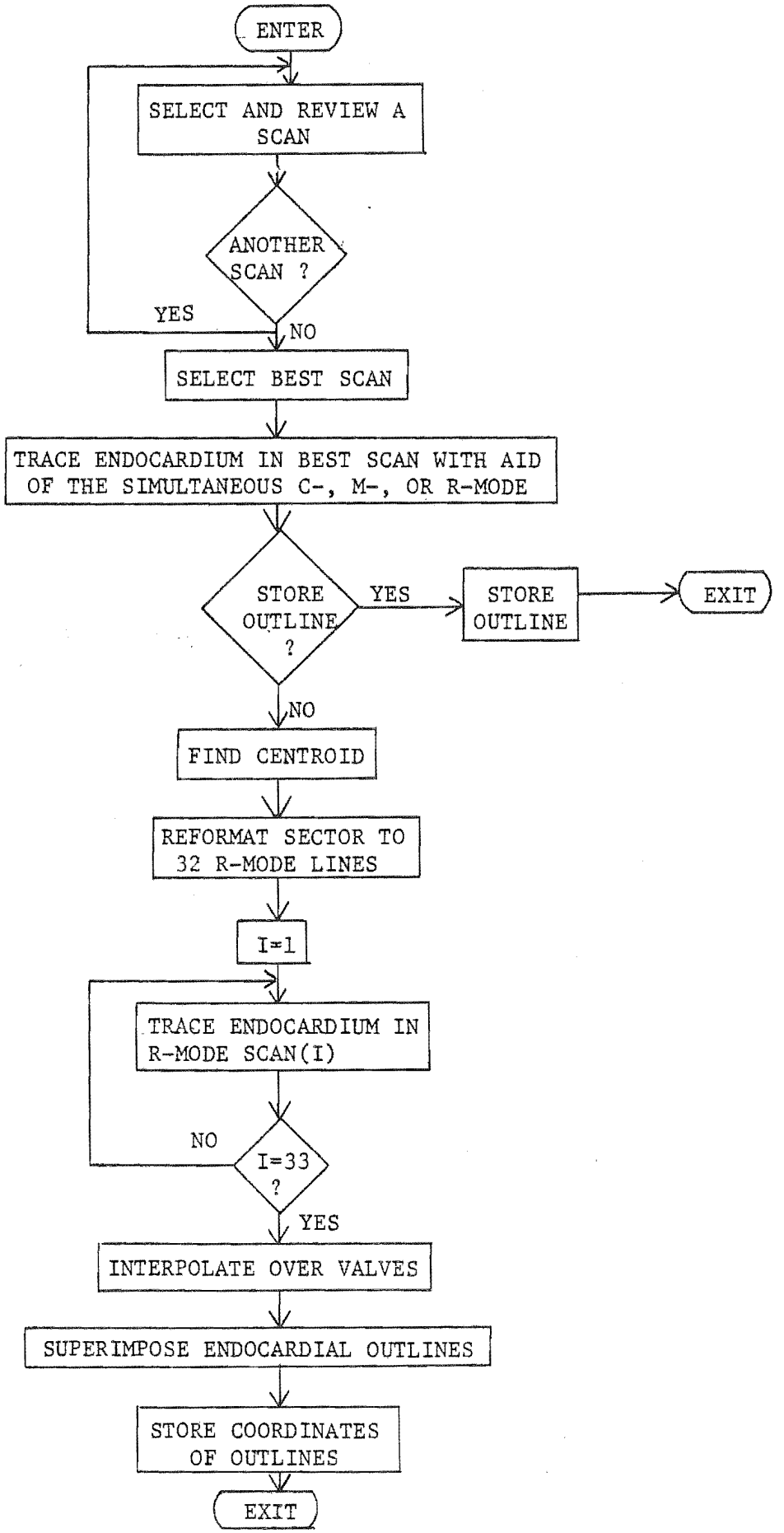

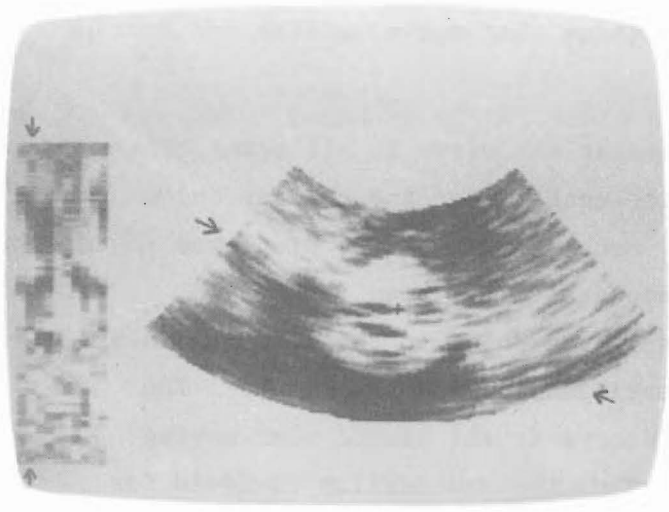

Figure 5.27
The simultaneous R-mode display. The lines which are common to both scans are marked by arrows.

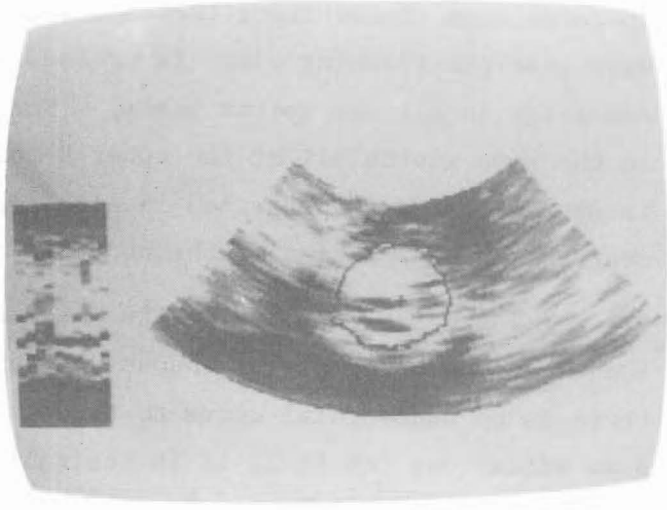

Figure 5.29
The endocardial outline traced with the aid of the simultaneous R-mode display.

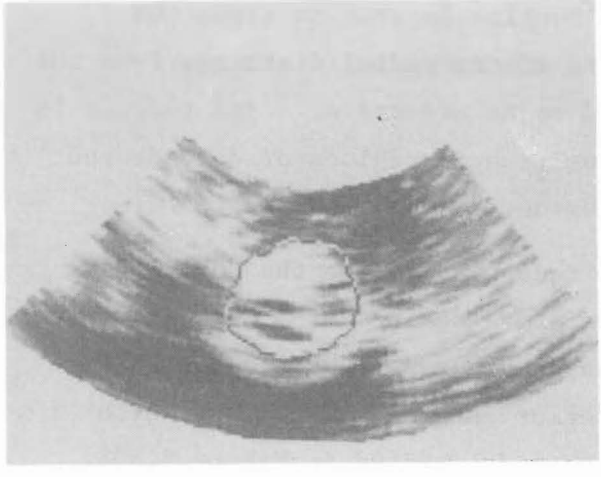

Figure 5.30a
The endocardial outline in Figure 5.20b determined using the outline tracing program. (Section 5.4.4)

Figure 5.30b
The endocardial for the scan shown in Figure 5.20c determined using the endocardial outline tracing program. (Section 5.4.4)

to save all of the pixel co-ordinates describing that curve on disk and exiting from the program.

If it is decided to continue to extract the curve in all scans, the computer then calculates the position of the centroid of the chamber and reconstructs 32 R-mode scans through it. Each R-mode scan is displayed in turn along with the sector scan in which the endocardium has been identified. The pixel in the R-mode scan which represents the point in the sector scan at which the endocardial position has been identified, is made to flash. The operator then traces along the endocardial curve in the R-mode scan making sure that the flashing pixel is crossed. Thus the endocardium is found for one point in all the sector scans. The endocardium is defined to the computer in the same way in all of the other R-mode scans. Thus the endocardial curve is extracted and is described in each scan in terms of polar co-ordinates centred at the position of the centroid of the scan nominated earlier.

There is one pitfall with this technique. The endocardium is seen in some scans as being discontinuous due to the presence of valves. Therefore there is no endocardial curve to trace along in some of the R-mode scans. In some situations (cf.§6.2) it is desirable to describe the endocardium in terms of a simple closed curve. An interpolation routine is used to close the curve in these regions. Linear interpolation of the radial distances from the reference centroid is used and has been found to be effective. The routine is also useful for estimating the endocardial position in regions of echo dropout preventing it from being identified in the R-mode.

Finally, all of the sector scans are redisplayed with the endocardial position identified using the co-ordinates recorded during R-mode tracing. The position defined in this way in the scans of Figures 5.20b and 5.20c are shown in Figures 5.30a and 5.30b. The posterior endocardial contour which could not be identified in Figure 5.20c has been delineated in Figure 5.30b. The operator checks that no gross tracing errors have been made, then the polar co-ordinates and position of the centroid relative to the apex of the sector are stored on disk.

This program was used to extract the endocardial contour in the wall motion and shape studies described in Chapter 6. Note that this method of obtaining wall motion data does so directly rather than by the usual method of calculating them from the wall positions traced in two-dimensional views of the ventricles.

5.5 DISCUSSION

In this chapter the construction of a device to interface a commercial cardiac sector scanner to a computer is described. The device was built specifically to enable series of sector scans taken through the heart cycle to be stored in a computer, in order to study the motion of the walls of the left ventricle. It is necessary for the endocardium to be readily identified in the scans before this can be done. Stop frame scans are often of such poor quality that the endocardium cannot be identified. In §5.3 the effectiveness of methods to process the computer-stored sector scans are considered. It has been found necessary to histogram-equalise the images to enable the endocardium to be seen. It can be identified even more readily if one defines a threshold sample value, below which the signal is rejected.

The noisy and speckled character of the sector scans can be reduced by low pass filtering. Of the techniques applied, local-average filtering has been found to be the most effective. Convolving the data with a weight array whose values simulate the echo shape was found to produce the visually most pleasing images.

Laplacian filtering the images to enhance the edges of details in the images had only limited value. The noise level of the images was high and Laplacian filtering amplifies the noise to an unacceptable level. This effect can be reduced if the images are first low-pass filtered.

The most effective regime, in terms of computer time for improving the scans to the stage where the endocardium can be identified, requires only that the data be echo-shape filtered and then displayed with histogram equalisation using a lower threshold cut-off.

As the sector scans often vary in character over different regions of the image, it is not appropriate to process an entire image with the same filter. A technique called 'regional filtering' was developed whereby different parts of a scan are processed with different filters. This technique is very useful for making the heart walls visible in regions of echo dropout. Much operator interaction is required to define the regions and to choose the best filtering technique. Therefore, regional filtering was not used when there were many scans to be processed.

In many series of sector scans the endocardium was seen in its entirity. In other series of scans the endocardium appeared discontinuous because of echo dropout or because it was confused with other structures in

the ventricles. These difficulties were overcome by reformatting the sector scans into C- and M-mode scans which allowed the endocardium to be identified by its motion. It was then possible to identify its position in the sector scans.

An extension of this, R-mode scanning, where the motion scans are reconstructed through a chosen point in the image, was found to be the most convenient technique to use.

A computer program was written which allows the endocardial position to be identified in a series of sector scans using these techniques. It was used in the wall motion studies described in Chapter 6.

CHAPTER 6

STUDIES OF LEFT VENTRICULAR SHAPE AND WALL MOTION

6.1 INTRODUCTION

Studies of the shape and motion of the left ventricular wall are presented in this chapter. Two groups of patients have been examined. The first was a group of normal volunteers with no history of cardiac disease. The second was a group of patients suffering from single-vessel coronary artery disease (CAD). A region of abnormal ventricular wall motion due to an infarction had been identified in each of the CAD patients when they had undergone routine angiography.

Abnormal wall motion is sometimes observed in normal subjects, and patients with infarctions do not necessarily exhibit wall motion abnormalities. However, abnormal wall motion in those with infarctions can often be induced by exercise (cf. Morganroth et al., 1981). Therefore, the members of the two groups were also studied while undergoing isometric exercise to allow infarcted regions to be more readily identified.

The effect of cardiac drugs on regional wall motion is of interest to clinicians. The drugs may cause ischaemic or infarcted regions of the myocardium to move in a more normal manner. The effects of two particular drugs on the CAD patients were also investigated.

Patients with CAD often have ventricles of different shapes to those of normal people. A method of mathematically describing ventricular shape has been developed. It has been applied to the ventricular outlines of the two groups to see if it is possible to quantitatively establish differences in ventricular shape.

6.2 A FOURIER SERIES DESCRIPTION OF LEFT VENTRICULAR SHAPE

6.2.1 Describing a Simple Closed Curve with a Fourier Series

Consider the simple closed curve in Figure 6.1. It can be described

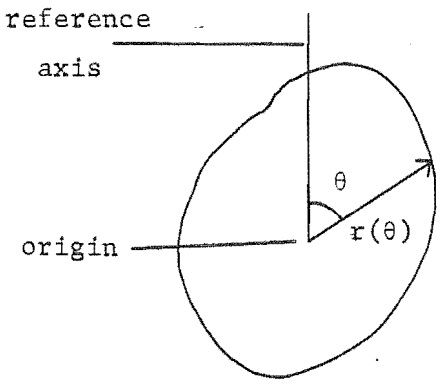

Figure 6.1 A simple closed curve and the polar co-ordinate system for (6.1)

in a trigonometrical Fourier series representation as

$$r(\theta) = \frac{a_o}{2} + \sum_{n=1}^{\infty} \{ a_n \cos(n\theta) + b_n \sin(n\theta) \} \qquad (6.1)$$

where

$$a_n = \frac{1}{2\pi} \int_{-\pi}^{+\pi} r(\theta) \cos(n\theta)\, d\theta \qquad (6.2)$$

$$b_n = \frac{1}{2\pi} \int_{-\pi}^{+\pi} r(\theta) \sin(n\theta)\, d\theta \qquad (6.3)$$

where r is the distance from an origin inside the curve at an angle θ from a reference axis through the origin. An insight into the physical significance of the coefficients can be obtained by examining Figure 6.2. The curve can be thought of as a circle of diameter a_o onto which are superimposed cosine and sine waves of frequency $2\pi/n$ and of amplitudes a_n and b_n. Superimposing a sinusoidal wave of frequency $2\pi/n$ has the effect of making a circle take on the shape of a cloverleaf with n leaves. The coefficients therefore may be used as descriptors of both the size and of the shape of the curve.

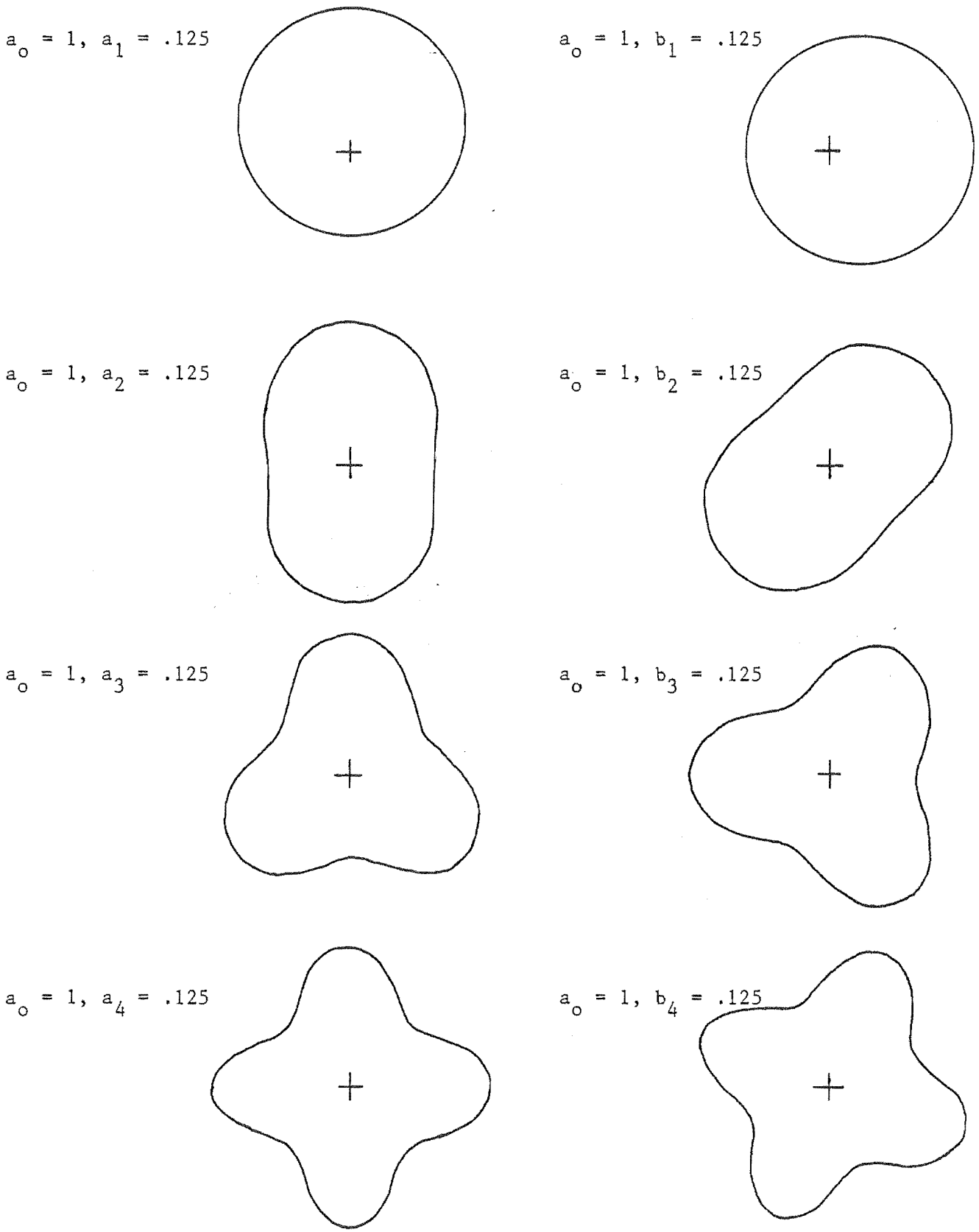

Figure 6.2 Examples of simple closed curves generated by evaluating (6.1) with the coefficient values stated (the values of all other coefficients are zero). The origin of the coordinate system with respect to each curve is marked '+', the reference axis points vertically up the page as in Figure 6.1.

A representation descriptive of shape only is obtained by defining normalised coefficients A_n and B_n where

$$A_n = \frac{a_n}{a_o} \qquad (6.4)$$

$$B_n = \frac{b_n}{a_o} \qquad (6.5)$$

These coefficients are descriptions of the shape of the curve only as they are normalised according to the average diameter of the curve.

When ventricular shape is described in such a way, it is necessary to define a reference axis and an origin. The difficulties involved in defining these are similar to those encountered when quantifying ventricular wall motion using angiography (cf. §3.3.1). It is necessary to make assumptions about the way in which the heart walls move when defining the reference axis and the origin. Even though the conventional angiographic assumptions for quantifying heart wall motion are not strictly correct, they are sufficiently realistic to allow diagnostically useful data to be obtained. A popular assumption which is used by those who study wall motion is that the walls move toward the ventricular centroid (cf. Azancot et al., 1978; Papapietro et al., 1978). This assumption is adopted when interpreting the studies reported in this chapter. When using a fixed-co-ordinate system the above-mentioned researchers consider the motion to be directed towards the position of the centroid in either the end-diastolic or end-systolic frame. If a floating system is used then the origin used is the centroid of the ventricle in each individual frame.

Even though there is no concensus of opinion as to which is the more diagnostically useful, it is reasonable to expect that a fixed origin is more appropriate for analysing regional wall motion. If a floating system is used to analyse a ventricle with one wall which is completely akinetic, the centroid moves towards that wall during systole. The result is that the akinetic wall and the opposite wall both appear to be hypokinetic. This difficulty is not encountered if a fixed co-ordinate system is used. Wall motion is analysed using both systems in this chapter.

When studying ventricular shape, a floating origin must be used to exclude the possibility of wall motion influencing the analysis. Such an origin is employed when studying shape in this chapter.

In angiographic studies, reference axes are often chosen so that they traverse certain landmarks such as the centre of the valve orifices and the apex. However, if one of these landmarks is in a region influenced by cardiac disease, the position of the reference axis is affected throughout the heart cycle. Also, choosing a reference system based on cardiac landmarks is often difficult when a ventricle is studied echocardiographically because in some views there are no suitable landmarks available. For example, in the transverse view of the left ventricle, the only structures seen are the two valve leaflets which are too mobile and not sufficiently separated to position a reference axis.

When a heart is scanned using two-dimensional echocardiography it is viewed through certain 'peep holes' around the rib cage. The patient is repositioned until the heart lines up with the peep holes. The echocardiographer then centres the image of the ventricle in the scan sector. Thus the ventricle is always aligned within the sector in the same manner. The reference axis I have chosen to use is a line parallel to the centre line of the sector scan and through the centroid of the ventricle. Thus it is an external reference axis.

6.2.2 A Practical Fourier Description

In practice, a finite order Fourier series must be used rather than an infinite series as in (6.1). So the summation is truncated to N terms. The studies reported in this section are directed towards determining how large N must be to adequately reproduce a ventricular outline. The coefficients of the finite series are obtained by performing the integrations in (6.2) and (6.3) numerically using a finite number of M points on the curve. The work described in this section was also directed towards determining how large M must be to estimate the magnitude of the coefficients to within a specified tolerance. A program was developed for estimating the accuracy of the coefficients (up to the Nth order) by numerically evaluating (6.2) and (6.3) over $M=2N+1$ points. It operates on data files created by the outline tracing program described in §5.4. In the tracing program an operator moves a cursor around the endocardial outline seen in a two-dimensional echocardiogram. This is done with the aid of the simultaneous R-mode display. A data file containing the co-ordinates of all of the pixels crossed by the cursor is

created. The file contains the co-ordinates of a number Q of pixels where $200 < Q < 350$.

The accuracy estimation program finds the centroid of the area defined by the co-ordinates in the data file created by the tracing program. This serves as a reference origin. An odd number $M=2N+1$ of equally spaced points on the outline are selected such that $0 \leq N \leq 19$. The integrals in (6.2) and (6.3) are evaluated numerically to obtain a_n and b_n values, using the points selected. They are evaluated for all n, i.e. for $0 \leq n \leq N$. The values of a_n and b_n thus obtained are printed out.

Graphs of a_n and b_n versus the number of points $M=2N+1$ used to estimate their values were drawn. A typical graph is presented in Figure 6.3. In this graph the estimates of b_n are seen to settle to relatively constant values quite quickly. Even when only 25 points on the curve are used, b_5 is well estimated. Observations of several such graphs indicated that estimates of a_n and b_n obtained using $M \geq 4n+5$ are relatively constant for all M.

The accuracy estimation program also analyses how well an Nth order summation using M points from the data file can reproduce all the co-ordinates in the file. Consider now the qth point in the co-ordinate data file produced by the tracing program. Let it be at a distance Z_q from the origin (i.e. the centroid). Also, let that point be at an angle θ_q to the reference axis (cf. Figure 6.1). The program selects 2N+1 points on the curve stored in the data file. The values of a_n and b_n for all n in the interval $0 \leq n \leq N$ are calculated by evaluating (6.2) and (6.3) using these points. The distances $r_{qn} = r(\theta_q)$ are calculated using (6.1) using an nth order summation. This is done for all points stored in the data file and for all n in the interval $0 \leq n \leq N$. An average error E_n is defined by

$$E_n = \sum_{q=1}^{Q} \frac{|Z_q - r_{qn}|}{Q} \qquad (6.6)$$

This is a measure of how well the outline produced by an nth order summation approximates the stored curve. The smaller the value of E_n the better the approximation.

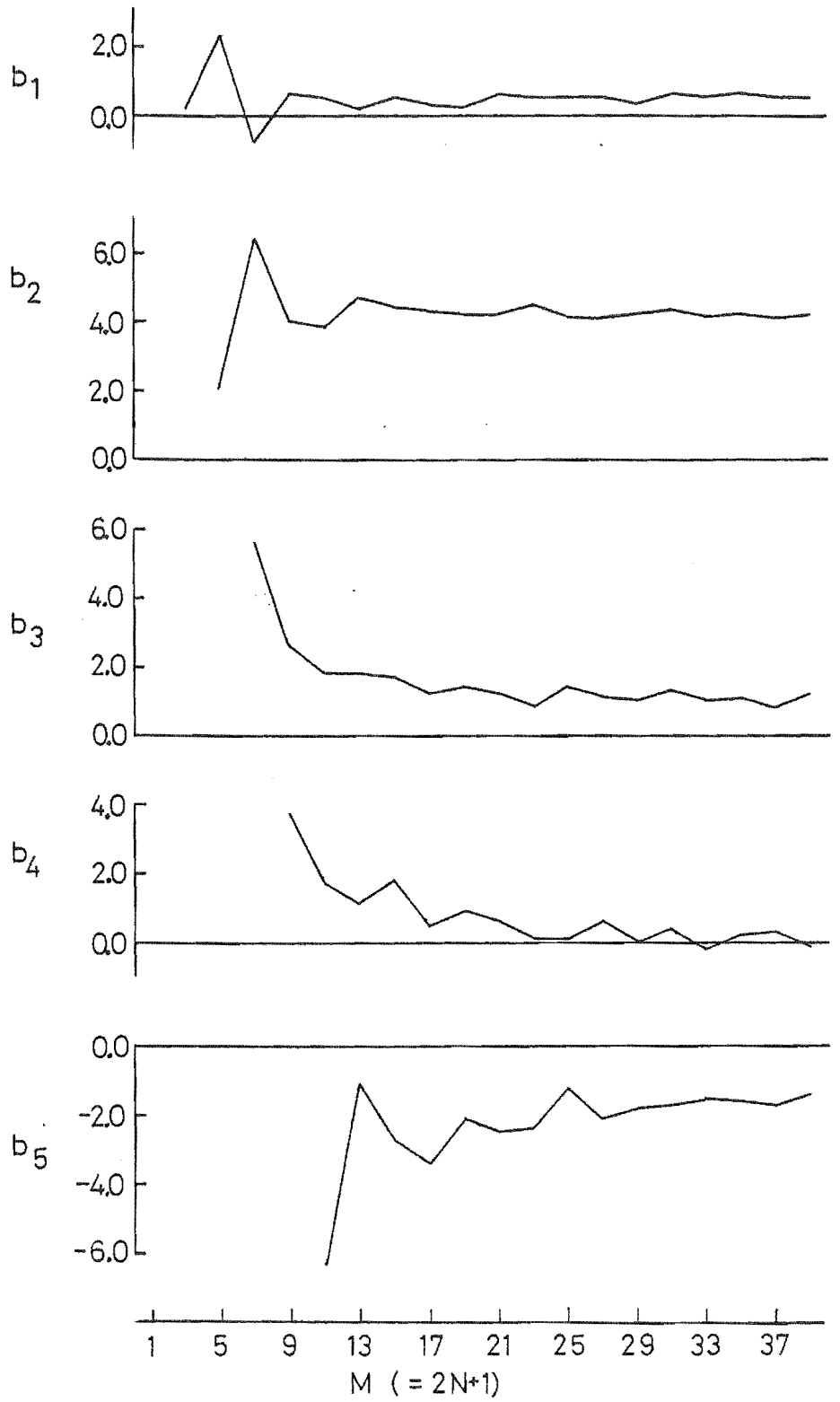

Figure 6.3 Typical graphs of b_n vs. M. The b_n values settle to their final values quite quickly.

Graphs of E_n versus n were also drawn for differing values of M=2N+1. A typical set of graphs for the same co-ordinate data file is presented in Figure 6.4. E_n is seen to reach a lower plateau value when $n \geq 5$. E_n eventually rises again when n becomes large because the corresponding values of a_n and b_n tend to be poorly estimated. It is also seen that E_n does not decrease significantly for $2N+1 \geq 29$. Thus it is considered sufficient to truncate the summation to 5 terms (N = 5). It is also considered sufficient to use only 32 points on the curve (i.e. M = 32) for the integrations in (6.2) and (6.3).

The above was confirmed by the following subjective analysis. The outlines stored in the co-ordinate data files were displayed on the video monitor. Curves reconstructed using the Fourier summation (6.1) were superimposed on the displayed outlines. This was done using M = 32 and $0 \leq N \leq 15$. It was observed that the outlines were reproduced quite well when M = 32 and $N \geq 5$. There was no noticible advantage to be gained by choosing $N > 5$. In fact, if N was chosen to be too large with M = 32, then high frequency oscillations appeared in the curves.

6.3 REGIONAL WALL MOTION STUDIES

6.3.1 Protocol

The echo sampling and scan processing systems (cf. §§5.2 - 5.4) were developed primarily to enable regional left ventricular wall motion to be studied quantitatively. It was envisaged that studies would be performed on subjects at rest and while undergoing isometric exercise. It was also planned to investigate the influence of some cardiac drugs on regional wall motion. The results of these studies are presented in this section.

The difficulties involved in quantifying regional wall motion in echocardiograms are similar to those experienced when using angiograms. There is still no accepted method of quantifying motion in angiograms. However, in angiographic studies, motion in terms of the displacement of walls from the ventricular centroid is often utilized. There are very few studies of regional wall motion using two-dimensional real-time echocardiograms. None use the displacement of walls from the ventricular centroid which is the analytic basis for the studies of wall motion presented in this chapter.

Data Collection

Two groups were to be studied: normal volunteers and patients suffering from coronary artery disease (CAD). All subjects were males. Some of the

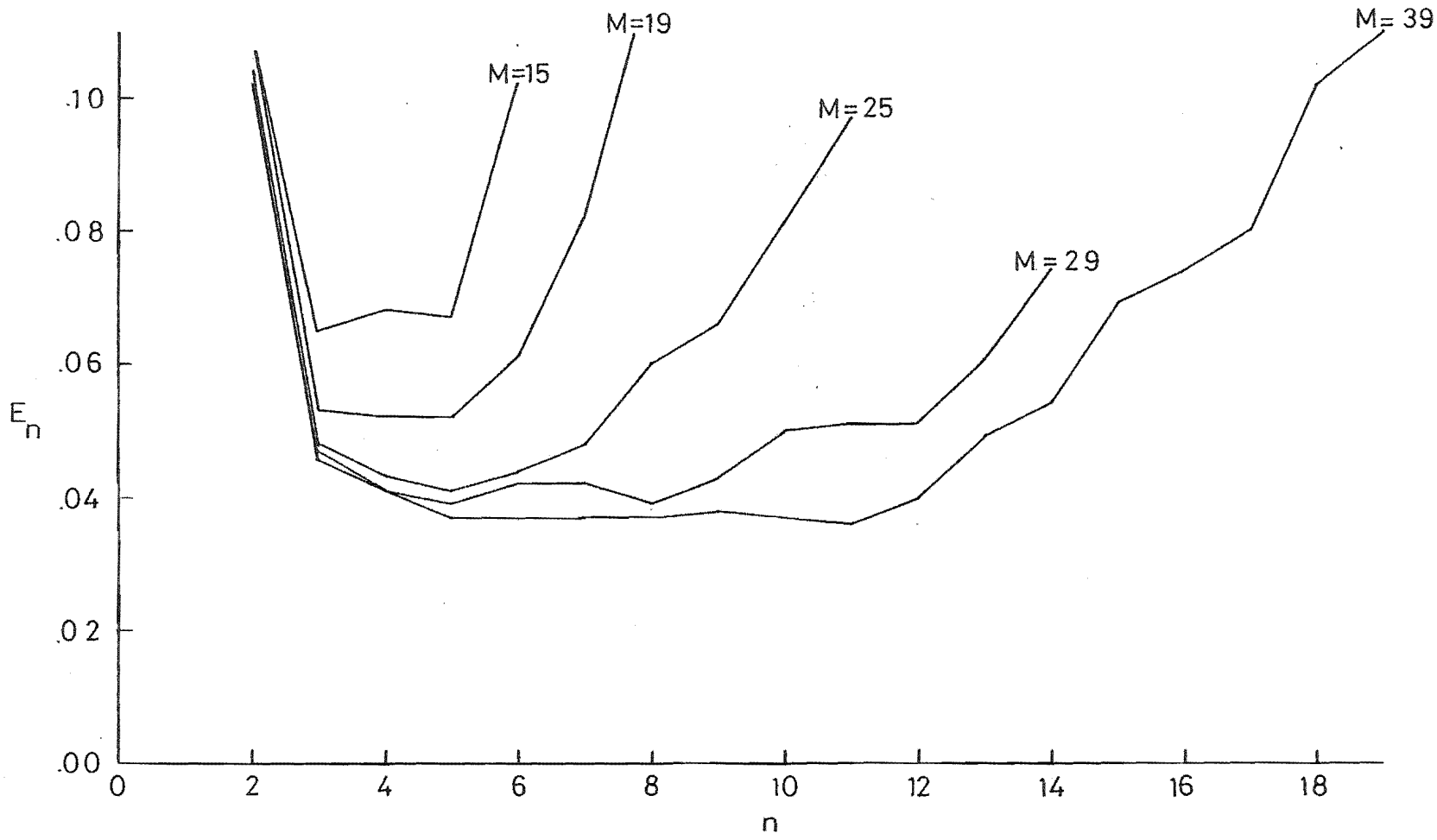

Figure 6.4 Typical graphs of E_n vs. n where $0 \leq n \leq N$ and $M = 2N + 1$.

investigations were performed in areas lacking the privacy necessary to study female subjects. A lower age limit of forty years was set since coronary artery disease is more prevalent in persons aged over forty.

Nine normal volunteers were selected, most were from the hospital staff. They had no history or symptoms of cardiac disease. The nine patients were selected from several hundred people who had been studied angiographically at the Princess Margaret Hospital in the previous eighteen months. They were known to suffer from single-vessel coronary artery disease. They also had an angiographically defined abnormal region of left ventricular wall motion. Five had an apical abnormality (either akenesia or aneurysm(cf. §3.3.1)); three had an inferior wall abnormality and one an anterior wall abnormality.

Several factors excluded subjects from participating in the study:

i) Patients with multiple-vessel coronary artery disease (cf. §3.2) Wall motion abnormalities in these patients would not have been localised.

ii) Patients taking large doses of cardiac medications. These medications may have modified the effects of the drugs to be studied.

iii) Obese subjects. Good quality scans could only be obtained in thin subjects (cf. §4.2).

iv) Patients whose cardiologists would not agree to their participation.

v) Patients whose cardiologists would not agree to the temporary suspension of minor drug therapy.

vi) Subjects who did not have easy access to the Princess Margaret Hospital.

It was originally planned to study the subjects in four of the standard views (cf. §4.2). These were the parasternal long axis view (LA), the apical four chamber view (4C), the parasternal short axis view at the level of the mitral valve (T1) and the parasternal short axis view at the level of the papillary muscles (T2). However, it became apparent that the scanner was incapable of obtaining a satisfactory scan in the T2 view. Therefore, only the first three views were eventually used.

A series of scans each covering a single heart beat was obtained. Scans were taken in subjects both at rest and during exercise. CAD patients were further studied at rest and exercise following the administration of cardiac drugs. The details of these interventions are now discussed.

Exercise involved the subject pulling on a spring-loaded handgrip. The handgrip was calibrated to indicate the amount of force being applied to it.

The maximum amount of force with which a subject could pull the handgrip with one hand was termed the 'maximal effort'. Each subject was required to hold the grip at 30% of his maximal effort for a period of three minutes. At the end of this period, a series of scans was obtained in one of the views. The subject then rested for two minutes before repeating the exercise. Scans in the other views were then obtained. Some subjects found the exercise protocol too strenuous. These subjects were scanned as soon as the exercise became excessive.

The two drugs used in the study of the CAD patients were nifedipine and metoprolol. Their effects on the heart are discussed in §§6.3.4 and 6.3.5 respectively. Patients taking any minor medications had these discontinued the night before the study. This was done to eliminate the cardiac effects of these drugs, otherwise masking of the effects of those drugs administered in the study would occur.

When nifedipine was used, the patient's heart rate and blood pressure were recorded immediately prior to the administration of a 10mg capsule of the drug. These parameters were recorded again after fifteen minutes. A decrease in blood pressure and an increase in heart rate confirmed that nifedipine had taken effect.

In the metoprolol studies, only the patient's heart rate was recorded. A decrease in the heart rate thirty minutes after the administration of a 50mg tablet of metoprolol indicated that the drug had taken effect. In both cases, echo studies with and without exercise were repeated once the drugs had taken effect.

Unfortunately, only eight of the nine patients were able to be studied with nifedipine and seven with metoprolol. Two of the patients would not return for a further study and one was unable to do so because of severe illness.

Data Processing

When the subjects were scanned in each view, a series of nine to eleven images of the left ventricle were obtained. Each covered slightly more than one heart cycle. The images were recorded on floppy disk and later transferred to RK05 hard disks on the PDP 11/10 computer. There they were echo-shape filtered and displayed on a T.V. monitor using histogram equalisation (cf. §5.3). The endocardial border was traced using the program described in §5.4. The position of 32 points on the outline traced from each

image were stored on disk.

Regional wall motion was analysed using the radial axis co-ordinate system illustrated in Figure 6.5.

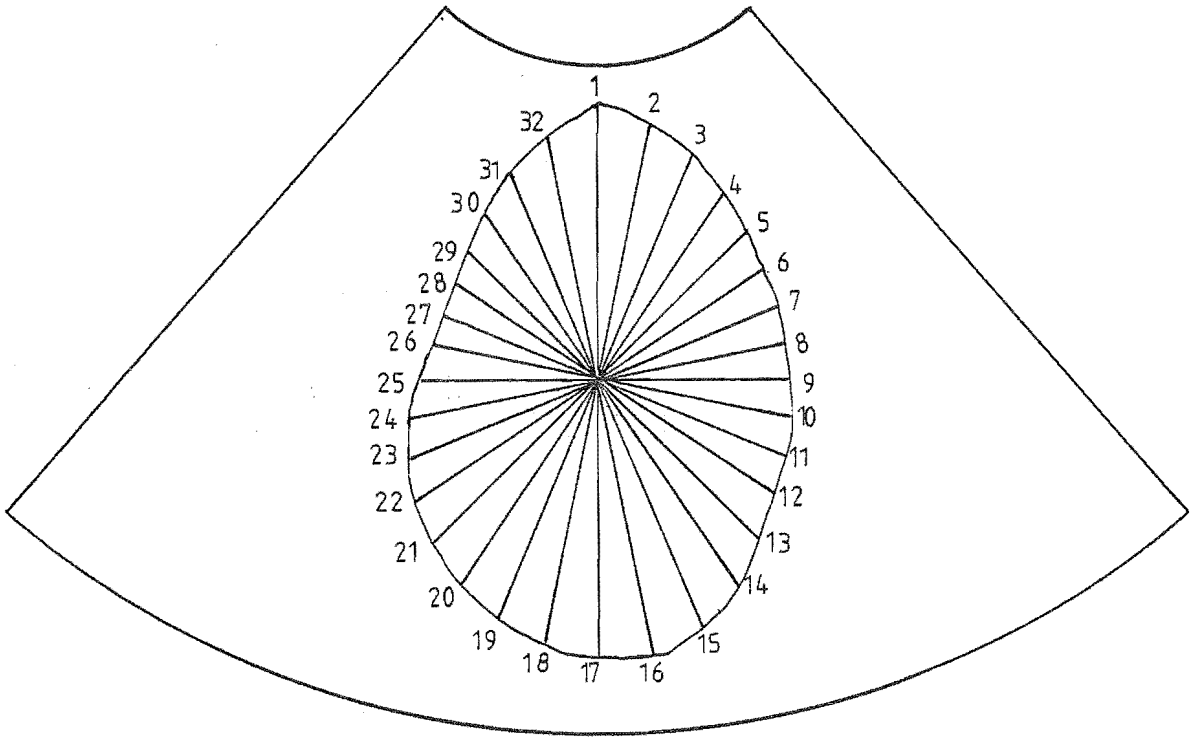

Figure 6.5 Radial co-ordinate system. The origin is at the ventricular centroid

Thirty-two radial axes are defined at equal increments of angle. They are numbered clockwise. Axis number 1 is parallel to the centre scan line of the sector and directed towards the transducer. The origin of the system may be 'floating' or 'fixed' (cf. §3.3.1). When a floating origin is used, the origin is at the centroid of the ventricle in each image. If a fixed origin is

used, it is set at the centroid of the ventricle in the frame displaying the smallest ventricle. This frame was considered to be the end-systolic frame. The wall motion data was analysed using both types of origin.

Wall motion was analysed using the percentage change in the centroid to-wall distance from end-systole to end-diastole. This percentage shortening S is defined as

$$S = \frac{R_D - R_S}{R_D} \times 100 \qquad (6.6)$$

where R_D = centroid-to-wall distance in the frame with largest ventricular area (end-diastolic frame)

R_S = centroid-to-wall distance in the frame with smallest ventricular area (end-systolic frame).

S is a useful parameter which has been widely applied to angiographic wall motion analysis (cf. §3.3)

The 32 points on the outline which are stored by the tracing program (cf. §5.4) are not necessarily those points where the radial axes intercept the ventricular outlines. It is necessary, therefore, to interpolate between the 32 stored points in order to calculate the lengths of the radial axes. This is achieved by fitting a curve to the 32 stored points by calculating a set of a_n and b_n $(0 \leqslant n \leqslant 5)$. To do this the integrals in (6.3) and (6.4) are evaluated using the 32 stored points and the radial-axis system's origin. The points where the radial axes cross the outline are then calculated using (6.1).

The mean percentage shortening $\bar{S}$ of the radial axes for each group of L studies is calculated by

$$\bar{S} = \sum_{k=1}^{L} \frac{S_k}{L} \qquad (6.7)$$

where S_k is the percentage shortening of the radial axis of the kth subject. Also the standard deviation σ_s of the S_k values is calculated by

$$\sigma_s = \sqrt{\frac{\sum_{k=1}^{L} (\bar{S} - S_k)^2}{(L-1)}} \qquad (6.8)$$

A convenient way of presenting the $\bar{S}$ values of each group is afforded by graphs of $\bar{S}$ versus radial axis number (see Figure 6.6). Wall motion abnormalities are easily identified in such graphs (cf. Figure 6.8c).

They are used in this thesis to compare the $\bar{S}$ values for the two groups under the various interventions used.

6.3.2 Reproducibility

There are four main factors which will cause variations in the estimates of S.

i) There are variations in the way the heart contracts from beat to beat (cf. Harris, 1974)

ii) It is difficult to scan the heart in exactly the same plane every time. This is partly because the heart is not rigidly fixed within the rib cage. It lies in a slightly different position each time a patient is examined.

iii) There is a range of cross-sections of the heart in which a similar view can be obtained.

iv) When using the tracing program (§5.4), an operator does not consistently trace the ventricular outline.

The following experiments were performed to determine the influence of these factors on S.

A young male volunteer was selected of whom good two-dimensional scans could be obtained. He was scanned seven times using the four-chamber view. Each time he was scanned, nine images of the heart were obtained. The nine images together had a duration of slightly more than one heart cycle. Between each scan he was made to sit up and lie back down. This was to re-orientate his heart within the rib cage. The echocardiographer then attempted to scan his heart in the same cross-section.

$\bar{S}$ and σ_s for the seven scans were calculated for each radial axis. Both a fixed and floating origin were used. $\bar{S}$ and σ_s are presented in Figures 6.6a and 6.6b respectively. These graphs show that $\frac{\sigma_s}{\bar{S}}$ is approximately 20% and σ_s 8% for each radial axis. They are unchanged when a fixed or a floating origin was used.

It is of interest to note that when a fixed origin was used, the shortening at the apex is less than at the mitral valve since the mitral valve moves downwards during systole more than the apex moves upwards. This effect is not as obvious when the floating origin was used. This is because the origin was placed very close to midway between the apex and the valve in each frame. The floating origin therefore tended to compensate for any apparent lack of shortening at the apex.

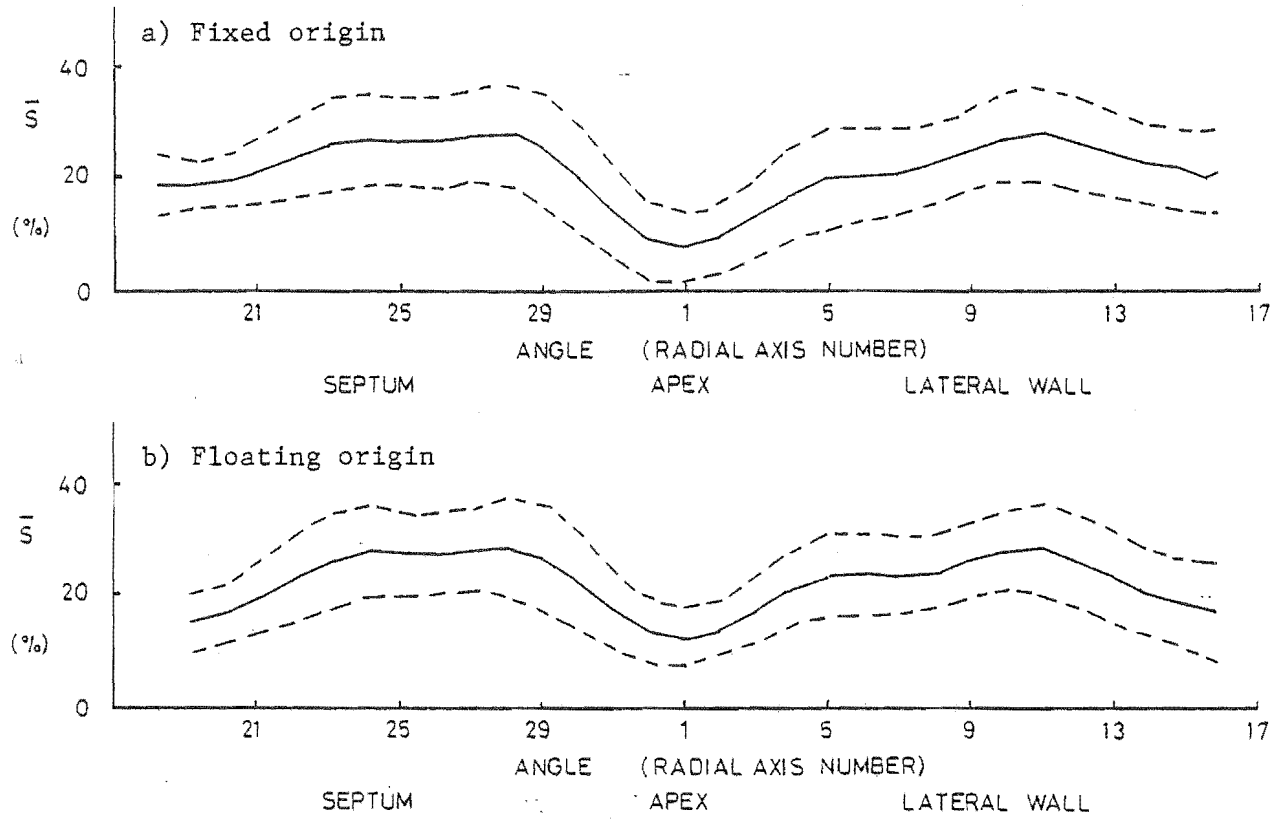

Figure 6.6 $\bar{S}$ values of normal volunteer scanned seven times. $\bar{S} \pm \sigma_s$ values shown as dashed lines.

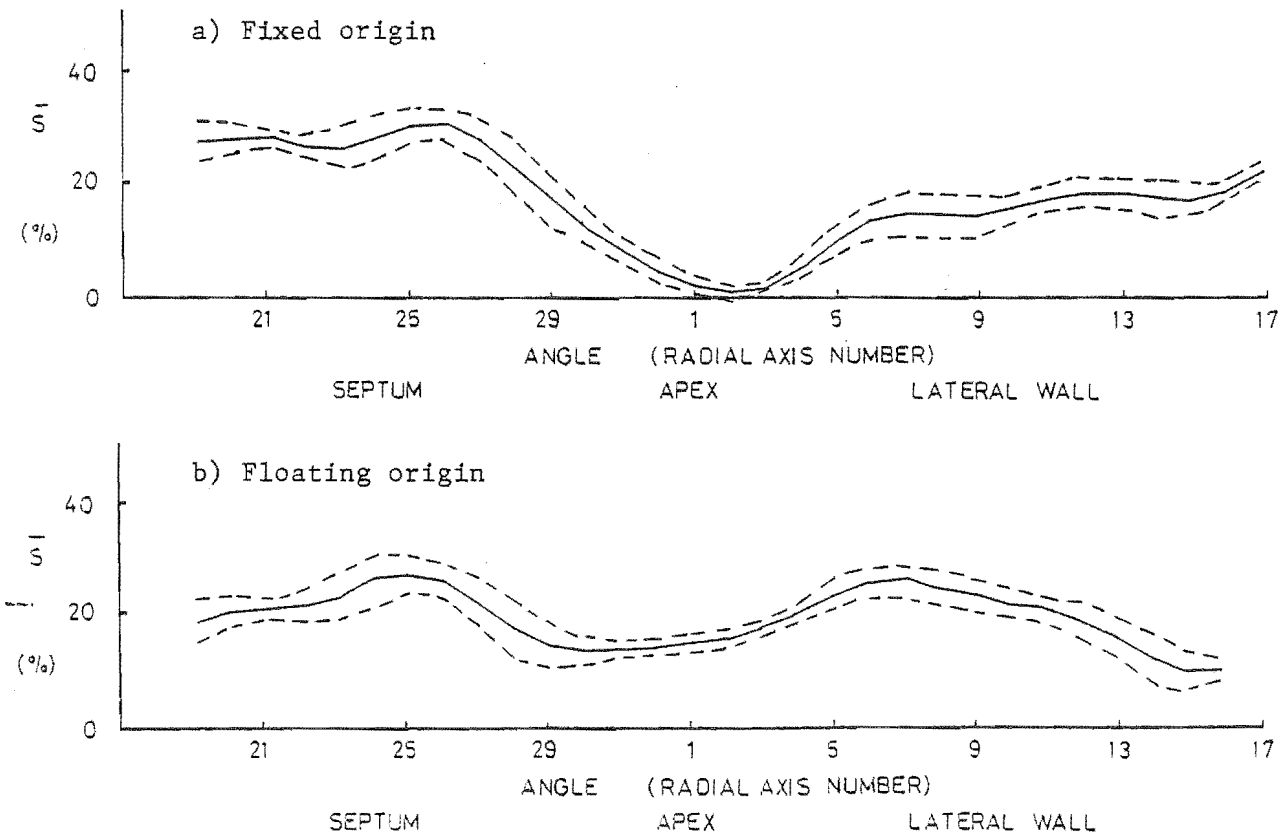

Figure 6.7 $\bar{S}$ values of a single set of scans of a normal volunteer in which the outlines were traced seven times. $\bar{S} \pm \sigma_s$ values shown as dashed lines.

The effect on S of operator interpretation of ventricular outline was also studied. The ventricular outline was traced seven times in one set of nine images. Graphs of $\bar{S}$ and σ_s versus radial axis number are presented in Figures 6.7a and 6.7b. σ_s is approximately 2% at the apex and near the mitral valve, and 4% at the septum and lateral walls. The tracing errors are therefore small in comparison to those encountered in the patient repositioning study (Figures 6a and 6b).

The effects of beat-to-beat variations were not investigated. To do this it would have been necessary to record scans continuously over several consecutive heart cycles. Igor is not capable of this. A delay of twenty seconds between two sets of scans is necessary when recording with Igor. The delay is to allow data to be transferred to disk and to allow the computer operator to prepare to record the next set of scans. Suspending respiration over several heart cycles minimizes respiration and organ movement artifacts. However, it also causes physiological changes which alter the heart's motion.

6.3.3 Exercise

Exercise causes the body's demand for oxygen to increase. To help meet this demand, the blood flow (and hence oxygen supply) increases. This is effected by an increase in heart rate.

The proportion of blood which is pumped from the ventricle at each beat is called the 'ejection fraction'. It is a measure of gross contractile motion of the walls. While it may be expected that this fraction gets larger to increase blood flow, this is not always so. If the exercise is initially low and is slowly increased, then the ejection fraction also increases (Zwehl et al., 1981, Foster et al., 1981). However, if a large exercise load is suddenly applied to the body, the ejection fraction decreases. This suggests that the myocardium becomes ischaemic (Foster et al., 1981). This phenomenon is often seen in subjects who undergo isometric exercise. The decrease in ejection fraction is due to an increase in end-systolic volume. Ludbrook et al. (1980) report, however, that in some subjects exercising isometrically, the ejection fraction stays the same or even increases.

As well as affecting gross contractile motion, exercise also induces regional wall motion abnormalities. This occurs in CAD patients (Morganroth et al., 1981; Mitamura et al., 1981; Wann et al., 1981). However, if exercise fails to induce regional wall motion abnormalities, CAD is not necessarily excluded (Morganroth et al., 1981).

Results of the effects of exercise on wall motion for normal volunteers

and CAD patients are now presented.

(A) Four chamber view

Graphs of $\overline{S}$ for the normal volunteers at rest and undergoing exercise are presented in Figures 6.8a and 6.8b. The corresponding graphs for five of the CAD patients are presented in Figures 6.8c and 6.8d. These patients had apical infarctions. The shortenings are calculated using a fixed origin. All other graphs of $\overline{S}$ presented later in this chapter are of data calculated relative to this origin.

In normal volunteers at rest, $\overline{S}$ is very similar along most parts of the wall. $\overline{S}$ is small in the region of the apex, indicating a lack of shortening there. Little change was induced by exercise apart from a small decrease in $\overline{S}$ along the septum. This is probably due to exercise-induced ischaemia (cf. Foster et al., 1981).

Two of the five apical infarction patients were studied twice. $\overline{S}$ was calculated over the seven studies. At rest, $\overline{S}$ is seen to be very large in certain regions of the septums of the CAD patients (compared Figure 6.8a with Figure 6.8c). This suggests that a region of hyperkinesia developed to compensate for the loss of contractility at the apex. This is seen in the real time scans of the patients. During exercise, $\overline{S}$ is reduced at most points on the lateral and septal walls. It is particularly noticable in the hyperkinetic region, which is no longer so obvious. These effects are probably due to exercise induced ischaemia. Similar effects are seen in corresponding graphs of shortening calculated using a floating centroid.

There are obvious differences between the graphs of the normal and apical infarct groups. $\overline{S}$ at the apex was less in the infarct group than the normal volunteers. This is so both at rest and during exercise, which suggests akinesia in this region. These results are consistent with findings angiography.

(B) Long axis views

The graphs of $\overline{S}$ for normal volunteers are presented in Figure 6.9. Adequate long axis views could be obtained in only five of the nine volunteers. Results for subjects at rest are presented in 6.9a and undergoing exercise in 6.9b. The corresponding graphs for the three CAD patients with inferior wall abnormality are presented in Figures 6.9c and 6.9d. These three patients were scanned twice, so that values of $\overline{S}$ were obtained for six sets of scans.

The inferior wall motion defects were not obvious using the real time scan. Since part of the inferior wall was visible in the parasternal long-axis

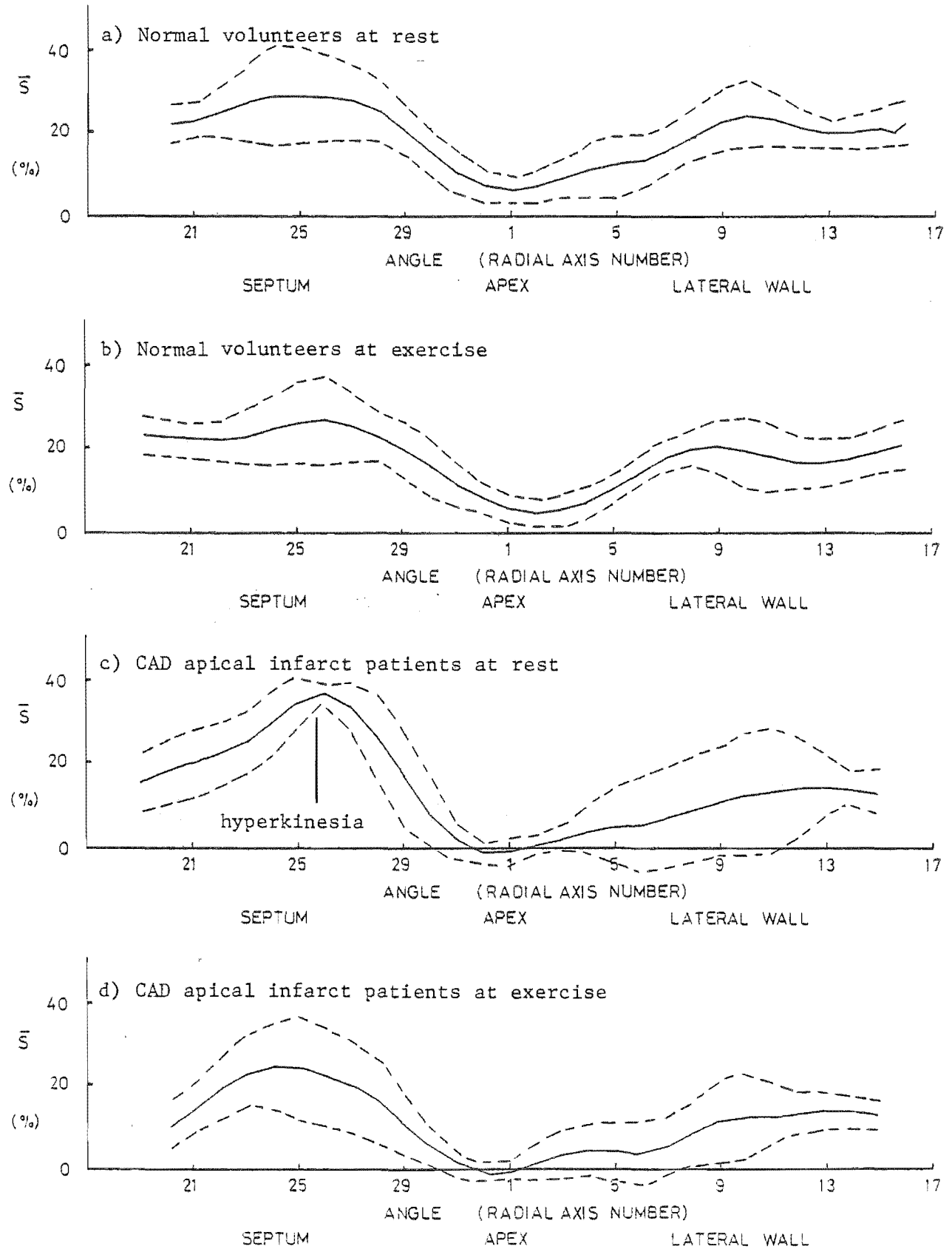

Figure 6.8 $\bar{S}$ values of subjects taken from the four chamber view at rest and exercise. $\bar{S} \pm \sigma_s$ values are shown as the dashed lines.

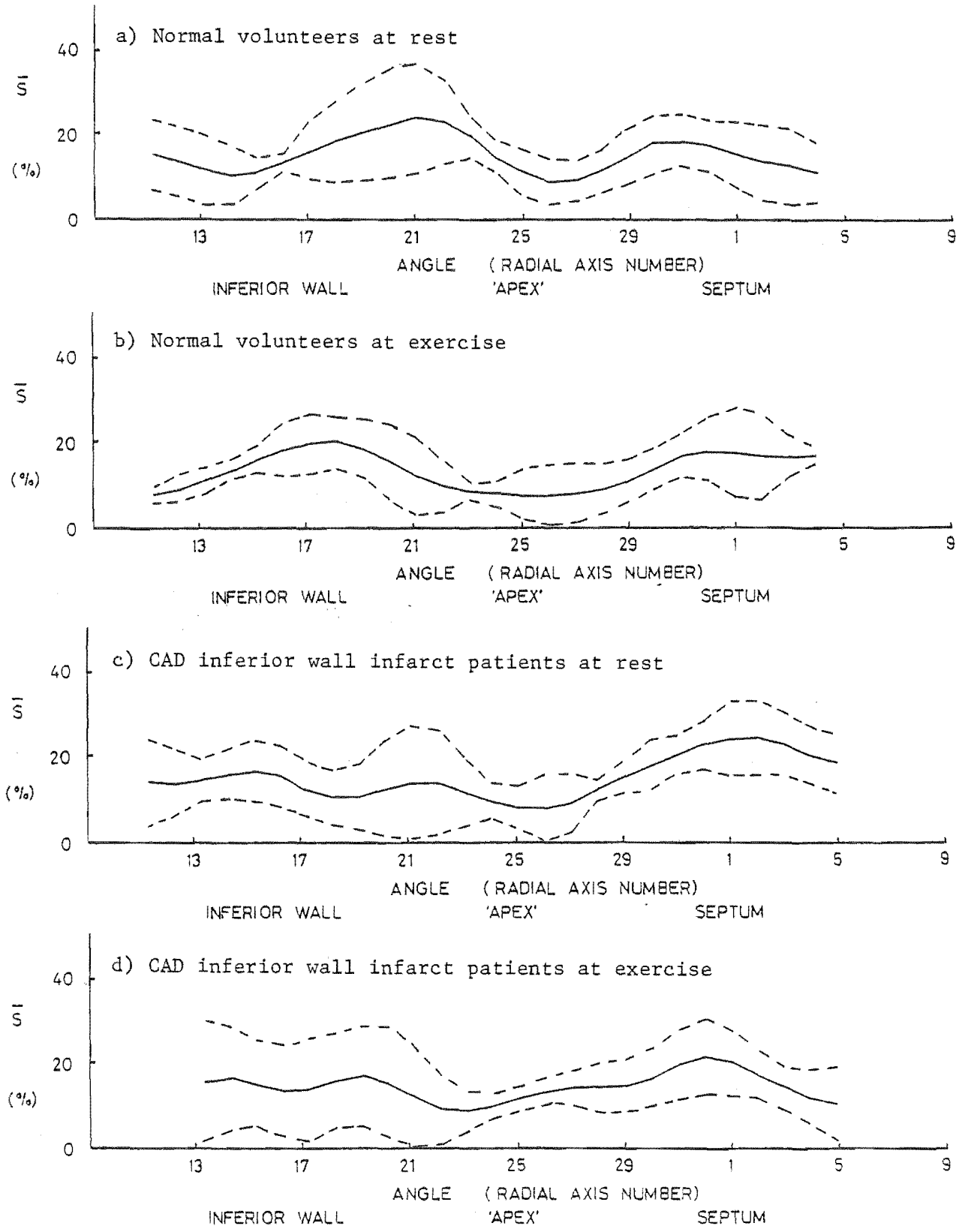

Figure 6.9 $\bar{S}$ values of subjects taken in the parasternal long axis view at rest and exercise. $\bar{S} \pm \sigma_s$ values are shown as the dashed lines.

view, it was expected that the region of abnormal wall motion be detected. However, there is little difference between the $\overline{S}$ graphs of patients at rest and at exercise. There was also little difference between the corresponding graphs of normal volunteers and CAD patients. Therefore, it was apparent that wall motion abnormalities of the inferior wall could not be reliably recognised in these patients.

Thus, while the long axis view is useful when analysing valve motion, it is of limited value when observing wall motion. The ventricular cross-section obtained in the long-axis view does not follow an imaginary axis from the centre of the base of the ventricle to the apex as may be expected. Instead the cross-section cuts through the lateral wall before the apex is reached. This is because of the restriction imposed by the orientation of the heart in the rib cage. The left ventricle appears truncated and a 'false apex' is seen where the cross-section cuts the lateral wall (Feigenbaum, 1981). Therefore, very little of the inferior wall and septum is seen. Instead, large areas of the lateral walls are seen. However, the direction of motion of the lateral wall is almost perpendicular to the plane of the scan. This motion is not in the plane of the scan and therefore, it was not studied.

(C) T1 and T2 views

Two views which I would have liked to study in detail were the short axis view at the level of the mitral valve (T1) and the short axis view at the level of the papillary muscles (T2) (cf. §6.3.1). However, because of technical difficulties in obtaining satisfactory images, the T2 views could not be obtained. Also, none of the patients studied had infarctions at the level of the T1 view, so motion in this view was not investigated.

We have recently tested modern two-dimensional scanners at the Princess Margaret Hospital which provide high quality images in the T2 view. It is expected that such a scanner will be purchased shortly which will allow motion seen in this view to be studied.

6.3.4 Nifedipine

Nifedipine belongs to the class of drugs called 'calcium antagonists'. It causes muscle fibres to relax. Therefore it reduces the contractility of normal myocardium. It also acts as a vasodilator, that is, it causes the internal diameter of the blood vessels to increase (Serruys et al., 1981). Vasodilation in turn causes the blood pressure to drop. As a result, the heart rate increases in an effort to maintain normal blood pressure.

Small doses of nifedipine also cause the ejection fraction to increase.

Some authors report that nifedipine appears to have a directly beneficial effect on the contractility of ischaemic myocardium (cf. Weintraub et al., 1982). The contractility of ischaemic (as opposed to normal or infarcted myocardium) increases. This is a result of improved blood flow caused by vasodilation.

The effects of nifedipine on $\overline{S}$ in four of the apical infarction patients were studied. The graphs of $\overline{S}$ at rest and exercise are presented in Figures 6.10a to 6.10d. A region of hyperkinesia (ischaemic myocardium) occurs at the edges of an infarcted area. This hyperkinetic area lies in the septum. The area becomes even more mobile after the administration of nifedipine. This was most pronounced in patients undergoing exercise. It also occurred at rest. In contrast, the apex itself (infarcted area) remained hypokinetic under the influence of nifedipine, both at rest and exercise.

These results indicate that nifedipine does increase the contractility of ischaemic myocardium as is suggested by Weintraub et al., (1982).

6.3.5 Metoprolol

Metoprolol belongs to the class of drugs called Beta-blockers (McDevitt, 1979), which generally act on the Beta receptors in the nervous conduction system of the heart, blood vessels and lungs. However, metoprolol is more specific. It acts only on the Beta receptors of the heart. It causes the heart to beat more slowly and reduces the force with which the heart contracts. As a result, the myocardium requires less oxygen. Thus, patients who have metoprolol administered to them can exercise more strenuously without experiencing distressing cardiac symptoms.

The effects of metoprolol on the values of $\overline{S}$ in three apical infarct patients are seen in Figures 6.11a to 6.11d. Whether the patients were at rest or exercising, the values of $\overline{S}$ for all regions of the ventricular wall decreased. This is probably because the force of contraction of the heart was reduced. The apex, however, still did not move. These effects are consistent with the known effects of metoprolol.

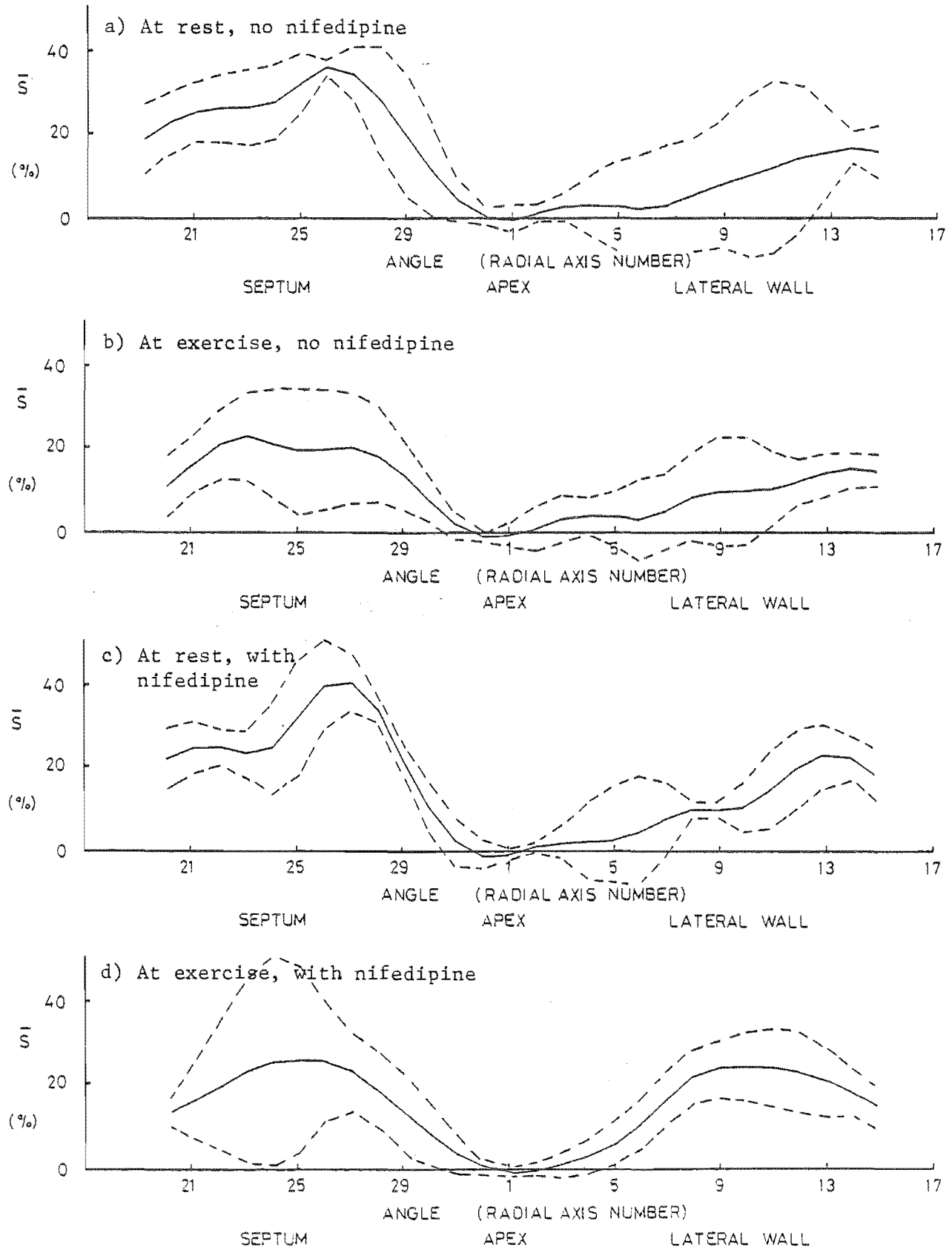

Figure 6.10 $\bar{S}$ values of CAD apical infarction patients taken from the apical four chamber view. $\bar{S} \pm \sigma_s$ values are shown by the dashed lines. Nifedipine study.

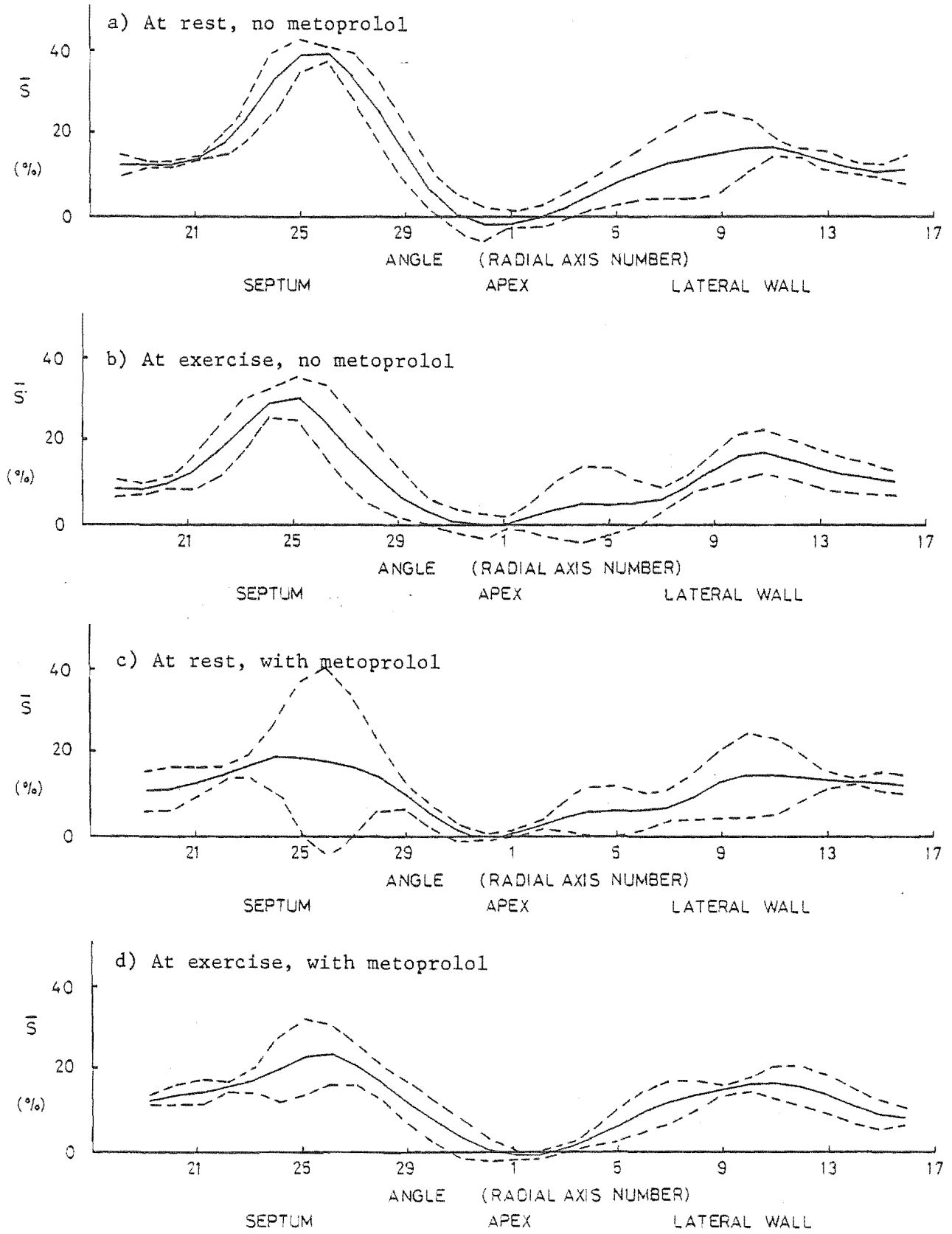

Figure 6.11 $\bar{S}$ values of CAD apical infarct patients taken from the apical four chamber view. $\bar{S} \pm \sigma_s$ values are shown by the dashed lines. Metoprolol study.

6.4 APPLICATION OF FOURIER SHAPE DESCRIPTORS

6.4.1 α_n Descriptors

Very few methods of quantifying left ventricular shape are reported in the literature. This is surprising as shape is often assessed qualitatively when diagnosing ventricular abnormalities (cf. §3.4). The normalised coefficients A_n and B_n of the Fourier series summation defined in §6.2 are descriptors of the shapes of closed curves. They may therefore be used as a basis for quantitatively assessing the shape of ventricular outlines.

Ten coefficients are used in the Fourier description, namely A_1 to A_5 and B_1 to B_5 (cf. (6.2), (6.3)). A clinician would probably prefer to assess ventricular shape by referring to a smaller number of descriptors. Not all of the A_n and B_n necessarily convey equal amounts of useful information. Those that are the least informative may be disregarded. For example A_1 and B_1 describe the eccentricity of the ventricle about the origin. By defining the origin as being at the ventricular centroid, the eccentricity is made to be negligible. Therefore A_1 and B_1 represent little significant information. Of the remaining coefficients (i.e. n>1), A_n and B_n tend to decrease as n increases. If the absolute error in estimating A_n and B_n is the same for all n then the estimates of A_n and B_n become relatively less accurate as n increases. Thus A_n and B_n for n = 2 or 3 are likely to be the most useful descriptors.

The number of descriptors is halved by combining A_n and B_n to obtain a set of descriptors α_n such that

$$\alpha_n = \sqrt{A_n^2 + B_n^2} \qquad n = 1,2,\ldots,5 \qquad (6.9)$$

The α_n descriptors have the advantage that they are insensitive to the direction of the reference axis (cf. Figure 6.1). Therefore it is irrelevant whether a fixed or a floating reference axis is used.

6.4.2 Reproducibility

If A_n, B_n and α_n are to be diagnostically useful, it must be possible to estimate their values reliably, within the variations to be expected each time the same patient is studied. The factors which introduce variations into recorded ventricular (and therefore values of A_n, B_n and α_n values) the same as are those which affect the estimates of S (cf. §6.3.2). These are:

i) the beat-to-beat variations

ii) the difficulties in aligning the heart with a peep hole in the ribcage

iii) the dissimilarity of several cross-sections of the heart which apparently provide the same view

iv) inconsistent tracing of the ventricular outlines

The data obtained to estimate the reproducibility of the S values was also used to determine the reproducibility of the A_n, B_n and α_n values. Examples of the ventricular outlines obtained in the reproducibility studies are presented in Figures 6.12 and 6.13. They display the outlines traced from end-systole to end-diastole.

Those in Figure 6.12 were obtained by retracing the same set of scans obtained of a volunteer over a single heart cycle. They are all very similar. This demonstrates that an operator is able to trace the same outline quite well.

Those in Figure 6.13 were obtained by tracing different sets of scans obtained of the same volunteer over different heart cycles. The volunteer was made to sit up between taking each set of scans. This was done to randomise the position of the heart within the body for each study. Thus all of the factors i) to iv) listed above affect the reproducibility. The outlines in Figure 6.13 are quite dissimilar to each other. This indicates that it is very difficult to obtain scans in the same cardiac cross-section each time the same patient is studied.

The dissimilarity of the outlines suggests that dissimilar estimates of A_n, B_n and α_n are likely to be obtained each time a patient is studied. Therefore it may be necessary to study the same patient repeatedly in order to average out these differences, and thus obtain reliable values of A_n, B_n and α_n. It was impractical for me to do this on a regular basis because it took me up to two hours to process the scans in each study. Even though the variations in the A_n, B_n and α_n values are large for each study of a single subject, reliable estimates can be obtained of the mean values of these either for normal or for CAD patients by averaging the estimates of the values of the subjects in each group.

The effects of operator interpretation of an outline on the A_n and α_n values for $1 \leqslant n \leqslant 4$ are illustrated by Figures 6.14 and 6.15. Graphs of B_n are not shown as they do not display any extra useful information. In Figures 6.14 and 6.15, frames 0 and 8 are at the end-diastolic points and frame 3 is at end-systole.

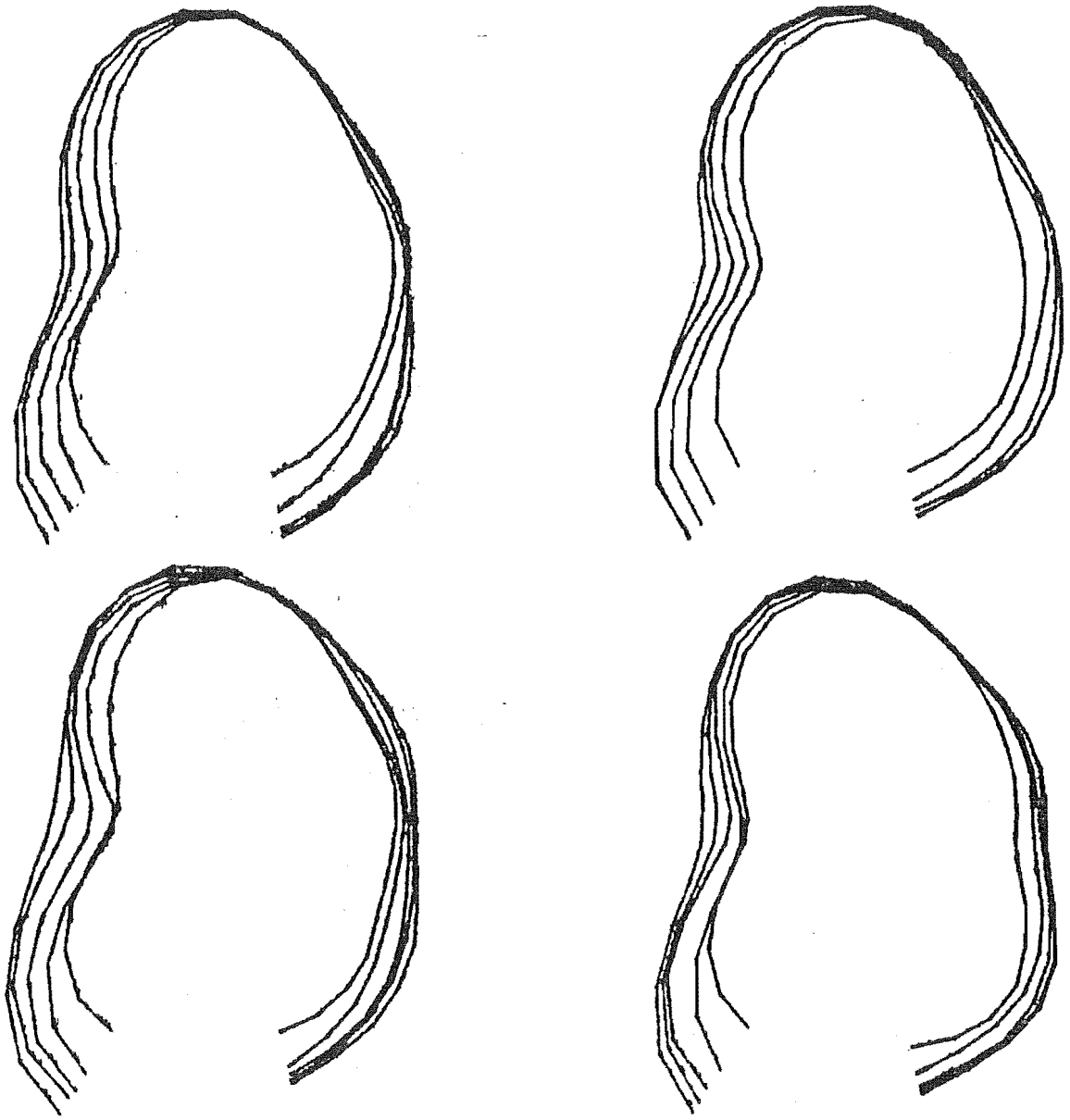

Figure 6.12 Four sets of ventricular outlines from end-systole to end-diastole. The four different sets of outlines were obtained by retracing the ventricular outlines in the same set of scans.

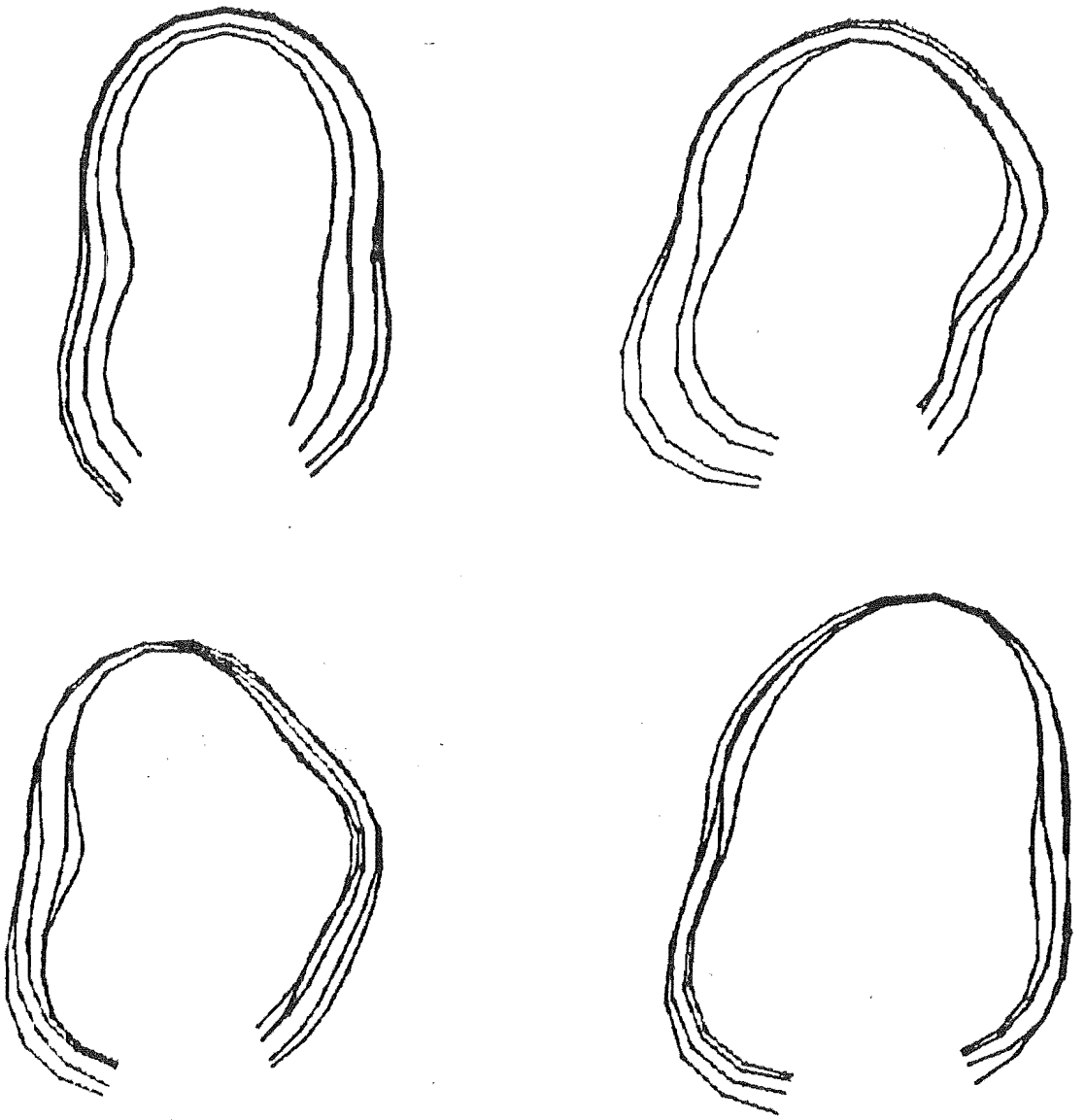

Figure 6.13 Four sets of ventricular outlines from end-systole to end-diastole. The four different sets of outlines were obtained by tracing the ventricular outlines in four different sets of scans. The scans were taken in the apical four chamber view. The scans were all taken of the same patient.

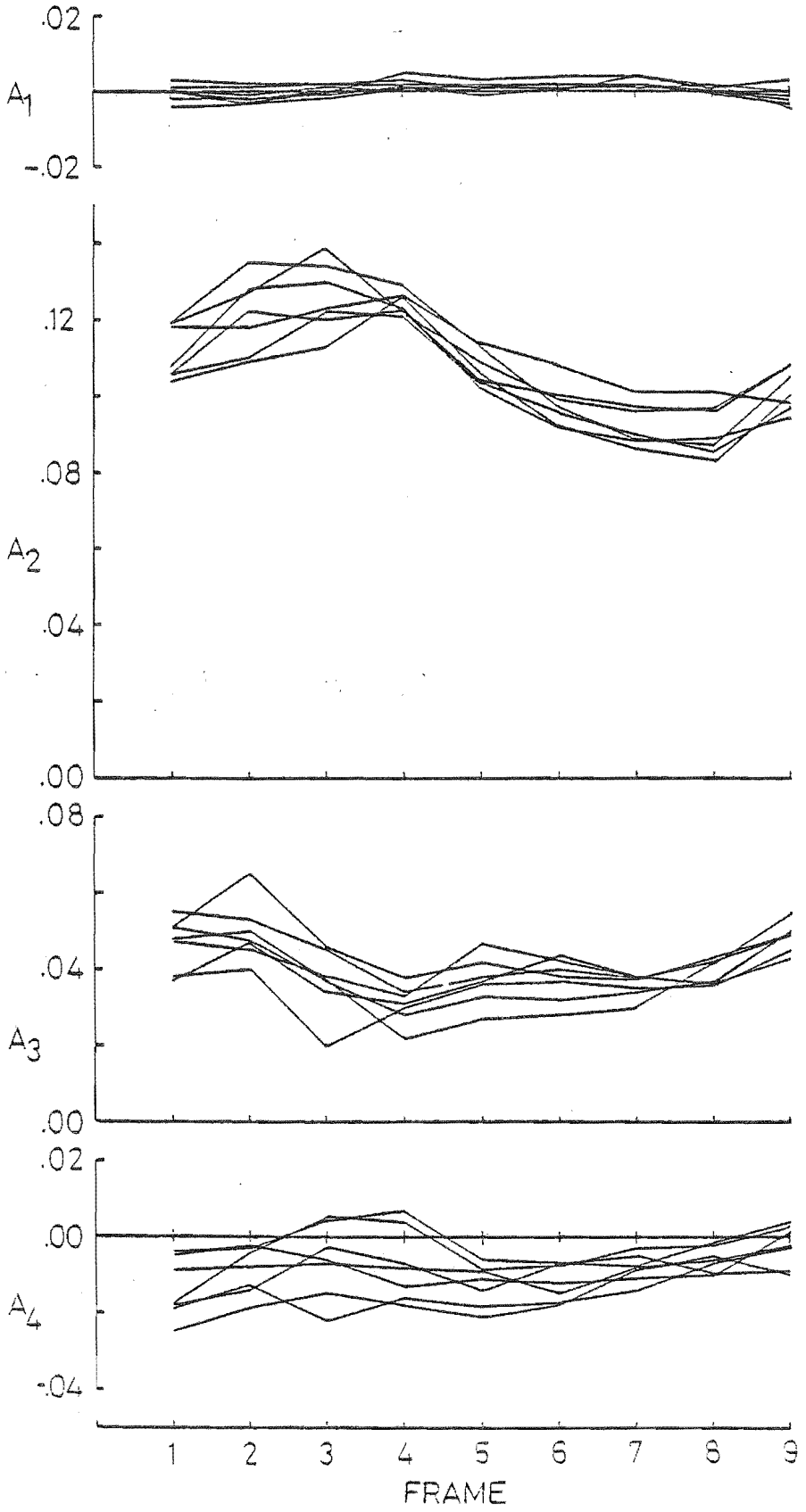

Figure 6.14 A_n values throughout the heart cycle of a normal volunteer. The same set of scans was traced seven times to give the seven curves in each graph.

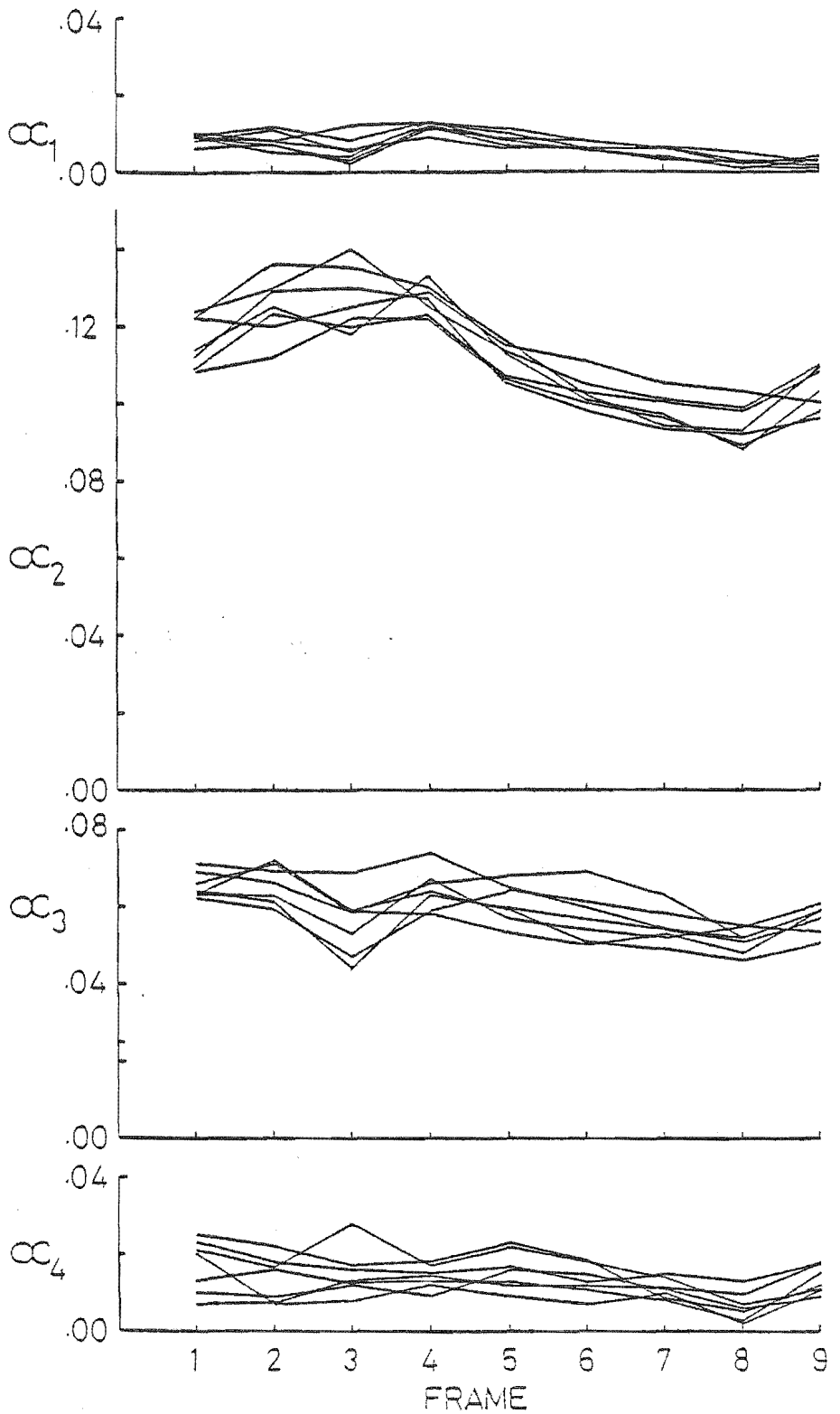

Figure 6.15 α_n values throughout the heart cycle of a normal volunteer. The same set of scans was traced seven times to give the seven curves in each graph.

The values of A_n and α_n vary in phase with the heart cycle. The spread of the values is not large. This indicates that A_n and α_n are not greatly affected by the operator's interpretation of the outline alone.

The combined effects of all four above-mentioned factors on the A_n and α_n values for $1 \leq n \leq 4$ are illustrated by Figures 6.16 and 6.17. The end-systolic points are at frame 0 and approximately at frame 7 and end-systole is at approximately frame 3. These points do not necessarily correspond to the same frame for each curve. They vary according to the heart rate of the volunteer when each study was performed. There are much greater spreads in the A_n and α_n values in these graphs than there are in Figures 6.14 and 6.15. This indicates that it is very difficult to obtain the same A_n and α_n values each time the same patient is scanned as all four factors contribute to the unreliability of the estimates of A_n and α_n. Note also that the α_n values have less spread than do the A_n values. Thus the α_n coefficients are potentially more useful than the A_n and B_n coefficients as their values can be estimated more reliably.

The mean α_n values ($\bar{\alpha}_n$) and the standard deviations ($\sigma_{\alpha n}$) of the data graphed in Figures 6.16 and 6.17 are presented in Table 6.1. $\bar{\alpha}_n$ and $\sigma_{\alpha n}$ are tabulated from the α_n values in the frames nearest end-diastole and in the frames nearest end-systole. The $\sigma_{\alpha n}$ values in this table for the α_n values obtained from Figure 6.17 (those representing all factors which cause variations in α_n) are several times greater than those obtained from 6.15 (those representing operator outline tracing variations only). Thus inconsistent interpretation of the outline by the operator who traces the outlines (cf. §5.4) has little effect on the reliability of the α_n values.

It is important to note that the $\sigma_{\alpha n}$ values obtained when the volunteer was repeatedly scanned are large compared to $\bar{\alpha}_n$. This confirms that a set of scans through a single heart cycle does not provide sufficient data to allow reliable α_n values to be obtained. But averaging the values of the parameters of several subjects of the same group enables reliable estimates of the mean values for each group obtained. Thus it is possible to identify differences in the α_n values of the subjects of the groups as a whole. It is also then possible to identify the effects of the exercise and drug interventions on the α_n values of the members of each group.

It is also seen that end-diastolic $\sigma_{\alpha n}$ values are much smaller than those obtained at end-systole. This is found to be true for the $\sigma_{\alpha n}$ values calculated from the data obtained by repeatedly scanning the same subject.

	Data from Fig 6.15 (Retracing same outline)				Data from Fig 6.17 (Rescanning same patient)			
	End-diastole		End-systole		End-diastole		End-systole	
ORDER(n)	$\bar{\alpha}_n$	$\sigma_{\alpha n}$	$\bar{\alpha}_n$	$\sigma_{\alpha n}$	$\bar{\alpha}_n$	$\sigma_{\alpha n}$	$\bar{\alpha}_n$	$\sigma_{\alpha n}$
1	.005	.001	.006	.003	.005	.002	.008	.002
2	.098	.005	.127	.007	.088	.022	.133	.040
3	.055	.004	.056	.008	.032	.010	.042	.019
4	.010	.002	.015	.006	.015	.005	.019	.007
5	.015	.003	.011	.004	.011	.005	.020	.012

Table 6.1 Mean and standard deviations of the α_n coefficient values of a normal 22 year old male.

It was also found to be true for the $\sigma_{\alpha n}$ values calculated from the data obtained by having an operator repeatedly trace the outlines in the same set of scans.

Now consider what happens when the same outline is traced repeatedly. The end-diastolic outline is always larger than the end-systolic outline. But the spatial resolution in each scan is the same. Therefore the a_n and b_n values (6.1 - 6.3) are obtained to the same precision at end-diastole as at end-systole. The α_n are obtained by normalising these according to the size of the curves (6.4, 6.5, 6.6). Therefore the α_n values at end-diastole tend to be relatively more precise and the $\sigma_{\alpha n}$ values are smaller.

Next consider what happens when the same volunteer is repeatedly studied. The $\sigma_{\alpha n}$ values being larger at end-systole than at end-diastole indicates that the ventricles contract differently during each heart cycle. Thus a different end-diastolic outline is attained in each cycle. They do, however, return to a more similar shape at the end of each cycle.

6.4.3 α_n Coefficients at Rest and at Exercise

Groups of the variation of the α_n values over the heart cycle which were obtained of subjects in the four-chamber view are presented in Figures 6.18 to 6.21. They were drawn using the wall position data collected for the studies reported in §6.3.3. The graphs apply to the following situations:

Figure 6.18 Normal volunteers at rest

Figure 6.19 CAD patients with apical infarctions at rest

Figure 6.20 Normal volunteers undergoing isometric exercise

Figure 6.21 CAD patients with apical infarctions undergoing isometric exercise.

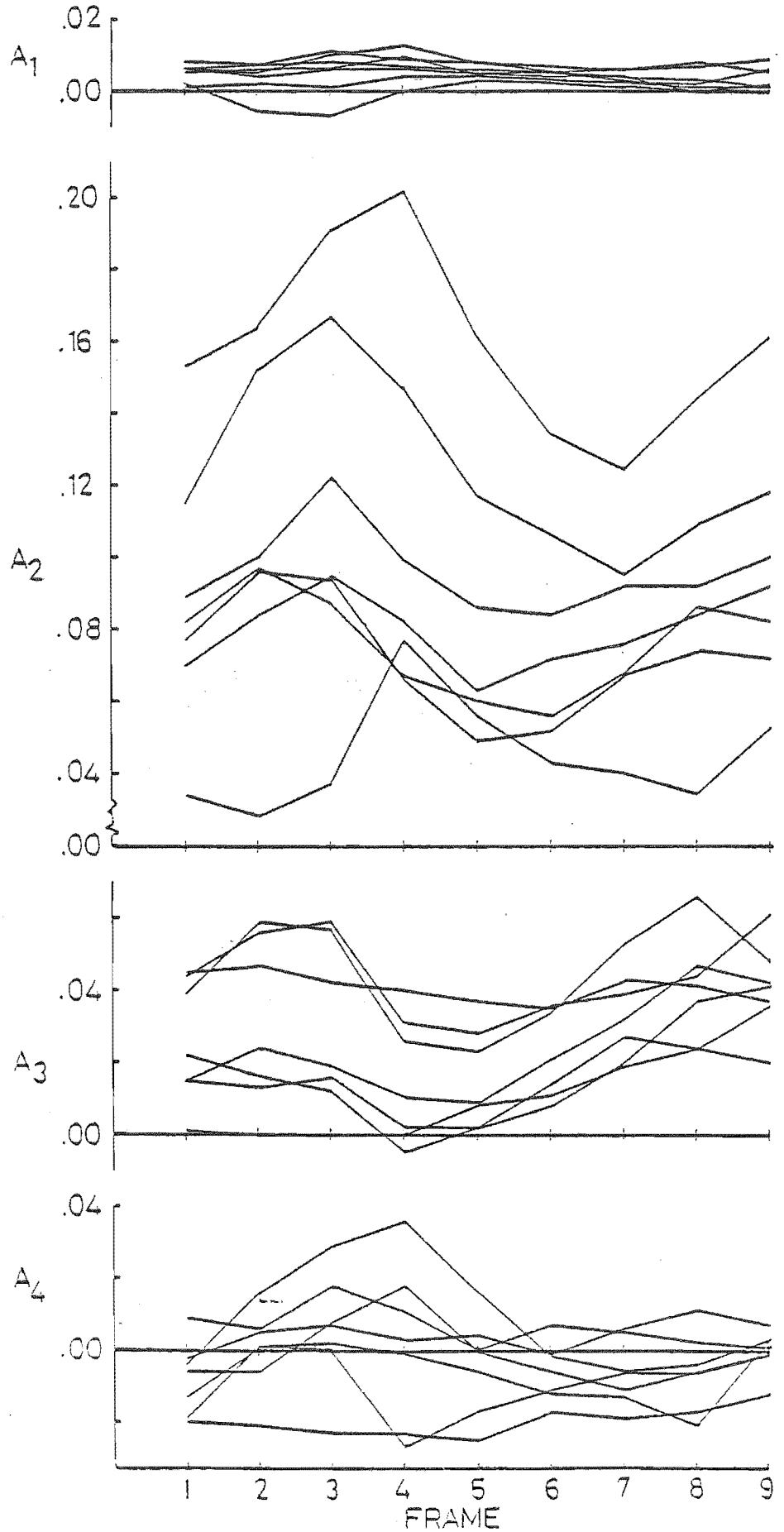

Figure 6.16 A_n values throughout seven different heart cycles of a normal volunteer.

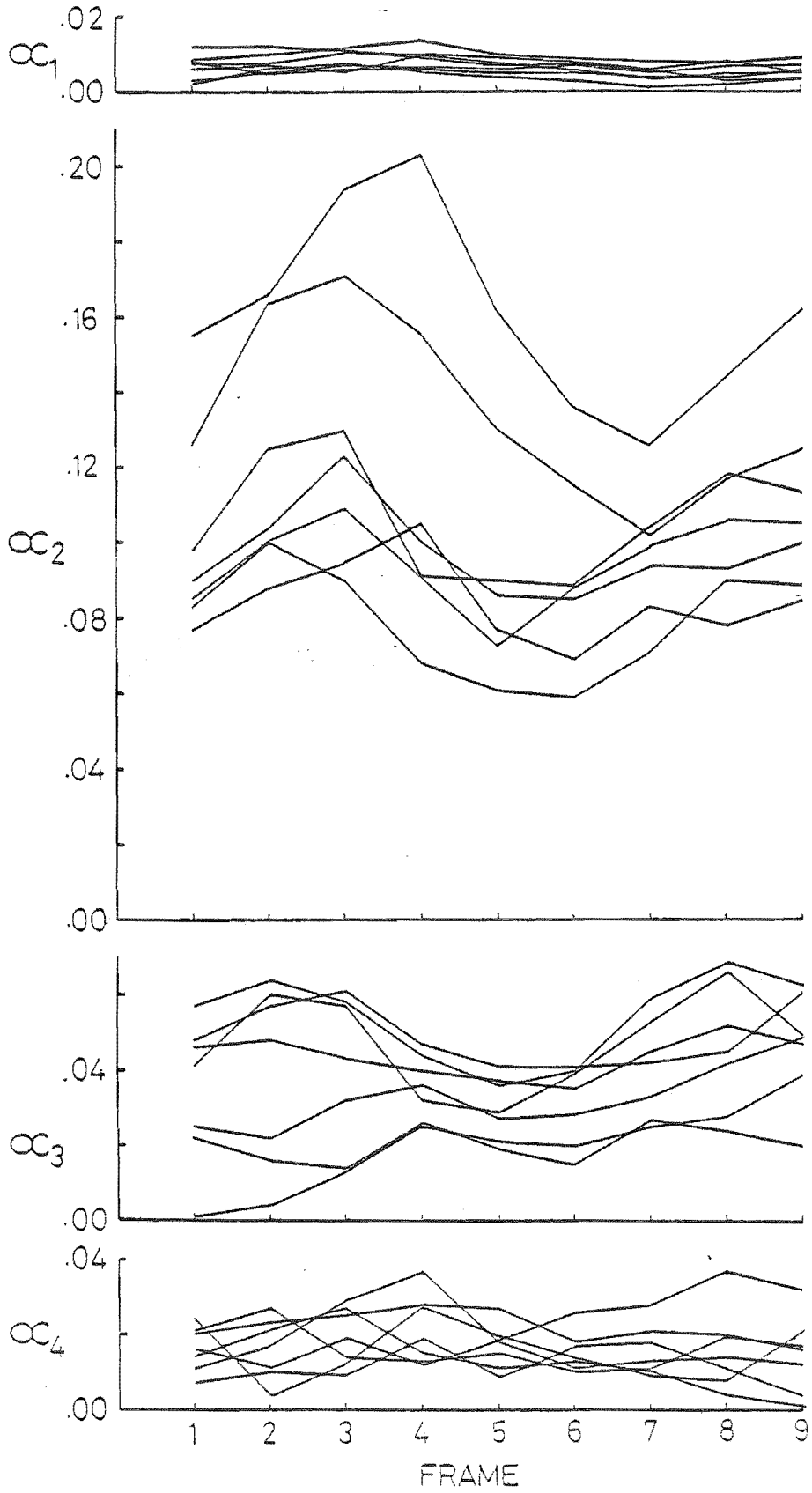

Figure 6.17 α_n values throuhout seven different heart cycles of a normal volunteer.

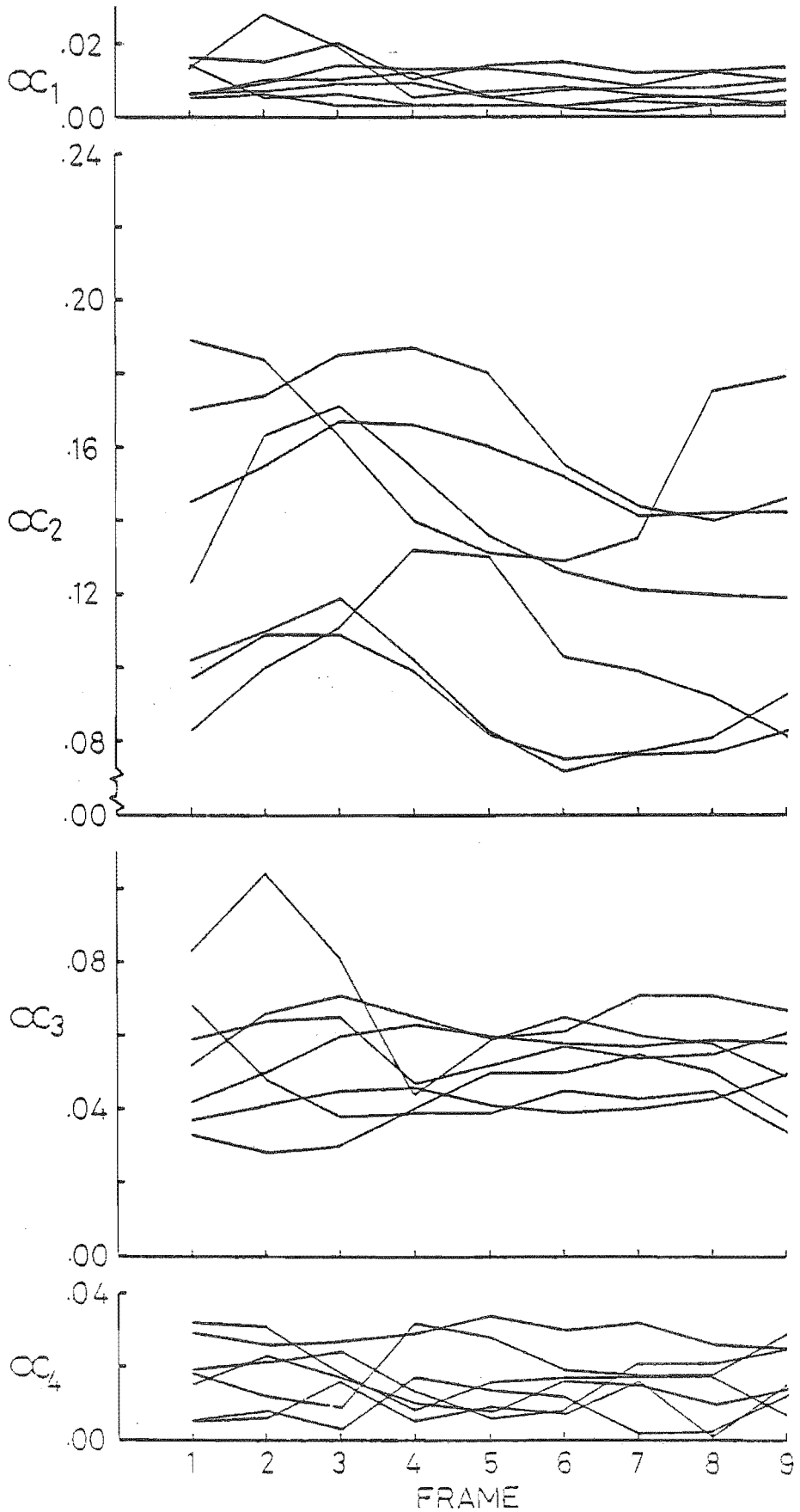

Figure 6.18 α_n values throughout heart cycles of normal volunteers at rest.

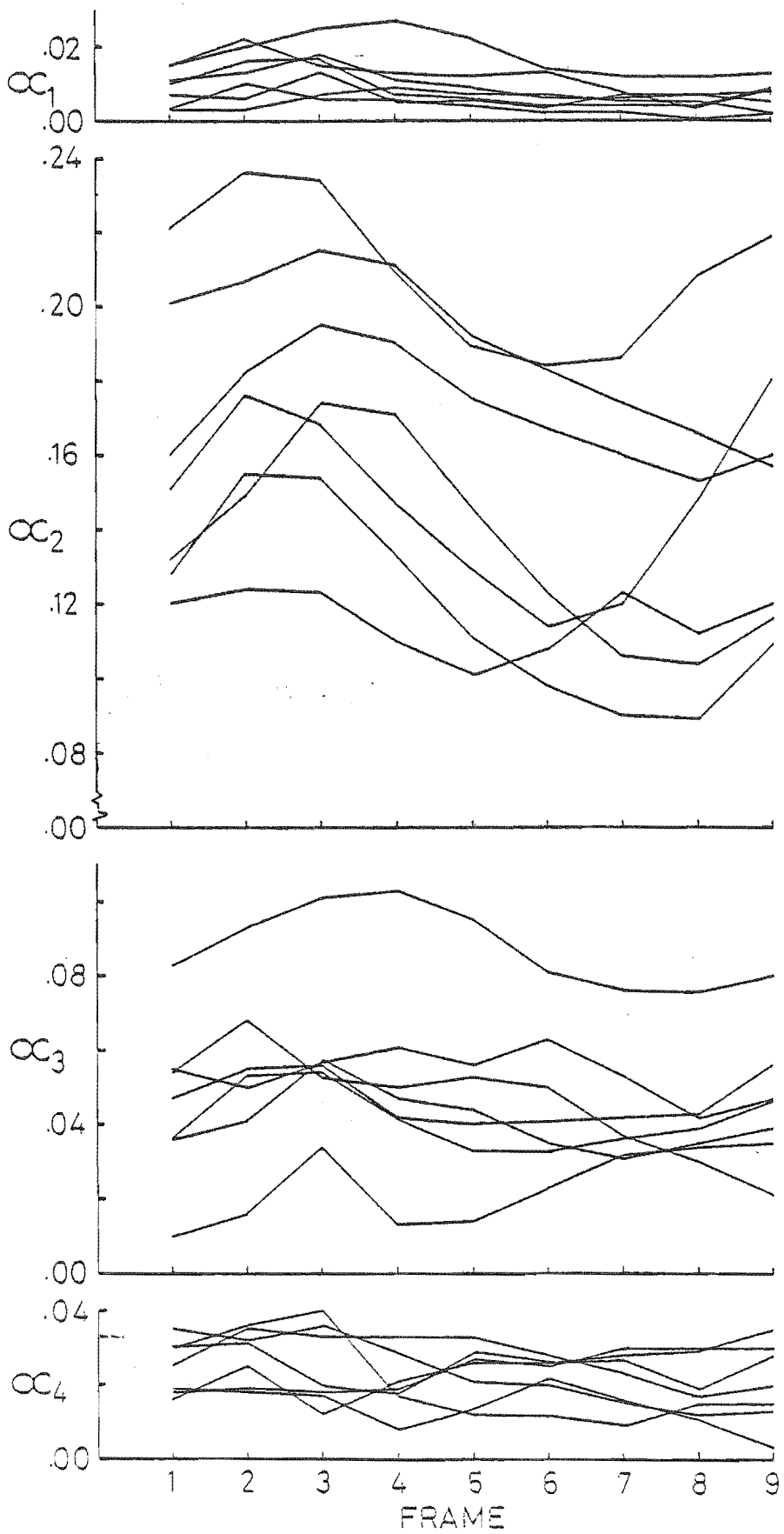

Figure 6.19 α_n values throughout heart cycles of CAD patients with apical infarctions at rest.

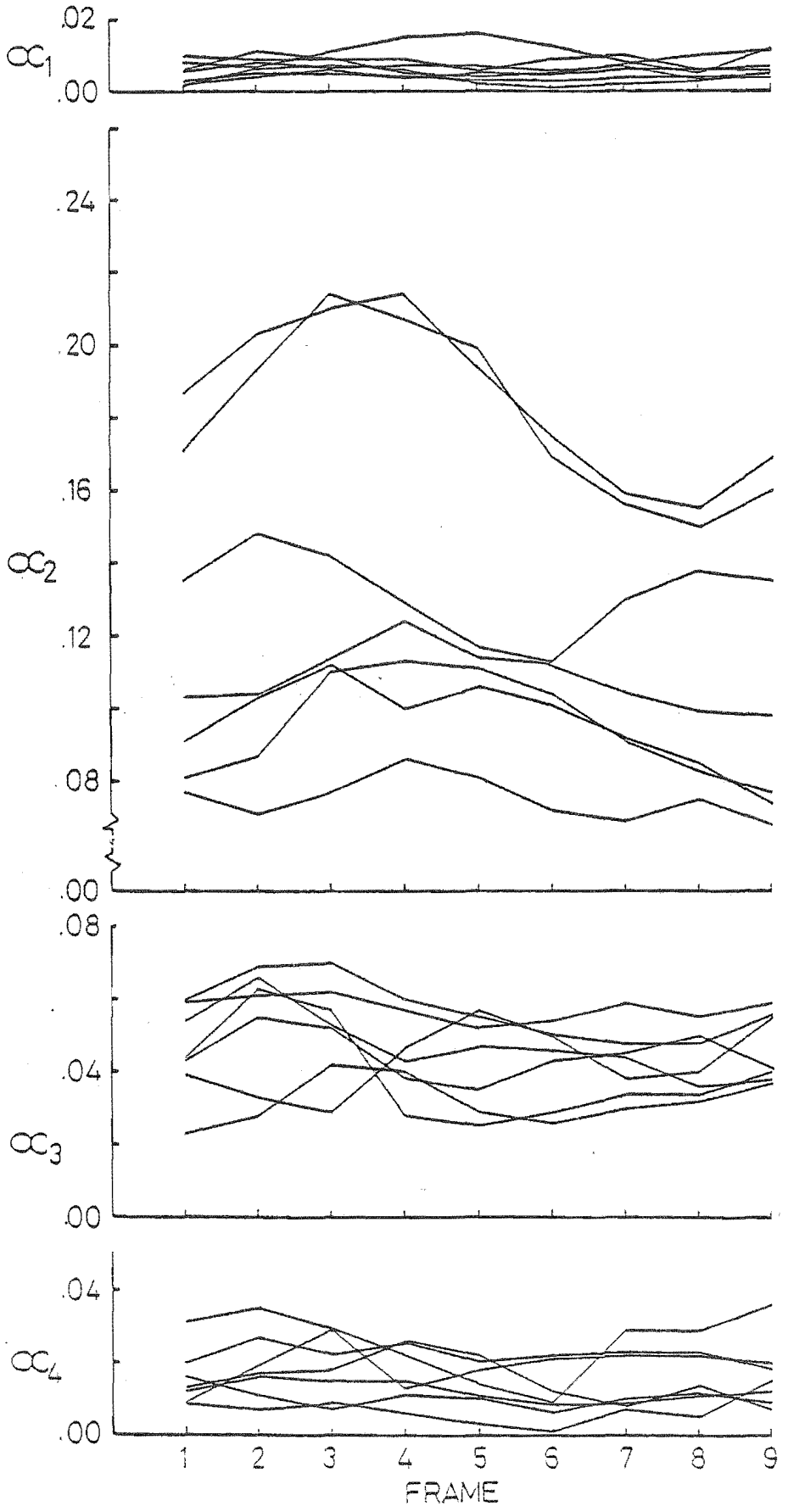

Figure 6.20 α_n values throughout heart cycles of normal volunteers undergoing isometric exercise.

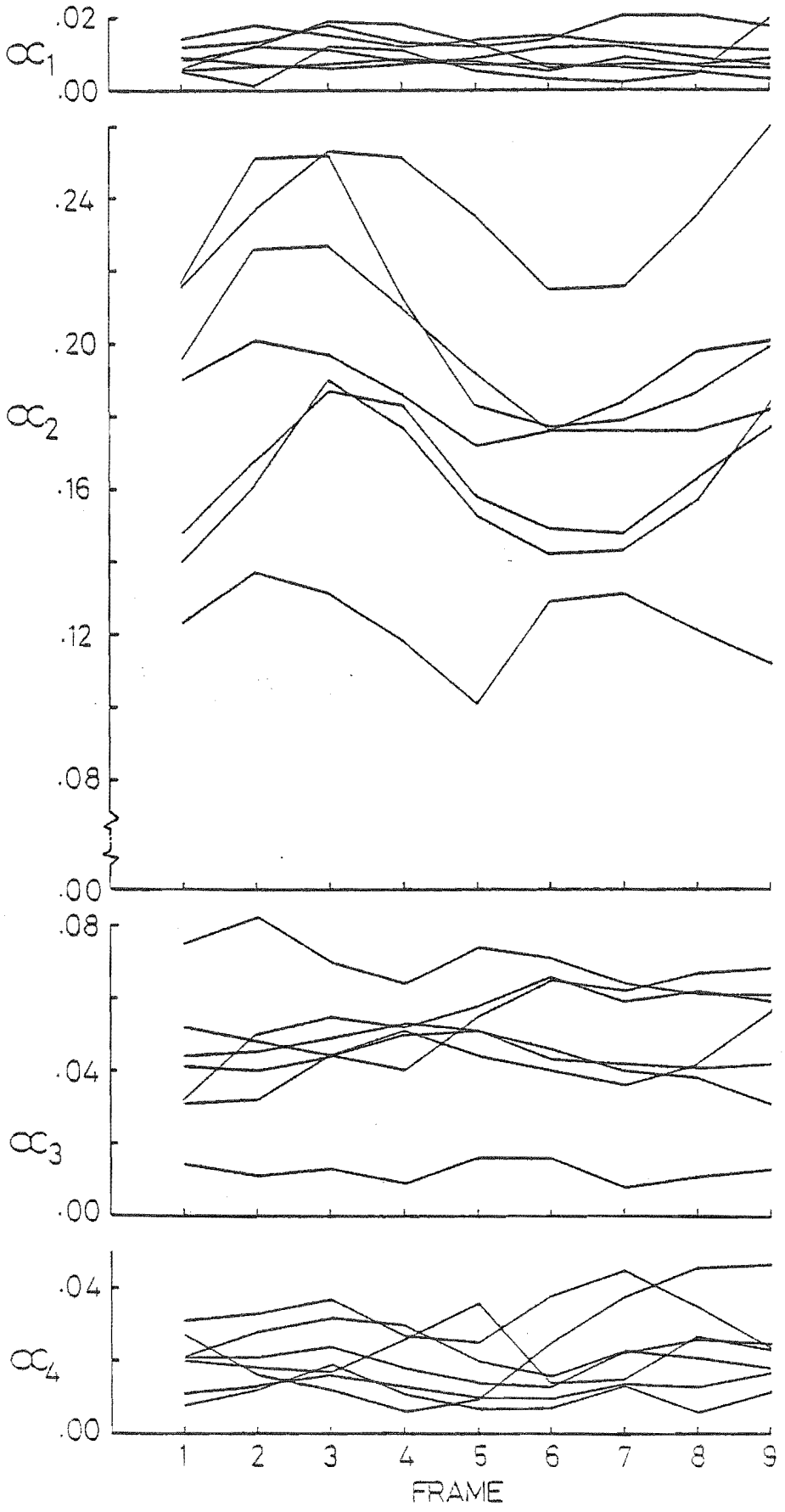

Figure 6.21 α_n values throughout heart cycles of CAD patients with apical infarctions undergoing isometric exercise.

The end-systolic points in these graphs are at frame 0 and at frames 6 to 8 depending on the subjects heart rate. Similarly the end-systolic point is at frame 3 or 4. These graphs demonstrate several important features of the α_n values. The first is that the α_n values vary in phase with the heart cycle. Second, most of the α_n values of the normal volunteers are the same as those of the CAD patients. Only the α_2 values are obviously different. They were generally larger for the CAD patients than for the normal volunteers. This is consistent with the CAD patients having elongated ventricles due to an aneurysm or akinesia at the apex (cf. Figure 6.2). Third, the spread of the α_n values in each graph is large. This is due to person-to-person differences in the values as well as to the factors considered in §§6.3.2 and 6.4.2. Care must be taken when interpreting these graphs. Conclusions which require more precise estimates of α_n to be available must not be made. The spread in the α_n values of a single patient is shown to be large (cf. §6.4.2). Therefore it is unreasonable to expect to be able to determine the effects of the interventions of the α_n values of the same subject from studies of a single beat. It is better to average the α_n values of each group of subjects to determine the effects of the interventions.

Several parameters derived from the α_n values are used to classify the subjects as having normally shaped ventricles or not. I have analysed the ability of the following parameters to classify the subjects:

a) the α_n values at end-systole (ES_n)
b) the α_n values at end-diastole (ED_n)
c) the maximum α_n value during the heart cycle (MAX_n)
d) the minimum α_n value during the heart cycle ((MIN_n)
e) the average α_n value over the heart cycle (AV_n)
f) the difference in the α_n values at end-systole and end diastole ($ES\text{-}ED_n$)
g) the difference in the maximum and minimum values of α_n during the heart cycle ($MAX\text{-}MIN_n$)

It is convenient to classify parameters a) to e) as 'absolute parameters' and f) to g) as 'difference parameters'.

It is also convenient to identify the mean value of each parameter calculated for a group of subjects by a superbar. Thus the mean value of ES_n is denoted by $\overline{ES}_n$.

Some of the parameters are essentially the same because the α_n values appear to change in phase with the heart cycle. For example, the MAX_n values are likely to be similar to the ES_n values, the MIN_n values to the ED_n values

and the $MAX\text{-}MIN_n$ values to the $ES\text{-}ED_n$ values.

The mean and standard deviations of the values of the above parameters were calculated for the four-chamber view studies of each group of subjects. This was done for $1 \leq n \leq 5$ and for the studies done at rest and at exercise. Graphs which compare the mean parameter values of the two groups of subjects are presented in Figure 6.22. Similar graphs which compare the mean parameter values of the two groups at exercise are presented in Figure 6.23.

The $\overline{ES}_n$ values are indeed similar to the $\overline{MAX}_n$, values (compare Figure 6.22a with Figure 6.22c, and Figure 6.23a with Figure 6.23c). Also, the $\overline{ED}_n$ values are similar to the $\overline{MIN}_n$ values (compare Figure 6.22b with Figure 6.22d, and Figure 6.23b with Figure 6.23d). However, the mean values of the difference parameters are dissimilar. The $\overline{ES\text{-}ED}_n$ values are always smaller than the $\overline{MAX\text{-}MIN}_n$ values (compare Figure 6.22f with Figure 6.22g, and Figure 6.23f with Figure 6.23g). Most of the $\overline{ES\text{-}ED}_n$ values are very small while all of the $\overline{MAX\text{-}MIN}_n$ values are greater than zero. The relatively large magnitude of the $\overline{MAX\text{-}MIN}_n$ values compared to the $\overline{ES\text{-}ED}_n$ values suggests that the former are poorly estimated. Thus the $\overline{MAX\text{-}MIN}_n$ values are noisy.

The differences between the mean parameter values of the two groups of subjects are now considered. The values for the subjects at rest are presented in Figure 6.22. The most obvious differences between the mean parameter values of the two groups are for the n=2 values. Those of the CAD patients are greater than those of the normal volunteers. This indicates that the ventricles of the CAD patients are elongated compared to those of the normal volunteers. Elongation due to the presence of apical aneurysm or akinesia is to be expected in the CAD patients. It should be noted that the increased mean parameter values of the CAD patients are more prominent at end-systole than at end-diastole (compare Figure 6.22a to Figure 6.22b, and Figure 6.22c with Figure 6.22d). This suggests that akinesia or aneurysm is most obvious at end-systole. This is consistent with what is observed in angiograms and echocardiograms of patients with apical infarctions.

Consider now the mean parameter values of the subjects at exercise. These are presented in the graphs in Figure 6.23. In general, the mean parameter values for n=2 of the normal patients do not change under exercise (compare Figure 6.22 to Figure 6.23). However those of the CAD patients do increase under exercise. This is consistent with ventricular abnormalities being produced by exercise in the CAD patients (cf. Morganroth et al., 1981, Mitamura et al., 1981; Wann et al., 1981). It is interesting to note that the

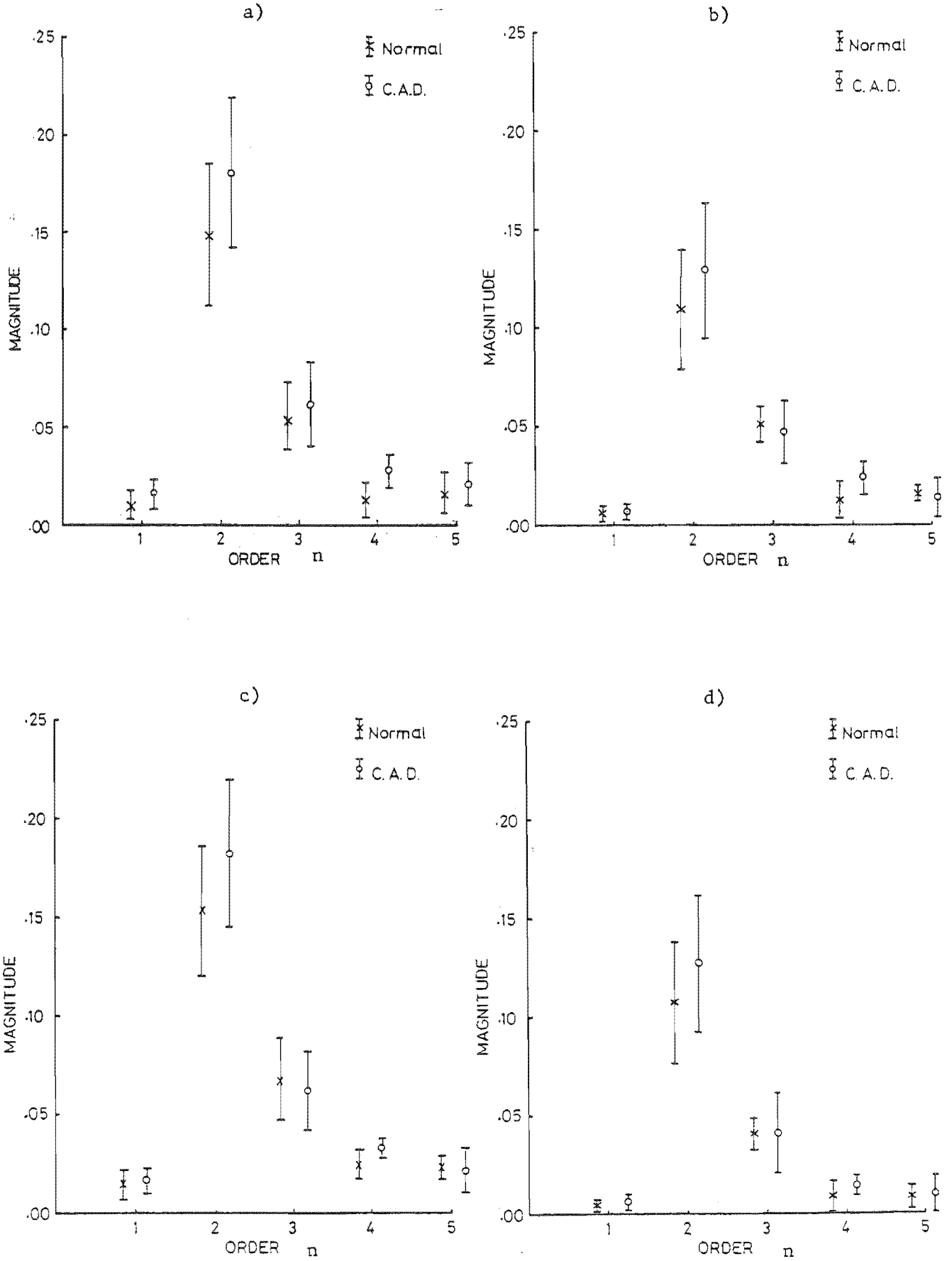
a)
b)
c)
d)
Normal
C.A.D.
MAGNITUDE
ORDER n
.25
.20
.15
.10
.05
.00
1
2
3
4
5

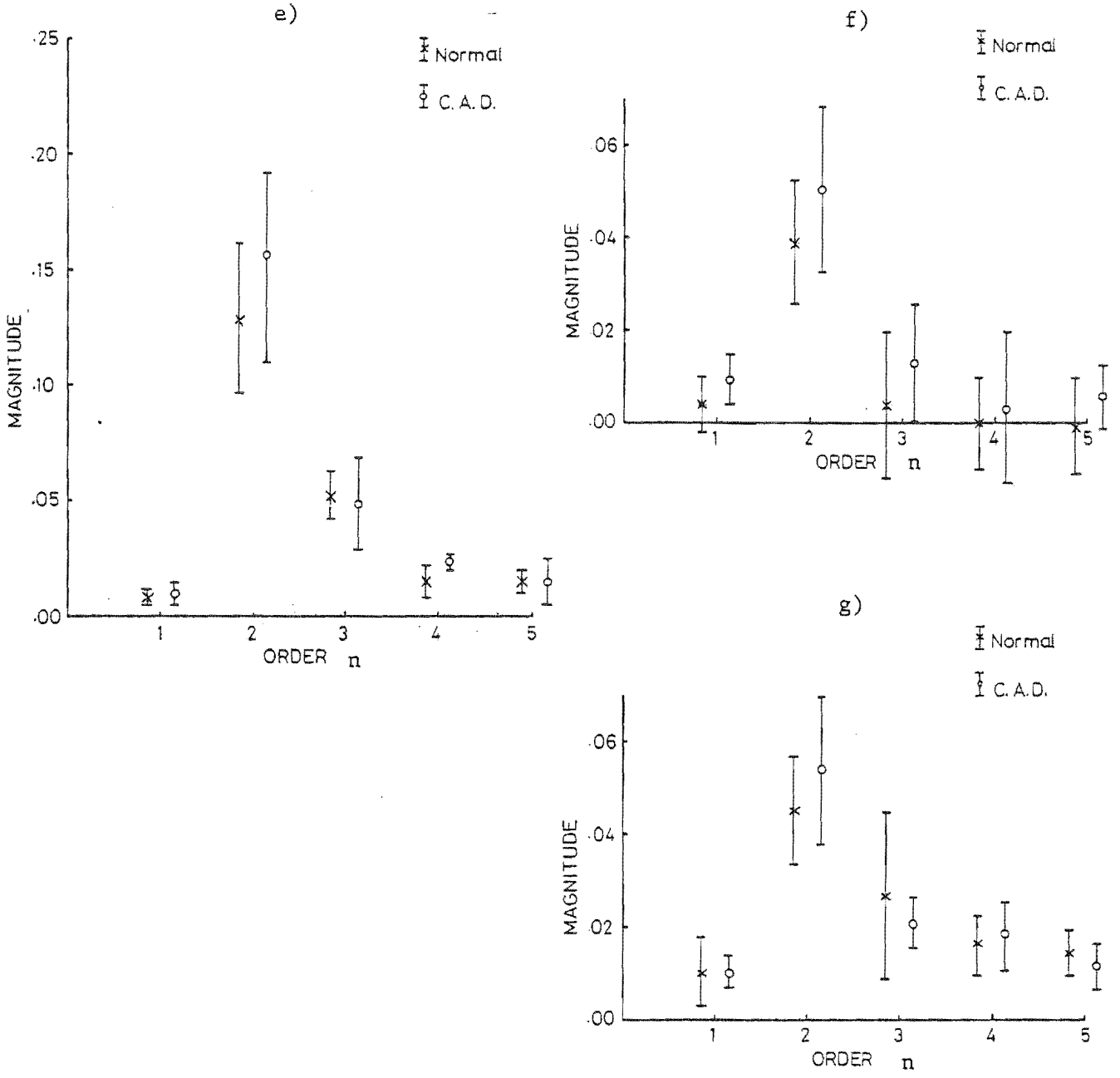

Figure 6.22 Means and standard deviations of parameter values of subjects at rest.

a) ES_n
b) ED_n
c) MAX_n
d) MIN_n
e) AV_n
f) $ES\text{-}ED_n$
g) $MAX\text{-}MIN_n$

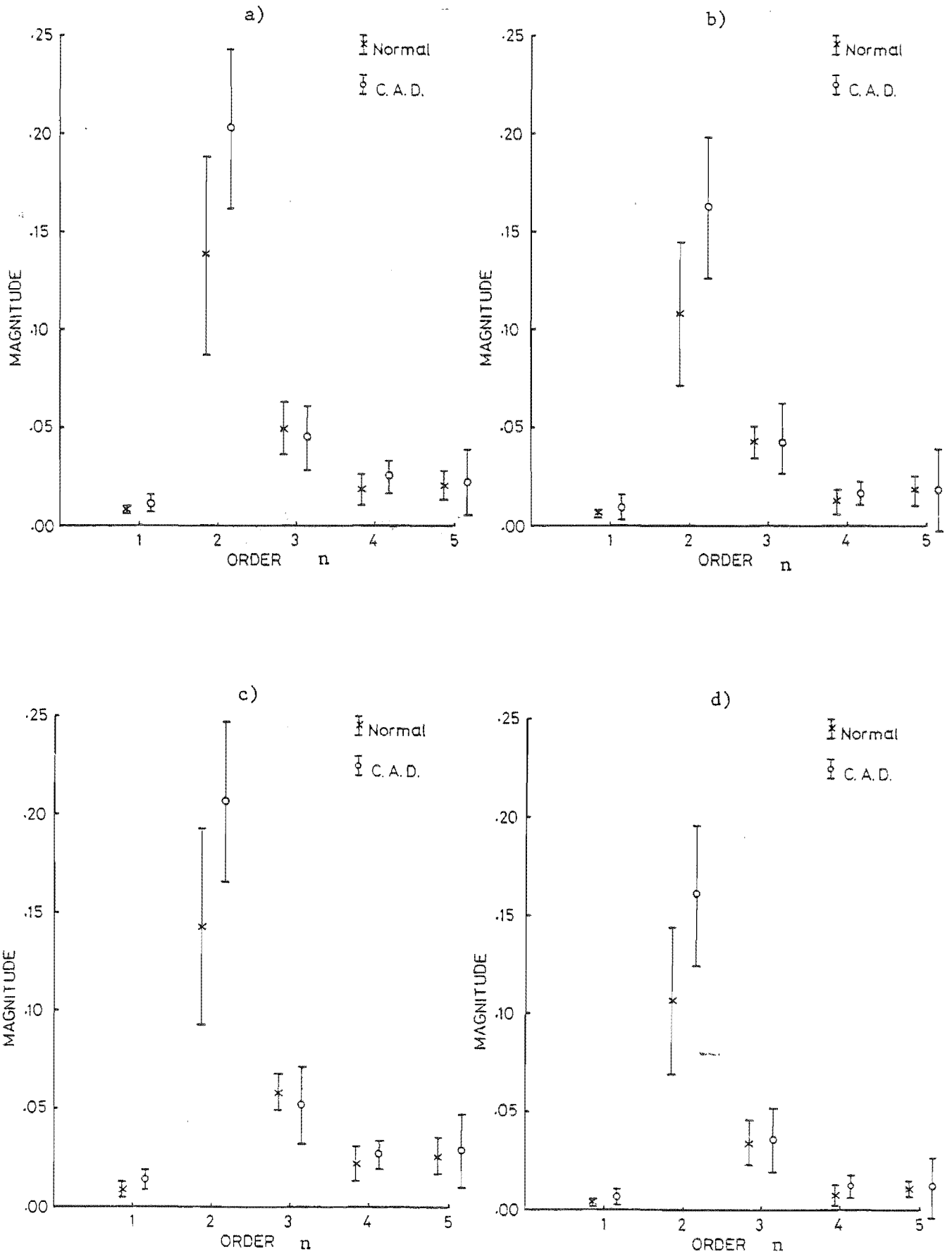
a)
b)
c)
d)
Normal
C. A. D.
MAGNITUDE
ORDER n
.25
.20
.15
.10
.05
.00
1
2
3
4
5

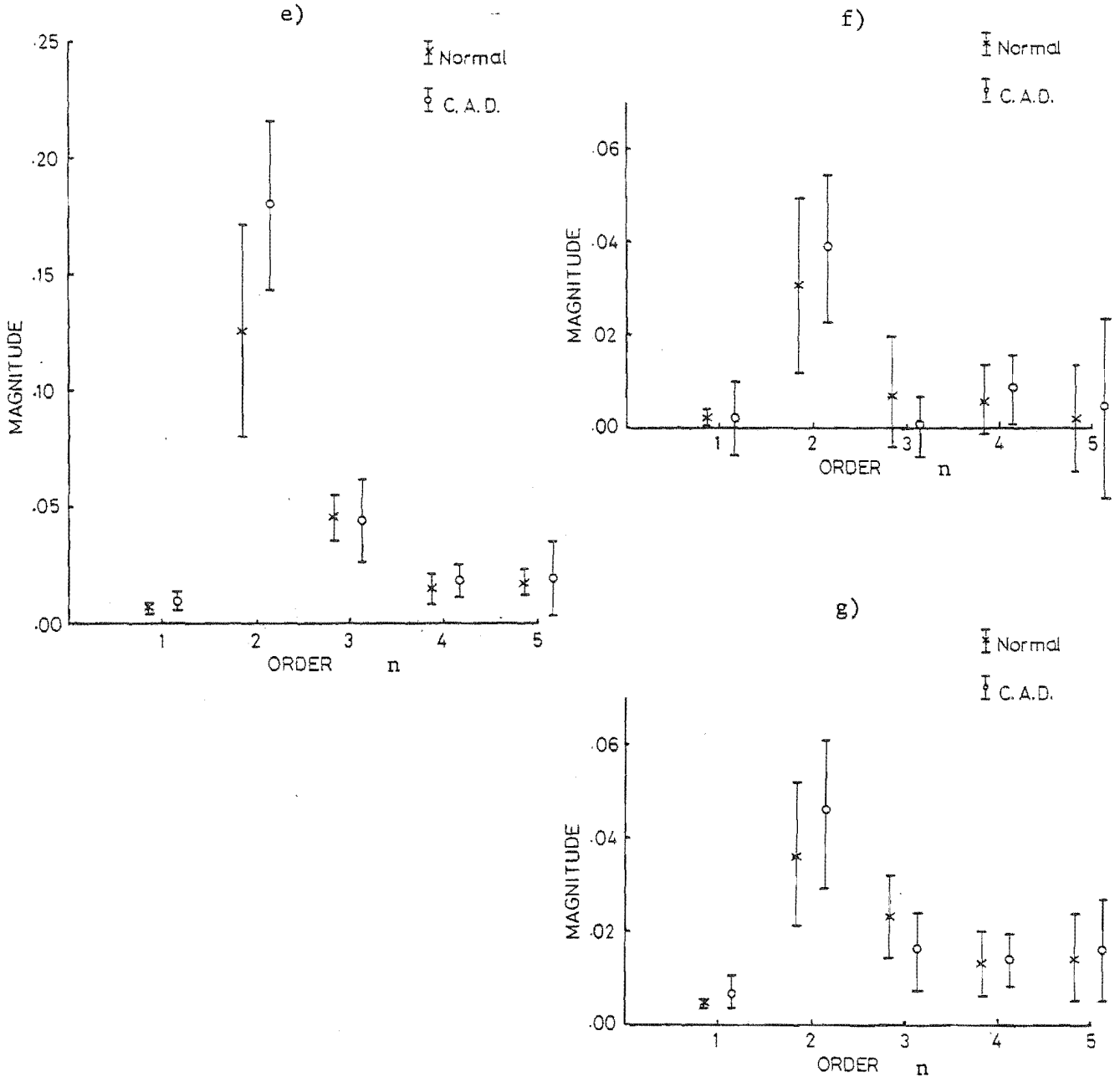

Figure 6.23 Means and standard deviations of parameter values of subjects undergoing isometric exercise.

a) ES_n

b) ED_n

c) MAX_n

d) MIN_n

e) AV_n

f) $ES\text{-}ED_n$

g) $MAX\text{-}MIN_n$

mean parameter values for n=2 in the CAD patients are now increased over those of the normals by about the same amount both at end-diastole and end-systole (compare Figure 6.23a and Figure 6.23b, and Figure 6.23c to Figure 6.23d). This is not what is observed at rest. Exercise therefore tends to induce shape abnormalities at end-diastole rather than at end-systole.

It was hoped to use the subjects' parameter values for n=2 as a means of characterising them as being normal or as having a ventricular wall abnormality. The following test was applied to their parameter values to do this. An upper normal limit was defined for each value as being one standard deviation greater than the mean parameter values of the normal volunteers. Subjects with parameter values greater than that limit were classified as having abnormal ventricles. All of the parameter values of all of the subjects were tested in this manner. The rests of the tests are presented in Table 6.2. In this table all subjects classified as having abnormal ventricles according to each parameter are marked by a '+'. Ideally, all of the CAD patients should be marked with a '+' and all of the normal volunteers should be unmarked. All of the subjects would then be correctly classified. This does not occur for any of the parameters. False positive and false negative results are encountered with each test. It is apparent, however, that the parameter values for n=2 of the CAD patients are generally greater than those of the normal volunteers.

While it is not possible to determine which parameter provides the most accurate classification of the subjects with the relatively small number of subjects studies, most of them appear to be able to do this to some extent. In 13 of the 14 parameters tested and presented in Table 6.2 there are more true positives than false positives, and more true negatives than false negatives.

6.4.4 Drugs

The effects of metoprolol and nifedipine on the shape parameters of the patient's ventricles were also investigated. Graphs of the parameters of the patients before and after taking nifedipine and metoprolol are presented in Figures 6.24 and 6.25 respectively.

Strong conclusions cannot be drawn from the effects of the drugs because so few patients were studied. Only four were studied with nifedipine and only three with metoprolol.

Nifedipine had little effect on the mean parameter values. Only the absolute parameter values for n=2 changed noticably after the patients took nifedipine and the changes were slight. The absolute parameter values for n=2 increased slightly indicating that the ventricles elongated under the

		EXERCISE							REST						
		ES_2	ED_2	$ES-ED_2$	TA_2	MAX_2	MIN_2	$MAX-MIN_2$	ES_2	ED_2	$ES-ED_2$	TA_2	MAX_2	MIN_2	$MAX-MIN_2$
N	1	+	+	+	+	+	+	+							
O	2									+				+	
R	3	+	+	+	+	+	+	+		+		+	+	+	
M	4										+		+		+
A	5														
L	6														
S	7														
	1	+	+		+	+	+		+	+		+	+	+	
	2		+				+		+	+	+	+	+	+	+
C	3	+	+	+	+	+	+	+	+	+		+	+	+	
A	4	+	+		+	+	+								
D	5	+						+							+
	6										+				+
	7	+	+	+	+	+	+	+			+				+

Table 6.2 Classification of subjects as having abnormal left ventricular shape parameter values. The abnormal shape parameters values are marked '+'

influence of nifedipine.

Metoprolol had the opposite effect. The absolute parameter values for n=2 decreased under the influence of metoprolol. This suggests that the ventricles became more circular.

6.5 DISCUSSION

In this chapter, quantitative results of studies of ventricular wall motion and shape have been reported. The studies were performed on a group of normal volunteers and a group of CAD patients. It was found to be difficult to obtain reliable estimates of parameters used to describe shape and

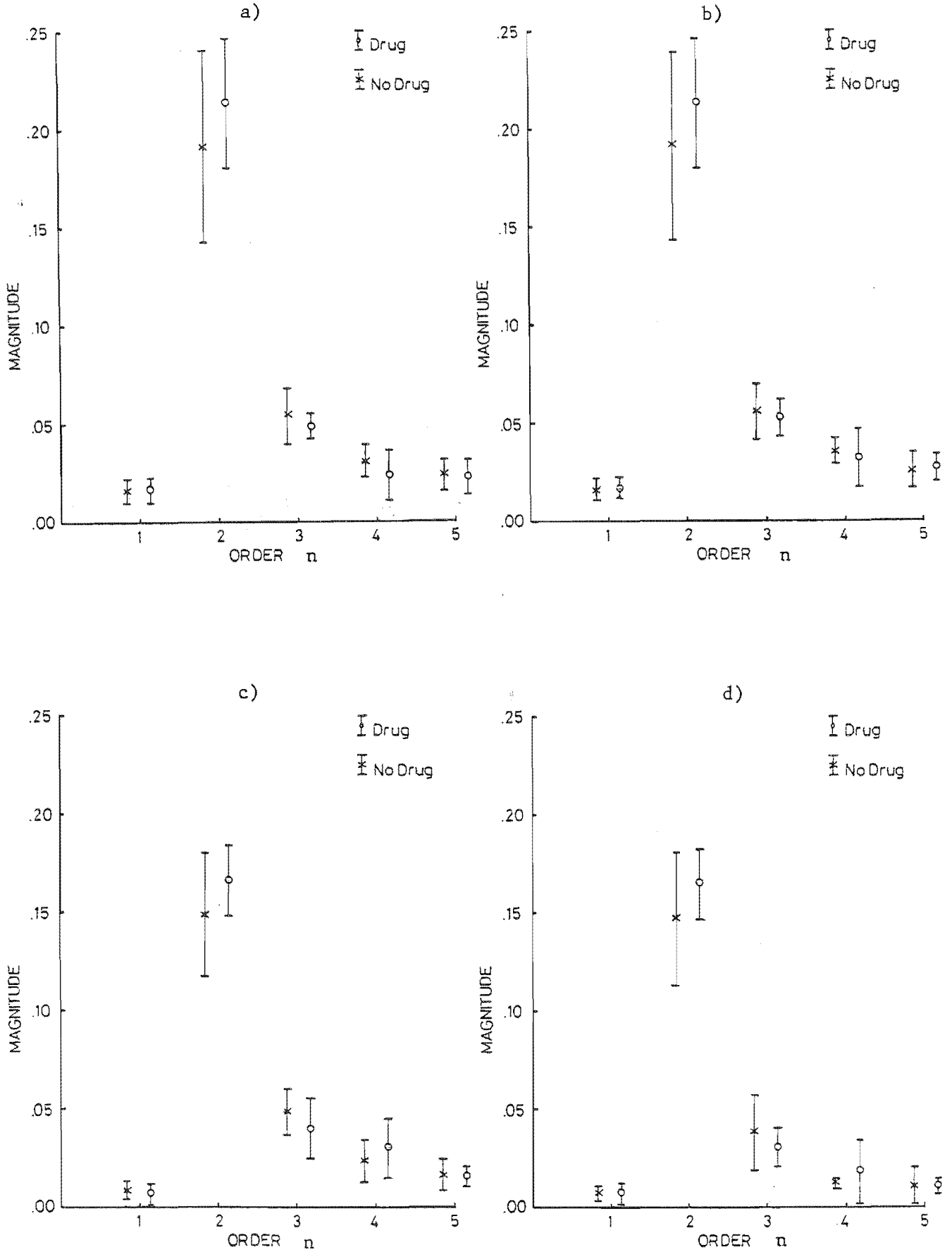
a)
b)
c)
d)
Drug
No Drug
MAGNITUDE
.25
.20
.15
.10
.05
.00
1
2
3
4
5
ORDER n

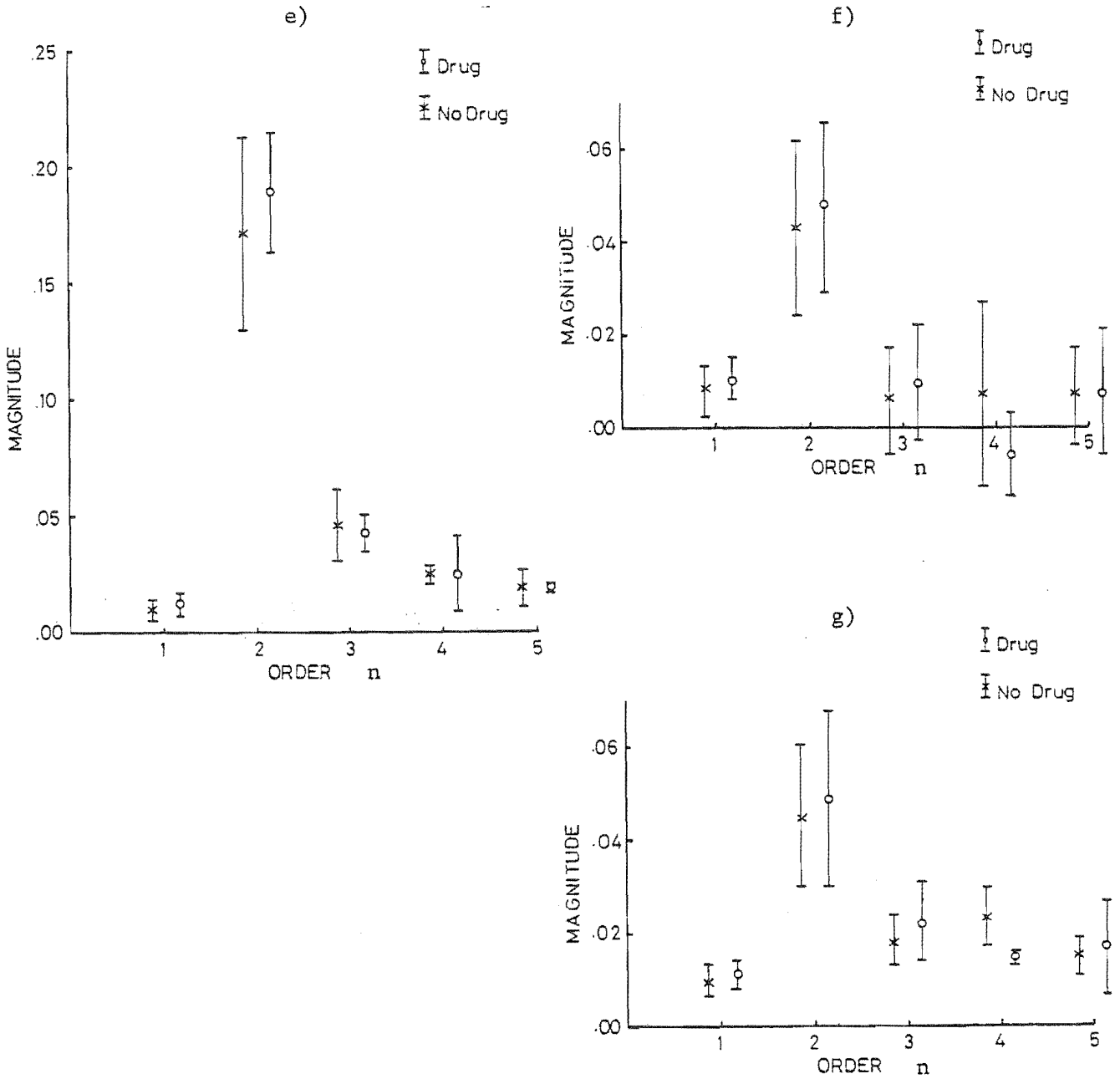

Figure 6.24 Means and standard deviations of parameter values of CAD patients with apical infarctions before and after taking nifedipine.

a) ES_n

b) ED_n

c) MAX_n

d) MIN_n

e) AV_n

f) $ES\text{-}ED_n$

g) $MAX\text{-}MIN_n$

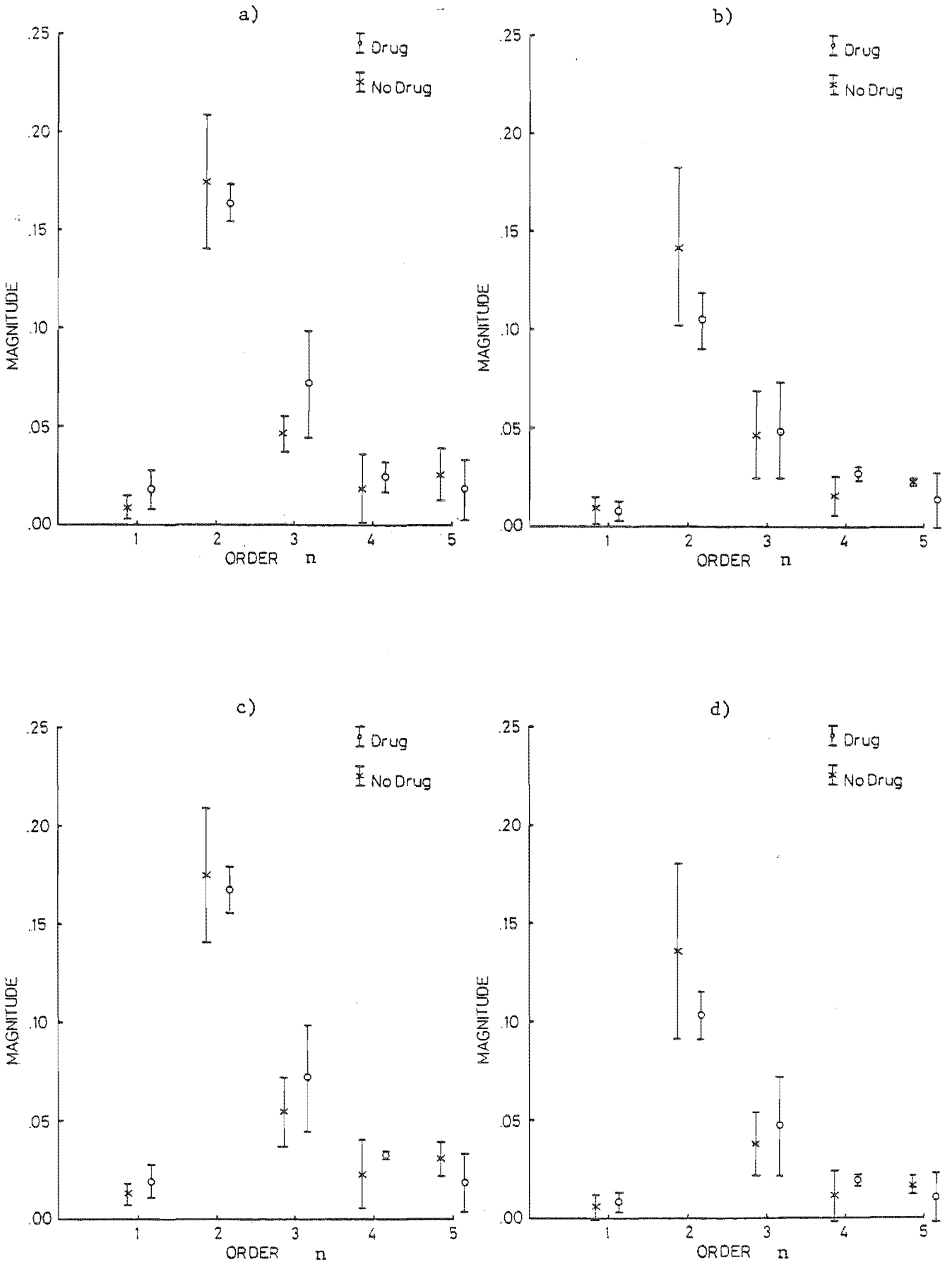
a)
b)
c)
d)
Drug
No Drug
MAGNITUDE
.25
.20
.15
.10
.05
.00
1
2
3
4
5
ORDER n

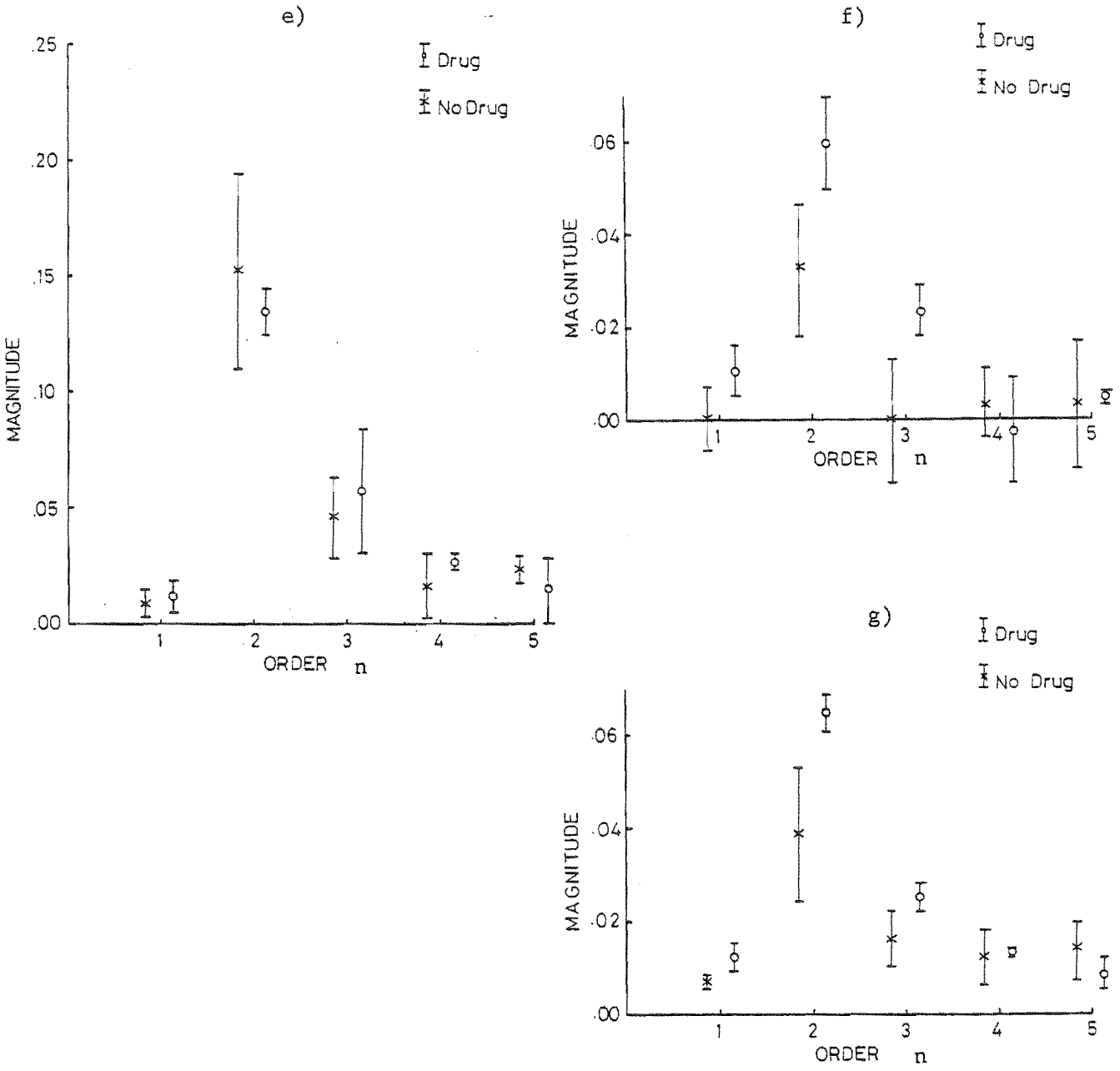

Figure 6.25 Means and standard deviations of parameter values of CAD patients with apical infarctions before and after taking metoprolol.

a) ES_n

b) ED_n

c) MAX_n

d) MIN_n

e) AV_n

f) $ES\text{-}ED_n$

g) $MAX\text{-}MIN_n$

motion. Therefore the mean values of the parameters of each group of which reliable estimates could be obtained were used to analyse differences in the wall motion and shape of the two groups.

Wall motion was measured in terms of the percentage shortening of 32 radial axes from end-diastole to end-systole. Motion was analysed using both a fixed and a floating centroid. It did not appear to matter which type of centroid was used when attempting to identify regions of abnormal wall motion.

The $\bar{S}$ values of normal volunteers at rest tended to be similar in all regions of the left ventricular wall. In patients who had an apical infarction, defects in wall motion were detected only in the four-chamber views. In these patients, a hyperkinetic region, characterised by an increase in percentage shortening, was detected. This was an area of ischaemic myocardium situated on the septal wall at the edge of an infarction. No regional wall abnormalities were detected in patients with inferior wall infarctions. A lot of motion seen in this view was due to lateral wall movement perpendicular to the scanning plane. Local in-plane contraction was barely visible. It is also possible that the scanning plane did not cross the affected region.

Isometric exercise affected the $\bar{S}$ values in a manner consistent with the presence of generalised ischaemia. The effects were most noticeable in CAD patients with apical infarctions, for whom the $\bar{S}$ values of the hyperkinetic regions decreased markedly.

The effects of nifedipine and metoprolol on the regional wall motion of the subjects were consistent with the known physiological effects of these drugs. Nifedipine was found to cause contractility of ischaemic myocardium to increase. This was most evident in the ischaemic regions near the infarctions where the $\bar{S}$ values increased markedly. Metoprolol, in contrast, caused the myocardium to contract less forcefully. Again the effects of this drugwere demonstrated best in the regions near the infarctions. The $\bar{S}$ values in those regions decreased to an almost normal level.

The shapes of the ventricular outlines of the subjects were quantified using the coefficients a_n and b_n of a fifth order trigonometric Fourier series representation (6.1). The parameters α_n, defined in §6.4.1, proved to be particularly useful descriptions of the shapes of ventricular outlines.

The values of $\bar{\alpha}_2$ for the CAD patients with apical abnormalities were generally larger than those of the normal volunteers. This was most obvious at end-systole. Increased $\bar{\alpha}_2$ values are consistent with ventricular elongation resulting from apical akinesia or aneurysm. Exercise increased the $\bar{\alpha}_2$values

of the CAD patients even further while those of the normal volunteers stayed the same. This was to be expected as exercise is known to enhance ventricular wall defects.

The effects of the drugs on the $\overline{\alpha}_2$ values reflected their effects on wall motion. Nifedipine, which increased the hyperkinesia of the walls, also increased the $\overline{\alpha}_2$ values. Metoprolol, in contrast, reduced the hyperkinesia and also reduced the $\overline{\alpha}_2$ values to make them more like those of the normal volunteers.

CHAPTER 7

CONCLUSIONS AND SUGGESTIONS FOR FUTURE WORK

Two-dimensional echocardiography has been a standard diagnostic technique for several years. It is considered to be superior to M-mode echocardiography as it allows complete ventricles to be seen in cross-section. Thus it permits the motion of different parts of the walls to be compared. The motion is analysed qualitatively rather than quantitatively. Quantitative analysis of ventricular wall motion is difficult for three reasons. The first of these is that complex hardware systems must be constructed to interface some sector scanners to the computers used to analyse the motion. Second, it is not yet known exactly how wall motion should be quantified. Even though quantification of wall motion using angiograms has been investigated for several years, there is still no concensus of opinion on which of the many systems tried produces the most diagnostically useful information from angiographic data. Third, extracting the ventricular outline cannot yet be done automatically using computers, so that a significant amount of operator intervention and time is required. This severely limits the amount of wall motion data which can be obtained.

Compared to the amount of research reported on quantification of ventricular wall motion, very little has been done to develop methods of quantifying ventricular shape. This is surprising because ventricular shape is analysed simultaneously with wall motion when a clinician diagnoses with the aid of cineangiograms.

This thesis describes the development of hardware and software which allows ventricular outlines to be extracted from real time two-dimensional echocardiograms. An interface to digitise echocardiograms and pass them through a PDP 11/10 computer was constructed. The images obtained were of poor quality and, in general, the endocardial border could not be easily identified. Image processing was used to improve the visual appearance of the images and to make the endocardium more obvious. It was found that the noisy appearance of the images was reduced by ' echo- shape' filtering. The endocardium was made to be more distinct by histogram equalising the images. Extraction of the endocardial border was performed interactively with the operator delineating it with a cursor. It was found that the position of the border could be determined more precisely by using the 'simultaneous scanning' techniques

developed during the research reported in this thesis. The 'simultaneous R-mode scan' was found to be particularly useful.

This thesis also describes studies of ventricular wall motion and shape. Two groups of subjects were studied: a group of normal volunteers and a group of patients with coronary artery disease. The time varying positions of the ventricular walls of the subjects were estimated. It was found to be very difficult to obtain similar echocardiograms each time the same patient was scanned, i.e. it was difficult to obtain reliable data specific to any one patient. Thus it was necessary to average the results of the analyses of several patients in order to determine the effects of the various interventions.

The subjects' ventricular wall motion was measured and recorded as the percentage change in the distance of the walls from the ventricular centroid. Both a fixed origin and a floating origin were used to analyse the motion. Similar estimates of the amplitude of the wall motion were obtained regardless of which origin was used. The wall motion of the subjects was measured with the subjects both resting and at exercise. A hyperkinetic region next to the infarcted regions was seen in patients with apical infarctions. The amplitude of motion of the hyperkinetic region decreased when the patients underwent isometric exercise.

The effects of two drugs on the regional wall motion of the patients with apical infarctions were investigated. The results were consistent with the known effects of the drugs. This suggests that quantitative analysis of echocardiographic images should be of use for determining the effects of other drugs on wall motion.

A method of quantifying ventricular shape using the coefficients of a Fourier series based shape description was investigated. It was found that the magnitude of some of the coefficients of patients with defects in the apices of their ventricles were larger than those of the normal volunteers. This correlated with the expected differences in ventricular shape between the two groups. Exercise was found to affect the coefficients of the patients with apical infarcts more than those of the normal volunteers. The effects of the drugs on the coefficients were consistent with the known properties of the drugs.

The following are suggestions of how this work may be further developed.

7.1 DATA COLLECTION

The Princess Margaret Hospital's SKI sector scanner was purchased in

1977. Now, five years later, it is considered to be obsolete. Modern sector scanners are capable of providing much clearer and more detailed images than can the SKI, since they have more sensitive receivers and digital image processing facilities. Therefore it is planned to replace the SKI with a modern fully-digital sector scanner within the next year. It is expected that Igor will be interfaced to it. Images with less noise and higher spatial resolution will then be available. It should be easier to detect the endocardium in these scans and it is possible that its position may be traced directly from the sector scans without having to resort to the simultaneous R-mode display.

Modern digital video disk units which may be used to interface a sector scanner to a computer are now commercially available. Some of the latest sector scanners may be directly interfaced to a computer. Echocardiograms stored on video tape are replayed into the scanner's main memory frame by frame from where they are passed to the computer. The ability to collect such large volumes of data has obvious advantages and Igor should be replaced by such a unit. Because every frame is recorded, the true end-diastolic and end-systolic frames are available for analysis. This is not the case with data collected by Igor, which records only a limited number of frames through the heart cycle. The end-diastolic and end-systolic frames are usually missed. In the studies reported in chapter 6, the frames displaying the largest and smallest ventricular volumes are nominated as the end-diastolic and end-systolic frames. Therefore the true values of the end-diastolic and end-systolic parameters are not always measured.

When recording scans with a video disk system or with a scanner which can be directly interfaced to a computer, the position of the ventricular walls will be recorded at many points throughout the heart cycle. Therefore it will be possible to study regional heart wall velocity. This is shown to be a diagnostically useful wall motion parameter by Blair et al. (1981).

The number of images collected by such a system is too large to be analysed using the interactive endocardial border tracing techniques described in this thesis. It would be necessary to develop a reliable, fully-automatic endocardial detection system. Even though such systems for analysing angiograms exist, it is a much more difficult task to develop such a system for echocardiograms. This is because echocardiograms contain more artifacts than do angiograms and it is very difficult to program a computer to recognise such artifacts.

Until such a detection system is developed it is really only feasible to extract the end-systolic and the end-diastolic outlines. Unless wall velocity is to be studied, the outlines at these two endpoints are usually the only ones required by most wall motion analysis techniques.

7.2 WALL MOTION AND SHAPE

A severe limitation on the reliability of echocardiographically obtained wall motion and shape data is demonstrated in chapter 6. Each time a patient is studied, a very different ventricular outline is observed in the scans. It is shown that this is caused by the heart contracting in a different manner in each heart cycle and/or by the difficulties encountered in trying to scan in the same cross-section. It was not possible to study these two factors independently with the equipment available and thus identify which is the greatest source of variation.

If the variation is primarily due to heart-beat to heart-beat changes then it will be necessary to average the cardiac shape and motion parameters calculated over several heart cycles. Should the variation be due more to aligning the patients' ventricles with the scanning 'peep holes' in between the ribs, then it will be necessary to study the patient several times. The patient will have to sit up in between each study to randomise the orientation of the heart for each scan. The parameter values obtained from each study must then be averaged to obtain reliable estimates of their magnitudes. Repositioning in between each study would make exercise testing intolerable for the patients as it would be necessary to repeat the whole exercise protocol each time. It would, in general, be difficult for the patient to sit up, lie down and be rescanned several times during the same test because it can take up to one minute to obtain a satisfactory scan. It was found that the patients could rarely maintain pressure on the handgrip exerciser for more than four minutes. Hence the studies could not be repeated very often.

It may well be that some of the heart-transducer orientation difficulties can be overcome by requiring certain cardiac landmarks (eg. the valves) to always appear in the same position and orientation in the same view. At present the definition of each view is relatively loose. There are many adjacent cross-sections of the heart which can be said to constitute the same view. This may sufficiently reduce the orientation variations to dispense with the need for patient repositioning.

Experiments to find a suitable scanning technique which gives reliable data for any one patient must be performed before any further studies of the

wall motion or shape parameters are carried out. There was too much variation in the data obtained in the experiments described in chapter 6 to allow the patients to be individually classified as normal or abnormal on the basis of the parameters used.

A comprehensive set of data of at least 50 patients with wall motion abnormalities in the same region must be gathered. Patients with apical abnormalities should be studied, since defects in such people can be recognised and quantified, whereas defects in other regions of the heart are not as easy to study. This data can then be analysed with many combinations of systems of co-ordinates, systems of reference and motion parameters. This should also be done with a group of 50 normal volunteers. The ability of each combination to classify the subjects as normal or abnormal could then be tested to determine which combination is the most diagnostically useful.

The data can also be used to find which of the shape parameters of §6.4 is best able to classify the subjects.

It was found that exercise can be used as an aid in discriminating between normal and CAD patients (§§6.3, 6.4). Therefore data should be collected with the subjects both at rest and at exercise, in order to assess exercise is as a discriminator.

The same studies should then be repeated for patients with known cardiac abnormalities in regions other than the apex in order to determine if these techniques can be used to detect abnormalities in these other regions.

The results of the drug intervention studies were in keeping with the known effects of the drugs used. The wall motion and shape description techniques may therefore be useful as means of studying the effects of other drugs on normal and ischaemic myocardium.

7.3 WALL MOTION VERSUS SHAPE

The term 'wall motion' is often employed in the wrong context, particularly when it is used to describe ventricular wall movement as seen in angiograms. 'Motion' has connotations of identifying the displacement and direction of movement of all points on the ventricular wall. Generally this is not the case. For the most part, only changes in the shape of the ventricle are displayed. The only points on the ventricular wall which can be precisely identified and followed are the edges of the valve orifices. In echocardiograms, however, it is possible to identify individual reflectors in the ventricular walls and follow them throughout the heart cycle (Hestenes et al., 1978).

It may be that a means of measuring shape change will provide a more reliable basis for detecting 'wall motion' abnormalities than do the techniques discussed in §3.3.1.

It would be worthwhile carrying out a series of psychophysical experiments to determine exactly how a cardiologist analyses 'wall motion' in angiograms and echocardiograms. Once it is known how a cardiologist does this, it may be possible to develop a system to do the same thing automatically and quantitatively.

REFERENCES

Ahuja A.S. 1972. "Effect of particle viscosity on propogation of sound in suspensions and emulsions", J. Acoust. Soc. Am. 51, 182-191.

Aks S.O. and Vezzetti D.J. 1980. "Ultrasonic scattering theory. I : Scattering by single objects", Ultrasonic Imaging 2, 85-101.

Alderman E.L., Schwarzkopf A., Ingels N.B., Daughters G.T., Stinson E.B., and Sanders W.J. 1979. "Application of an externally referenced, polar co-ordinate system for left ventricular wall motion analysis", in Computers in Cardiology 1979, 207-210.

Andreae J.H. and Edmonds P.D. 1961. "Two megacycle interferometer", J. Scient. Instrum. 38, 508.

Angelsen B.A.J. 1980. "A theoretical study of the scattering of ultrasound from blood", IEEE Trans. BME - 27, 61-67.

Argyle E. 1971. "Techniques for edge detection", Proc. IEEE Trans. C-21, 667-676.

Atkinson P. and Berry M.V. 1974. "Random noise in ultrasonic echoes diffracted by blood", J. Phys. A : Math., Nucl. Gen. 7, 1292-1302.

Azancot I., Vannier D., Kedra A.W., Rosengarten M., Slama R. and Bouvrain Y. 1978. "Angiographic frame-by-frame computerized evaluation of overall and regional left ventricular wall motion", in Computers in Cardiology 1978, 281-284.

Azancot I., Vannier D., Vannier A., Slanna R., and Bouvrain Y. 1979. "Utilization of a mini computer for analysis and database management of hemodynamic parameters for routine and research applications", in Computers in Cardiology 1979, 441-444.

Ballantine H.T., Bolt R.H., Hveter T.F. and Ludwig G.D. 1950. "On the detection of intracranial pathology by ultrasound", Science, N.T., 112, 525-528.

Ballantine H.T., Hueter T.F. and Bolt R.H. 1954. "On the use of ultrasound for tumour detection", J. Acoust. Soc. Am. 26, 581.

Balocchi R., Benassi A., Bencivelli W., Pierotti D. and Valli G. 1977. "A system for off-line analysis of left ventricular angiographic images by the use of a mini computer", in Computers in Cardiology 1977, 363-367.

Bamber J.C., Hill C.R., King J.A. and Dunn F. 1979. "Ultrasonic propogation through fixed and unfixed tissues", Ultrasound in Med. & Biol. 5, 159-165.

Barnes R.W., Nomeir A.M., Pardue G.T. and Nuss P.H. 1975. "An Ultrasound receiver with programmable time gain control", J. Clin. Ultrasound 3, 121-124.

Barrett W.A., Clayton P.D. and Warner H.R. 1976. "A system for evaluation and refinement of left ventricular border recognition algorithms", in Computers in Cardiology 1976, 251-253.

Barrett W.A., Clayton P.D. and Warner H.R. 1980. "Determination of left ventricular contours : A probabilistic algorithm derived from angiographic images", Comp. and Biomed. Res. 13, 522-548.

Baruthio J., Chambron J., Mossard J.M. and Voegtlin R. 1979. "Accuracy of the ventricular models and localisation of the contraction anomalies in cineangiocardiography", in Computers in Cardiology 1979, 157-160.

Bastiaans O.L., Meltzer R.S., Vogel J.A., McGhine J., Roelandt J. and Verbeek P.W. 1980. "Quantitative left ventricular analysis from two-dimensional echocardiography", in Computers in Cardiology 1980, 235-238.

Bates R.H.T. and Dunlop G.R. 1977. "Inverse scattering and tomography", Ultrasonics International 1977 (Conference Proceedings), I.P.C. Science and Technology Press, Guildford, U.K., 104-110.

Bates R.H.T., Lewitt R.M., McDonnell M.J., Milner M.D. and Peters T.M. 1978. "Practical image processing", Phys. Technol. 9, 101-107.

Beard C.I., Hays T.H. and Twersky V. 1967. "Scattering by random distributions of spheres versus concentrations", IEEE AP-15, 99.

Beaver W.L. 1977. "Phase error effects in phased array beam steering", in Ultrasonic Symposium Proceedings, IEEE Cat #77CH1264-ISU, 264-267.

Besse P., LeGoff G., Gouverneur G., Page A., Beaune J., Delaye J., Lorino H., Nitenberg A., Laurent D., Boitaud J., Harvey P.J. and Guitton F. 1977. "Present status of a computing system for treatment of hemodynamic and cineangiographic data (SYSCORMORAM)", in Computers in Cardiology 1977, 369-375.

Blair T.J., Clayton P.D., Klausner S.C., Jeppson G.M. and Liddle H.V. 1981. "Changes in velocity of segmental wall motion following coronary artery bypass surgery", in Computers in Cardiology 1980, 75-79.

Bolson E.L., Kilman S., Sheehan F. and Dodge H.T. 1980. "Left ventricular segmental wall motion - a new method using local direction information", in Computers in Cardiology 1980, 245-248.

Bonn N., Lancee C.T., van Zwieten G., Kloster F.E. and Roelandt J. 1973. "Multiscan echocardiography 1. technical description", Circulation 48, 1066-1074.

Bowen T., Connor W.G., Nasoni R.L., Pifer A.E. and Sholes R.R. 1979. "Measurement of the temperature dependence of the velocity of ultrasound in soft tissues", Ultrasonic Tissue Characterisation 2, M. Linser Ed., NBS Spec. Publ. #525, 57-61.

Braun M. and Robinson D.E. 1980. "Model studies of angular behaviour of acoustic backscatter", Ultrasound in Med. & Biol. 6, 377-382.

Braunwald E. 1980 "Heart Disease", Saunders, Philadephia.

Brinkley J.F., Moritz W.E. and Baker D.W. 1978. "Ultrasonic three-dimensional imaging and volume from a series of arbitrary sector scans", Ultrasound in Med. and Biol. 4, 317-327.

Brooks R.A. and DiChiro G. 1976. "Principles of computer assisted tomography (CAT) in radiographic and radioisotope imaging", Phys. Med. Biol. 21, 689-732.

Brower R.W. and Meester G.T. 1976. "Computer based methods for quantifying regional left ventricular wall motion from cine ventriculograms", in Computers in Cardiology 1976, 55-62.

Brower R.W., ten Katen, H.J. and Meester G.T. 1978. "Direct method for determining regional myocardial shortening after bypass surgery from radiopaque markers in man", Am. J. Cardiol, 41, 1222-1229.

Brower R.W. 1980. "Evaluation of pattern recognition rules for the apex of the heart", Cathet. and Cardiovas. Diag., 145-157.

Brower R.W. and Meester G.T. 1980. "Quantitative cardiomorphology of the left ventricle: a new approach to the measurement of regional wall motion", in Computers in Cardiology 1980, 67-72.

Brunt J.N.H., Taylor C.J. and Rowlands D.J. 1979. "A software based system for geometrical analysis of left ventricular cineangiograms", in Computers in Cardiology 1979, 437-440.

Carstensen E.L., Li. K. and Schwan H.P. 1953. "Determination of the acoustic properties of blood and its components", J. Acoust. Soc. Am. 25,286.

Carstensen E.L. and Schwann H.P. 1959a. "Acoustic properties of hemoglobin solutions", J. Acoust. Soc. Am. 31, 305-311.

Carstensen E.L., Schwan H.P. 1959b. "Absorption of sound arising from the presence of intact cells in blood", J. Acoust. Soc. Am. 31, 185.

Carstensen E.L. 1979. "Absorption of sound in tissues", Ultrasonic Tissue Characterisation 2, M. Linzer Ed., NBS Spec. Publ. #525, 29-36.

Chernow A. 1960. "Wave Propagation in Random Medium", New York, McGraw-Hill.

Chivers R.C. and Hill C.R. 1975. "A spectral approach to ultrasonic scattering from human tissue : methods, objectives and backscattering measurements", Phys. Med. Biol. 20, 799-815.

Chivers R.C. 1978. "Phase and amplitude fluctuations in the propagation of acoustic waves in lossless inhomogeneous continua with velocity, density and bulk modulus variations", Ultrasound in Med. & Biol. 4, 353-361.

Chow C.K. and Kaneko T. 1972. "Automatic boundary detection of the left ventricle from cineangiograms", Comp. and Biomed. Res. 5, 388-410.

Chow C.K. and Kaneko T., 1973. "Boundary detection and volume determination of the left ventricle from a cineangiogram", Comp. Biol. Med. 3, 13-26.

Clayton P.D., Harris L.D., Rumel S.R. and Warner H.R. 1974. "Left ventricular videometry", Comp. and Biomed. Res. 7, 369-379.

Cohen M., Peskin C., Teichholz L. and Thornton J. 1980. "The tangent vector as a reference frame free method of analysis of left ventricular shape and shape change", in Computers in Cardiology 1980, 257-260.

Daughters G.T., Schwarzkopf A., Mead C.W. Stinson E.B., Alderman E.L. and Ingels N.B. 1980. "A clinical evaluation of five techniques for left ventricular wall motion assessment", in Computers in Cardiology 1980, 249-252.

de Billy M. and Quentin G.J. 1979. "Methods of analysis for backscattering from tissues", Ultrasonics 17, 85-91.

De Coodt P.R., Mathey D.G. and Swan H.J.C. 1976. "Automated analysis of the left ventricular diameter time curve from echocardiographic recordings", Comp. and Biomed. Res. 9, 549-558.

De Jong L.P. and Slager C.J. 1975. "Automatic detection of the left ventricular outline in angiographs using television signal processing techniques", IEEE BME. 22, 230-237.

Dekker D.L. and Piziali R.I. 1972. "An analysis of ultrasound characteristics related to computerized echocardiology", 25th ACEMB, Florida 1972

De Maria A.N., Bommer A., Joye J.A. and Mason D.T. 1980. "Cross sectional echocardiography : Physical principles, anatomic planes, limitations and pitfalls", Am. J. Cardiol, 46, 1097-1108.

Dines K.A. and Kak A.C. 1979. "Ultrasonic attenuation tomography of soft tissues", Ultrasonic Imaging 1, 16-23.

Doornbos P. and Somer J.C. 1972. "An electrically variable analogue delay line achieved by fast consecutively commuted capacitors", Prog. Rpt., Institute of Medical Physics, Utrecht, 109-113.

Dunlop G.R. 1978. "Ultrasonic Transmission Imaging", Ph.D. Thesis, Univ. of Canterbury, New Zealand.

Dunn F. and Brady J.K. 1973. "Ultrasonic absorption in biological media", Biofizika 18, 1063-1066.

Dunn F. and Brady J.K. 1974. "Ultrasonic absorption in biological media", Biophysics 18, 1128-1132.

Dunn F. 1976. "Ultrasonic attenuation, absorption, and velocity in tissues and organs", Ultrasonic Tissue Characterisation 1, M. Linzer Ed. NBS. Spec. Publ. #453, 21-28.

Dussik K.T. 1942. "Possibility of using mechanical high frequency vibrations as a diagnostic aid", Z. Neurol. Phychiat. 174, 153-168.

Dussik K.T., Dussik F. and Wyt L. 1947. "Auf dem wege zur hyperphonographic des gehirnes", Wien. med. Wschr. 97, 425-429.

Eastman G.A. 1971. "Television Waveform Processing Circuits", 4th ed. Tektronix

Edwards W.D., Tajik A.J. and Seward J.B. 1981. "Standardized nomenclature and anatomic basis for regional tomographic analysis of the heart", Mayo Clin. Proc. 56, 479-497.

Eklundh J.O. and Rosenfeld A. 1980. "Some relaxation experiments using triples of pixels", IEEE SMC-10, 150-163.

Feigenbaum H. 1976. "Echocardiography", 1st Ed., Lea and Febiger, Philadelphia.

Feigenbaum H. 1981. "Echocardiography", 2nd Ed., Lea and Febiger, Philadelphia.

Fields S. and Dunn F. 1973. "Correlation of echocardiographic visualisation of tissue with biological composition and physiological state", J. Acoust. Soc. Am. 54, 809.

Foster C., Anholm J.D., Hellman C.K., Carpenter J., Pollock M.L. and Schmidt D.H. 1981. "Left ventricular function during sudden strenuous exercise", Circulation 63, 592-596.

Freese M. and Lyons E.A. 1977. "Ultrasonic backscatter from human liver tissue : its dependence on frequency and protein/lipid composition", J. Clin. Ultra. 5, 307-312.

Freese M. and Lyons E.A. 1979. "Dependence of ultrasound backscatter from human liver tissue on frequency and protein/lipid composition", Ultrasonic Tissue Characterisation 2, M. Linzer Ed., NBS Spec. Publ. #525, 157-163.

Frei W. 1978. Personal communication to W.K. Pratt. In Digital Image Processing W.K. Pratt, Wiley, New York, 316-318.

Fry W.J. and Dunn F. 1962. "Ultrasound : analysis and experimental methods in biological research", in Physical Techniques in Biological Research, (ed. W.L. Nastuk) vol. IV, Academic Press, N.Y., 261-394.

Fujita M., Sasayama S., Kawai C., Eiho S. and Kuwahara M. 1981. "Automatic processing of cineventriculograms for analysis of regional myocardial function", Circulation 63, 1065-1074.

Gammell P.M., Le Croissette D.H. and Heyser R.C. 1979. "Temperature and frequency dependence of ultrasonic attenuation in selected tissues", Ultrasound in Med. & Biol. 5, 269-277.

Gammell P.M. 1981. "Improved ultrasonic detection using the analytical signal magnitude", Ultrasonics 19, 73-76.

Garcia E., Gueret P., Bennett M., Corday E. Zwehl W., Meerbaum S., Sorday S., Swan H.J.C. and Berman D. 1981a. "Real time computerization of two-dimensional echocardiography", Am. Heart J. 101, 783-792.

Garcia E., Bennett M., Gueret P., Zwehl W., Meerbaum S., Swan H.J.C. and Corday E. 1981b. "A computer system for acquisition in real time, processing and display of two-dimensional echocardiographic images", in Computers in Cardiology 1980, 81-86.

Garrison J.B., Weiss J.L., Maughan W.L., Tuck O.M., Guier W.H. and Fortuin N.J. 1977. "Quantifying regional wall motion and thickening in two-dimensional echocardiography with a computer-aided contouring system", in Computers in Cardiology 1977, 25-35.

Geiser E.A., Lupkiewicz S.M., Christie L.G., Ariet M., Conetta D.A. and Conti C.R. 1980. "A framework for three-dimensional time-varying reconstruction of the human left ventricule: sources of error and estimation of their magnitude", Comp. and Biomed. Res. 13, 225-241.

Geiser E.A., Ariet M., Conetta D.A., Lupkiewicz S.M., Christie L.G. and Conti R.C. 1982. "Dynamic three-dimensional echocardiographic reconstruction of the intact human left ventricle : technique and initial observations in patients", Am. Heart J. 103, 1056-1065.

Gibson D.G. and Brown D.J. 1975. "Continuous assessment of left ventricular shape in man", Brit. Heart J. 37, 904-910.

Gibson D.G., Prewitt T.A. and Brown D.J. 1976. "Analysis of left ventricular wall movement during isovolumic relaxation and its relation to coronary artery disease", Brit. Heart J. 38, 1010-1019.

Gibson D.G., Doran J.H., Traill T.A. and Brown D.J. 1978a. "Regional abnormalities of left ventricular wall movement during isovolumic relaxation in patients with ischemic heart disease", Europ. J. Cardiol., 7/Supple., 251-264.

Gibson D.G., Brown D.J. and Logan-Sinclair R.B. 1978b. "Analysis of regional left ventricular wall movement by phased array echocardiography", Br. Heart J. 40, 1334-1338.

Glover G.H. 1977. "Characterisation of in vivo breast tissue by ultrasonic time of flight computed tomography", in Proc. Nat. Bur. Stand. 2nd Int. Symp. Ultrasonic Tissue Characterisation, Gaithersbury, 221.

Glover G.H. and Sharp J.C. 1977. "Reconstruction of ultrasound propagation speed distributions in soft tissue : time-of-flight tomography", IEEE Trans. SU-24, 229-234.

Gonzalez R.C. and Wintz P. 1977. "Digital Image Processing", Addison-Wesley, Mass.

Gore J.C. and Leeman S. 1977. "Ultrasonic backscattering from human tissues : a realistic model", Phys. Med. Biol. 22, 317-326.

Goss S.A. and Dunn F. 1974. "Concentration dependence of ultrasonic absorption in aqueous solutions of bovine serum albumin", Ultrasonics Symposium Proceedings, IEEE Cat. #74 CHO896-1SU, 65-68.

Gray H. 1973. "Gray's Anatomy",(Ed. R. Warwick, P.L. Williams), 35th Ed., Longman, Edinburgh, 599-618.

Green P.S., Schaeffer L.F., Jones E.D. and Suarez J.R. 1974. "A new high-performance ultrasonic camera", in Acoustical Holography, vol.5. (Ed. P.S. Green), Plenum Press, N.Y., 493-503.

Greenleaf J.F., Johnson S.A., Lee S.L., Herman G.T. and Wood E.H. 1974. "Algebraic reconstruction of spatial distributions of acoustic absorption with tissues from their two-dimensional acoustic projections", in Acoustic Holography, vol. 5, (Ed. P.S. Green), Plenum, New York, 591-603.

Greenleaf J.F., Johnson S.A., Samayoa W.F. and Duck F.A. 1975. "Algebraic reconstruction of spatial distributions of acoustic velocities in tissue from their time-of-flight profiles", in Acoustical Holography, vol. 6, (Ed. N. Booth) Plenum Press, New York, 71-90.

Greenleaf J.F. and Bahn R.C. 1981. "Clinical imaging with transmissive ultrasonic computerized tomography", IEEE BME-28, 177-185.

Greenspan M. and Tscheigg C.E. 1957. "Speed of sound in water by a direct method", J. Res. Natn. Bur.Stand. 59, 249-254.

Gueret P., Meerbaum S., Wyatt H.L., Uchiyama T., Lang T.W. and Corday E. 1980. "Two-dimensional echocardiographic quantitation of left ventricular volumes and ejection fraction importance of accounting for dyssynergy in short-axis reconstruction models", Circulation 62, 1308-131

Guttner W., Fielder G. and Patzold J. 1952. "Vber ultraschallabbildvngen am menschlichen shadel", Acustica 2, 148-156.

Harris L.D., Clayton P.D., Marshall H.W. and Warner H.R. 1974. "A technique for the detection of asynergistic motion in the left ventricle", Comp. and Biomed. Res. 7, 380-394.

Heffernan P.B. 1981. "Aspects of Modelling in Medicine", Ph.D. Thesis, University of Canterbury, New Zealand.

Henry W.L., De Maria A., Gramiak R., King D.L., Kisslo J.A., Popp R.L., Sahn D.J., Schiller N.B., Tajik A., Teichholz L.E. and Weyman A.E. 1980. "Report of the American Society of Echocardiography Committee on nomenclature and standards in two-dimensional echocardiography", Circulation 62, 212-217.

Herrick J.F. and Krusen F.H. 1954. "Ultrasound and medicine. A survey of experimental studies", J. Acoust. Soc. AM. 26, 236-240.

Hestenes J.D., Heng M.K., Ledbetter D.C., Wyatt H.L., Meerbaum S. and Corday E. 1978. "Quantification of circumferential segmental shortening motions from ultrasound sector scanner images in dogs after induced ischemia", in Computers in Cardiology 1978, 389-392.

Heyser R.C. and Le Croissette D.H. 1974. "A new ultrasonic imaging system using time delay spectrometry", Ultrasound in Med. and Biol. 1, 119-131.

Hirsch M., Sanders W.J., Popp R.L. and Harrison D.C. 1973. "Computer processing of ultrasonic data from the cardiovascular system", Comp. and Biomed. Res. 6, 336-346.

Hooghoudt T.E.H., Slager C.J., Reiber J.H.C., Serruys P.W., Schuurbiers J.C.H. and Meester G.T. 1981. "Regional contribution to global ejection fraction used to assess the applicability of a new wall motion model to the detection of regional wall motion in patients with asynergy", in Computers in Cardiology 1980, 253-256.

Horowitz R.S. and Morganroth J. 1982. "Immediate detection of early high-risk patients with acute myocardial infarction using two-dimensional echocardiographic evaluation of left ventricular regional wall motion abnormalities", Am. Heart.J. 103, 814-822.

Hostetler M.S., Roemer L.E., Malindzak G.S., Cauffield E.J. and Petrovick M.L. 1980. "A microprocessor-controlled echocardiographic tracking system", IEEE BME-27, 249-254.

Hounsfield G.N. 1973. "Computerised transverse axial scanning (tomography). Part I. Description of system", Brit. J. Radiol. 46, 1016-1022.

Hueter T.F. and Bolt R.H. 1951. "An ultrasonic method for outlining the cerebral ventricles", J. Acoust. Soc. AM. 23, 160-167.

Hundt E.E., Trautenberg E.A. 1980. "Digital processing of ultrasonic data by deconvolution", IEEE Trans. SU-27, 249-252.

Ide M. 1974. "Image formation processing for pulse echo scanning methods", in Ultrasonic Imaging and Holography, (Ed. G.W. Stroke, W.E. Kock, Y. Kikuchi and J. Tsujiuchi), Plenum Press, New York, 159-189.

Iinuma K., Kidokoro T., Ogura I., Takamizawa K., Seo Y., Hshiguchi M and Uchiumi I. 1979. "High resolution electronic-linear scanning ultrasonic diagnostic equipment", Ultrasound in Med. and Biol. 5, 51-59.

Ingels N.B., Mead C.W., Daughters G.T., Stinson E.B. and Alderman E.L. 1978. "A new method for assessment of left ventricular wall motion", in Computers in Cardiology 1978, 57-61.

Ingels N.B., Daughters G.T., Stinson F.B. and Alderman E.L. 1979. "Dynamic geometry of the left ventricle in intact unanaesthetized man:- motion of specific midwall sites in the 30° right anterior oblique projection", in Computers in Cardiology 1979, 153-155.

Ito K., Yokoi H. and Tatsumi T. 1974. "Quantitative color ultrasonography. Computer aided simultaneous tomogram method", in Ultrasonics in Medicine (Ed. M. de Vlieger, D.N. White and V.R. McCready), Exerpta Medica, Amsterdam, 366-372.

Jensch P., Ameling W., Kubalski W., Heuck N., Meyer J. and Effert S. 1981. "A data acquisition and processing system for sequences of ultrasound echoes and video images", in Computers in Cardiology 1980, 227-230.

Johnson S.A., Greenleaf J.F., Chu A., Sjostrand J.D., Gilbert B.K. and Wood E.H. 1975. "Reconstruction of material characteristics from highly refraction distorted projections by ray tracing", in Topical Meeting on Image Processing for 2-D and 3-D Reconstruction from Projections: Theory and Practice in Medicine and the Physical Sciences, Stanford Univ.

Johnston R.L., Goss, S.A., Maynard V., Brady J.K., Frizzell L.A., O'Brien W.D. and Dunn F. 1979. "Elements of Tissue Characterisation. Part 1. Ultrasonic propagation properties", Ultrasonic Tissue Characterisation 2, Ed. M. Linzer, NBS Spec. Publ. #525, 19-27.

Kadaba M.P., Bhagat P.K. and Wu V.C. 1980. "Attenuation and backscattering of ultrasound in freshly excised animal tissues", IEEE Trans. BME-27, 76-83.

Kambe T., Nishimura K., Hibi N., Sakakibara T., Kato T., Fukui Y., Arakawa T., Tatematsu H., Miwa A., Tada H. and Sakamoto N. 1977. "Clinical application of high speed B mode echocardiography", J. Clin. Ultra. 5, 202-207.

Keshavan H.R. and Srinath M.D. 1978. "Enhancement of noisy images using an interpolative model in two dimensions", IEEE SMC-8, 247-258.

Kirsch R. 1971. "Computer determination of the constituent structure of biological images", Comp. and Biomed. Res. 4, 315-328.

Kishimoto T. 1959. "Ultrasonic absorption in bones", Acustica 8, 179-180.

Klausner S.C., Blair T.J., Bulawa W.F., Jeppson G.M., Jensen R.L. and Clayton P.D. 1982. "Quantitative analysis of segmental wall motion throughout systole and diastole in the normal human left ventricle", Circulation 65, 580-590.

Klepper J.R., Brandenburger G.H., Mimbs J.W., Sobel B.E. and Miller J.G. 1981. "Application of phase-insensitive detection and frequency dependent measurements to computed ultrasonic attenuation tomography", IEEE BME-28, 186-201.

Kol'tsova I.S. and Mikhailov I.G. 1970. "Scattering of ultrasonic waves in heterogenous systems", Sov. Phys. Acoust. 15, 390.

Kossoff G. 1972. "Improved techniques in ultrasonic cross sectional echography", Ultrasonics 10, 221-227.

Kossoff G. and Garrett W.J. 1972. "Ultrasonic film endoscopy for placental localisation", Aust. N.Z. J. Obstet. Gynaecol. 12, 117-121.

Kossoff G. 1979. "Analysis of focussing action of sperically curved transducers", Ultrasound in Med. and Biol. 5, 359-365.

Kremkau F.W. and Carstensen E.L. 1972. "Macromolecular interaction in sound absorption", Proc. of Workshop of Ultras. and Bio. Tiss., F.D.A., Maryland, 37-42.

Kremkau F.W. and Carstensen E.L. 1973. "Molecular Interaction in the absorption of ultrasound in fixed erythrocytes", J. Acoust. Soc. Am. 53,1448-1451.

Kremkau F.W., McGraw C.P. and Barnes R.W. 1979. "Acoustic properties of normal and abnormal human brain", Ultrasonic Tissue Characterisation II, Ed. M. Linzer, NBS Spec. Publ. #525, 81.

Kronik G., Slany J. and Mosslacher H. 1979. "Comparative value of eight M-mode echocardiographic formulas for determining left ventricular stroke volume : a correlative study with thermodilation and left ventricular single-plane cineangiography", Circulation 60, 1308-1316.

Latson L.A., Cheatham J.P. and Gutgesell H.P. 1981. "Resolution and accuracy in two dimensional echocardiography", Am. J. Cardiol. 48, 106-110.

Ledley F.D. and Wilson J.B. 1974. "Computer analysis of ultrasound cardiograms", Comp. Biol. Med. 4, 27-41.

Leighton R.F., Nelson A.D., Andrews L.T. and Gupta M. 1979. "Altered sequence of regional left ventricular wall motion in patients with coronary heart disease", in Computers in Cardiology, 1979, 149-152.

Lele P.P., Mansfield A.B., Murphy A.J., Namery J. and Serapati N. 1976. "Tissue characterisation of ultrasonic frequency dependent attenuation and scattering", Proc. 1st Inst. Symp. Ultrasonic Tissue Characterisation, (Ed. M. Linzer), 167-206.

Lev A., Zucker S.W. and Rosenfeld A. 1977. "Iterative enhancement of noisy images", IEEE Trans. SMC-7, 435-442.

Lewitt R.M. and Bates R.H.T. 1978a. "Image reconstruction from projections : I : general theoretical considerations", Optik 50, 19-33.

Lewitt R.M. and Bates R.H.T. 1978b. "Image reconstruction from projections : III : projection completion methods (theory), Optik 50, 189-204.

Lewitt R.M. and Bates R.H.T. 1978c. "Image reconstruction from projections : IV : projection completion methods (computational examples)", Optik 50, 269-278.

Lewitt R.M., Bates R.H.T. and Peters T.M. 1978. "Image reconstruction from projections : II : modified back-projection methods", Optik 50, 85-109.

Ligtvoet C., Vogel J., Van Egmond F. and Vletter W. 1977. "Direct conversion of real time two-dimensional echocardiographic images", Ultrasonics IS, 89-92.

Lizzi F., Katz L., St Louis L. and Coleman D.J. 1976. "Applications of spectral analysis in medical ultrasonography", Ultrasonics 14, 77-80.

Lizzi F.L. and Elbaum M.E. 1979. "Clinical spectrum analysis techniques for tissue characterisation", Ultrasonic Tissue Characterisation 2, M. Linzer Ed., NBS Spec. Publ. #525, 111-119.

Ludbrook P.A., Byrne J.D., Reed F.R. and McKnight R.C. 1980. "Modification of left ventricular diastolic behaviour by isometric handgrip exercise", Circulation 62, 357-370.

McDevitt D.G. 1979. "Adrenoceptor blocking drugs: clinical pharmacology and therapeutic use", New Ethicals and Med. Prog. 16, 119-144.

McDicken W.N. 1981. "Diagnostic Ultrasonics : Principles and Use of Instruments", 2nd Edn. John Wiley, New York.

McKeighen R.E. and Buchin M.P. 1977. "New techniques for dynamically variable electronic delays for real time ultrasonic imaging", Ultrasonics Symposium Proceedings, IEEE Cat. #77 CH1264-ISU, 250-254.

McSherry D. 1973. "Digital processing systems for diagnostic ultrasound data", Proc. of the Second World Congress on Ultrasonics in Med, Rotterdam, 325-331.

McSherry D. 1974. "Computer processing of diagnostic ultrasound data", IEEE Trans. SU-21, 91-97.

McSherry D.H. and Keller J.R. 1974. "Ultrasonic cardiac imaging and image enhancement techniques", Ultrasonic Symposium Proceedings, IEEE Cat. #74 CHO896-ISU, 5-11.

Manes G.F., Atzeni C., Susin C. and Somer J.C. 1979. "A new delay technique with application to ultrasound phased-array imaging systems", Ultrasonics 17, 225-229.

Markham J.J., Beyer R.T. and Lindsay R.B. 1951. "Absorption of sound in fluids", Rev. Mod. Phys. 23, 355-411.

Matzuk T., Skolnick M.L. 1978. "Novel ultrasonic real time scanner featuring servo controlled transducers displaying a sector image", Ultrasonics 16, 171-178.

Maurer G. and Nanda N.C. 1981. "Two-dimensional echocardiographic evaluation of exercise-induced left and right ventricular asynergy: correlation with thallium scanning", Am. J. Cardiol. 48, 720-727.

Meerbaum S., Wyatt H.L., Heng M., Cobo J. and Corday E. 1980. "Assessment of cardiac function in the dog by cross-sectional echocardiography", in Cardiac Dynamics, Martinus Nijhoff, The Hague, 405-415.

Melen R.D., Macouski A. and Meindl J.D. 1979. "Application of integrated electronics to ultrasonic medical instruments", Proc. IEEE. 67, 1274-1285.

Melton H.E. and Thurstone F.L. 1978. "Annular array design and logarithmic processing for ultrasonic imaging", Ultrasound in Med. Biol. 4, 1-12.

Milan J. and Taylor K.J.W. 1975. "The application of the temperature-color scale to ultrasonic imaging", J. Clin. Ultra. 3, 171-173.

Mimbs J.W., O'Donnell M., Bauwens D., Miller J.W. and Sobel B.E. 1980. "The dependence of ultrasonic attenuation and backscatter on collagen content in dog and rabbit hearts", Circulation Research 47, 49-58.

Mimbs J.W., O'Donnell M., Miller J.G. and Sobel B.L. 1981. "Detection of cardiomyopathic changes induced by doxorubicin based on quantitative analysis of ultrasonic backscatter", Am. J. Cardiol, 47, 1056-1060.

Mitamura H., Ogawa S., Hori S., Yamazaki H., Handa S, and Nakamura Y. 1981. "Two-dimensional echocardiographic analysis of wall motion abnormalities during handgrip exercises in patients with coronary artery disease", Am. J. Cardiol, 8, 711-719.

Modestino J.W., Ashkar G.P., Fries R.W. and Kaufman H. 1976. "Computer evaluation of dynamic left ventricular volume from serial analysis", in Computers in Cardiology 1976, 211-218.

Morgan C.L., Trought W.S., Clark W.M., Von Ramm O.T. and Thurstone F.L. 1978. "Principles and applications of a dynamically focused phased array real time ultrasound system", J. Clin. Ultra. 6, 385-391.

Morganroth J., Chen C.C., David D., Sawin H.S., Naito M., Parrotto C. and Meixell L. 1981. "Exercise cross-sectional echocardiographic diagnosis of corconary artery disease", Am. J. Cardiol. 47, 20-26.

Morse P.M. and Feshbach H. 1953. "Mathematical Methods of Theoretical Physics", Vol. 1., McGraw-Hill, N.Y.

Morse P.M. and Ingard K.U. 1968. "Theoretical Acoustics", McGraw-Hill, N.Y.

Mountford R.A. and Wells P.N.T. 1972a. "Ultrasonic liver scanning : the A-scan in the normal and cirrhosis", Phys. Med. Biol. 17, 261-269.

Mountford R.A. and Wells P.N.T. 1972b. "Ultrasonic liver scanning : the quantitative analysis of the normal A-scan", Phys. Med. Biol. 17, 14-25.

Moynihan P.F., Parisi A.F. and Feldman C.L. 1981. "Quantitative detection of regional left ventricular contraction abnormalities by two-dimensional echocardiography. I. Analysis of methods", Circulation 63, 752-760.

Myers G.H., Thumin A., Feldman S., Santis G. de and Lupo F.J. 1972. "A miniature pulser-preamplifier for ultrasonic transducers", Ultrasonics 10, 87-89.

Nicholas D. and Hill C.R. 1975. "Acoustic bragg diffraction from human tissues", Nature 257, 305-6.

Nicholas D. 1976. "Ultrasonic Scattering and Structure of Human Tissue", Ph.D. Dissertation, Univ. of London.

Nixon J.V. and Saffer S.I. 1978. "Three-dimensional echocardiography", Circulation 57 and 58 : II-157.

O'Brien W.D. and Dunn F. 1971. "Ultrasonic examination of the Hemoglobin dissociation process in aqueous solutions of guanidine hydrochloride", J. Acoust. Soc. Amer. 50, 1213-1215.

O'Donnell M. and Miller J.G. 1979. "Mechanisms of ultrasonic attenuation in soft tissues", Ultrasonic Tissue Characterisation 2, M. Linzer Ed., NBS Spec. Publ. #525, 37-40.

O'Donnell M., Mimbs J.W., Sobel B.E. and Miller J.G. 1979. "Ultrasonic attenuation in normal and ischaemic myocardium", Ultrasonic Tissue Characterisation 2, M. Linzer Ed., NBS Spec. Publ. #525, 63-71.

O'Neil H.T. 1949. "Theory of focussing radiators", J. Acoust. Soc. Amer. 21, 516-526.

Ophir J. et al. 1974. "The CUPAD system : real time handling of randomly acquired clinical ultrasound data", in Ultrasound in Medicine, Vol.1. (Ed. Denis White), Plenum Press, New York.

Ophir J. and Maklad N.F. 1979. "Digital scan converters in diagnostic ultrasound imaging", Proc. IEEE 67, 654-664.

Papapietro S.E., Smith L.R., Hood W.P., Russell R.O., Rackley C.E., and Rogers W.J. 1978. "An optimal method for angiographic definition and quantification of regional left ventricular contraction", in Computers in Cardiology 1978, 293-295.

Parisi A.F., Moynihan P.F., Folland E.D. and Feldman C.L. 1981. "Quantitative detection of regional left ventricular contraction abnormalities by two-dimensional echocardiography II. Accuracy in coronary artery disease", Circulation 63, 761-767.

Parker D.L., Pryor T.A. and Ridges J.D. 1979. "Enhancement of two-dimensional echocardiographic images by lateral filtering", Comp. and Biomed. Res. 12, 265-277.

Parry R.J. and Chivers R.C. 1979. "Data of the velocity and attenuation of ultrasound in mammalian tissues", Ultrasonic Tissue Characterisation 2, Ed. M. Linzer, NBS Spec. Publ. #525, 343-360.

Pauly H. and Schwan H.P. 1971. "Mechanism of absorption of ultrasound in liver tissue", J. Acoust. Soc. Am. 50, 692-697.

Pellan J.R. and Galt J.K. 1946. "Ultrasonic propagation in liquids : I. Application of pulse techniques to velocity and absorption measurements at fifteen megacycles", J. Chem. Phys. 14, 608-614.

Platt W.R. 1969. "Color Atlas and Textbook of Hematology", J.B. Lippincott, Philadelphia.

Ponder E. 1945. "The paracrystalline state of the rat red cell", J. Gen. Physiol. 29, 89-102.

Pratt W.K. 1978."Digital Image Processing",John Wiley New York.

Pryor T.A., Parker D.L. and Ridges J.D. 1978. "Comparison of regional wall motion parameters between angiographic and echocardiographic images". in Computers in Cardiology 1978, 63-68.

Reiber J.H.C., Slager C.J., Schuurbiers J.C.H. and Meester G.T. 1978. "Contouromat-A hard-wired left ventricular angio processing system. II. Performance evaluation", Comp. and Biomed. Res. 11, 503-523.

Reid J.M., Sigelman R.A., Nauser M.G. and Baker D.W. 1969. "The scattering of ultrasound by human blood", The Proceedings of the Eighth ICMBE.

Reid J.M. 1976. "The scattering of ultrasound by tissues", Ultrasonic Tissue Characterisation 1, M. Linzer Ed., NBS Spec. Publ. #453, 29-47.

Roberts L.G. 1965. "Machine perception of three-dimensional solids", in Optical and Electro-optical Information Processing (Ed. J. Tippett et al.), M.I.T. Press, Mass., 159-197.

Robinson D.E., Jellins J. and Kossoff G. 1970. "The C.A.L. four channel solid state echo-encephaloscope", Ultrasonics 8, 93-96.

Robinson D.E. 1972. "Ultrasonic systems for medical diagnostic visualization", M.I.T. Quart. Progr. Rep. 104, 289.

Robinson D.E., Knight, P.C., Kossoff G. and Chen F. 1981. "Developments in computer processing of ultrasonic echo data", Australasian Physical and Engineering Sciences in Medicine 4, 83-90.

Robinson E.P., Pryor T.A., Wellard S.J., Jones D.S. and Ridges J.D. 1976. "Recognition of left ventricular borders using two-dimensional echocardiographic images", Comp. and Biomed. Res. 9, 247-261.

Rosenfeld A. 1970. "A non-linear edge detection technique", Proc. IEEE letters 58, 814-816.

Rosenfeld A. and Thurston M. 1971. "Edge and curve detection for visual scene analysis", IEEE Trans. C-20, 562-569.

Rosenfeld A. and Kak A.C. 1976. "Digital Picture Processing", Academic Press, New York.

Round W.H. 1977. "Investigations of a Ray Tracing Model of Ultrasound Traversing the Human Eye", M. Sc. Thesis, University of Surrey, U.K.

Round W.H., Bones P.J., Ikram H. and Bates R.H.T. 1982. "Digitising and processing echocardiographic images", Aust. Phys. Eng. Sci. Med 5, 113-121.

Serruys P.W., Brower R.W., ten Katen H.J., Bom A.H. and Hugenholtz P.G. 1981. "Regional wall motion from radiopaque markers after intravenous and intracoronary injectors of nifedipine", Circulation 63, 584-591.

Shepertycki T.H. and Morton B.C. 1979. "An interactive computer graphic modelling approach in detecting left ventricular wall motion abnormalities", in Computers in Cardiology 1979, 215-218.

Shott J.D., Melen R.D. and Meindl J.D. 1976. "The cascade charge coupled device : A single-chip lens for ultrasonic imaging systems", IEEE Solid State Circuits Conf., Philadephia, 200-201.

Shung K.K., Sigelmann R.A. and Reid J.M. 1976a. "The scattering of ultrasound by red blood cells", Ultrasonic Tissue Characterisation 1, Ed. M. Linzer, NBS Spec. Publ. 453, 207-212.

Shung K.K. Sigelmann R.A. and Reid J.M. 1976b. "Scattering of ultrasound by blood", IEEE Trans. BME-23, 460-467.

Shung K.K. and Reid J.M. 1977. "Ultrasonic scattering from tissues", IEEE Ultrasonics Symposium Proceedings 1977, 230-233.

Shung K.K., Sigelmann R.A. and Reid J.M. 1977. "Angular dependence of scattering of ultrasound from blood", IEEE BME-24, 325-331.

Sigelmann R.A. and Reid J.M. 1972. "Analysis and measurement of ultrasound backscattering from an ensemble of scatterers excited by sine-wave bursts", J. Acoust. Soc. Am. 53, 1351-1355.

Silverman M.E. and Schlant R.C. 1974. in"The Heart"3rd Ed. (Ed. J.W. Hurst, R.B. Logue, R.C. Schlant, N.K. Wenger), McGraw-Hill, New York, 20-34.

Sims H.V. 1969. "Principles of Pal Colour Television and Related Systems", Ilfte Books, London.

Skorton D.J., McNary C.A., Child J.S., Newton F.C. and Shah P.M. 1981. "Digital image processing of two-dimensional echocardiograms : identification of the endocardium", Am. J. Cardiol, 48, 479-486.

Slager C.J., Reiber J.H.C., Schuurbiers J.C.H. and Meester G.T. 1978. "Contourmat - A hard-wired left ventricular angio processing system 1: design and application", Comp. and Biomed. Res. 11, 491-502.

Slager C.J., Hooghoudt T.E.H., Reiber J.H.C., Schuurbiers J.C.H., Booman F. and Meester G.T. 1979. "Left ventricular contour segmentation from anatomical handmark trajectories and its application to wall motion analysis", in Computers in Cardiology 1979, 347-350.

Smalling R.W., Skolnick M.H., Myers D., Shabetai R., Cole J.C. and Johnston D. 1976. "Digital boundary detection, volumetric and wall motion analysis of left ventricular cineangiograms", Comp. Biol. Med. 6, 73-85.

Sobel K. 1973. in "Pattern Classification and Scene Analysis", Duda R.O. and Hart P.E., Wiley, N.Y.

Somer J.C. 1968. "Electronic sector scanning for ultrasonic diagnosis". Ultrasonics 6, 153-159.

Somer J.C. and Dael J.W.J.M. van. 1972. "Application of a non-linear processing technique to ultrasound pulse echo systems for improving angular resolution", in Ultrasonics in Biology and Medicine, (Ed. L. Filipczynski), Polish Scientific Publishers, Warsaw, 201-213.

Stack R. and Kisslo J. 1980. "Evaluation of the left ventricle with two-dimensional echocardiography", Am. J. Cardiol. 46, 1117-1124.

Surridge A.D. 1980a. "Frequency shift of an acoustic wavetrain due to atmospheric absorption", Acustica 44, 207-211.

Surridge A.D. 1980b. "On frequency dependent backscattering of an acoustic wavetrain in the atmosphere", Acustica 46, 289-292.

Tajik A.J., Seward J.B., Hagler D.J., Mair D.D. and Lie J.T. 1978. "Two-dimensional real time ultrasonic imaging of the heart and great vessels : technique, image orientation, structure identification, and validation", Mayo Clin. Proc. 53, 271-303.

Tasto M. 1974. "Motion extraction for left-ventricular volume measurement", IEEE BME-21, 207-213.

Taylor K.J.W., Carpenter D.A. and McCready V.R. 1973. "Grey scale echography in the diagnosis of intrahepatic disease", J. Clin. Ultra. 1, 184-187.

Thurstone F.L. and Abbott J.G., 1977. "Actual time scan conversion and image processing in a phased array ultrasound imaging system", Ultrasonic Symposium Proceedings, IEEE Cat. #77CH1264-ISU, 247-249.

Treitel S. and Robinson E.A. 1966. "The design of high-resolution digital filters", IEEE Trans. GE-4, 25-38.

Trussell H.J. 1977. "A fast algorithm for noise smoothing based on a subjective criterion", IEEE SMC-7, 677-678.

Tsotsos J.K., Covvey H.D., Mylopoulos J., Zucker S. and Wigle E.D. 1979. "Alven : a system for LV segmental wall motion analysis", in Computers in Cardiology 1979, 445-446.

Tukey J.W. 1971. "Exploratory Data Analysis", Addison-Wesley, Reading, Mass.

Twersky V. 1962a. "On scattering of waves by random distributions - I : Freespace scatterer formalism", J. Math. Phys. 3, 700-715.

Twersky V. 1962b. "On scattering of waves by random distributions - I : two space scatterer formalism", J. Math. Phys. 3, 724-734.

Twersky V, 1962c. "On a general class of scattering problems", J. Math. Phys. 3, 716-723.

Twersky V, 1964. "Acoustic bulk parameters of random volume distributions of small scatterers", J. Acoust. Soc. Am. 36, 1314-1329.

Ueda K., Kuwaki K. and Inone K. 1980. "Three-dimensional display and volume determination of the left ventricle by two-dimensional echography", (abstr.) Am. J. Cardiol. 45, 471.

Urick R.J. 1947. "A sound velocity method for determining the compressibility of finely divided substance", J. Appl. Phys. 18, 983.

Van Wijk van Brievingh R.P. 1975. "Quantitative Videoangiography", Delft University Press.

Varian. 1980. Varian V-3400 brochure.

Verbeek P.W., Bastiaans O.L. 1977. "Search-free structure extraction applied to M-mode echocardiograms and chromosome images", in Computers in Cardiology 1977, 281-284.

Vezzetti D.J. and Aks. S.O. 1980. "Ultrasonic scattering theory II : scattering from composites", Ultrasonic Imaging 2, 195-212.

Visser C.A., Kan G., Lie K.I., Becker A.E. and Durrer D. 1982a. "Apex two-dimensional echocardiography - alternative approach to quantification of acute myocardial infarction", Br. Heart J. 47, 461-471.

Visser C.A., Kan G., David G.K., Lie K.I. and Durrer D. 1982b. "Echocardiographic cineangiographic correlation in detecting left ventricular aneurysm : a prospective study of 422 patients", Am. J. Cardiol. 50, 337-341.

Vollmann W. 1982. "Resolution enhancement of ultrasonic B-scan images by deconvolution", IEEE Trans. SU-29, 78-83.

Von Ramm O.T. and Thurstone F.L. 1976. "Cardiac imaging used a phased array ultrasound system", Circulation 53, 258-262.

Waag R.C. and Lerner R.M. 1973. "Tissue macro-structure determination with swept-frequency ultrasound", Proc. Ultrasonics Symposium, IEEE #73CHO 807-8SU, 63-66.

Waag R.C., Lee P.P.K., Lerner R.M., Hunter L.P., Gramiak R. and Schenk E.A. 1979. "Angle scan and frequency-swept ultrasonic scattering characterisation of tissue", Ultrasonic Tissue Characterisation 2, Ed. M. Linzer, NBS Spec. Publ. 525, 143-152.

Wallis R.H. 1976. "An approach for the space variant restoration and enhancement of images", in Proceedings Symposium on Current Mathematical Problems in Image Science, Monterey California, November 1976.

Wann L.S., Faris J.V., Childrens R.H., Dillon J.C., Weyman A.E. and Feigenbaum H. 1979. "Exercise cross-sectional echocardiography in ischaemic heart disease", Circulation 60, 1300-1308.

Weintraub W.S., Hattori S., Agarwal J.B., Bodenheimer M.M., Banka V.S., and Helfant R.H. 1982. "The effects of nifedipine on myocardial blood flow and contraction during ischaemia in the dog", Circulation 65, 49-53.

Wells P.N.T. 1977."Biomedical Ultrasonics",Academic Press, London.

Weyman A.E., Wann L.S., Caldwell R.L., Huruwitz R.A., Dillon J.C. and Feigenbaum H. 1979. "Negative contrast echocardiography : a new method for detecting left-to-right shunts", Circulation 59, 498.

Whiting J.F., Koch R., Price D.C., Kojrowicz E., McCaffrey J.F. and Cavaye G. 1981. "Ultrasonic computer assisted tomography of the breast", Presented at 21st Conference on PSEMB, Melbourne, August 17-21, 1981.

Wild J.J. 1950. "The use of ultrasonic pulses for the measurement of biologic tissues and the detection of tissue density changes", Surgery 27, 183-187.

Wild J.J. and Reid J.M. 1952. "Further pilot echographic studies on the histologic structure of tumours of the living intact human breast", Am. J. Pathol. 28, 839-861.

Wyatt H.L., Heng M.K., Meerbaum S., Hestenes J.D., Colso J.M., Davidson R.M. and Corday E. 1979. "Cross-sectional echocardiography I. Analysis of mathematic models for quantifying mass of the left ventricle in dogs", Circulation 60, 1104-1113.

Wyatt H.L., Heng M.K., Meerbaum S., Gueret P., Hestenes J., Dula E. and Corday E. 1980a. "Cross-sectional echocardiography : II. Analysis of mathematic models for quantifying volume of the formalin-fixed left ventricle", Circulation 61, 1119-1125.

Wyatt H.L., Meerbaum S., Heng M.K., Gueret P. and Corday E. 1980b. "Cross-sectional echocardiography III. Analysis of mathematic models for quantifying volume of symmetric and asymmetric left ventricles", Am. Heart. J. 100, 821-828.

Zahn C.T. and Roskies R.Z. 1972. "Fourier descriptors for plane closed curves", IEEE C-21, 269-281.

Zatz L.M., Marich K.W., Green P.S., Lipton M.J., Suarez J.R. and Macouski A. 1975. "Real time imaging with a new ultrasonic camera : Part II. Preliminary studies in normal adults", J. Clin. Ultras. 3, 17-22.

Zwehl W., Gueret P., Meerbaum S., Holt D. and Corday E. 1981. "Quantitative two-dimensional echocardiography during bicycle exercise in normal subjects", Am. J. Cardiol 47, 866-873.

APPENDIX A

CIRCUIT DIAGRAMS

OF

IGOR

Controller Board

I.C. type	Identification number in diagram
7400	7,32
7408	1
74S11	8
7414	23
7417	38
7432	17,19
7476	5,6
7490	2,14
74107	13,16,20,21
74123	15,18
74192	3,4,25-37
8556	9-12

All thumbwheel inputs are tied to +5V through 470 ohm resistors.

Power requirements: +5V

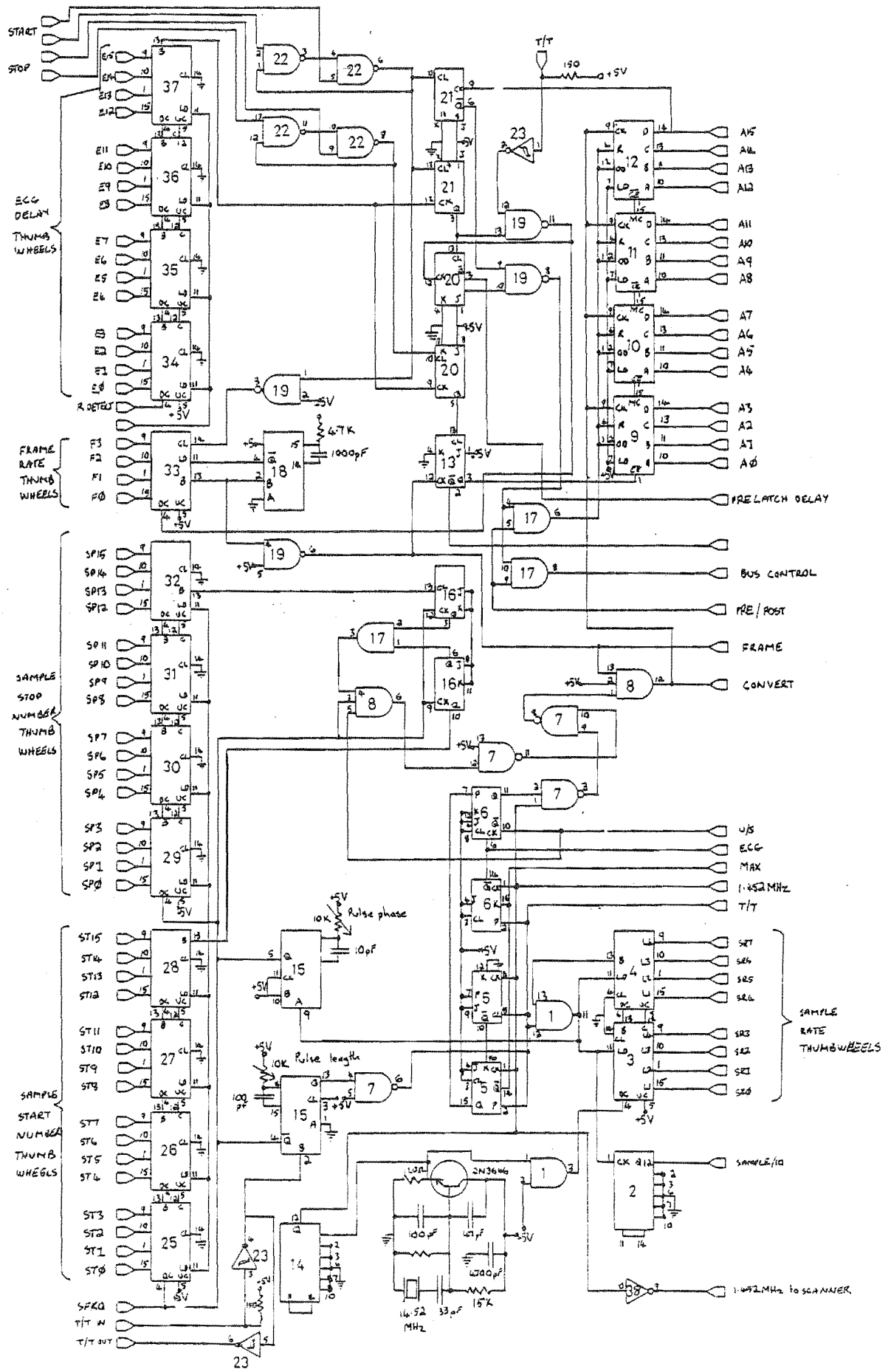

Controller Board

Analogue Signal Processor Board

I.C. type	Identification number in diagram
LM741	17
LM301	16,18-22
CD4051	14
74S02	9,10,11
7404	1
7408	4
74S11	8,12
74S30	13
7473	2,3,7
74123	15
8095	5,6

Power requirements: +5V, +15V, -15V

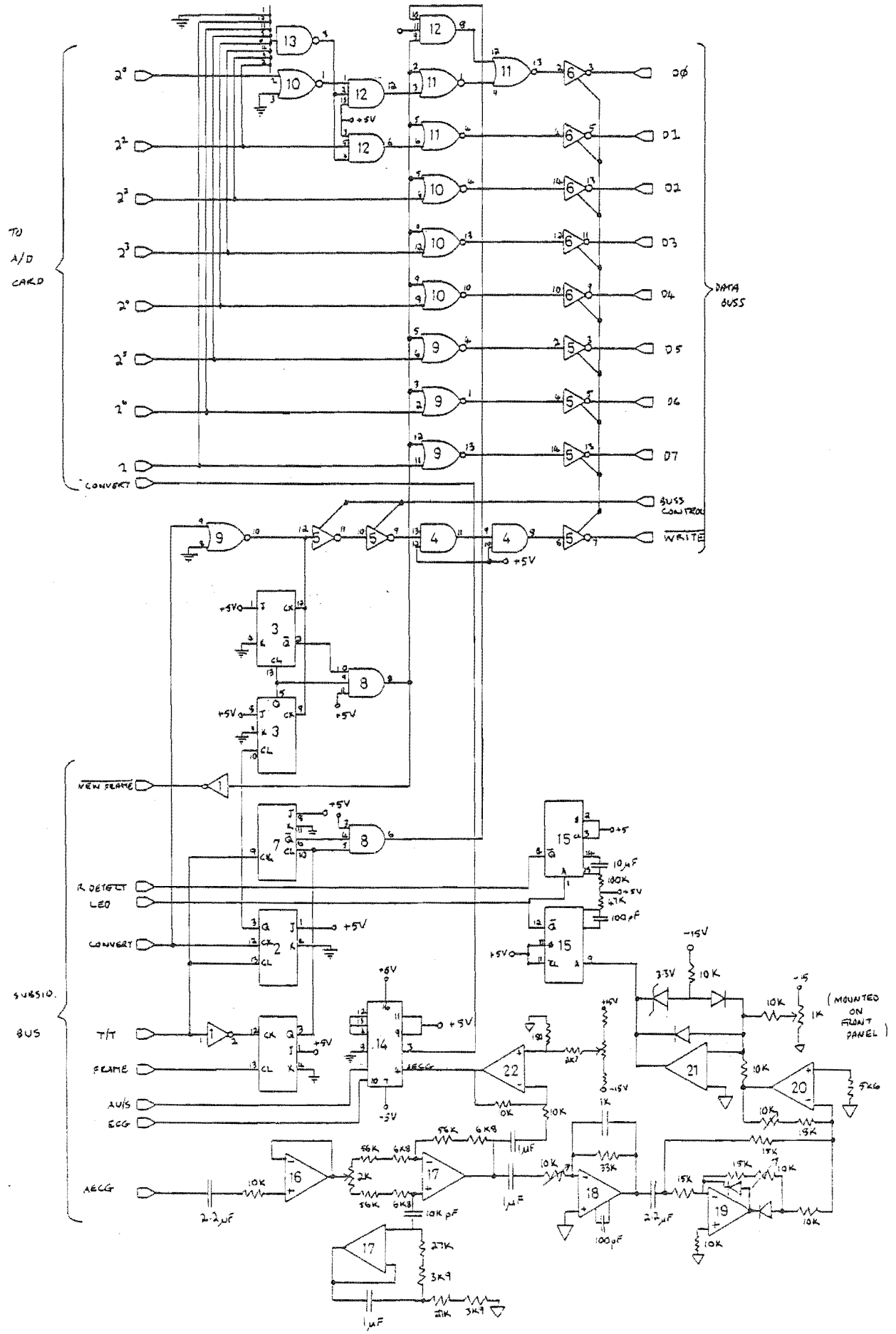

Analogue Signal Processor Board

Analogue to Digital Converter Board

TDC1007PCB board used. This plugs directly into the Analogue Signal Processor Board

TDC1007PCB

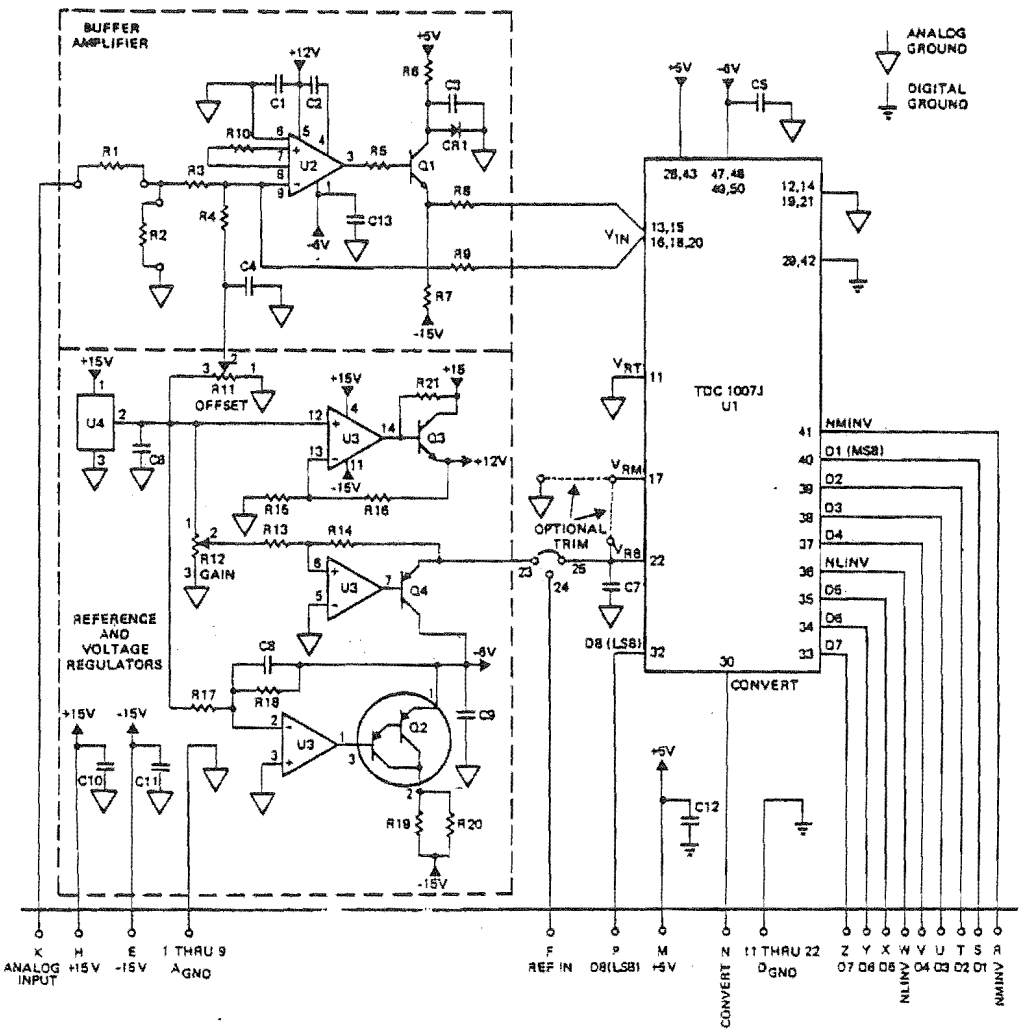

PARTS LIST

RESISTORS

R1	0Ω*	1/4W	2%
R2	82Ω*	1/4W	2%
R3	1.0KΩ		2%
R4	4.2KΩ	1/4W	2%
R5	10Ω	1/4W	2%
R6	56Ω	1/4W	5%
R7	240Ω	2W	5%
R8	6.8Ω	1/2W	5%
R9	2.0KΩ	1/2W	2%
R10	†	1/4W	2%
R11	2.0KΩ	1/4W	MULTITURN CERMET POT
R12	2.0KΩ	1/4W	MULTITURN CERMET POT
R13	21.4KΩ	1/4W	2%
R14	21.4KΩ	1/4W	2%
R15	11.3KΩ	1/4W	2%
R16	42.2KΩ	1/4W	2%
R17	21.5KΩ	1/4W	2%
R18	51.1KΩ	1/4W	2%
R19	24Ω	2W	10%
R20	24Ω	2W	10%
R21	392Ω	1/4W	2%

DIODES

CR1	1N4001

CAPACITORS

C1	0.1μF	50V
C2	†	50V
C3	0.1μF	50V
C4	0.1μF	50V
C5	0.1μF	50V
C6	1.0μF	10V
C7	10.0μF	10V
C8	0.001μF	50V
C9	100.0μF	10V
C10	10.0μF	20V
C11	10.0μF	20V
C12	10.0μF	10V
C13	0.1μF	50V

TRANSISTORS

Q1	2N5836
Q2	2N6034
Q3	2N2222
Q4	2N2907

INTEGRATED CIRCUITS

U1	TRW TDC1007J
U2	PLESSEY SL541C
U3	MOTOROLA MLM2902
U4	MOTOROLA MC1403U

MISCELLANEOUS

A1	CAMBION 64 PIN SOCKET 704-4064-01-04-12 FOR U1**
A2	THERMALLOY HEAT SINK 60738 FOR Q2
A3	TRW CINCH EDGE CONNECTOR 251 22 30 160
A4	PRINTED CIRCUIT BOARD TRW TPC1007
A5	MOORE SYSTEMS STITCH WELD PINS 700508 FOR R1, R2

* INPUT IMPEDANCE AND RANGE SELECT (75Ω, 1V OPTION SUPPLIED)

** A ZERO INSERTION FORCE SOCKET (TEXTOOL PN 232-2601-00-0606, 2 REQUIRED) MAY BE SUBSTITUTED BY THE USER.

† AMPLIFIER COMPENSATION COMPONENTS

TRW LSI PRODUCTS

Analogue-to-Digital Converter Board

Memory Selector Board

I.C. type	Identification number in diagram
7404	3,6
7432	1,2
74122	4
8205	7,8
LM555	5

Power requirements: +5V

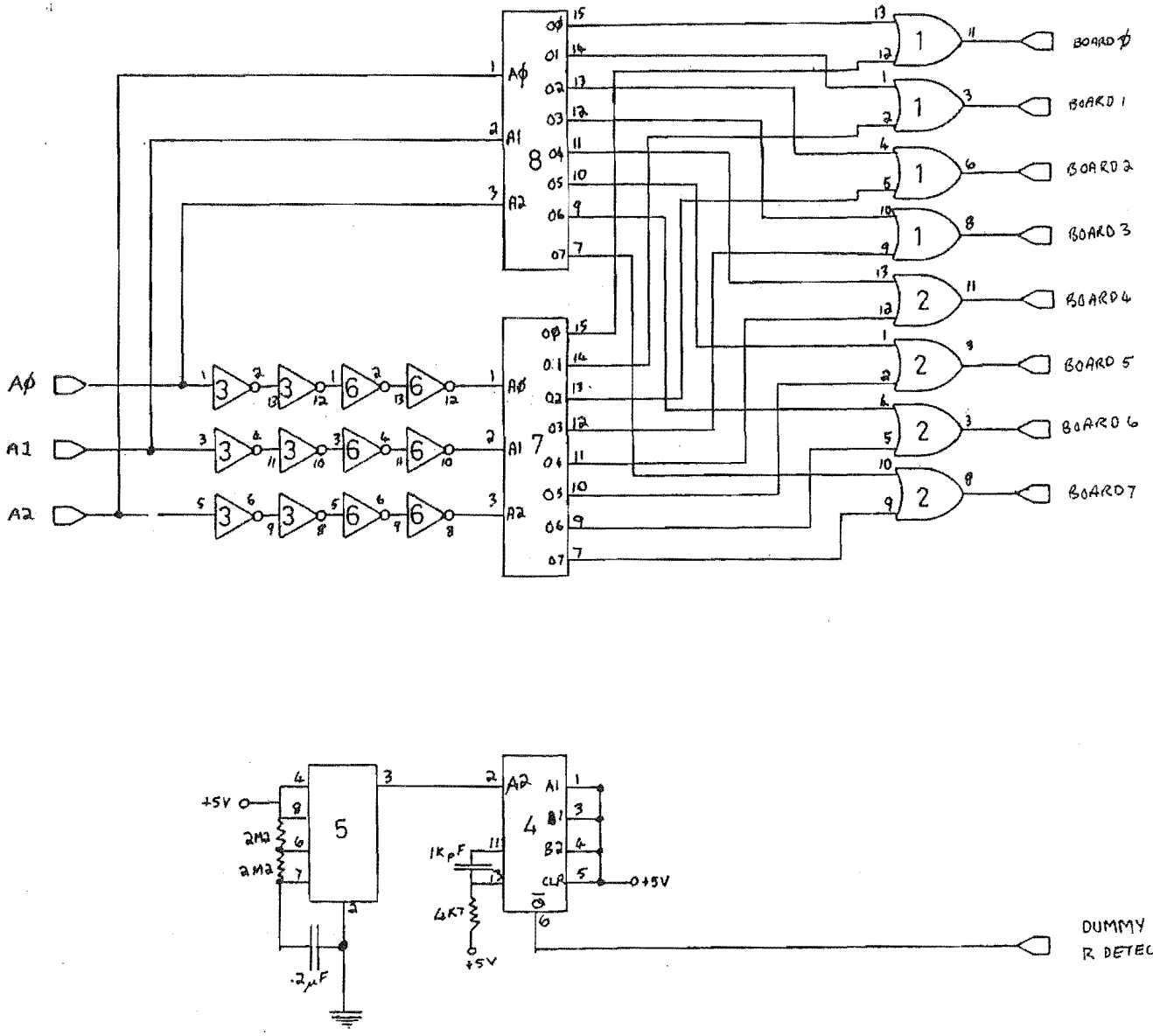

Memory Selector Board

Multiplexer Board (8 required)

I.C. type	Identification number in diagram
74LS02	6
74LS08	8
74LS123	7
74LS374	3,10,12
8096/8098	9,11,13
8216/8226	1,2,4,5

Power requirements: +5V

This board plugs directly into buss. Memory boards plug into this board.

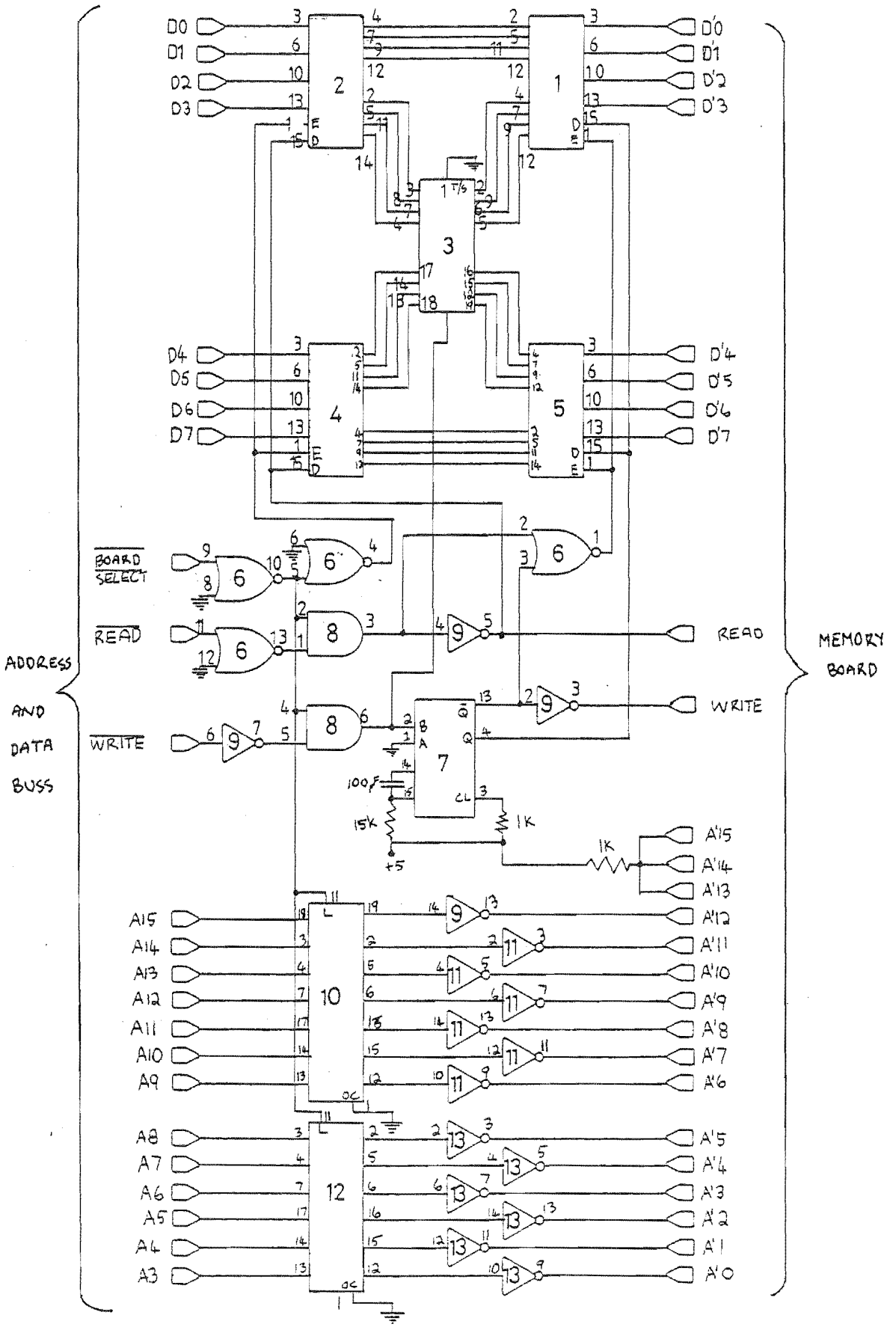

Multiplexer Board

DAVCO Memory Boards (8 required)

I.C. type	Identification number in diagram
8226/8216	1,2
8205	3,4
Octal DIP switch	5
MM2102	6-69

Power requirements: +5V

This diagram has been simplified for clarity. Only 3 memory chips are shown There are 8 rows of 8 chips on the board to store the data.

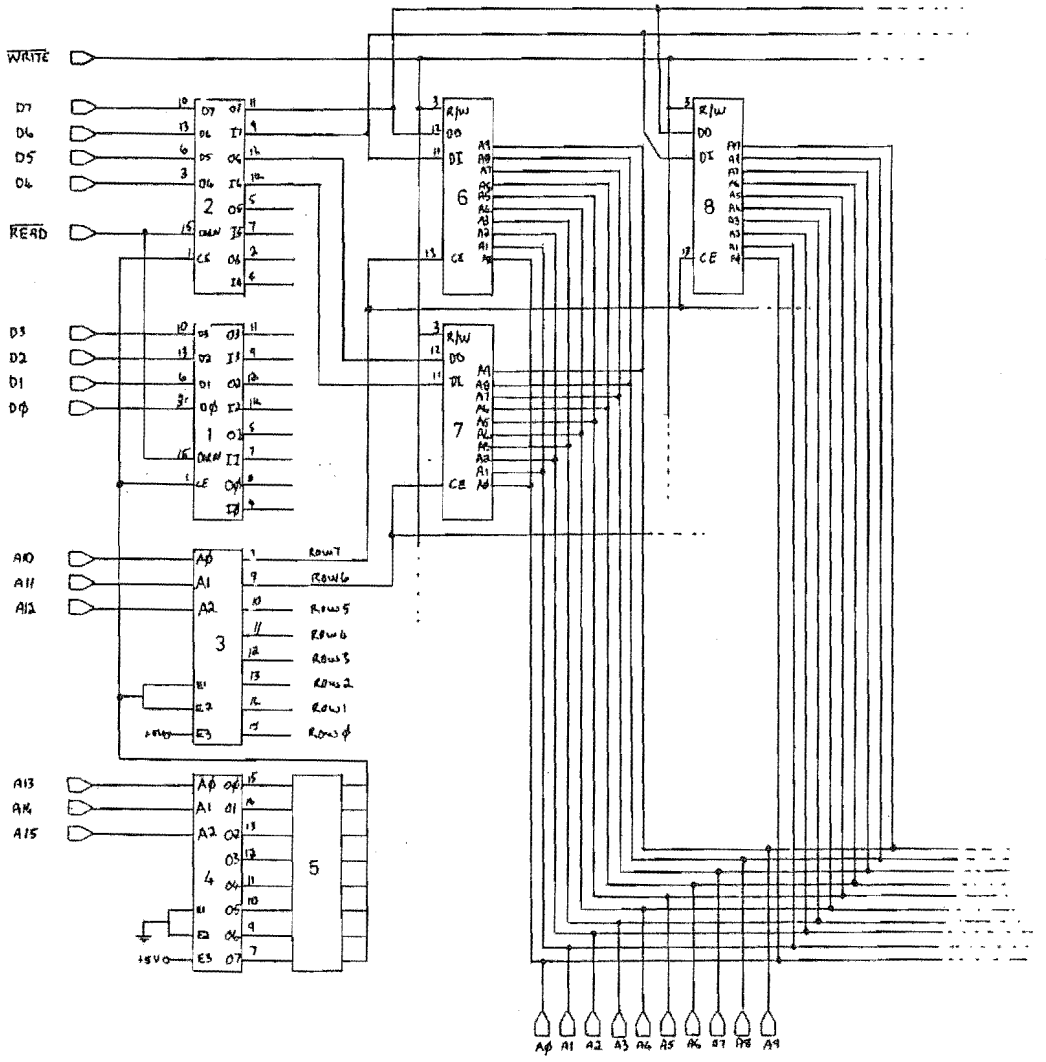

DAVCO Memory Board

Parameter Display Board

I.C. type	Identification number in diagram
7400	23
7404	5,16
7408	12
7410	4,15
7432	13
7473	3,7,14,22
7490	1,10,9,24
74161	18-21
74C925	6,11,17
Octal DIP switch	25,26

Power requirments: +5V

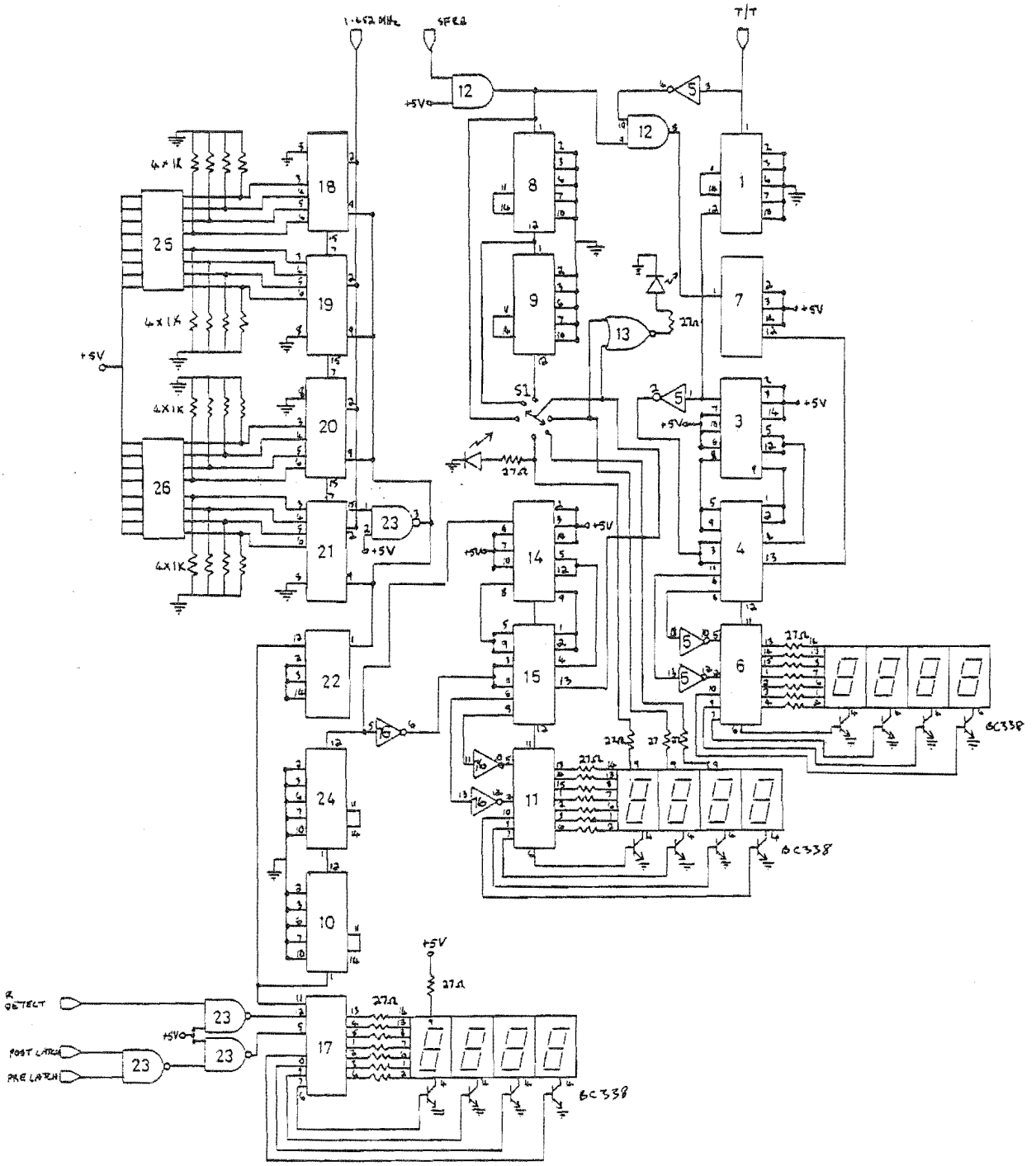

Parameter Display Board

Computer Interface Board

I.C. type	Identification number in diagram
7400	6,9
7404	1
74LS14	4
7417	2,3
74123	5,7
8095	13
8226	8,12
8556	10,11,14,15

Power requirements: +5V

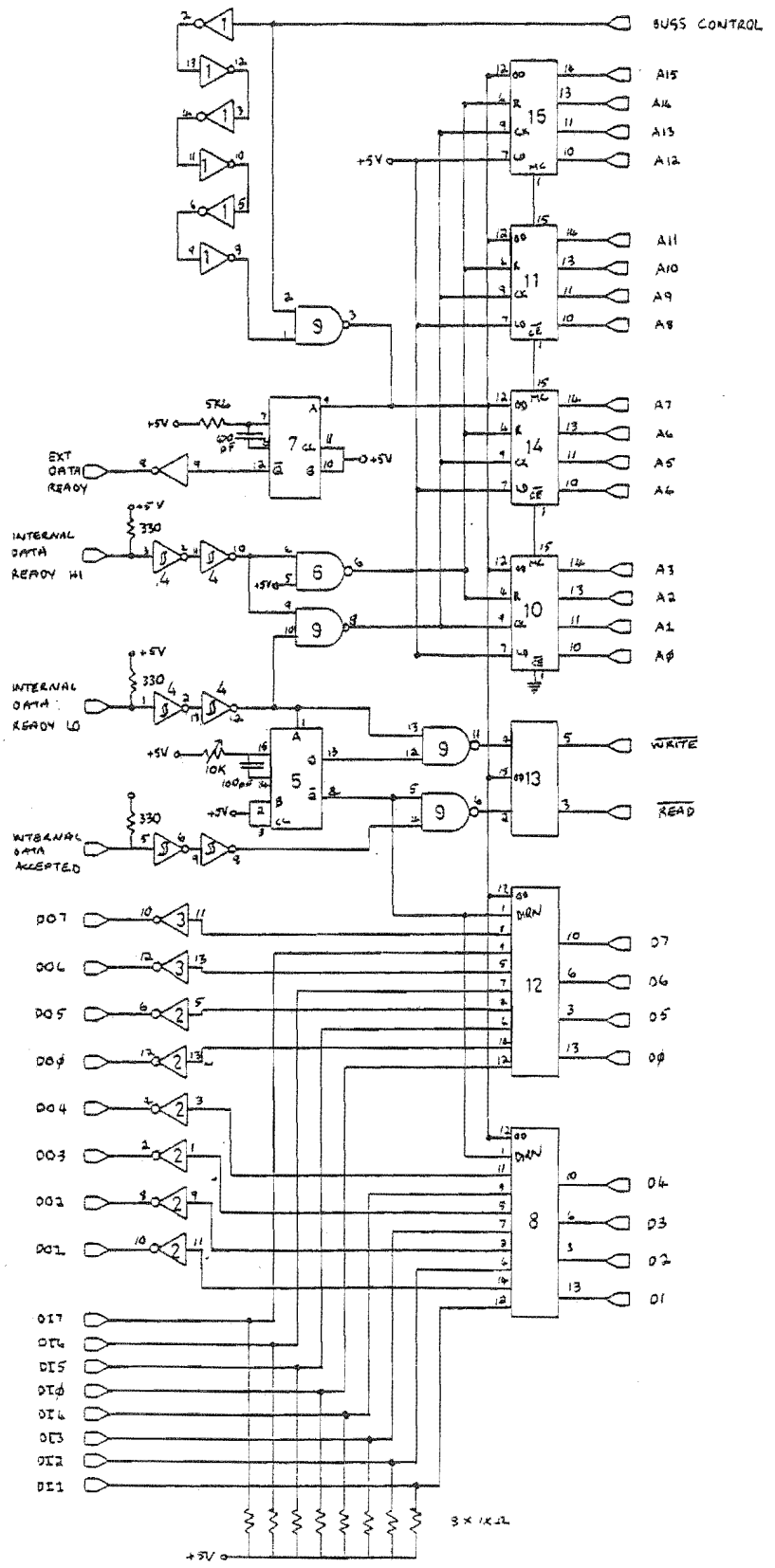

Computer Interface Board

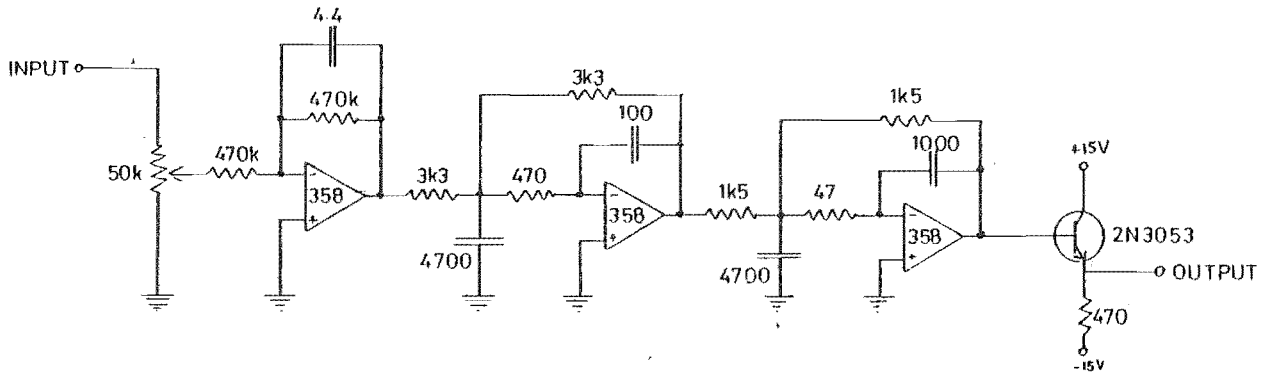

358 = LF358

Power: ±15V

Echo-train Filter and Buffer

APPENDIX B

The following experiment was used as a means of testing and calibrating Igor.

Theory

Consider a pulse of ultrasound emitted by a medical transducer (cf.§2.3.1). The shape of the intensity spectrum of such a pulse is considered by some researchers to be Gaussian (cf. Dines and Kak, 1979). That is, it is of the form

$$I(f) = I_o \exp\{-\alpha(f_o-f)^2\} \qquad (A.1)$$

where I_o is the intensity at the centre frequency f_o of the spectrum and α is a measure of the width of the spectrum (cf. Figure A.1).

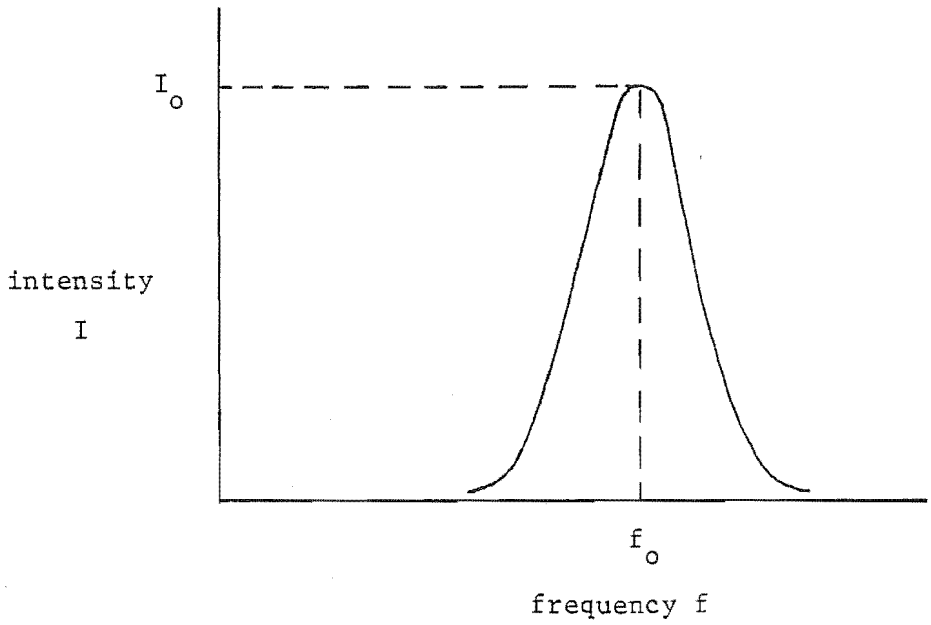

Figure A.1 Intensity spectrum of an ultrasonic pulse (Gaussian shaped).

Suppose now, that the pulse is reflected off a planar boundary perpendicular to the path of the pulse. The spectrum of the reflected pulse is

$$I_p(f) = PI_o \exp\{-\alpha(f_o-f)^2\} \qquad (A.2)$$

where P is the fraction of the incident pulse reflected by the boundary. P is the same for all frequencies of the spectrum (cf. Wells, 1977, p 138). However, if the pulse is scattered off a wire whose diameter is appreciably less than one wavelength then the spectrum of the backscattered pulse is (cf. 1.13)

$$I_w(f) = AI_o f^3 \exp\{-\alpha(f_o-f)^2\} \qquad (A.3)$$

where A is a constant. Similarly, if the pulse is reflected off a particle all of whose dimensions are appreciably smaller than one wavelength (i.e. a subwavelength particle), the spectrum of the scattered pulse is (cf. 1.15).

$$I_s(f) = BI_o f^4 \exp\{-\alpha(f_o-f)^2\} \qquad (A.4)$$

where B is a constant. It can be seen from (A.3) and (A.4) that the higher-frequency components of the incident pulse are backscattered more strongly than those of the lower frequencies. Thus the subwavelength wires or scatterers act as high pass filters.

A typical spectrum for a pulse of sound emitted by a medical ultrasonic transducer is presented in Figure A.2. It has a centre frequency f_o = 1.9 MHz and a bandwidth of 600 KHz (at the - 3dB points). Superimposed on it is the spectrum of the same pulse after it has been backscattered from a subwavelength particle. The spectrum of the scattered pulse was calculated using (A.4). It is normalised so that the intensities at the centre frequencies of the incident and scattered pulse spectra are the same. The spectrum of the scattered pulse also appears to be Gaussian in shape. However, it appears to be 'shifted' slightly to a higher frequency (cf. Surridge, 1980a, 1980b). The centre frequency f_s of the scattered pulse may be found by solving

$$\frac{dI_s(f)}{df} = 0 \qquad (A.5)$$

for f. Thus it can be shown that

$$f_s = \frac{f_o}{2} + \sqrt{\frac{f_o^2}{4} + \frac{2}{\alpha}} \qquad (A.6)$$

Similarly it can be shown that the centre frequency f_w of the spectrum of the pulse scattered off a thin wire is

$$f_w = \frac{f_o}{2} + \sqrt{\frac{f_o^2}{4} + \frac{3\alpha}{2}} \qquad (A.7)$$

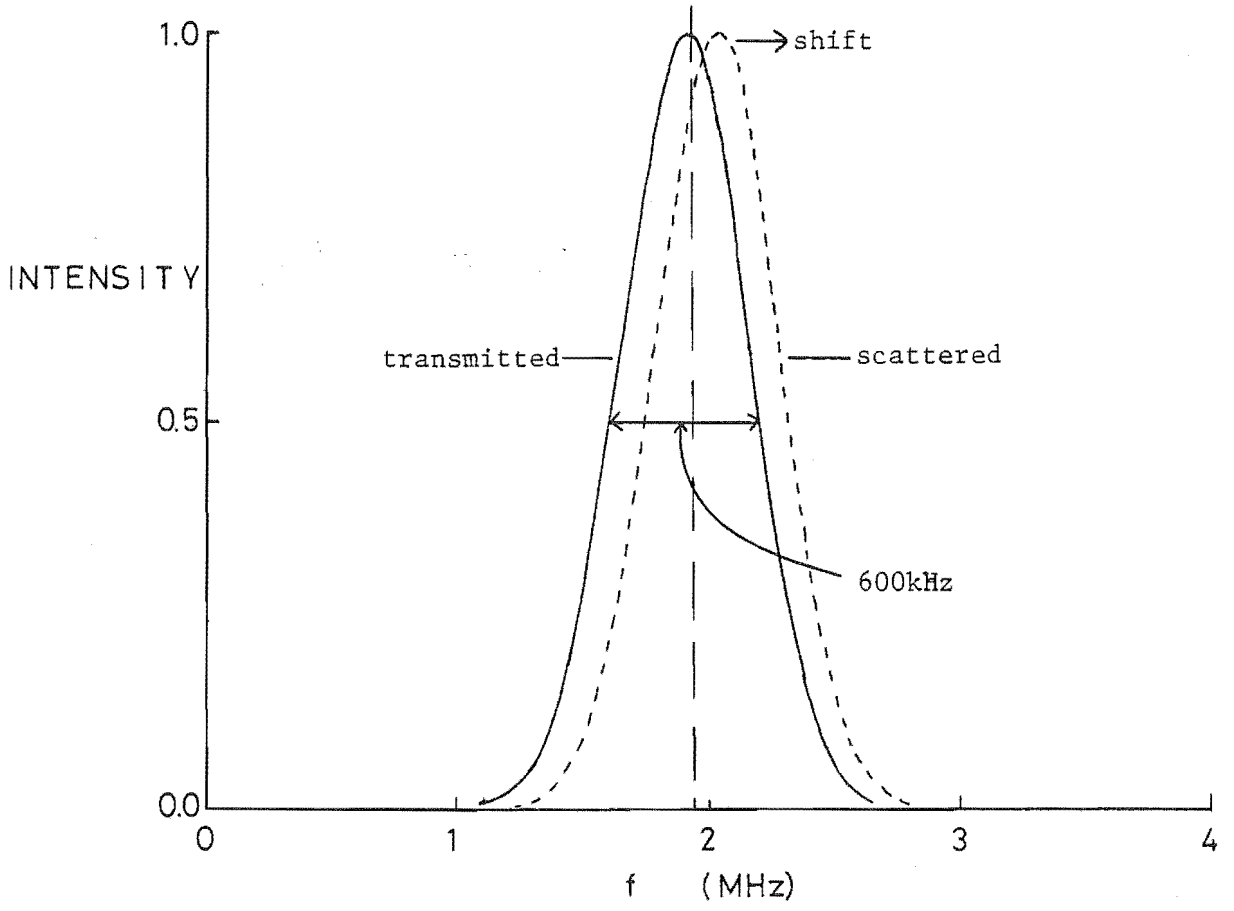

Figure A.2 Shift in the centre frquency of a pulse of ultrasound when it is scattered off a subwavelength particle.

The magnitude of the shift in the centre frequency of the pulse shown in Figure A.1 when scattered off a subwavelength particle is calculated using (A.6) to be 100 KHz. In the same manner, the shift in the centre frequency for the pulse when scattered off a thin wire is calculated to be 80 KHz using (A.7).

Method

The following experiment was performed to see if the predicted shift in the centre frequency of a pulse from a medical transducer scattered off a thin wire can be detected. Apparatus of the kind indicated in Figure A.3 was assembled.

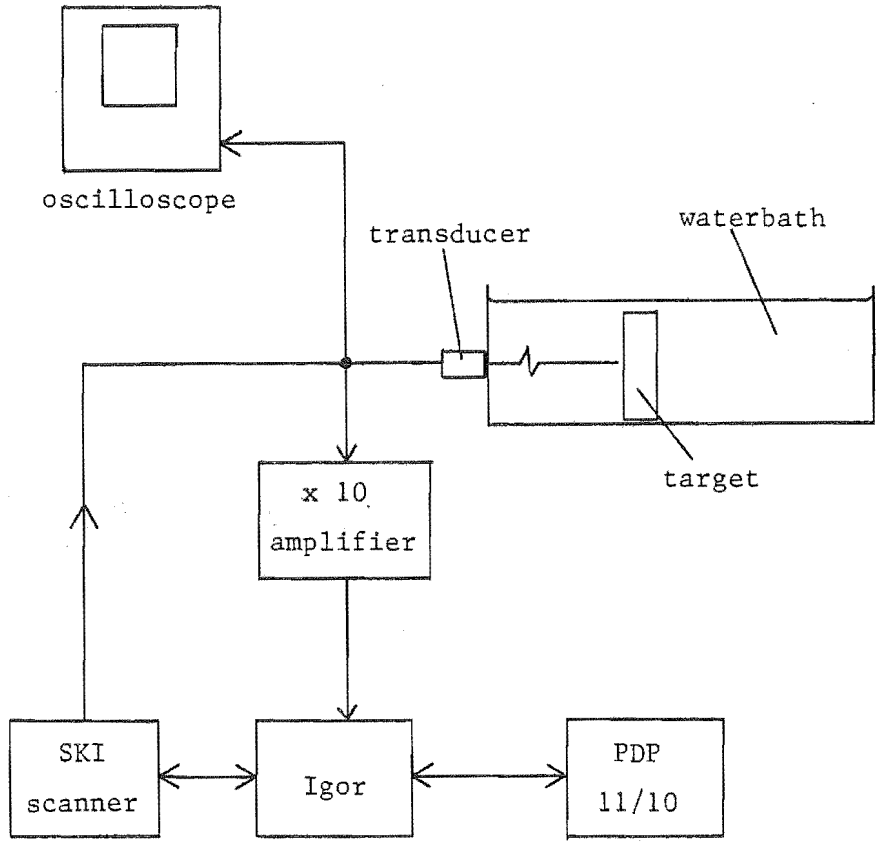

Figure A.3 Apparatus assembled to measure frequency shift.

A transducer (1.9 MHz nominal centre frequency, 2 cm diameter) was arranged to irradiate a target immersed in a water bath. The target was either a polished perspex block or a grid of copper wires (see Fig. A.4). The transducer was excited by the SKI scanner. A target was placed in the ultrasonic beam and aligned to be perpendicular to the beam. This was achieved by rotating the target until the largest echo of the target was displayed on the oscilloscope. The echoes received by the transducer were passed to Igor via an amplifier with a gain of 10. The echo train was sampled by Igor at 7.26 MHz and recorded on disk. This was then done with the other target, at the same transducer-to-target range. The experiment was

then repeated with the targets at different ranges from the transducer.

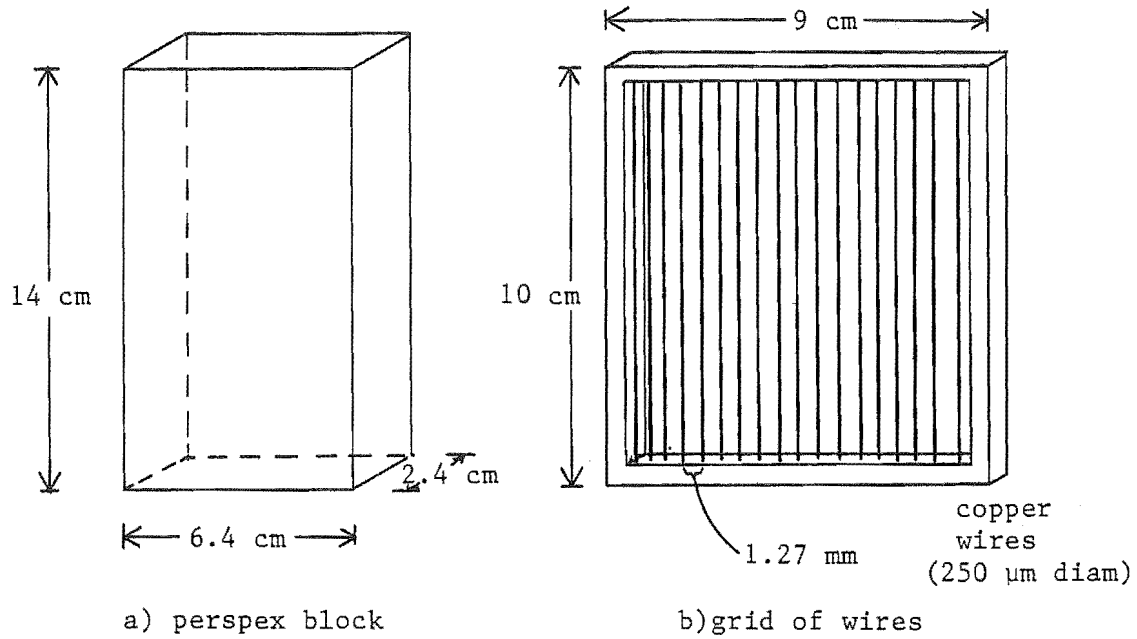

a) perspex block b) grid of wires

Figure A.4 Targets used in scattering experiment.

The intensity spectra of the backscattered pulses were then calculated. This was achieved by computing the real and imaginary components of the spectra of the echoes using the Fast Fourier Transform (cf. Gonzalez and Wintz, 1977). The intensity spectra was then calculated by

$$I(f) = \{Re(f)\}^2 + \{Im(f)\}^2 \qquad (A.8)$$

where Re(f) is the real component of the spectrum at frequency f, Im(f) is the imaginary component of the spectrum at frequency f. See Figure A.5. The centre frequency (f_o or f_w) of each spectrum was considered to be that with the highest intensity. These were found for each spectrum and are graphed in Figure A.6. In this graph it is seen that the centre frequencies of the echoes scattered off the wire grid were higher than those scattered off the perspex block in all cases except two. On average the shift in the centre frequency is 130 KHz. This is approximately the size of the shift in the centre frequency which was expected (cf. Figure A.2).

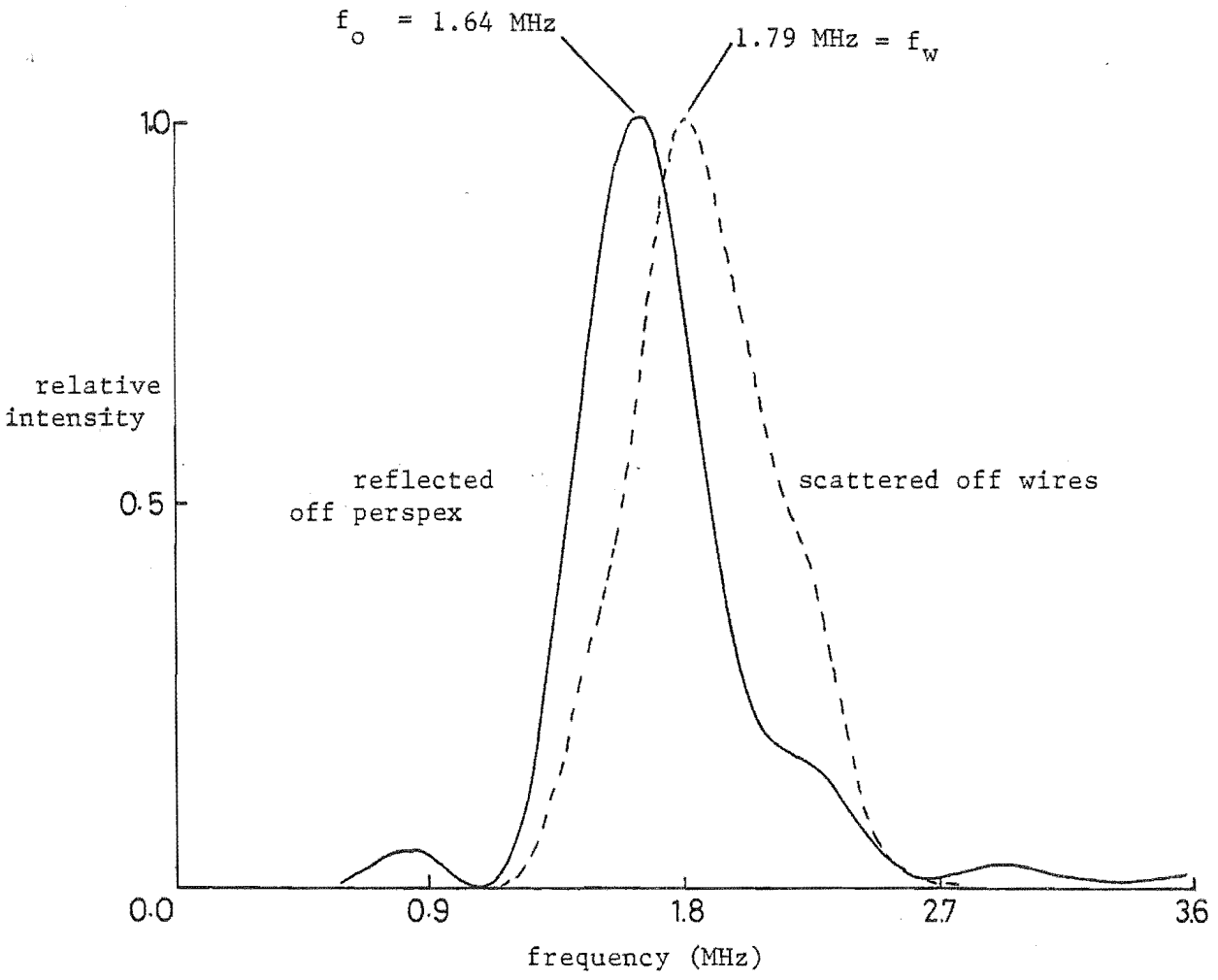

Figure A.5 Spectra of ultrasound pulses after being scattered off the perspex block and off the wire grid. Targets were positioned 23mm away from the transducer.

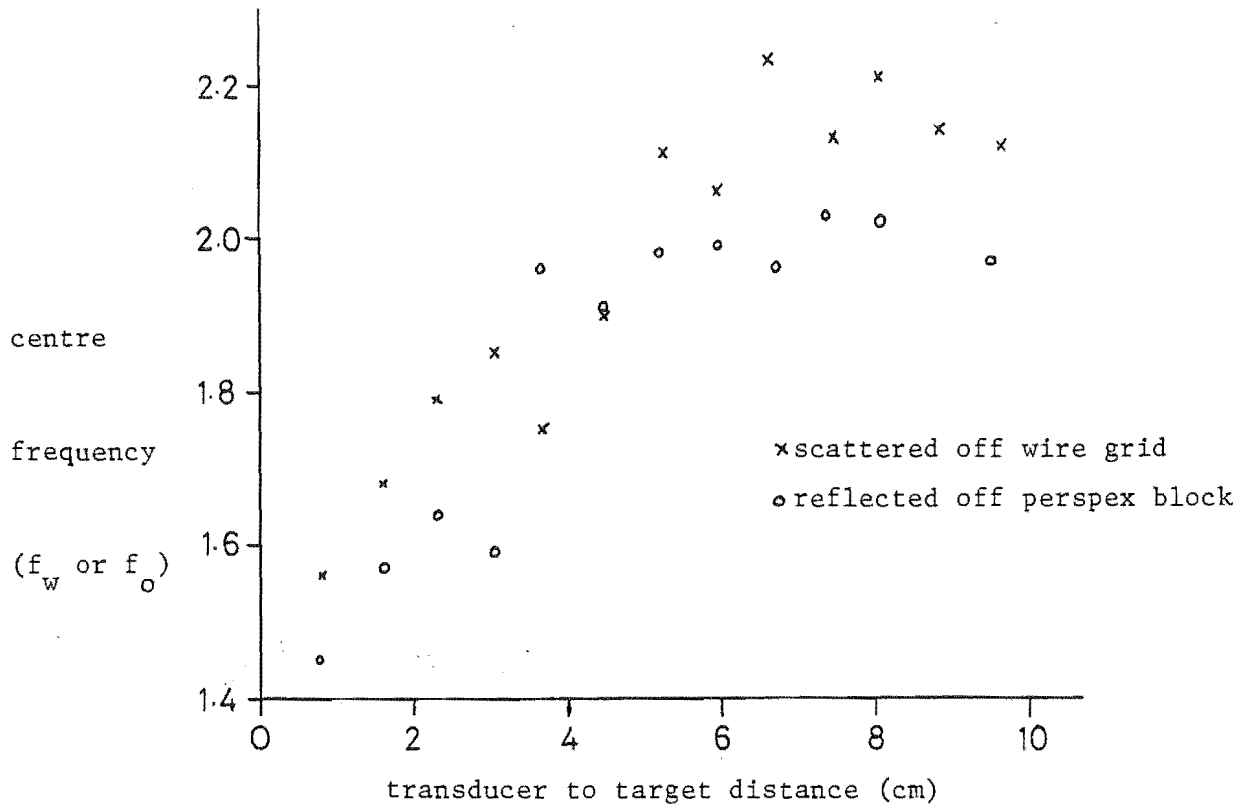

Figure A.6 Graph of centre frequencies of spectra of pulses scattered off perspex block and wire grid at different transducer to target separations.